PERTURBATIONS IN THE A $^1\Pi$ STATE OF THE ISOTOPOMERS OF CO AND THE COMET-TAIL SYSTEM OF $^{12}C^{16}O^+$

CHANDRAN HARIDASS

PERTURBATIONS IN THE A $^1\Pi$ STATE OF THE ISOTOPOMERS OF CO

AND

THE COMET-TAIL SYSTEM OF $^{12}C^{16}O^+$

BY

Chandran Haridass

A thesis submitted to the School of Graduate

Studies in partial fulfillment of the

requirements for the degree of

Doctor of Philosophy

Department of Physics and Physical Oceanography

Memorial University of Newfoundland

May 1996

St. John's Newfoundland

DEDICATED TO MY PARENTS

ACKNOWLEDGMENTS

It is my pleasure to express my deep gratitude to my supervisor, Professor S. P. Reddy for his constant encouragement and guidance in the various stages of my research projects and other academic pursuits.

I am indebted to Dr. K. P. Huber, Steacie Institute of Molecular Sciences, N. R. C., Ottawa, for his guidance and help in using the jet discharge experimental setup and the 10.6 m vacuum grating spectrograph. I am grateful to Professor. André Le Floch, Department de Physique, Universite de Tours, France for his computer program to perform the deperturbation analysis. I sincerely thank Drs. J. K. G. Watson, Steacie Institute of Molecular Sciences, Peter Bernath, Chemistry Department, University of Waterloo, C. Amiot, Laboratoire Aimé Cotton, Orsay Cédex, France, and C. V. V. Prasad, Chemistry Department, University of Victoria for their stimulating and useful discussions. My thanks are due to other members of the supervisory committee, Drs. M. Morrow and N. D. Foltz and also to Drs. M. J. Clouter, N. Rich, and R. Goulding for the valuable discussions.

I extend my thanks to the following technical personnel for their help in completing the research project: Mr. Chris Harris, Steacie Institute of Molecular Sciences, N. R. C., Ottawa. Messers. M. Ryan, and W. Holly for the mechanical work; T. Perks, M. Hatswell for their skilful glass blowing; R. Guest for some drafting work; and R. Bradley for some photographic work. It is a pleasure to thank Mrs. Joy Simmons for her skilful typing of a part of the thesis. I also express my sincere thanks to Mr. Cliff Stamp for some computational work and also to Miss. Wicke, summer student, Steacie Institute

of Molecular Sciences, N. R. C., Ottawa for her help in recording the spectra.

I thank Memorial University of Newfoundland and Department of Physics for financial support in the form of a Graduate fellowship and a Graduate Teaching Assistantship and Dr. Reddy for support from his NSERC grant.

I am indebted to Professor. N. Krishnamurthy, Madurai Kamaraj University, Madurai, India, who inspired me to undertake research in molecular spectroscopy.

I extend my heart-felt thanks to my wife, Shobha, and daughter, Kiran, for their patience and understanding when I had to spend extended periods in the laboratory. Finally, I wish to express my sincere regards to my parents for their blessings and encouragement.

ABSTRACT

The electronic band spectra of the neutral molecule $^{12}C^{16}O$, its isotopomers $^{13}C^{16}O$, $^{12}C^{18}O$, and $^{13}C^{18}O$, and the molecular ion $^{12}C^{16}O^+$ are of considerable importance in astrophysics and atmospheric physics. The rotational emission spectra of these molecules are routinely used in millimetre radio astronomy to map the molecular densities in the interstellar medium. These molecules are present in circumstellar envelopes, and cometary and planetary atmospheres. The molecular ion CO^+ has applications in the study of radiative heating of hypersonic space craft at escape velocity and in the atmospheric fringe of Venus.

The vacuum ultraviolet spectra of the fourth positive ($A\ ^1\Pi$ - $X\ ^1\Sigma^+$) system of carbon monoxide isotopomers $^{12}C^{18}O$ and $^{13}C^{18}O$ excited in the anode column of a hollow-cathode discharge tube, and of the isotopomers $^{13}C^{16}O$ and $^{13}C^{18}O$ generated in emission in a jet discharge apparatus were photographed in the spectral region 1370 - 1935 Å on a 10.6 m vacuum grating spectrograph. Detailed rotational analysis for thirty nine bands of the three isotopomers of the A-X system has been carried out. Several perturbations occurring in the $A\ ^1\Pi$ state due to its neighbouring states e $^3\Sigma^-$, a′ $^3\Sigma^+$, d $^3\Delta_i$, I $^1\Sigma^-$, and D $^1\Delta$ were observed. From a deperturbation analysis, the deperturbed molecular constants, were obtained for the $A\ ^1\Pi$ state as well as for the perturbing states of the three isotopomers. Perturbing parameters and mixing coefficients which characterize perturbations were also derived.

Using the experimental data of the fourth positive system of the three isotopomers, the term values of the $A\ ^1\Pi$, v=0 to 9 levels of $^{13}C^{16}O$, v=1 and 2 levels of $^{12}C^{18}O$, and

v=1 level of $^{13}C^{18}O$ were determined. The term values of the Rydberg states B $^1\Sigma^+$, v=0 and 1, C $^1\Sigma^+$, and E $^1\Pi$, v=0 were calculated for the isotopomers $^{12}C^{18}O$ and $^{13}C^{18}O$, by combining the present data and those of the B $^1\Sigma^+$ - A $^1\Pi$, C $^1\Sigma^+$ - A $^1\Pi$, and E $^1\Pi$ - A $^1\Pi$ systems taken from the literature. The molecular constants of Rydberg states B, C, and E were determined from the calculated term values.

The comet-tail (A $^2\Pi_i$ - X $^2\Sigma^+$) system of $^{12}C^{16}O^+$ occurring in the cathode glow of a hollow cathode discharge tube and photographed in the spectral range 3345 - 8500 Å at high resolution was reinvestigated. Spin-splitting of the rotational levels of all the analyzed ten bands was observed. The observed intensity distribution of the branches is in good agreement with theoretical calculations. Rotational constants were obtained for the A $^2\Pi_i$ and X $^2\Sigma^+$ states from a global fit of the present data of the comet-tail system and the infrared and microwave data available from the literature.

CONTENTS

CHAPTER 1

INTRODUCTION

1.1 Importance of Molecular Spectra in Atmospheric Physics and Astrophysics

With the development of quantum mechanics great progress has been made in the experimental studies and theoretical understanding of the electronic spectra of diatomic molecules. Information about the vibration and rotation of the nuclei and the electronic structure of the molecules are provided by their electronic spectra. Properties such as chemical valence can be understood from the electronic structure. Electronic, vibrational and rotational energy levels of a molecule can be obtained very precisely from a detailed analysis of its electronic spectrum. From a knowledge of the vibrational frequencies and the anharmonicities of a molecule, forces between the constituent atoms and its dissociation energy can be estimated. The rotational analysis of the electronic bands of a molecule gives accurate values of the moments of inertia and internuclear separations in various energy states. It also provides information on the nature of the coupling between the rotational motion of the molecule, as well as information about the possible perturbations between the energy levels of different electronic states. Thermodynamic properties such as specific heat, entropy, and free energy can be estimated from the vibrational and rotational partition functions. From the vibrational and rotational constants of the electronic states and other molecular data, intensities of the bands of the electronic spectra can be calculated.

Molecular spectra play a very important role in the investigations of atmospheric and

astrophysical phenomena. A few examples of these are the molecular absorption spectrum of the earth's atmosphere, the emission band spectra of the aurorae, the radiations from the night and the twilight sky which are produced in the upper layers of the atmosphere, the cometary spectra, and the spectrum of lightning. The presence of all natural isotopomers of CO, namely, $^{12}C^{16}O$, $^{13}C^{16}O$, $^{12}C^{18}O$, and $^{13}C^{18}O$ was established in the solar spectra by Farrenq *et al.* (1991) from a high resolution study using an infrared Fourier transform spectrometer. The emission of radiation from the earth's atmosphere gives rise to band spectra due to several molecular species. For example, the spectrum of the night sky reveals band spectra of N_2, O_2, and NO; the N_2^+ bands have been observed in the twilight; the spectra of aurorae consist of the N_2 and N_2^+ bands. The main features of the auroral spectra are very similar to those obtained in a hollow-cathode discharge in nitrogen. Important information about the physical conditions and the compositions of the atmospheric layers can be obtained from a study of their spectra. The temperatures and depths of the atmospheres of the celestial objects are estimated from the intensity distribution of their emission spectra. The absorption spectra of the planetary atmospheres confirm the presence of polyatomic molecules such as CO_2, CH_4, NH_3, e.g., CO_2 in Venus, earth's atmosphere, and Mars; CH_4 in many planets; NH_3 in Jupiter and Saturn. Cometary spectra are a good example of the application of molecular spectra to astrophysics. The ion tail of a comet consists of molecular ions such as CO^+, N_2^+, H_2O^+, etc., and its dust tail consists of mostly dust particles. The coma of a comet gives radiation emitted by the molecular radicals, C_2, CN, OH, NH, NH_2, etc., which is

overlapped by a weak continuum with Fraunhofer atomic lines, arising from the reflection of sunlight by the solid particles of the cometary nuclei. The band spectra emitted in the coma (head of the comet) and the nucleus are different from those occurring in the tail. Molecules such as CO, etc., are present in interstellar space. Temperatures of the stars can be determined from their emission spectra. These types of investigations are necessary to understand the nuclear processes through which the energy is released in these objects.

1.2 Electronic Configurations and Spectra of the Isotopomers of CO and CO^+

The number of electrons in the outer most shells of the constituent atoms of the molecule determines its binding character and the nature of the electronic states. The ground state electronic configurations of the carbon and oxygen atoms are

$$\text{C: K } 2s^2\ 2p^2; \quad \text{O: K } 2s^2\ 2p^4 \qquad [1.1]$$

The ground state electronic configuration of CO molecule is written as (Mulliken, 1932)

$$\text{K K } (z\sigma)^2\ (y\sigma)^2\ (w\pi)^4\ (x\sigma)^2 \quad : X\ ^1\Sigma^+. \qquad [1.2]$$

The other low lying excited states are obtained by promoting one of the $x\sigma$ electrons of the ground state configuration to the $v\pi$ orbital and one of the $w\pi$ electrons to the $v\pi$ orbital. The resulting configurations and states are represented as

$$- \ - \ - \ - \ (w\pi)^4\ (x\sigma)\ (v\pi) \ : \ a\ ^3\Pi_r \text{ and } A\ ^1\Pi \qquad [1.3]$$

and

$$(w\pi)^3\,(x\sigma)^2\,(v\pi) \;:\; a'\,{}^1\Sigma^+,\ e\,{}^1\Sigma^-,\ d\,{}^1\Delta,$$

$$D'\,{}^1\Sigma^+,\ I\,{}^1\Sigma^-,\ \text{and}\ D\,{}^1\Delta. \qquad [1.4]$$

The $D'\,{}^1\Sigma^+$ state in Eq.[1.4] has been observed by Wolk and Rich (1983). Higher excited states of CO are obtained by raising one of the $x\sigma$ electrons of the ground state expressed in Eq.[1.2] to the $u\sigma$ orbital and one of the $w\pi$ orbitals to the $u\sigma$ orbital. They are

$$(w\pi)^4\,(x\sigma)\,(u\sigma) \;:\; {}^3\Sigma^+ \text{ and } {}^1\Sigma^+ \qquad [1.5]$$

and

$$(w\pi)^3\,(x\sigma)^2\,(u\sigma) \;:\; {}^3\Pi_i \text{ and } {}^1\Pi. \qquad [1.6]$$

To date none of the four states referred to in Eqs. [1.5] and [1.6] has been observed. Further higher excited states of CO are obtained by promoting one of the $x\sigma$ electrons to the Rydberg orbitals $3s\sigma$, $3p\sigma$, and $3p\pi$, etc., which are written as

$$(w\pi)^4\,(x\sigma)\,(3s\sigma) \;:\; b\,{}^3\Sigma^+ \text{ and } B\,{}^1\Sigma^+ \qquad [1.7]$$

$$(3p\sigma) \;:\; j\,{}^3\Sigma^+ \text{ and } C\,{}^1\Sigma^+ \qquad [1.8]$$

$$(3p\pi) \;:\; e\,{}^3\Pi_i \text{ and } E\,{}^1\Pi \qquad [1.9]$$

Lefebvre-Brion *et al.* (1964) have shown that the Rydberg states converge to the ground state of the CO^+ molecule. The observed molecular states of CO and their RKR potential energy curves below 95000 cm^{-1} given by Tilford and Simmons (1972) are shown in a modified form in Fig. 1.1. The electronic spectrum of CO in the spectral region 600-8600 Å has been extensively studied both in emission and absorption. From the known 24 electronic states of CO, a total of 30 electronic transitions are observed. Of these, the prominent band systems are (i) the Ångström ($B^1\Sigma^+$-$A^1\Pi$) system (4100-6600 Å), ii) the

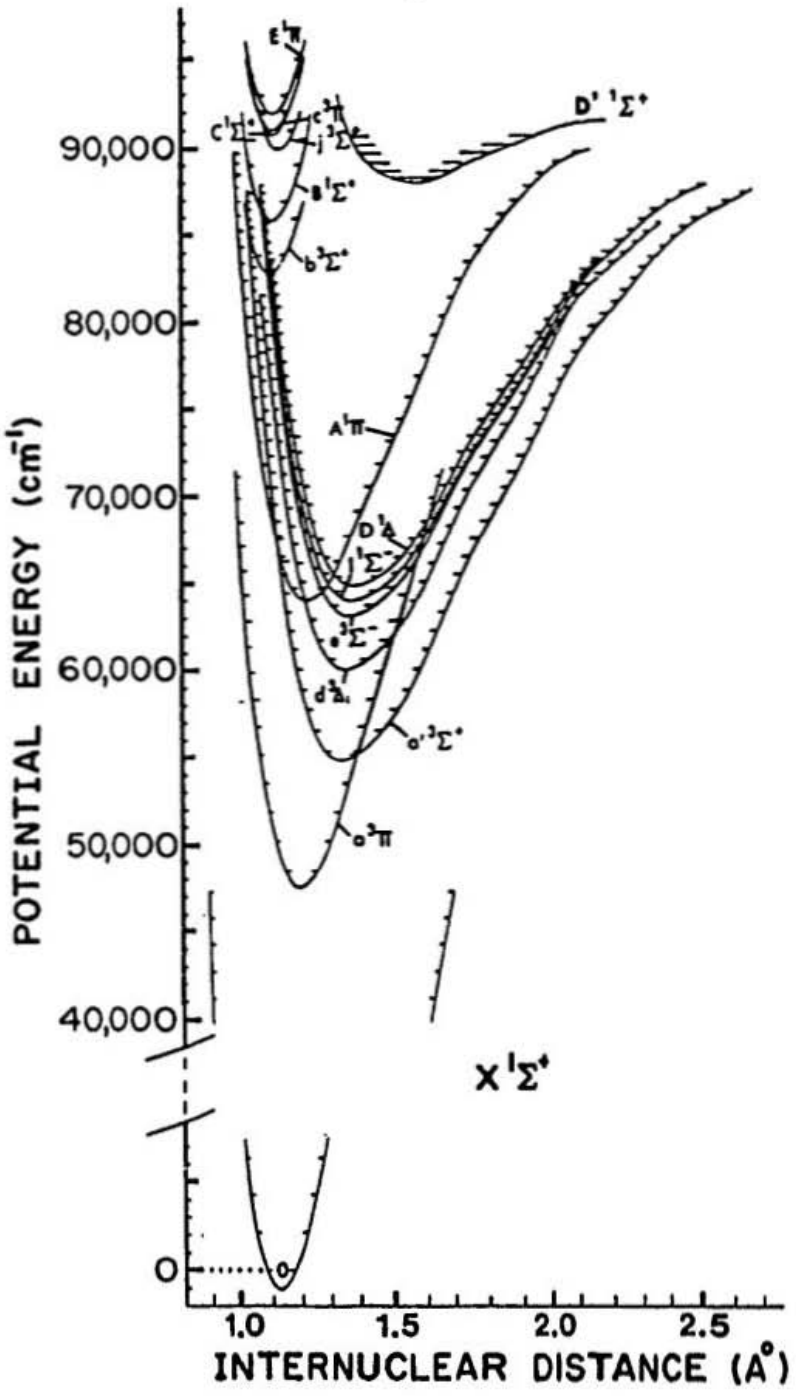

Figure 1.1 RKR potential energy curves for the electronic states of $^{12}C^{16}O$ below 95000 cm^{-1} (adopted from Tilford and Simmons, 1972).

Herzberg ($C^1\Sigma^+$-$A^1\Pi$) system (3680-5705 Å), iii) the third positive ($b^3\Sigma^+$-$a^3\Pi_i$) system (2600-3800 Å), and iv) the fourth positive ($A^1\Pi$-$X^1\Sigma^+$) system (1140-2800 Å).

The CO^+ molecular ion is obtained by the removal of one electron from the CO molecule. The electronic configuration of the ground state of the CO^+ molecule arises by the removal of an electron from $x\sigma$ orbital of the ground state ($X^1\Sigma^+$) of the CO molecule and is written as

$$K\ K\ (z\sigma)^2\ (y\sigma)^2\ (w\pi)^4\ (x\sigma)\ :\ X^2\Sigma^+ \qquad [1.10]$$

The electronic configurations of the first three excited states are

$$K\ K\ (z\sigma)^2\ (y\sigma)^2\ (w\pi)^3\ (x\sigma)^2\ :\ A^2\Pi_i \qquad [1.11]$$

$$--\ -\ -\ (w\pi)^4\ (x\sigma)^2\ :\ B^2\Sigma^+ \qquad [1.12]$$

$$--\ -\ -\ (w\pi)^3\ (x\sigma)\ (v\pi)\ :\ C^2\Delta_r \qquad [1.13]$$

The electronic states $X^2\Sigma^+$ and $A^2\Pi_i$ dissociate into $C^+(^2P)$ and $O(^1P)$ atoms. The Rydberg-Klein-Rees (RKR) potential energy curves modified from Krupenie (1966) for the $X^2\Sigma^+$, $A^2\Pi_i$, and $B^2\Sigma^+$ states which are of interest in the present work along with that of the ground state ($X^1\Sigma^+$) of neutral CO are given in Fig. 1.2 (adopted from Krupenie, 1966). The three prominent band systems arising from the three well known electronic states X, A, and B of the CO^+ molecule are i) the comet-tail ($A^2\Pi_r$-$X^2\Sigma^+$) system (3080-8500 Å), ii) the Baldet-Johnson ($B^2\Sigma^+$-$A^2\Pi_i$) system (3315-4236 Å), and iii) the first negative ($B^2\Sigma^+$-$X^2\Sigma^+$) system (1800-3152 Å). The transition $C^2\Delta_r$-$A^2\Pi_i$ was first observed at lower resolution by Marchand *et al.* (1969), who assigned the vibrational quantum numbers for the observed bands. Later, Cossart and Cossart-Magos (1990) observed

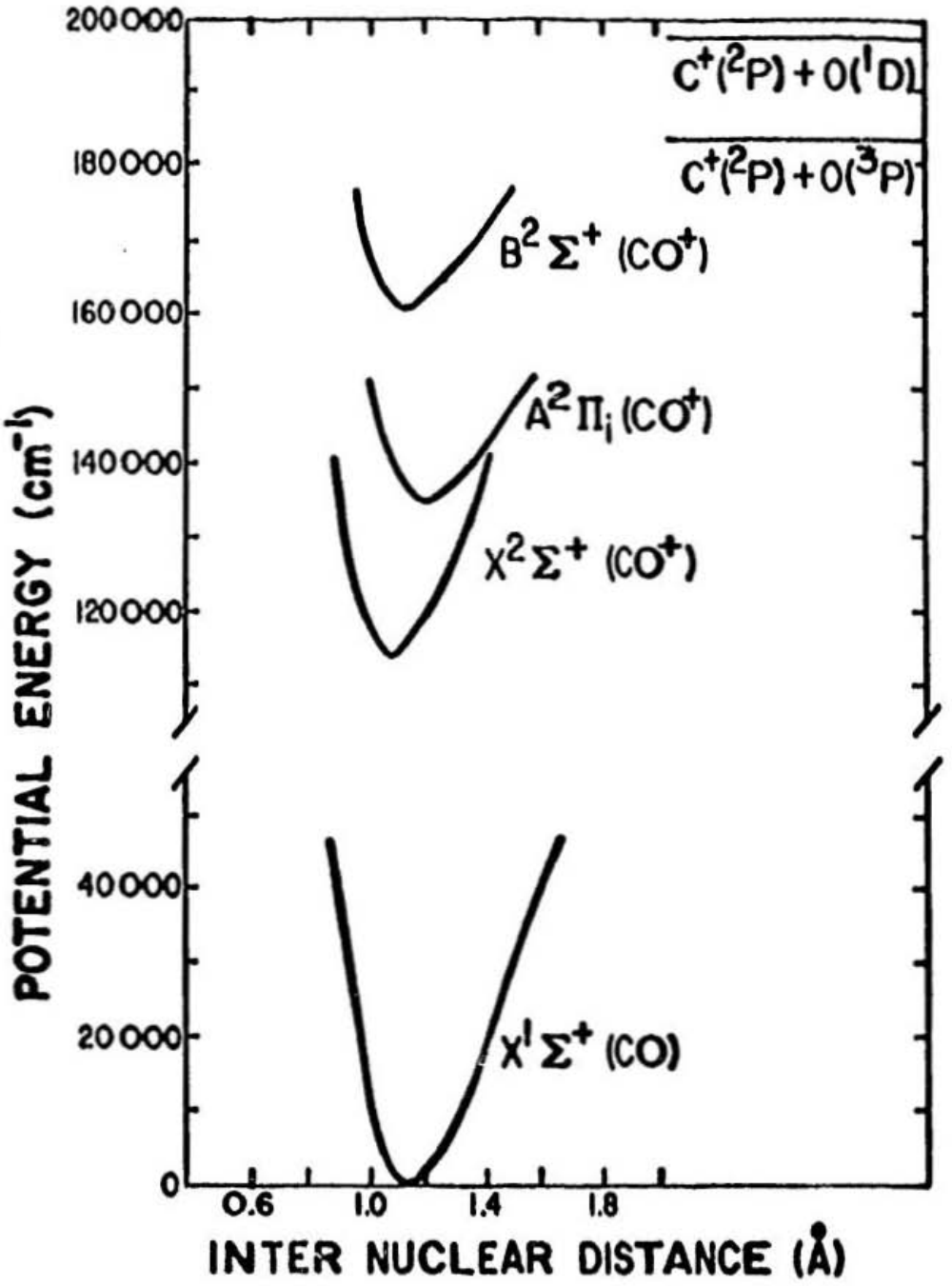

Figure 1.2 RKR potential energy curves for the ground state of CO and X, A, B states of CO^+ (adopted from Krupenie, 1966).

several bands of this system in the presence of Ne and performed the rotational analysis of the 0-2, 1-1, and 2-2 bands.

1.3 Importance of the Fourth Positive System of CO and the Comet-tail System of CO^+

The molecule CO and the molecular ion CO^+ are constituents of solar atmospheres, comet tails, interstellar space and planetary atmospheres. Hence their spectra are of great importance in astrophysical phenomena. The observation of the pure rotational emission line of CO from interstellar space by Wilson et al. (1970), supports the contention that CO is by far the most abundant molecule among the diatomic molecules, in the interstellar medium. From radio-astronomical observations, the abundance ratios $^{12}C/^{13}C$ and $^{16}O/^{18}O$ were obtained for the interstellar medium and compared with the theoretical models (see Auduoze 1977). Spectroscopic studies of astronomical objects by rockets and satellites in recent times, extending the spectral range to the vacuum ultraviolet region, have increased their importance in astrophysics. CO has been extensively observed in a variety of enviornments such as stars (Tsuji, 1986), planets (Encrenaz, 1990), circumstellar and interstellar media (Huggins, 1987), and in the supernova 1987A (Meikle et al., 1989). Wiedemann and Ayres (1991) and Allard et al. (1992) have shown that CO is a major opacity source in the infrared region in cool stellar atmospheres, where transitions occur inside the ground $X\ ^1\Sigma^+$ state. A rocket spectrum obtained by Smith and Stecher (1971) provided the first observation of the interstellar electronic transitions of

CO.

Deslandres (1888) was the first to the study CO emission spectrum. He observed the strong ultraviolet emission bands of CO and named them the fourth positive system and this is now identified as the $A\ ^1\Pi - X\ ^1\Sigma^+$ system. Gerö (1936) and Onaka (1957) studied this system in emission in medium resolution and identified rotational lines up to J=55 for some bands. Simmons et al. (1969) made high resolution measurements of this system in absorption. The first comprehensive study of the $A\ ^1\Pi$ state of CO was performed by Field (1971) and Field et al. (1972) by constructing the appropriate energy matrix and fitting all the available absorption, emission and radio frequency data involving the $A\ ^1\Pi$, a $^3\Pi$, and the perturbing states. This systematic analysis provided fully- deperturbed band origins and rotational constants for the $A\ ^1\Pi$, v=0 to 23 levels and the perturbing states. The perturbation analysis of the data of the A-X system of $^{12}C^{16}O$ initially carried out by Field (1971) has been extended to high J values for the v=0 level by Le Floch et al. (1987) and for the levels v=1 to 4 by Le Floch (1989). This deperturbation analysis has provided the final vibrational and rotational parameters showing a smooth variation with v to within the experimental errors, predicted term values for incompletely observed levels, and mixing coefficients for each interaction. Some of the resulting mixing coefficients were used by Le Floch et al. (1990) to analyze the available life time measurements of both short-lived levels of $A\ ^1\Pi$ and long-lived levels of triplet states.

The bands of the fourth positive system of CO are extensively used in

astrophysics. Goldberg et al. (1965) and Porter et al. (1967) have detected the A-X bands in absorption in the VUV solar spectrum. In the extreme UV solar spectrum, the A-X fluorescence excited by the atomic lines C_{II} and C_{IV} has been observed by Bartoe et al. (1978). The same fluorescence is also observed in the spectrum of giant Arcturus (Ayres, 1981). From the measured line intensities of the A-X system of sunspots in the UV region by Jordan et al. (1979), the solar minimum tempertaure was determined by Marcis and Petropoulos (1983).

The isotopomers of CO were also observed in the stars, planetary nebulae, novae, and interstellar space. With the *International Ultraviolet Explorer (IUE)*, Hanson et al. (1992) observed both $^{12}C^{16}O$ and $^{13}C^{16}O$ in the direction of 20 Aql, and Welty and Fowler (1992) studied these isotopes toward HD 210121. A detailed investigation of these isotopes toward ζOph was made by Sheffer et al. (1992) and Lambert et al. (1994) using the Goddard High-Resolution Spectrograph (GHRS) on the *Hubble Space Telescope (HST)*. Mitchell et al. (1990) have measured numerous absorption lines with $0 \leq J'' \leq 24$ between $X\ ^1\Sigma^+$, v=0 and 1 for both $^{12}C^{16}O$ and $^{13}C^{16}O$ toward several young stellar objects. The presence of stable carbon isotopes ^{12}C and ^{13}C in the solar system in the ratio 11.0 : 0.122 by number and ^{16}O, ^{17}O, and ^{18}O in the ratio $23.7 : 9.04 \times 10^{-3} : 4.76 \times 10^{-2}$, relative to unity for Si was well documented by Grevesse et al. (1991) and Andres and Grevesse (1989). All combinations of the isotopomers of CO, except $^{13}C^{17}O$, have been detected in the radio emission from dense galactic gas clouds. The ratio of the isotopes shows the effects of nuclear processing and isotopic fractionation. According to Hanson

et al. (1992), the isotopic fractionation of CO depends on the competing processes of charge exchange through the reaction

$$^{13}C + {}^{12}C^{16}O \rightleftharpoons {}^{13}C^{16}O + {}^{12}C + 36\ K. \qquad [1.1]$$

This reaction favours the production of $^{13}C^{16}O$ where temperatures are low ($T < 36$ K), and UV photodissociation, which enhances the more abundant $^{12}C^{16}O$ through self-shielding in the absorption lines.

To identify the isotopomers of CO in astrophysical objects and to obtain precise estimates for the abundance ratios of isotopes, it is essential to have accurate laboratory data. It is customary to study the spectra of isotopically substituted molecules in order to unambiguously identify the emitter of a particular band system or confirm the vibrational numbering in an electronic state, etc. In the absence of published transition frequencies of a band system for isotopomers, standard isotopic relations are used to predict these frequencies (Herzberg 1991). For a perturbed band, as in the case of the fourth positive system, the results of such calculations are often misleading since they fail to account for the perturbations of the A $^1\Pi$ state by a number of overlapping singlet and triplet states. The deperturbation analysis of the perturbed bands not only gives information about the perturbed state but also provides spectroscopic information about the perturbing states.

There is a great need in laser spectroscopic studies to understand the fine structure of the valence state A $^1\Pi$ of CO. Various techniques have been used to measure the life times and collision rates for the A state. Interpretation of rotationally resolved lifetime

measurements carried out by laser techniques requires accurate conventional spectroscopic data, such as, extra line assignments and mixing coefficients. Knowledge about the lifetime of the excited state is important in gas kinetic studies to set up experiments for determining collision and reaction rates, as well as for modelling media such as terrestrial and planetary atmospheres where chemical processes are interacting with radiation. Lifetimes are very closely connected to the basic properties such as transition moments and their variation with internuclear distance, perturbations, nonradiative decay, predissociations, fluorescence, etc. of molecular states. From a detailed study of perturbations, accurate mixing coefficients and the deperturbed life times of both the perturbed and the perturbing states can be determined.

The spectra of the molecular ion CO^+ are also of considerable importance in astrophysical phenomena. For example, the comet-tail ($A\ ^2\Pi_i$ - $X\ ^2\Sigma^+$) band system of CO^+ was first observed in the tail of comet Morehouse 1908c by Pluvinel and Baldet (1909, 1911); measurements by Erickson et al. (1981) have provided strong evidence of CO^+ in Orion molecular cloud 1; Dixon and Woods (1975) observed CO^+ terrestrially by microwave spectroscopy. The comet-tail system of CO^+ which occurs in the region 3080-8500 Å has applications in the study of radiative heating of the hypersonic fringe of the planet Venus which contains a considerable amount of CO_2. Precise laboratory data on the spectra of CO^+ will be very useful in the study of the spectra resulting from the astrophysical phenomena mentioned above. For these reasons, a systematic study of the comet-tail band system of $^{12}C^{16}O^+$ has been undertaken.

1.4 Present Investigation

One of the aims of the present research project is to record and analyze the spectra of the A $^1\Pi$ - X $^1\Sigma^+$ system of the isotopomers $^{13}C^{16}O$, $^{12}C^{18}O$, and $^{13}C^{18}O$ in the spectral region 1370 -1935 Å under high resolution. The other aim is to study the perturbations present in the spectra and obtain deperturbed molecular constants for not only the A $^1\Pi$ state but also for the perturbing states. The third aim is to calculate the term values of several vibrational levels of A $^1\Pi$ state of $^{13}C^{16}O$, $^{12}C^{18}O$, and $^{13}C^{18}O$. It is also the aim of the present work to obtain accurate molecular constants for the A $^2\Pi_i$ and X $^2\Sigma^+$ states of the molecular ion CO^+ from the high resolution study of its comet-tail (A $^2\Pi_i$ - X $^2\Sigma^+$) system. The anode column of a hollow-cathode discharge tube and a jet discharge apparatus were used to excite the isotopomers $^{13}C^{16}O$, $^{12}C^{18}O$, and $^{13}C^{18}O$. Their emission spectra were photographed on a 10.6 m vacum grating spectrograph at Steacie Institute of Molecular Sciences, Ottawa. The molecular ion $^{12}C^{16}O^+$ was excited in the cathode column of the hollow-cathode discharge tube and its emission spectrum was photographed under medium and high resolutions. The design of the hollow-cathode discharge tube is such that it facilitates the study of both anode and cathode glows independently. The jet discharge over more conventional sources is preferred because the former produces spectra of comparatively low rotational temperature where the low-J lines are clearly identified and free from overlaps. Details of the hollow-cathode discharge tube and jet discharge apparatus, the spectrogaphs used, and the experimental procedures followed are presented in Chapter 2.

The theory of electronic spectra and perturbations pertinent to the present investigation is reviewed in Chapter 3. This chapter also discusses various contributions to the tot¬l molecular Hamiltonian H. The energy matrix and fitting procedure used to obtain deperturbed molecular constants and perturbation parameters are described in this chapter.

Chapters 4 to 8 of this thesis are written in such a way that each chapter constitutes a full paper in a peer-reviewed scientific journal. Chapters 4 and 6 have already appeared in the Journal of Molecular Spectroscopy (Haridass, C., Reddy, S. P., and Le Floch, A. C., *J. Mol. Spectrosc.* **167**, 334 (1994) and *ibid* **167**, 424 (1994)), and Chapter 7 has been published in the Astrophysical Journal (Haridass, C., and Huber, K. P., *Astrophys. J.* **420**, 433 (1994)). The results of Chapters 5 and 8 will soon be communicated to one of the peer-reviewed journals. Because of this, the reader will find the sections on "Introduction" in chapter 4 to 7 to be somewhat repetitive. The author appeals to the examiners and readers of the thesis to keep this in mind.

The fourth positive ($A\ ^1\Pi - X\ ^1\Sigma^+$) system of the carbon monoxide isotopomers $^{12}C^{18}O$ and $^{13}C^{18}O$ excited in the anode column of a hollow-cathode discharge tube, was observed in the spectral region 1710 - 1935 Å for the first time and photographed on a 10.6 m vacuum grating spectrograph at Steacie Institue of Molecular Sciences, National Research Council, Ottawa. The rotational structure of five bands (A,v=1, and 2 and X, v=2 to 6) of the isotopomer $^{12}C^{18}O$ and two bands (A, v=1 and X, v=4 and 5) of $^{13}C^{18}O$ was analyzed. Several perturbations were observed in the $A\ ^1\Pi$ state of both isotopomers.

The observed perturbations are in good agreement with those estimated by theoretical calculations. The effective molecular constants were obtained for the A $^1\Pi$ state as well as for the perturbing states of both isotopomers. Pertubation parameters and mixing coefficients which characterize each perturbation were also derived. The details of these results are presented in Chapter 4.

The vacuum ultraviolet spectra of the A $^1\Pi$ - X $^1\Sigma^+$ system of the isotopomer $^{13}C^{18}O$ generated in emission in a jet discharge occurring in the region 1460 -1670 Å were observed for the first time and photographed under high resolution. The deperturbation analysis of the rotational structure of nineteen bands was carried out. Strong and weak perturbations were observed in seven levels (v′=0, 1, 2, 4, 6, 7,and 9) of the A $^1\Pi$ state. The 1-0 band of the intercombination e $^3\Sigma^-$ - X $^1\Sigma^+$ system was observed because of "intensity borrowing" from the main A - X system. Accurate deperturbed constants for the A $^1\Pi$ state and the perturbing states have been determined. Perturbation parameters and mixing coefficients which characterize each perturbation were also derived. The results of this investigation are presented in Chapter 5.

Using the experimental data of the A $^1\Pi$ - X $^1\Sigma^+$ system of the isotopomers $^{12}C^{18}O$ and $^{13}C^{18}O$ given in Chapter 4, the term values of the A $^1\Pi$, v=1 and 2 levels of $^{12}C^{18}O$ and v=1 level of $^{13}C^{18}O$ were calculated. The term values of the Rydberg states B $^1\Sigma^+$, v=0 and 1, C $^1\Sigma^+$, v=0, and E $^1\Pi$, v=0 were also calculated for these two isotopomers by combining our data of the A-X system and those of the B $^1\Sigma^+$ - A $^1\Pi$, C $^1\Sigma^+$ - A$^1\Pi$, and E $^1\Pi$ - A$^1\Pi$ systems taken from the literature. From the calculated term values, the

molecular constants for the B, C, and E states of $^{12}C^{18}O$ and $^{13}C^{18}O$ were determined. The interaction between the C and E states was taken into account in determining these constants. The details of these results are outlined in Chapter 6.

Twenty three bands of the fourth positive system of $^{13}C^{16}O$ occurring in the region 1370 - 1600 Å were photographed at high resolution in emission from a jet discharge in mixtures of argon and $^{13}CO_2$. The rotational structure of thirteen of these bands was analyzed. The term values for the A $^1\Pi$, v=0 to 9 levels have been calculated. The mixing coefficients of strongly perturbed v=0 and 6 levels have been evaluated. In addition, the ^{13}C isotope shifts have been measured for several multiplets in the spectra of C_I and C_{II}. The results obtained for the A-X system of $^{13}C^{16}O$ isotopomer are presented in Chapter 7.

Following our recent work (Haridass, C., Prasad, C. V. V., and Reddy S. P., *Astrophys. J.* **388**, 669 (1992)), the comet-tail (A $^2\Pi_i$ - X $^2\Sigma^+$) system of $^{12}C^{16}O^+$ occurring in the region 3345 - 8500 Å was reinvestigated. The spin splitting of the rotational levels was observed in all the bands of this system. The observed intensity distribution of the branches of this system is in good agreement with those estimated by theoretical calculations. The data of the rotational lines of ten bands of this system, the microwave data of Bogey et al. (1983) and infrared data of Davies and Rothwell (1985) were analyzed in a global fit using the effective Hamiltonian for the $^2\Pi$ state given by Brown et al. (1979) and the molecular constants were derived for the A $^2\Pi_i$ and X $^2\Sigma^+$ states. The details of the results are given in Chapter 8.

REFERENCES

Allard, F., Scholz, M., and Wehrse, R., *Rev. Mex. Astron. Astrofis.* **23**, 203 (1992).

Anders, E., and Grevesse, *Geochim. Cosmochim. Acta*, **53**, 197 (1989).

Audouze, J., in CNO Isotopes in Astrophysics (Dordrecht: Reidel), 5 (1977).

Ayres, T. R., Moos, H. W., and Linsky, J. L., *Astrophys. J.* **248**, L137 (1981).

Bamford, D. J., Filseth, S. V., Foltz, M. F., Hepburn, J. W., and Moore, C. B., *J. Chem. Phys.* **82**, 3032 (1985).

Bartoe, J. D. F., Brueckner, G. E., Sandlin, G. D., Van Hoosier, M. E., and Jordan, C., *Astrophys. J.* **223**, L51 (1978).

Bogey, M., Demuynck, C., and Destombes, J. L., *J. Chem. Phys.* **79**, 4704 (1983).

Brown, J. M., Colbourn, E. A., Watson, J. K. G., and Wayne, F. D., *J. Mol. Spectrosc.* **74**, 294 (1979).

Cossart, D., and Cossart-Magos, C., *J. Mol. Spectrosc.* **141** 59 (1990).

Davies, P. B., and Rothwell, W. J., *J. Chem. Phys.* **83**, 5450 (1985)

Deslandres, H., C. R. Acad. Sci. (Paris), **106**, 842 (1888).

Dixon, T. A., and Woods, R. C., *Phys. Rev. Lett.* **34**, 61 (1975).

Encrenaz, T., *Rep. Prog. Phys.* **53**, 793 (1990).

Erickson, N. R., Snell, R. L., Loren, R. B., Mundy, L., and Plambeck, R. L., *Astrophys. J.* **245**, L83 (1981).

Farrenq, R., Guelachvilli, G., Sauval, A. J., Grevesse, N., and Farmer, C. B., *J. Mol. Spectrosc.*, **149**, 375 (1991).

Field, R. W., Ph. D thesis, Harvard University (1971).

Field, R. W., Wicke, B. G., Simmons, J. D., and Tilford, S. G., *J. Mol. Spectrosc.* **44**, 383 (1972)

Gero, L., *Z. Phys.* **99**, 52 (1936).

Goldberg, L., Parkinson, W. H., and Reeves, E. M., *Astrophys. J.* **141**, 1293 (1965).

Grevesse, n., Lambert, D. L., Sauval, A. J., van Dishoeck, e. F., Farmer, C. B., and Norton, R. H., *Astronomy and Astrophys.* **242**, 488 (1991).

Hancock, G., and Zacharias, H. *Chem. Phys. Lett.* **82**, 402 (1981)

Hancock, G., and Zacharias, H., "Quantum Electronics and Electro-Optics" (P. L. Knight Ed), 145, Wiley, New York, (1983).

Hanson, M. M., Snow, T. P., and Black, J. H., Astrophys. J, **392**, 571 (1992).

Ho, P., and Smith, A. V., *Chem. Phys. Lett.* **90**, 407 (1982)

Hodgson, R. T., *J. Chem. Phys.* **55**, 5378 (1971).

Huggins, P. J., *Astrophys. J.* **313**, 400 (1987).

Jordan, C., Bartoe, J. D. F., Brueckner, G. E., Nicolas, K. R., Sandlin, G. D., and Van Hoosier, M. E., *Astron. Soc.* **187**, 473 (1979).

Krupenie, P. H., "The Band Spectrum of Carbon Monoxide", Nat. Bur. Stand., NBS 5, Washington, D.C. (1966).

Lambert, D. L., Sheffer, Y., Gilliland, R. L., and Federman, S. R., *Astrophys. J.* **420**, 756 (1994)

Lefbvre-Brion, H., Moser, C. M., and Nesbet, R. K., *J. Mol. Spectrosc.* **13**, 418 (1964).

Le Floch, A. C., Ph. D. thesis, Univ. Paris-Sud (1989).

Le Floch, A. C., Rostas, J., and Rostas, F., *Chem. Phys* 142, 261 (1990).

Le Floch, A. C., Launay, F., Rostas, J., Field, R. W., Brown, C. M., and Yoshino, K., *J. Mol. Spectrosc.* **121**, 337 (1987).

Marchand, J., D'Incan, J., and Janin, J., *Spectrochim. Acta* **25A**, 605 (1967).

Marcis, C., and Pertopoulos, B., "7th European Regional Astronomy Meeting, Florence, Dec. 1983."

Meikle, W. P. S., Allen, D. A., Spyromillo, J., and Varani, G. F., *Mon. Not. R. astron. Soc.* **238**, 193 (1989).

Mitchell, G. F., Maillard, J.-P., Allen, M., Beer, R., and Belcourt, K., *Astrophys. J.* **363**, 573 (1990).

Mulliken, R. S., 1932. Rev. Mod. Phys. **4**, 1.

Onaka, R., *J. Chem. Phys.* **26**, 1763 (1957)

Pluvinel, A. B., and Baldet, F., *C. R. Acad. Sci.* Paris, **148**, 759 (1909).

Pluvinel, A. B., and Baldet, F., *Astrophys. J.* **34**, 89 (1911).

Porter, J. R., Tilford, S. G., and Widing, K. G., *Astrophys. J.* **147**, 172 (1967).

Sheffer, Y., Federmann, S. R., Lambert, D. L., and Cardelli, J. A., *Astrophys. J.* **397**, 482 (1992).

Simmons, J. D., Bass, A. M., and Tilford, S. G., *Astrophys. J.* **155**, 345 (1969).

Smith, A. M., and Stecher, T. P., *Astrophys. J.* **164**, L43 (1971).

Tilford, S. G., and Simmons, J. D., *J. Phys. Chem. Ref. Data* **1**, 147 (1972).

Tsuji, T., *Annu. Rev. Astron. Astrophys.* **24**, 89 (1986).

Vallee, F., Wallace, S. C., and Lukasik, J., *Opt. Commun.* **42**, 148 (1982).

Wannier, P. G., Penzias, A. A., and Jenkins, E. B., 1982, ApJ, **254**, 100.

Welty, D. E., and Fowler, J. R., *Astrophys. J.* **393**, 193 (1992).

Wiedemann, G., and Ayres, T. R., *Astrophys. J.* **366**, 277 (1991).

Wilson, R. W., Jefferts, K. B., and Penzias, A. A., *Astrophys. J.* **162**, L43 (1970).

Wolk, G. L., and Rich, J. W., *J. Chem. Phys.* **79**, 12 (1983).

CHAPTER 2

EXPERIMENTAL TECHNIQUES

The Fourth Positive ($A^1\Pi$ - $X^1\Sigma^+$) system of the carbon monoxide isotopomers $^{13}C^{16}O$, $^{12}C^{18}O$ and $^{13}C^{18}O$ was excited in the anode column of a hollow-cathode discharge tube and in a jet discharge apparatus and photographed on a 10.6 m vacuum spectrograph. The comet-tail ($A^2\Pi_i$ - $X^2\Sigma^+$) system of the carbon monoxide ion $^{12}C^{16}O^+$ was excited in the cathode column of the hollow-cathode discharge tube and was photographed on medium and high resolution optical spectrographs. In this chapter, the sources of molecular excitation, their mechanisms, and the spectrographs used are described. The experimental procedure and the measurement of the spectra are also briefly presented here.

2.1 Sources of Molecular Excitation

a) The hollow-cathode discharge tube

A schematic diagram of the hollow-cathode discharge tube and the associated gas-handling system is shown in Fig. 2.1. The main features of this discharge tube are a copper hollow cathode (H), a Kovar-Pyrex seal (K), and Pyrex glass body (PG), a tungsten anode (T), a cathode window (W_C) and an anode window (W_A). The hollow-cathode, 75 mm long, 17 mm in outer diameter and 1 mm in wall thickness, was silver-soldered to the Kovar tube 19 mm in inner diameter of the Kovar-Pyrex seal. The Pyrex section of this seal was joined to the Pyrex glass body, 145 mm long and 50 mm in outer

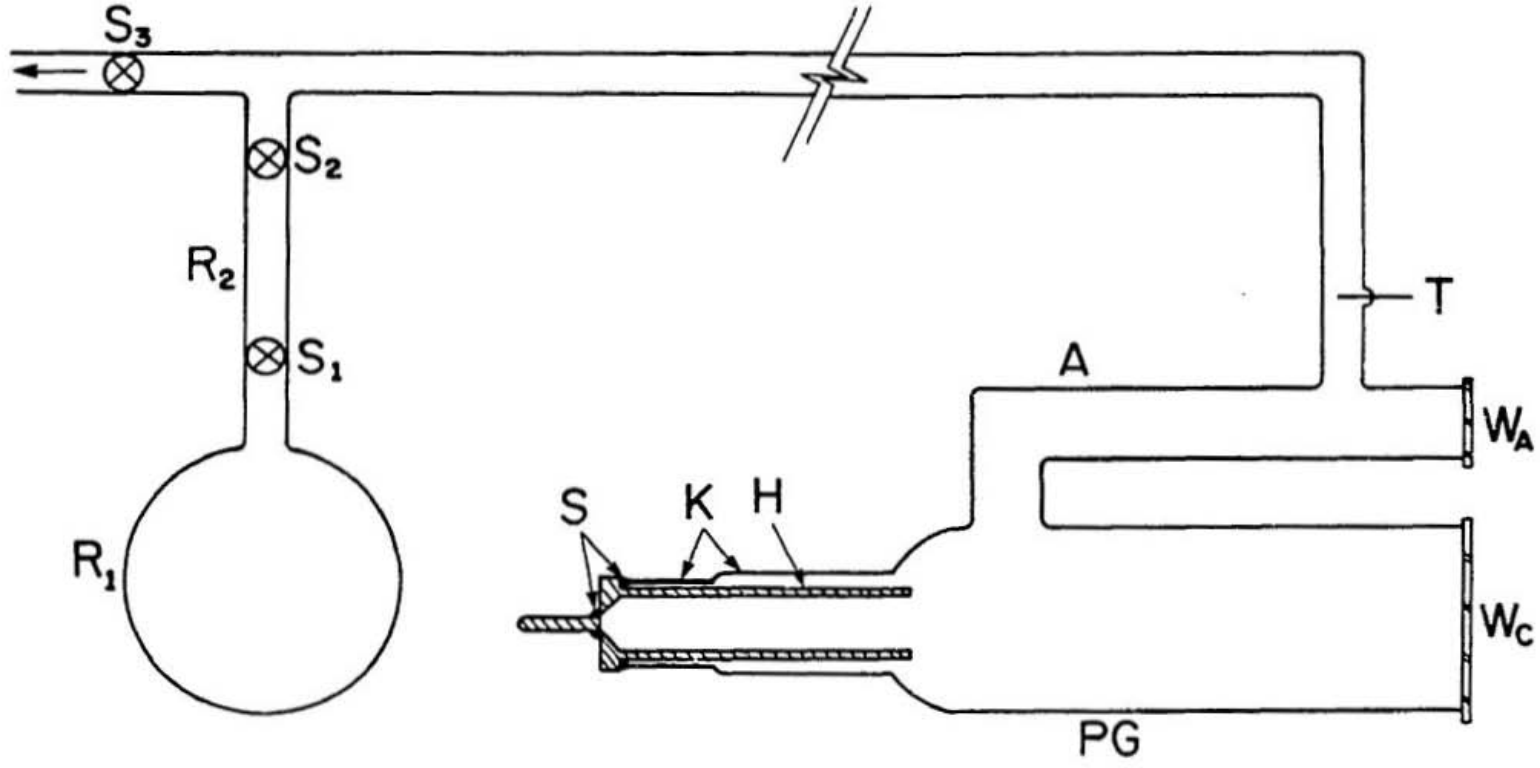

Figure 2.1 A Schematic diagram of the hollow-cathode discharge tube and the asscociated gas handling system. R_1 and R_2: reservoirs; S_1, S_2, and S_3: stop cocks; S: silver soldering; K: Kovar-Pyrex seal; H: copper hollow-cathode; PG: Pyrex glass body; A: anode branch; W_A and W_C: quartz windows; T: tungsten anode.

diameter. The anode arm (A), 20 mm in outer diameter, branches off from the main body of the discharge tube. The tungsten anode was fused into the side branch of the anode arm. The S1-UV quartz windows (W_A) and (W_C), each 3.0 mm thick supplied by Esco Products Inc., were attached to the ground end-surfaces of the anode and cathode branches of the discharge tube with Torr Seal (a low vapour pressure resin supplied by Varian Associates, Inc.). In Fig. 2.1, R_1 is the primary reservoir of the experimental gas ($^{12}C^{16}O$, $^{12}C^{18}O$, or $^{13}C^{18}O$) and R_2 is the corresponding secondary reservoir.

The main advanta$_{\text{ge}}$ of the hollow-cathode discharge tube is the provision of separate columns for anode and cathode, which facilitate photographing the two glows independently. Reddy and Prasad (1989) have demonstrated that in a hollow-cathode the cathode glow is a rich source of positive molecular ions (e.g., CO^+, N^+_2, CO^+_2) and the anode column consists exclusively of neutral (e.g., CO, N_2, NO, etc.) molecules. Moreover, spectral broadenings such as Doppler, pressure, and Stark broadenings are minimized in a hollow-cathode excitation unlike the excitations in straight d.c. arcs and conventional electrodeless discharges. In the present study the Fourth Positive System of $^{12}C^{18}O$ and $^{13}C^{18}O$ was excited in the anode column, and the comet-tail system of $^{12}C^{16}O^+$ was excited in the cathode column, of this discharge tube. An applied d.c. voltage of 1.1 kV from a power supply unit rated at 2 kV and 0.25 A was used to maintain the CO^+ discharge in the cathode column. Under normal operating conditions, an applied d.c. voltage of 1.1 kV gave a current of 60-65 mA and the pressure inside the discharge was approximately 0.8 Torr. A steady CO discharge was maintained with a 1.3

kV d.c. voltage and ~ 90 mA current.

b) Jet discharge apparatus

The experimental arrangement of the jet discharge apparatus, used in the excitation of the A-X spectra of $^{13}C^{16}O$ and $^{13}C^{18}O$ is shown in Fig. 2.2. A mixture of argon and the experimental gas expands in one dimension from a high pressure reservoir through a slit nozzle, 5 mm long and ~ 0.020 mm wide into the low pressure region from where it is removed by an Edwards EH500/E2M80 pump combination having a capacity of 140 litres/s. The slit (S), formed by two knife edges of X-Acto blades bevelled on one side, is isolated not only from the tungsten anode (T) situated at the center of the Pyrex tube, connecting with the slit-nozzle assembly, but also from the grounded booster and the rotary pump combination (not shown in figure) acting as the cathode for the d.c. discharge. The tip of the anode which is at 1 mm upstream from the slit-nozzle is carefully centered both longitudinally and laterally. A voltage of 600 V is applied to the tungsten anode to maintain a d.c. discharge at a current of ~ 60 mA. With the discharge running, a thin sheet of luminous gas expands from the tip of the anode in a plane normal to the slit direction. The direction of observation is parallel to the slit direction and is through the thin emission zone at approximately 2 mm downstream from the nozzle orifice. Under normal operating conditions, the pressure in the reservoir is ~ 300 Torr. Light emitted from the jet discharge is collected by a lithium fluoride spherical lens (L_1) and subsequently predispersed and refocussed onto the slit (S_1) of the spectrograph by LiF

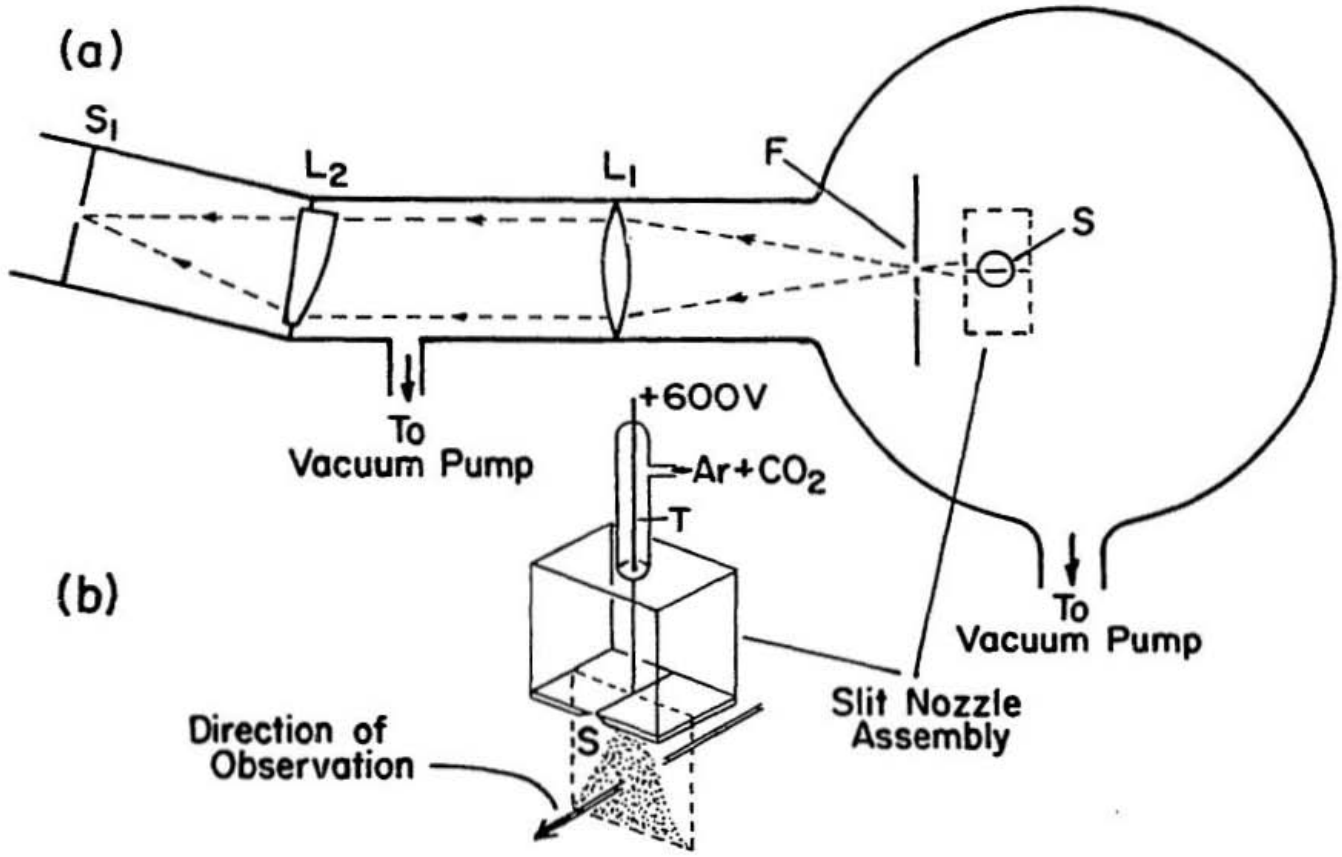

Figure 2.2 a) A Schematic diagram of the cross-sectional view of the jet discharge arrangement. S: slit-nozzle [see (b)]; F: fore slit; L_1: lithium fluoride spherical lens; L_2: quartz or lithium flouride prism/cylinder combination acting as a predisperser; S_1: slit of the spectrograph.
b) Slit-nozzle arrangment. S: slit (length: 5 mm and width: 20 μm); T: tungsten anode.

prism/cylinder combination (L_2). The pump and the nozzle assembly could be rotated around a pivot underneath the predispersor (L_2) making it possible to select and isolate a narrow wavelength region in the higher orders of the 10.6 m concave grating spectrograph. The preference of a jet discharge over more conventional sources stems from the fact that the former, in contrast to the latter, produces spectra of comparatively low rotational temperature where low-J lines are clearly identified and are relatively free from overlaps by the returning R and P branches of strongly degraded bands. With the advent of the supersonic jet expansion technique very low rotational temperatures have been achieved. For example, Liverman et al. (1979) using a pulsed supersonic free jet have observed the lowest rotational temperature of 0.17 K from the fluorescence excitation spectrum of oxalyl fluoride ($C_2F_2O_2$). Smalley et al. (1974, 1975) from the study of supersonic expansion of NO_2 seeded in Ar achieved a rotational temperature of 3 K. In all the experiments mentioned above, the chemical intermediates have been produced either by electron bombardment or laser photolysis. Obi et al. (1983) have demonstrated that a laser is not necessary for the photochemical production of free radicals in a jet. The free radical HNO was formed by irradiating a mixture of H_2, NO, Ar and Hg by a simple Hg lamp. A rotational temperature of approximately 16 K was achieved for cooled HNO from the laser-induced fluorescence. Droege and Engelking (1983) showed the presence of cooled (rotational temperature about 11 K) OH radical from the emission of a corona discharge in a mixture of H_2O and He in the downstream from the nozzle. Huber and Sears (1985) and Huber and Vervloet (1992) have obtained

low rotational temperatures between 20-30 K for the emission spectra of NO and N_2 in the jet expansion. In the present work, the rotational temperatures are found to be considerably higher and are of the order of 200 K to 300 K, where the emitting species is the product of reactions involving larger parent molecules. Veeken and Reuss (1985) studied the infrared laser absorption of CO_2 clusters by a jet discharge using both the slit and pinhole nozzles. The conclusions arrived at from their study are: 1) the use of a slit nozzle expansion yields a much higher spectral resolution (a factor of 10) than from a circular nozzle expansion with the same gas flow. 2) From the observed rotational temperatures it is found that a slit source with a width D produced more clusters than a circular source with a diameter D at the same stagnation pressure. 3) The slit nozzle produces line shapes with a sharp maximum in contrast to the circular nozzle which produces a broad maximum. The molecules emerging from a pinhole nozzle may have substantial velocity components along the line of observation. Huber and Sears (1985) and Huber and Vervloet (1992) using a pinhole nozzle in their jet discharge apparatus have documented the resulting Doppler effects of line shapes and line positions for spectra in the visible and near infrared regions. In the vacuum ultraviolet region, the line shapes and positions would be proportionately larger and might effect the peak positions of the individual lines by as much as 0.20 cm^{-1}, or by more than 5 times the expected accuracy of our measurements (0.03 cm^{-1}). In order to avoid these complications, the two dimensional jet expansion from a pinhole nozzle was replaced by a one-dimensional expansion from a slit nozzle, following the recommendations by Veeken and Reuss

(1985). The slit construction is a simplified version of the design given by Comer and Foster (1993).

2.2 Excitation Mechanisms

a) The hollow-cathode discharge

When a d.c. voltage is applied across the electrodes of a hollow-cathode discharge tube, electrons released from the cathode accelerate through the tube. The accelerated electrons collide with the molecules or atoms of the experimental gas and excite them to different higher atomic states or molecular rotational, vibrational and electronic states. Since these excited states are unstable, the atoms and molecules will relax to the lower energy states through the emission of electromagnetic radiation. The emission is maintained as long as the discharge tube is subjected to the electric field. The free electrons released from the cathode acquire sufficient kinetic energy to produce positive moleuclar ions in the collision process. The ions concentrate around the cathode and the excited neutral molecules spread out into the anode branch of the discharge tube.

b) The jet discharge

When a mixture of an experimental gas and a large quantity of a monatomic carrier gas such as argon or helium at high pressure is ejected into an evacuated chamber through a small nozzle (or orifice), under conditions where the flow of the mixture is many times faster than a sound wave, a jet of the mixture is pushed out of the nozzle.

In the absence of viscous forces, heat conduction, and shock waves, the expansion is isentropic, and an isentropically expanding gas must cool. The cooling of the gas implies that the expansion converts random thermal motion in the static gas into directed motion in the expanding gas. This free jet expansion is illustrated in Fig. 2.3. In this figure, the conditions down stream from the nozzle are indicated for various multiplets (X/D) of the nozzle diameter D (Miller 1984), where X is the distance from the nozzle and D is the diameter of the nozzle It is assumed that the pressure behind the nozzle is 10 atmospheres of helium at room temperature. The arrows indicate the conversion of random velocities of the gas behind the nozzle to uniform velocity in front of it. Thus the free jet expansion "monochromatizes" the gas velocity. The Mach number, M which is the ratio of the flow velocity to the local speed of the sound increases as the distance (X/D) increases. However, the value of M will not increase indefinitely as a function of X/D and the decreasing frequency of collisions causes M to approach a limiting value. The most important physical property is the width of the velocity distribution which is a direct measure of the translational temperature of the gas. For X/D = 10, this width corresponds to a temperature of less than 5 K and subsequently drops to 0.4 K. Under more extreme conditions the translational temperature can approach 0.01 K. These low temperatures characterize the energies of the collisions that occur in the expanding gas. As a result of these collisions, the internal degrees of freedom of the molecules, i.e., the vibrational and rotational energy levels will relax toward these same low temperatures. The density of the gas and the probability of collisions decrease as the expansion

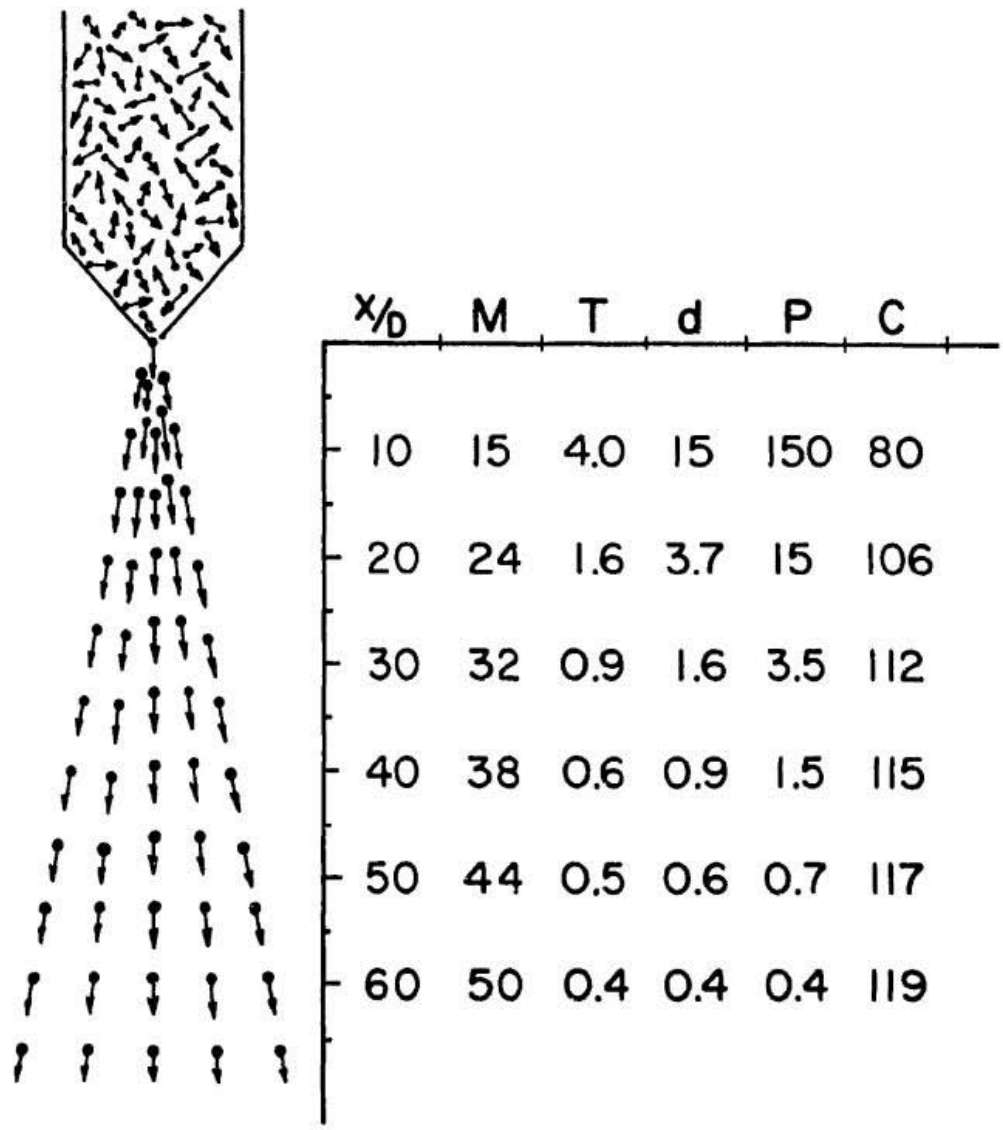

Figure 2.3 A Schematic diagram of a free jet expansion. The scale refers to measuring distance (X/D) downstream in units of the nozzle diameter (D). M: Mach number; T: temperature in Kelvin, d: density (in torr at S.T.P); P: pressure in millitorr; C: number of collisions between X/D = 5 and the indicated point. (adopted from Miller 1984).

proceeds. In supersonic and static gas expansions, condensation is a slow process. Cooling requires only two body collisions, while condensation requires three body or higher order collisions to form nuclei around which condensation takes place. A common method for limiting condensation is to use a large amount of carrier gas such as helium or argon and small quantity of the experimental molecular gas. In the supersonic free jet expansion, most of the collisions will be between the carrier gas atoms. When a rare gas is used as carrier gas the intermolecular forces in the mixed-gas expansion are on average much weaker than in a pure molecular expansion, thus greatly reducing condensation.

2.3 Spectrographs

a) The 3.4 m Jarrell-Ash Ebert grating spectrograph

A schematic diagram of the optical layout of this spectrograph is shown in Fig. 2.4. In this instrument light from the source (LS) is incident directly upon the upper section of the concave mirror (M) (with radius of curvature 6.655 m, diameter 0.406 m, and numerical aperture f/35) after passing through two quartz cylindrical lenses (L_1) (a collimating lens, 0.100 m in focal length and 0.030 m in diameter) and (L_2) (a condensing lens 0.450 m in focal length and 0.030 m in diameter) and a slit (S) (width 30 μm). The concave mirror collimates the light onto the grating (G). The dispersed light from the grating is then focused onto the photographic plate (P) by the lower section of the concave mirror. The plate holder which holds two 5.08 cm x 25.45 cm photographic plates can be tilted on its vertical axis to obtain the best focus for a fixed slit position.

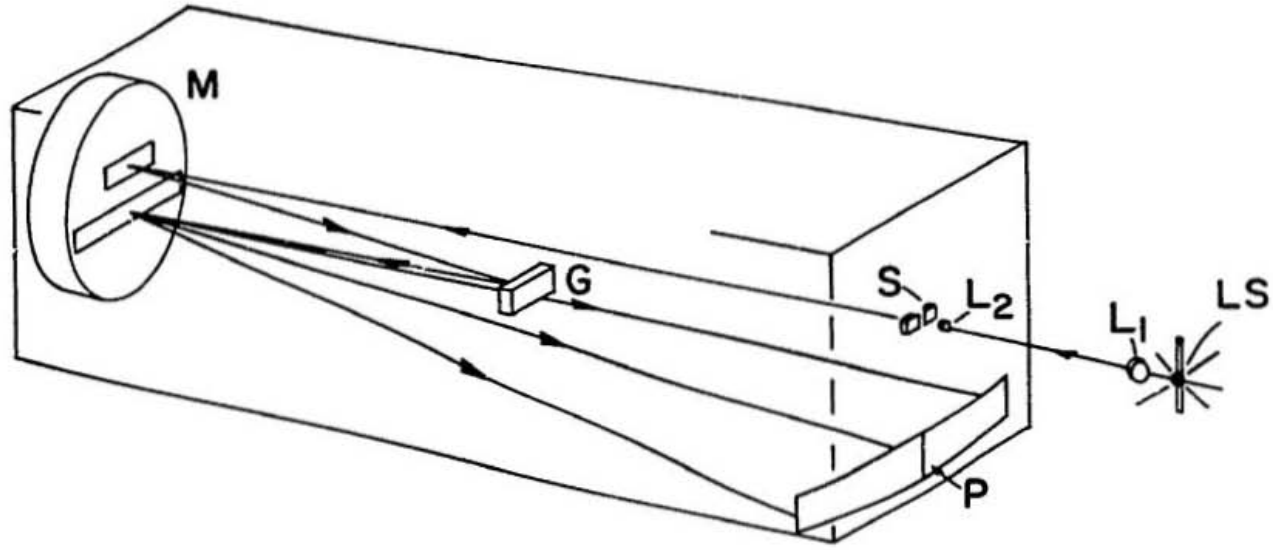

Figure 2.4 Optical layout of the 3.4 m Jarrell - Ash Ebert grating spectrograph with a polychromatic light beam. LS: light source; L_1: quartz cylindrical source lens; L_2: quartz cylindrical slit lens; S: slit of the spectrograph; M: spherical collimating mirror; G: grating; and P: photographic plate.

The tilt of the plate holder is found to have a linear dependence on the grating angle.

A Bausch and Lomb plane grating with 1200 grooves/mm and blazed at 1.4 μm and an MIT echelle grating (300 grooves/mm blazed at 5.7 μm) are available for this spectrograph. The ruled area of each of these gratings has a width of 186 mm and groove length of 63 mm. In the present work the Bausch and Lomb grating was used in the second, third and fourth orders. The measured reciprocal dispersions of the spectra are 0.34 Å/mm at 3450 Å in the fourth order and 0.28 Å/mm at 5100 Å in the second order.

b) 10.6 m vacuum grating spectrograph

The general layout of the spectrograph is shown in Fig. 2.5 (Douglas and Potter (1962)). Light from the source after passing through a lithium fluoride prism and cylindrical lens combination (not shown in this figure) falls on the slit (E) which can be adjusted in width and length without breaking the vacuum. This light can be blocked by a shutter which is a small mirror oriented in such a way that when it blocks the light from the source, it reflects the light from the reference source (an iron hollow-cathode). Light after passing through the slit is incident on the concave grating (A) (radius of curvature 10.685 m, ruled area 198 mm x 100 mm), mounted on a turn table (B) which can slide along the rails (C) directed toward the slit. The dispersed light from the grating is then focused onto the photographic plate which is inside a plate holder mounted on a rigid aluminum-alloy beam (F). The plate holder has a length of 0.93 m and holds two plates, each of size 5 cm x 45 cm. A small side tank (H) (0.15 m in diameter and 1.00 m long)

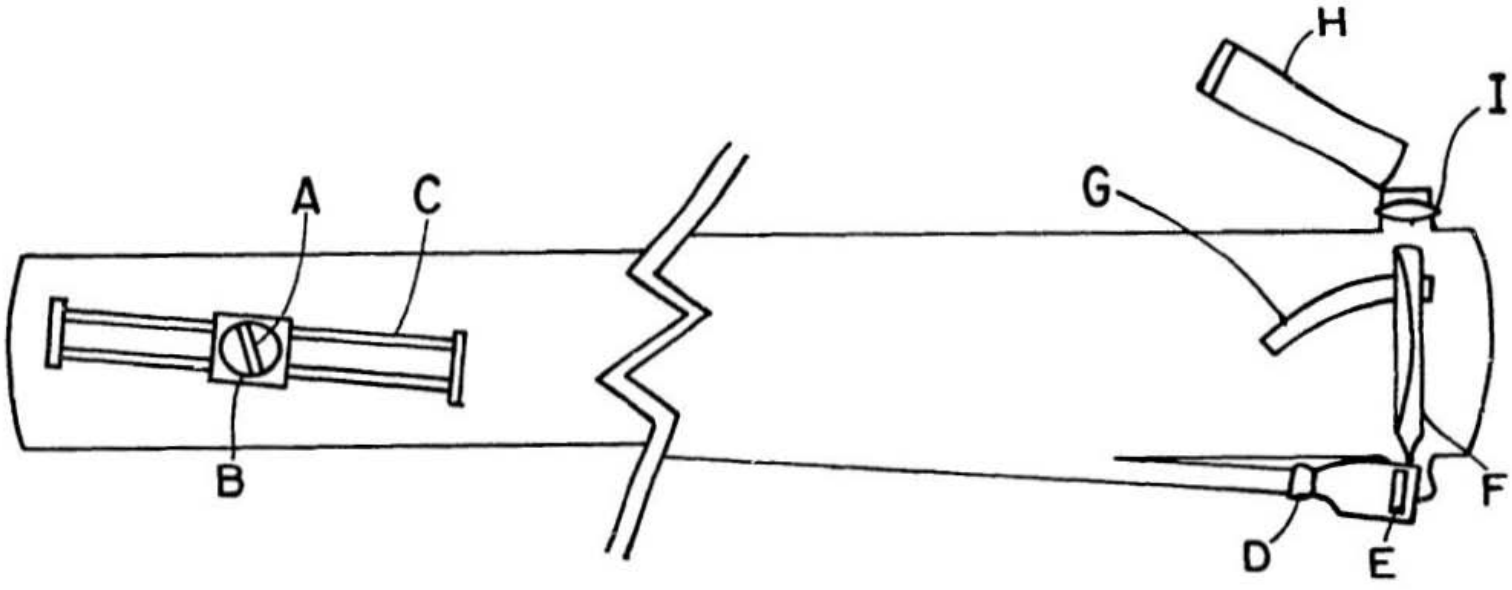

Figure 2.5 General layout of the 10.6 m vacuum grating spectrograph. A: concave diffraction grating; B: turntable for the diffraction grating; C: steel rails; D: 10-cm gate valve; E: slit of the spectrograph; F: rigid aluminum - alloy beam; G: curved metal beam; H: small vacuum tank (for removing the plate holder from the main vacuum tank); I: 15 cm gate valve. (adopted from Douglas and Potter, 1962).

is joined to the main vacuum tank and it allows introduction of the photographic plate or removal from the vacuum tank without breaking the vacuum. A gate valve (I) can close this opening between the main vacuum system and the small tank. In order to remove the plate holder from the spectrograph, the small tank is first swung into position directly adjacent to the gate valve. The small chamber is evacuated by a mechanical pump and the gate valve is opened. By means of a rack and pinion (not shown in the diagram), the plate holder is driven on small wheels to the small tank. After closing the gate valve the air is admitted into the small chamber.

The spectrograph is evacuated by two parallel pumping systems. The larger system consists of Edwards 1500 liters/s oil diffusion pump followed by a 52 litre/s Kinney mechanical pump. Pumping for at least twelve hours gives good vacuum when the initial pressure of the interior is one atmospheric. After achieving good vacuum the larger system is shut off and the tank is pumped continuously by a smaller system consisting of National Research Corporation fractionating pump followed by a small booster and a 1 litre/s Kinney mechanical pump. The spectrograph equipped with a normal incidence concave grating with 600 grooves/mm and blazed at 12,000 Å was used in the seventh and eighth orders in the present work.

2.4 Experimental Procedure

Carbon dioxide ($^{13}C^{16}O_2$) gas with a purity of 99.1 atom % of ^{13}C, and an impurity of 5.1 atom % of ^{18}O supplied by Matheson Gas Products was used to study the fourth

positive ($A\ ^1\Pi - X\ ^1\Sigma^+$) system of $^{13}C^{16}O$. The $^{12}C^{18}O$ gas with a purity of 97.6% of ^{18}O and the $^{13}C^{18}O$ gas with specified purities of 98% of ^{13}C and 95.7% of ^{18}O, both supplied by Merck Sharpe & Dohme Canada Ltd. were used for the study of the A-X system excited in the anode column of the hollow cathode discharge tube. For the study of the same system of the $^{13}C^{18}O$ isotopomer in the jet discharge, the $^{13}C^{18}O_2$ gas having a purity of 99.1 atom % of ^{13}C, and 99.9 atom % of ^{18}O supplied by Isotech, Ohio, was used.

The discharge tube and the secondary reservoir R_2 in the gas-handling system (see Fig. 2) were thoroughly evacuated. A small quantity of the experimental gas ($^{12}C^{16}O$, $^{12}C^{18}O$ or $^{13}C^{18}O$) from the primary reservoir R_1 was admitted into R_2 by opening the stop cock S_1. Direct-current voltages of 1100 V (for CO^+) and 1300 V (for $^{12}C^{18}O$ and $^{13}C^{18}O$) were applied between the electrodes of the discharge tube. The gas from R_2 was then admitted into the discharge tube through stop cock S_2 and the discharge was initiated with a tesla coil. In the present work, the experiment was carried out under stagnant conditions of the gas. The pressure of the gas inside the discharge tube was regulated until a bright, stable characteristic discharge was maintained. To maintain a steady discharge with a characteristic glow, it was necessary to reevacuate the discharge tube and admit a fresh sample of the gas intermittently.

The emission spectra of CO^+ in the region 3000-8000 Å was photographed under medium dispersion of the Bausch and Lomb spectrograph and under high resolution of this instrument as well as on the Jarrell-Ash spectrograph. The slit width was maintained at 0.020 mm for the former and 0.030 mm for the latter. Kodak SWR, Spectrum

Analysis No.1, 103 a-O, 103-F, and 1-N plates were used to record the spectra in different spectral regions. Corning and Hoya glass filters were used to eliminate overlapping orders of the spectra. Exposure times ranged from 1 min to 12 hrs depending on the intensity of the band, sensitivity of the photographic plates, and the transmittance of the filters. The photographic plates were developed in Kodak developer D-19 at room temperature for about 4 minutes and were then fixed in Kodak fixer.

The $A^1\Pi$ - $X^1\Sigma^+$ system of the carbon monoxide isotopomers $^{12}C^{18}O$ and $^{13}C^{18}O$ excited in the anode column of a hollow cathode discharge tube was recorded in the spectral region 1710-1935 Å on the 10.6 m vacuum grating spectrograph. For the jet emission experiment on this system of $^{13}C^{16}O$ and $^{13}C^{18}O$, argon seeded with $^{13}C^{16}O_2$ and $^{13}C^{18}O_2$ respectively was expanded from a high pressure reservoir through a slit nozzle 5 mm long and approximately 0.020 mm wide into the low pressure region from where it was removed by a diffusion pump having a capacity of 140 litres/s. A d.c. voltage of 600 V applied to the anode was sufficient to maintain a steady jet discharge at a current of 60 mA. The emission spectra of $^{13}C^{16}O$ in the region 1370-1600 Å and $^{13}C^{18}O$ in the region 1460-1670 Å under high resolution were photographed on the 10.6 m vacuum spectrograph using the slit width of 0.020 mm. The Overlapping orders of the spectra were eliminated by using a lithium fluoride prism/cylinder combination. Exposure times were ~ 3 hr for each of the $^{12}C^{18}O$ and $^{13}C^{18}O$ spectra with the hollow-cathode excitation and from 10 to 90 min for the spectra of $^{13}C^{16}O$ and $^{13}C^{18}O$ with the jet excitation method. The spectra were recorded on Kodak SWR plates.

2.5 Measurement of Spectra

Two different types of measuring devices have been used in the present work. First a linear comparator supplied by the Gaertner Optical Company, Chicago, was used to measure spectra of CO^+, $^{12}C^{18}O$ and $^{13}C^{18}O$. The least count of the instrument is 1 μm, but the readings can be estimated to an accuracy of 0.2 μm. The Following procedure was used to calculate the vacuum wavenumbers of the rotational lines photographed in the Jarrell-Ash Ebert grating spectrograph. The positions of the band heads, rotational lines, and the standard Fe-Ne lines were measured and their comparator readings d were recorded. The air wavelength λ_{air} of the standard Fe-Ne lines taken from Crosswhite (1975) and their comparator readings were fitted to a least-squares polynomial:

$$\lambda_{air} = \sum_{i=0} a_i (d-d_0)^i \ , \qquad [2.1]$$

where d_0 is the comparator reading of the first standard line and the a_i are the least-squares coefficients. In most of the cases a second degree polynomial fit was found to be adequate and gave standard deviations of 0.03 Å and 0.003 Å for the medium and high resolution spectra respectively. Using the coefficients a_i, the wavelengths in air of the band heads and the rotational lines were calculated from Eq. [2.1]. They were then converted to vacuum wavenumbers ν (cm^{-1}) by using Edlen's formula (1953) for the refractive index n for air,

$$n = 1 + 6432.8 \times 10^{-8} + \frac{2942810}{146 \times 10^8 - \nu^2} + \frac{25540}{41 \times 10^8 - \nu^2} \ , \qquad [2.2]$$

where $\nu = \frac{10^8}{n \times \lambda_{air}}$, ($\lambda_{air}$ in Å).

For the spectra photographed on the vacuum grating spectrograph and measured on the Gaertner comparator, the vacuum wavenumbers of the rotational lines were calculated by recording the comparator readings d of the rotational lines and the standard Fe-Ne lines. The vacuum wavelength λ_{vac} of the standard Fe-Ne lines taken from Crosswhite (1975) and their comparator readings were fitted to Eq. [2.1]. A second degree polynomial fit was found to be adequate and gave a standard deviation of 0.001 Å for the high resolution spectra. Using the coefficients a_i, the vacuum wavenumbers ($\nu = 1/\lambda_{vac}$ in cm^{-1}) were calculated from Eq. [2.1]

The second instrument is a semiautomatic measuring device at the National Research Council Laboratory and was used to measure the A-X system of $^{13}C^{16}O$ and $^{13}C^{18}O$ photographed on the 10.6 m vacuum spectrograph. In this device the measuring microscope is replaced by a photoelectric scanning device which displays line contours on an oscilloscope screen. The comparator readings are automated with electronic devices and the results are recorded on a floppy disk. The positions of the rotational lines and the standard Fe-Ne lines were measured and their comparator readings d were recorded. Three random vacuum wavelengths λ_{vac} of the standard Fe-Ne lines taken from Crosswhite (1975) were used to obtain the coefficients a_i of the polynomial in Eq.[2.1]. The numerical calculations were performed by a personal computer. In most cases a third

or fourth order polynomial fit was found to be adequate. The standard deviations were found to be 0.0015 to 0.0030 Å for high resolution spectra. The personal computer then calculates the vacuum wavenumbers ($\nu = 1/\lambda_{vac}$) of the rotational lines and plots the spectra.

REFERENCES

Comer, K. R., and Foster, S. C., *Chem. Phys. Lett.* **202**, 216 (1993).

Crosswhite, H. M., *J. Res. Natl. Bur. Stand.* **79 A**, 17 (1975).

Douglas, A. E., and Potter, J. G., *Appl. Optics* **1**, 727 (1962).

Droege, A. T., and Engelking, p. C., *Chem. Phys. Lett.* **96**, 316 (1983).

Edlen, B., *J. Opt. Soc. Amer.* **43**, 339 (1953).

Huber, K. P., and Sears, T. J., *Chem. Phys. Lett.* **113**, 129 (1985).

Huber, k. p., and Vervloet, M., *J. Mol. Spectrosc.* **153**, 17 (1992).

Liverman, M. G., Beck, S. M., Monts, D. L., and Smalley, R. E., *J. Chem. Phys.* **70**, 192 (1979).

Miller, T. A., *Science* **223**, 545 (1984).

Obi, K., Matsumi, Y., Takeda, Y., Mayama, S., Watanabe, H., and Tsuchiya, S., *Chem. Phys. Lett.* **95**, 520 (1983).

Reddy, S. P., and Prasad, C. V. V., *J. Phys. E.* **22**, 306 (1989).

Smalley, R. E., Ramakrishna, B. L., Levy, D. H., and Wharton, L., *J. Chem. Phys.* **61**, 4363 (1974).

Smalley, R. E., Wharton, L., and Levy, D. H., *J. Chem. Phys.* **63**, 4977 (1975).

CHAPTER 3

THEORY OF THE ELECTRONIC SPECTRA AND PERTURBATIONS

The theory of the electronic spectra and perturbations of diatomic molecules relevant to the present work is outlined in this chapter. For a detailed discussion of this topic, the reader is referred to Mullikan (1931, 1932), Hougen (1970), Lefebvre-Brion and Field (1986), and Herzberg (1991).

3.1 Vibrational and Rotational Structures of Electronic Band Systems

(i) Electronic and vibrational terms

Under the Born-Oppenheimer approximation, with the exclusion of translational and nuclear spin energies, the total energy E (in ergs) of a diatomic molecule is represented as the sum of its electronic energy E_e, vibrational energy E_v, and rotational energy E_r:

$$E = E_e + E_v + E_r. \qquad [3.1]$$

The term value T (in cm^{-1}) of an energy level is given by

$$T = E/hc = T_e + G(v) + F_v(J), \qquad [3.2]$$

where v and J are the vibrational and rotational quantum numbers, respectively, and $T_e = E_e/hc$, $G(v) = E_v/hc$ and $F_v(J) = E_r/hc$ are the electronic, vibrational and rotational terms, respectively. The wavenumber v (in cm^{-1}) of a spectral line corresponding to a transition between the rotational levels of an upper (T′) and a lower (T″) electronic state is given by

$$\begin{aligned}\nu &= T' - T'' \\ &= (T_e' - T_e'') + [G'(v') - G''(v'')] + [F_v'(J') - F_v''(J'')] \\ &= \nu_e + \nu_v + \nu_r \, . \end{aligned} \qquad [3.3]$$

For a given electronic transition $\nu_e = T_e' - T_e''$ is the system origin and $\nu_e + \nu_v = \nu_0$ is the band origin, where $\nu_v = G'(v') - G''(v'')$, $\nu_r = F_v'(J') - F_v''(J'')$. In the first approximation, the electronic terms T_e for different multiplet components of an electronic state can be expressed as

$$T_e = T_0 + A\Lambda\Sigma_s, \qquad [3.4]$$

where T_0 is the electronic term neglecting electron spin, and A is the spin orbit coupling constant. The quantum number Λ corresponds to the angular momentum Λ which is the component along the internuclear axis of the electron orbital angular momentum **L**. Similarly, Σ_s corresponds to the projection Σ_s of the electron spin angular momentum $\vec{S}$ along the internuclear axis. The electronic states are designated as Σ, Π, Δ, ϕ, ..., corresponding to Λ = 0, 1, 2, 3, ..., respectively. The Λ = 0 (Σ) electronic states are designated as Σ^+ and Σ^- depending on whether the electronic wavefunction ψ_e remains unchanged or changes sign upon reflection through any plane containing the internuclear axis. The number of components of **S** projected along the internuclear axis is referred to as multiplicity of the state and is given by 2S + 1, where S is the total electron spin angular momentum quantum number. For all the singlet electronic states, S = 0. An electronic state is referred to as "regular" or "inverted" if the spin-orbit coupling constant A is positive or negative respectively. The vibrational term G(v) of an electronic state is given by

$$G(v) = \omega_e(v + 1/2) - \omega_e x_e(v + 1/2)^2 + \omega_e y_e(v+1/2)^3 + \ldots , \qquad [3.5]$$

where ω_e is the vibrational constant and $\omega_e x_e$, $\omega_e y_e$, etc., are the anharmonic constants.

(ii) Vibrational structure of the electronic spectra and isotope shifts

The wavenumber $\nu_{v'v''}$ of a vibrational transition neglecting the rotational contribution is given by

$$\begin{aligned}\nu_{v'v''} &= \nu_e + G'(v') - G''(v'') \\ &= \nu_e + \omega_e'(v'+1/2) - \omega_e' x_e'(v'+1/2)^2 + \omega_e' y_e'(v'+1/2)^3 + \ldots \\ &\quad -\omega_e''(v''+1/2) + \omega_e'' x_e''(v''+1/2)^2 - \omega_e y_e''(v''+1/2)^3 - \ldots \end{aligned} \qquad [3.6]$$

The system origin ν_e and the vibrational constants ω_e, $\omega_e x_e$ and $\omega_e y_e$ for both upper (′) and lower (″) levels can be obtained from the least-squares fit of the band origins ν_0 estimated from the rotational analysis of many bands of an electronic band system. In the absence of such an analysis, the band heads may be used to estimate the vibrational constants but these are not as accurate as the ones obtained from the rotational analysis.

The relation between the vibrational constants ω_e', $\omega_e' x_e'$, and $\omega_e' y_e'$ of an isotopomer and the corresponding constants ω_e, $\omega_e x_e$, and $\omega_e y_e$ of an ordinary molecule are given by the following expressions:

$$\omega_e' = \rho\omega_e, \quad \omega_e' x_e' = \rho^2 \omega_e x_e, \quad \text{and} \quad \omega_e' y_e' = \rho^3 \omega_e y_e , \qquad [3.7]$$

where $\rho = |\mu/\mu'|^{1/2}$ and μ, and μ' are the reduced masses of the ordinary molecule and its isotopomer, respectively. The wavenumber $\nu_{v'v''}'$ of a vibrational transition of the isotopomer is given by

$$\nu^{i}_{v'v''} = \rho\omega_e'(v'+1/2) - \rho^2\omega_e'x_e'(v'+1/2)^2 + \rho^3\omega_e'y_e'(v'+1/2)^3 + \ldots$$
$$-\rho\omega_e''(v''+1/2) + \rho^2\omega_e''x_e''(v''+1/2)^2 - \rho^3\omega_e''y_e''(v''+1/2)^3 + \ldots \quad [3.8]$$

The vibrational isotope shift $\Delta\nu = \nu_{v'v''} - \nu_{v'v''}^{i}$ can be represented by

$$\Delta\nu = (1-\rho)\,[\omega_e'(v'+1/2) - \omega_e''(v''+1/2)]$$
$$-(1-\rho^2)\,[\omega_e'x_e'(v'+1/2)^2 - \omega_e''x_e''(v''+1/2)^2]$$
$$+(1-\rho^3)\,[\omega_e'y_e'(v'+1/2)^3 - \omega_e''y_e''(v''+1/2)^3] + \ldots \quad [3.9]$$

(iii) Coupling between rotational and electronic motions

The interactions between the various angular momenta of the molecule cause the splitting of the rotational level in the multiplet states. Hund classified five different coupling cases. Of these five, the two most important ones known as Hund's case (a) and case (b), are represented in Fig. 3.1 and will be discussed here.

Hund's Case (a): In this case, each of the orbital angular momentum **L** and the spin angular momentum **S**, of the electrons is separately coupled to the internuclear axis of the molecule giving the resultant angular momentum Ω along the same axis as

$$\Omega = \Lambda + \Sigma_s, \quad [3.10a]$$

The quantum number Ω associated to this angular momentum Ω is given by

$$\Omega = \Lambda + \Sigma_s, \quad [3.10b]$$

where Σ_s has 2S+1 values (-S, -S+1, ... S-1, and S) for a given S, and hence the total angular quantum number Ω also has 2S+1 values for a given value of Λ. Thus the electronic state $^2\Pi$ (Λ = 1 and S = 1/2) has two spin-orbit coupling components $^2\Pi_{1/2}$

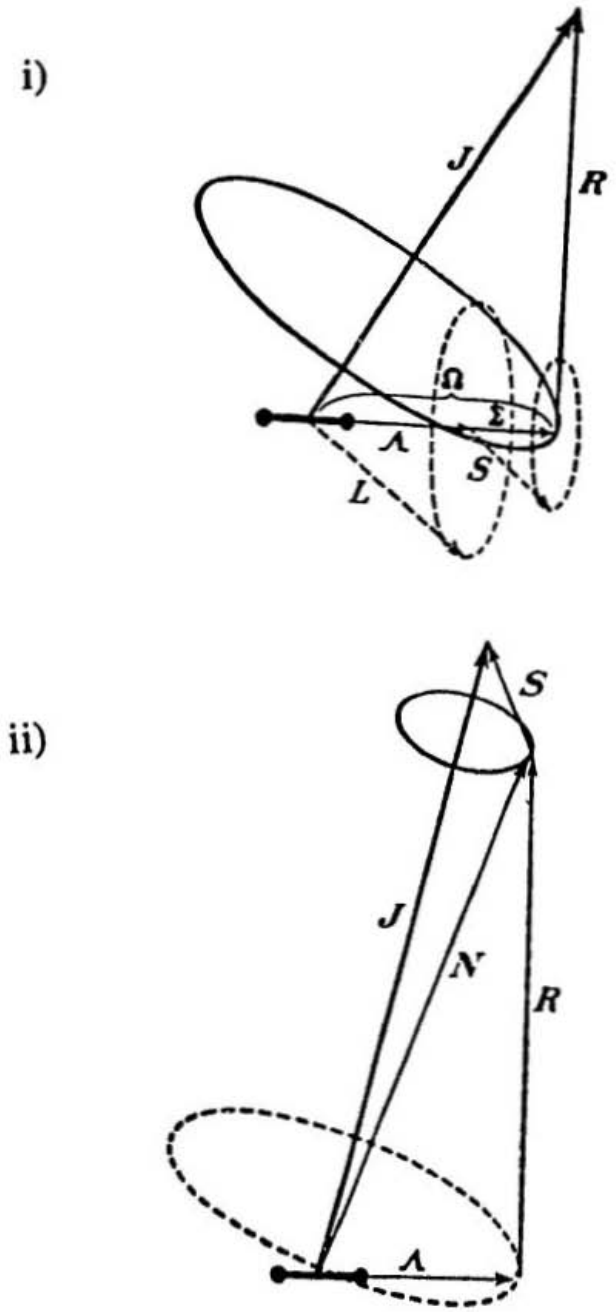

Figure 3.1 Vector diagrams for angular momenta: i) Hund's case (a) and ii) Hund's case (b) (see text for details).

and $^2\Pi_{3/2}$ corresponding to Ω=1/2 and Ω=3/2, respectively. In Hund's case (a), nuclear rotational angular momentum **R** and the electronic angular momentum Ω combine to form the total angular momentum **J** and the associated quantum number J has the values

$$J = \Omega, \Omega+1, \Omega+2 \ldots . \qquad [3.11]$$

Both J and Ω are either integers or half integers depending on whether the multiplicity (2S+1) of the state is odd or even. The splitting of the degeneracy that arises for the electronic states with $\Lambda \neq 0$ is referred to as Λ-type doubling, which is due to a weak coupling between the rotational motion of the nuclei and the orbital motion of the electrons.

Hund's Case (b): In Hund's case (b) the electron spin angular momentum **S** is weakly coupled to the internuclear axis, so that it is not possible to define an angular momentum Ω unlike in Hund's case (a). However, the total angular momentum **N** of the molecule is formed by the resultant of the vectors Λ and **R**. The quantum number N corresponding to this angular momentum takes the values

$$N = \Lambda, \Lambda+1, \Lambda+2 . \qquad [3.12]$$

The total angular momentum **J** of the molecule is given by the vector sum of **N** and **S**. For a given N, the quantum number J has the values :

$$J = N+S, N+S-1, N+S-2, \ldots |N-S| . \qquad [3.13]$$

Thus each rotational level N has (2S+1) components which represent the multiplicity of the electronic state. In this case, J can be either an integer or a half integer depending on whether the multiplicity of the state is odd or even. The $\Sigma(\Lambda = 0)$ state always belongs to Hund's case (b), whereas the multiplet Π (Λ=1), Δ (Λ=2), etc., states belong

to either Hund's case (a) or Hund's case (b).

The Hund's coupling cases represent ideal limiting cases which are a good approximation to the observed spectra. But large deviations from these limiting cases are found because of neglected interactions in the idealized coupling cases, in particular, the change in relative magnitudes of the interactions with increasing rotation. Thus, for a particular electronic state it is possible to observe a transition from one coupling case to another for increasing rotation. Recently in our laboratory, for the ground electronic state $^2\Pi_r$ of $^{15}N^{18}O$ (Wang et al., 1996), a transition from case (a) to case (b) has been observed at high J values.

(iv) Rotational terms of the electronic states and their parity

The rotational terms of a given vibrational level of a singlet electronic state are represented by

$$F_v(J) = B_v[J(J+1) - \Lambda^2] - D_v[J(J+1) - \Lambda^2]^2 + ... \qquad [3.14]$$

and those of a multiplet electronic state belonging to Hund's case (a) neglecting the Λ-type doubling are given by

$$F_v(J) = B_v[J(J+1) - \Omega^2] - D_v[J(J+1) - \Omega^2]^2 + ..., \qquad [3.15]$$

where B_v and D_v are rotational and centrifugal distortion constants, respectively. The constants B_v and D_v can be expressed in terms of the vibrational quantum number v and the equilibrium molecular constants as

$$B_v = B_e - \alpha_e (v+1/2) + \gamma_e (v+1/2)^2 + ... \ , \qquad [3.16]$$

and

$$D_v = D_e + \beta_e (v+1/2) + ... \ , \qquad [3.17]$$

where $B_e = h/8\pi^2 c\mu r_e^2$, and $D_e = 4B_e^3/\omega_e^2$ (Kratzer's relation). Here, μ is the reduced mass of the molecule, r_e represents the equilibrium internuclear distance, ω_e is the equilibrium vibrational constant, $\alpha_e << B_e$, $\gamma_e << \alpha_e$, and $\beta_e << D_e$. When the Λ- doubling is taken into account the expression for the term energies becomes more complicated. For example, for a $^2\Pi$ state, matrix elements of the molecular Hamiltonian H in a Hund's case (a) basis set have been developed by Brown et al. (1978, 1979). The form of these will be discussed in detail in a subsequent section. The best practical procedure for calculating the energies is to compute the matrix elements of H and diagonalize them.

The rotational terms of a $^2\Sigma^+$ state in Hund's case (b) are given by the following expressions:

$$F_{1e}(N) = B_v N(N+1) - D_v N^2(N+1)^2 + (1/2)\gamma_v N \qquad [3.18]$$

and

$$F_{2f}(N) = B_v N(N+1) - D_v N^2(N+1)^2 - (1/2)\gamma_v (N+1) . \qquad [3.19]$$

Here $F_{1e}(N)$ and $F_{2f}(N)$ refer to the components having J=N+1/2 and J=N-1/2 respectively, and γ_v is referred to as the spin-splitting constant or the spin-rotation interaction constant. In terms of the rotational quantum number J, the above rotational terms are expressed as:

$$F_{1e}(J) = B_v (J-1/2)(J+1/2) - D_v (J-1/2)^2(J+1/2)^2 + (1/2)\gamma_v (J-1/2) \qquad [3.20]$$

and

$$F_{2f}(J) = B_v (J+1/2)(J+3/2) - D_v (J+1/2)^2(J+3/2)^2 - (1/2)\gamma_v (J+3/2) . \qquad [3.21]$$

(Note: γ_v in Eqs. [3-18] to [3-20] is different from γ_e in Eq. [3.16]).

The positive or negative **parity** of a rotational level of an electronic state depends upon whether the total eigenfunction ψ of the molecule remains unchanged or changes

sign upon reflection at the origin. Kopp and Hougen (1967) used the following convention in labelling the rotational levels e and f with half integer J values:

"Levels with parity $+(-1)^{J-1/2}$ are e levels and those with parity $-(-1)^{J-1/2}$ are f levels."

Later Brown et al. (1975) extended this convention to the rotational levels with integer J values which can be stated as:

"Levels with parity $+ (-1)^J$ are e levels and those with parity $- (-1)^J$ are f levels."

3.2 General Remarks on Perturbations

Perturbations are generally viewed as occurrence of molecular energy levels at unexpected positions. Theoreticians consider perturbations when calculated quantities disagree with the corresponding experimental quantities because important interaction terms are neglected in the calculations. The observed regularity of the pattern can be generally represented in a simple algebraic representation in which the term value T_{vJ} of a band spectrum is considered as a simple, and rapidly-convergent polynomial function of the rotational and vibrational quantum numbers v and J.

The term values of a given electronic state are expressed in the form of a double power series by Dunham (1932) which is given by

$$T_{vJ} = \sum_{l,m} Y_{lm} (v+1/2)^l [J(J+1)]^m . \qquad [3.22]$$

The above polynomial expression is simply a translation of the expectation of a smooth

variation in the v and J quantum numbers. Perturbations may be viewed as a failure of a subset of the observed v, J levels to be accommodated by the empirical energy level expression defined by a majority of the sampled levels. Perturbations are also recognized when a band which appears as unperturbed in isolation from other vibrational bands disagrees with an interpretation of its rotational constant or vibrational energy representation

$$B_v = \sum_l Y_{l1} (v+1/2)^l \qquad [3.23]$$

or

$$G(v) = \sum_l Y_{l0} (v+1/2)^l \, . \qquad [3.24]$$

The Dunham expression (Eq. [3.22]) is based on the concept of potential energy curve which obeys Born-Oppenheimer approximation and the neglect of certain couplings between the angular momenta associated with the nuclear rotation, electron spin, and electron orbital motion. The concept of potential energy curve provides self consistency checks for molecular constants given by the Kratzer relation (Kratzer, 1920) (which is valid for harmonic or Morse potentials)

$$D_e = 4B_e^3/\omega_e^2 \qquad [3.25]$$

and the Pekeris relation (Pekeris, 1934) (which is valid for a Morse potential)

$$\alpha_e = (6 B_e^2/\omega_e) [(\omega_e x_e/B_e)^{1/2} - 1] \, . \qquad [3.26]$$

The indication of the presence of unsuspected perturbation can be found when fitted constants satisfy the above mentioned consistency checks.

3.3 The Molecular Hamiltonian H

The perturbations can be studied by constructing a deperturbation model which is represented by a Hamiltonian H given by

$$H = H^{o} + H', \qquad [3.27]$$

where H^{o} is the zero-order model consisting of functions like the potential energy curve V(R), an electronic eigenfunction $\phi(v,R)$, a set of ro-vibronic eigenvalues and eigenfunctions E_{vJ} and $X_{vJ}(R)$, and H′ represents the neglected terms that couple the zero-order functions with different electronic states. The perturbation parameters in the above constructed deperturbation model should govern the strength of the perturbation. By refining the molecular structural parameters of the Hamiltonian H, the deperturbation model is made to account for the properties of all observed levels. The deperturbation model should describe equally well the strongly perturbed and relatively perturbation-free levels.

The molecular Hamiltonian in the absence of an external magnetic or electric field is given by

$$H = H_{o} + H_{rot} + H_{fs} + H_{hfs}, \qquad [3.28]$$

where H_{o} is the nonrelativistic Hamiltonian for electronic energies in the Born-Oppenheimer approximation and gives the vibronic term energy T_{v} for the allowed vibrational states of different electronic states. The last term H_{hfs} is the Hamiltonian for the hyperfine structure and is rarely resolved in the optical spectra and hence it is neglected here. The term H_{rot} represents the Hamiltonian describing the rotation of the nuclei. The term H_{fs} (relativistic part of the Hamiltonian) describes the fine structure of

the rotational levels. Now the terms H_{rot} and H_{fs} will be considered in detail.

(a) The rotational Hamiltonian $\mathbf{H_{rot}}$:

The rotational part of the Hamiltonian is expressed as (Hougen, 1970)

$$\begin{aligned} H_{rot} &= B\,\mathbf{R}^2, \\ &= (1/2\mu R^2)\mathbf{R}^2 \\ &= (1/2\mu R^2)(R_x^2 + R_y^2), \end{aligned} \qquad [3.29]$$

where B is the rotational operator, μ is the reduced mass, R is the internuclear separation, and $\mathbf{R}$ is the nuclear rotation angular momentum operator. $R_z = 0$ since $\mathbf{R}$ is perpendicular to the z direction. The operator H_{rot} can be reexpressed in a convenient form from the definition of the total angular momentum $\mathbf{J} \equiv \mathbf{R} + \mathbf{L} + \mathbf{S}$ as

$$\begin{aligned} H_{rot} &= (1/2\mu R^2)\,[(J_x - L_x - S_x)^2 + (J_y - L_y - S_y)^2] \\ &= (1/2\mu R^2)\,[(J^2 - J_z)^2 + (J^2 - J_z)^2 + (S^2 - S_z^2) \\ &\quad + (L^+S^- + L^-S^+) - (J^+L^- + J^-L^+) - (J^+S^- + J^-S^+)], \end{aligned} \qquad [3.30]$$

where $J^{\pm} = J_x \pm iJ_y$, $L^{\pm} = L_x \pm iL_y$, $S^{\pm} = S_x \pm iS_y$. The first three terms $[(J^2 - J_z^2)$, $(L^2 - L_z^2)$, and $(S^2 - S_z^2)]$ have exclusive diagonal matrix elements and represent the rotational energy in the Hund's case (a) $|JM\Omega\Lambda S\Sigma\rangle$ basis function given by

$$E_{rot}(R) = (h^2/2\mu R^2)[J(J+1) - \Omega^2 + S(S+1) - \Sigma^2 + L(L+1) - \Lambda^2]. \qquad [3.31]$$

The remaining three terms of the rotational operator (Eq. 3.30] which are neglected in the Born-Oppenheimer approximation and couple the orbital, spin and total angular momenta are responsible for perturbations between different electronic states. They are classified as:

1. The spin-electronic operator $H_{SE} = (1/2\mu R^2)\,(L^+S^- + L^-S^+)$ which gives rise to

homogeneous spin-electronic ($\Delta\Omega = 0$) perturbations.

2. The **L**-uncoupling operator $H_{RE} = (1/2\mu R^2)\,(J^+L^- + J^-L^+)$ which causes heterogeneous ($\Delta\Omega = \pm 1$) electronic-rotational perturbations.

3. The **S**-uncoupling operator $(1/2\mu R^2)\,(J^+S^- + J^-S^+)$ which is also responsible for heterogeneous electronic-rotational perturbations.

The spin-electronic operator:

The selection rules for the off-diagonal elements of the operator H_{SE} are $\Delta\Sigma = 0$, $\Delta\Lambda = -\Delta\Sigma = \pm 1$ and $\Delta S = 0$. The operator L^+S^- can be written as

$$L^+S^- = \sum_i l_i^+ \sum_j s_j = \sum_i l_i^+ s_i^- + \sum_{i \neq j} l_i^+ s_j^- . \qquad [3.32]$$

The summation involves two-electrons for both l^+ and s^- operators and can give non-zero matrix elements between wavefunctions that differ by two spin-orbitals. The rotational operator $B = \hbar^2/2\mu R^2$ acts on the vibrational part of the wavefunction and hence the matrix elements are written as

$$B_{vv'} = \langle v|B|v'\rangle = B_v \delta_{vv'}. \qquad [3.33]$$

The contribution of H_{SE} compared to the contribution from H_{SO} (spin orbit) is small for the CO molecule.

The L-uncoupling operator:

The selection rules for this operator are $\Delta\Omega = \Delta\Lambda = \pm 1$, and $\Delta S = 0$. It is responsible for the transition from Hund's case (a) to Hund's case (d) (Herzberg, 1991) as J increases. The total matrix element of the BJ^+L^- operator is proportional to $|J(J+1) - \Omega(\Omega-1)|^{1/2}$. The **L**-uncoupling perturbations result in a large and strong J-

dependent Λ-doubling for non-Rydberg states. The Λ doubling of a $^1\Pi$ state due to interaction with a $^1\Sigma$ state via the **L**-uncoupling operator is observed for the CO molecule.

The S-uncoupling operator:

The selection rules for this operator are $\Delta S = 0$, $\Delta\Omega = \Delta\Sigma = \pm 1$, and $\Delta\Lambda = 0$ and the operator mixes different components of the same multiplet electronic state. It is responsible for the transition from Hund's case (a) to case (b) as J increases. The total interaction from the $-2B\mathbf{J}\cdot\mathbf{S}$ term which result from Eq. [3.30] is given by

$$\langle {}^{2S+1}\Lambda_{\Omega,v}|-B(J^+ S^- + J^- S^+)|{}^{2S+1}\Lambda_{\Omega+1,v+1}\rangle = -2\,(B_e^3/\omega_e)^{1/2}\,(v+1)^{1/2}\,|J(J+1) - \Omega(\Omega+1)|^{1/2} \times [S(S+1) - (\Omega-\Lambda)(\Omega-\Lambda+1)]^{1/2}\,, \qquad [3.34]$$

with phase convention for $S^{\pm}$ operator of the form

$$S^{\pm}\,|S,\Sigma\rangle = +\hbar[S(S+1) - \Sigma(\Sigma\pm1)]^{1/2}\,|S,\Sigma\pm1\rangle. \qquad [3.35]$$

The vibrational part of the $B\mathbf{J}\cdot\mathbf{S}$ matrix element gives

$$\langle v|B|v\rangle \equiv B_v \qquad [3.36]$$

if the S uncoupling operator acts between two components of a multiplet state that belongs to the same vibrational quantum number. This operator causes perturbations between the Ω spin component of the v^{th} level and the $\Omega \pm 1$ components of the $(v+1)^{th}$ level of the same electronic state if there is a near degeneracy between them. For heavier molecules the crossing of rotational levels are observed when the spin splitting between the spin substates of one vibrational level is slightly smaller than the vibrational interval.

(b) The relativistic fine structure Hamiltonian $\mathbf{H_{fs}}$**:**

The term H_{fs} is given by the sum of three terms as:

$$H_{fs} = H_{SO} + H_{SR} + H_{SS}, \qquad [3.37]$$

where the spin-orbit operator H_{SO} represents interaction between the spin and the orbital angular momenta of the electrons, the spin-rotation operator H_{SR} represents the electron spin and rotational angular momenta of the nuclei, and the spin-spin operator H_{SS} accounts for the interaction between the spins of different electrons. These interactions remove the spin degeneracy of the levels of an electronic state and give rise to the multiplet or zero-field splitting. They are also responsible for mixing states of the same multiplicity or different multiplicities thus providing a mechanism for observing forbidden transitions and homogeneous ($\Delta\Omega = 0$, $\Delta S = 0, \pm 1$) perturbations. A brief description of each term is given below:

(i) The spin-orbit operator $\mathbf{H_{SO}}$**:**

The Hamiltonian operator for spin-orbit and spin-other orbit interactions may be explicitly written in electron coordinates and velocities (Van Vleck ,1951), and may also be reduced in the molecule fixed coordinate frame (Veseth, 1970) as

$$H_{SO} = \frac{\alpha^2}{2}\sum_i \left[\frac{Z_A}{r_{iA}^3} l_{iA}\cdot s_{iA} + \frac{Z_B}{r_{iB}^3} l_{iB}\cdot s_i\right] - \frac{\alpha^2}{2}\sum_{i\neq j}\frac{1}{r_{ij}^3}(r_{ij}\times p_i)\cdot(s_i + 2s_j) \qquad [3.38]$$

where α ($= e^2/\hbar c$) is the fine-structure constant. The first part of Eq. [3.38] is a single electron operator and represents spin-orbit coupling of each electron in the field of the two nuclei with charges Z_A and Z_B. The second term is a two electron operator and is due to interelectronic interactions. It has the effect of partially counterbalancing the field of the bare nuclei. The spin-orbit Hamiltonian can be represented by one electron operator

(Field et al. 1972) as

$$H_{SO} = \sum_i \hat{a}_i \, l_i \cdot s_i \quad \text{with} \quad \hat{a}_i l_i = \sum_K \frac{\alpha^2}{2} \frac{Z_{eff,K}}{r_{iK}^3} l_{iK} \,, \qquad [3.39]$$

where l_{ik} is the orbital angular momentum of the electron i about the nucleus K, and $Z_{eff,K}$ is the effective charge of the K^{th} nucleus, and $\hat{a}$ is an operator that acts only on the radial part of the wavefunction. Expanding $l_i \cdot s_i = l_{iz} \cdot s_{iz} + 1/2(l_i^+ s_i^- + l_i^- s_i^+)$, the Hamiltonian can be written as

$$H_{SO} = \sum_i \hat{a}_i \left[l_{iz} \cdot s_{iz} + 1/2(l_i^+ s_i^- + l_i^- s_i^+) \right] . \qquad [3.40]$$

The first term ($l_{iz} \cdot s_{iz}$) in the Hamiltonian H_{SO} is used when two states belong to the same values of Λ and Σ quantum numbers. The selection rules are $\Delta\Lambda = \Delta\Sigma = 0$ and $\Delta S = 0$ or ± 1 (Kayama and Baird (1967)). The diagonal matrix elements for two interacting states having the same value of S and $\Lambda \neq 0$ has the form

$$\langle \Lambda,\Sigma,S,\Omega,v \; | H_{SO} | \; \Lambda,\Sigma,S,\Omega,v \rangle = A_{Av} \, \Lambda\Sigma, \qquad [3.41]$$

where A_{Av} is the spin-orbit coupling constant. According to Eq. [3.41] the fine structure levels are expected to be equally spaced with an interval of $A\Lambda$. Nonzero off-diagonal matrix elements occur mainly between states belonging to the same configuration having selection rules $\Delta\Lambda = \Delta\Sigma = 0$ but $\Delta S = 1$. When the two interacting states are far from each other, the effect causes only second-order effects called isoconfigurational spin-orbit effects which are important in understanding the strong spin-orbit transition to the Hund's

case (c) limit. A transition from case (a) to case (c) is possible if the interacting states are near degenerate. The matrix elements for the second part of Eq. [3.40], i.e., $(l_i^+ s_i^- + l_i^- s_i^+)$, are calculated if the two interacting states differ by $\Delta\Lambda = \pm 1$ and $\Delta\Sigma = \pm 1$, for a given signed value of Ω. These interactions between states of different symmetries are very common and are observed in the present work.

(ii) The spin-rotation operator $\mathbf{H_{SR}}$**:**

The operator H_{SR} accounts for the interaction between the electron spins and the magnetic field arising from molecular rotation. Kayana and Baird (1967) and Green and Zare (1977) derived an expression for the microscopic Hamiltonian in Hund's case (a) basis which is given by

$$H_{SR} = -2g_s\mu_B\mu_n(M/I)\left[\sum_i\sum_K Z_K\left(\frac{R_{GK}\cos\theta_{iK}}{r_{iK}^2}s_i\right)\right]\cdot R, \qquad [3.42]$$

where μ_B is the Bohr magneton, μ_n represents the nuclear magneton $(=m/M)\mu_B)$,(m/M) is the ratio of the mass of the electron to that of the proton, I is the molecular moment of inertia, Z_K is the nuclear charge, R_{GK} is the distance of nucleus K from the center of mass, θ_{iK} is the angle between the electron coordinate r_{iK} and the molecular space-fixed axis. Eq.[3.42] can be expressed for a diatomic molecule when I is related to the rotational constant B_v as

$$H_{SR} = -\ 1.05\times10^{-4}\ B_v\left[\sum_i\left(\frac{Z_A R_{GA}\cos\theta_{iA}}{r_{iA}^2} + \frac{Z_B R_{GB}\cos\theta_{iB}}{r_{iB}^2}\right)S_i\right]\cdot R. \qquad [3.43]$$

The effective form for the spin-rotation Hamiltonian for a case (a) basis is given by Brown and Watson (1977) as

$$H_{SR} = \gamma \mathbf{R} \cdot \mathbf{S} = \gamma (\mathbf{J} - \mathbf{L} - \mathbf{S}) \cdot \mathbf{S}$$

$$= \gamma (\mathbf{N} - \mathbf{L}) \cdot \mathbf{S}. \qquad [3.44]$$

For the case (b) basis, this operator is represented by

$$H_{SR} = \gamma \mathbf{N} \cdot \mathbf{S}. \qquad [3.45]$$

The diagonal matrix elements of H_{SR} in the case (a) basis for both operators in Eq. [3.44] and [3.45] are given by

$$\langle \Lambda,S,\Sigma,\Omega \ |H_{SR}| \ \Lambda,S,\Sigma,\Omega\rangle = \gamma \, |\Sigma^2 - S(S+1)|,$$

and

$$\langle \Lambda,S,\Sigma,\Omega \ |H_{SR}| \ \Lambda,S,\Sigma,\Omega\rangle = \gamma \, |\Omega\Sigma - S(S+1)|. \qquad [3.46]$$

The diagonal matrix elements obtained from Eq. [3.45] which are particularly useful for the case (b) basis is given by

$$\langle N,J,S,\Lambda \ |\boldsymbol{H}_{SR}| \ N,J,S,\Lambda\rangle = (\gamma/2)\,|J(J+1) - N(N+1) - S(S+1)| \ . \qquad [3.47]$$

There exists an off-diagonal matrix element for this operator for the selection rules $\Delta\Omega=\Delta\Sigma= \pm 1$, $\Delta\Lambda= 0$, and $\Delta S= 0$, and is represented by

$$\langle \Lambda,S,\Sigma,\Omega,v\,|H_{SR}\,|\Lambda,S,\Sigma\pm1,\Omega\pm1,v\rangle = \langle \Sigma,\Omega,v\,|(\gamma/2)J^{\pm}\,S^{\mp}|\Sigma\pm1,\Omega\pm1,v\rangle$$

$$=(\gamma/2)\ |J(J+1) - \Omega(\Omega\pm1)|^{1/2}\ |S(S+1) - \Sigma(\Sigma\pm1)|^{1/2} \qquad [3.48]$$

This off-diagonal matrix element is similar to the one obtained for the operator $\mathbf{H}_{rot}$ (**S**-uncoupling), but its sign is opposite to that of the B_v contribution.

(iii) The spin-spin operator $\mathbf{H}_{SS}$**:**

This operator represents the interaction energy between the magnetic dipoles

associated with the spins of two different electrons. The expression for two electron operators is given by

$$H_{ss} = -\alpha^2 \sum_{i<j} \frac{1}{r_{ij}^5}\left[3(\boldsymbol{r}_{ij}\cdot\boldsymbol{s}_i)(\boldsymbol{r}_{ij}\cdot\boldsymbol{s}_j) - (\boldsymbol{s}_i\cdot\boldsymbol{s}_j) r_{ij}^2\right]. \qquad [3.49]$$

where α is the spin-spin constant (this constant is different from the fine structure constant $\alpha = e^2/\hbar c$ in the expression for the spin-orbit Hamiltonian H_{so}) . The selection rules for this operator are $\Delta S = 0, \pm 1, \pm 2$, $\Delta\Sigma = -\Delta\Lambda = 0$ or ± 1 or ± 2 and $\Delta\Omega = 0$. The spin-spin interaction is zero for both the singlet and doublet Σ states. The effective spin-spin Hamiltonian with $\Delta S = \Delta\Sigma = 0$ is represented by

$$H_{ss} = (2/3)\lambda(3S_z^2 - \boldsymbol{S}^2). \qquad [3.50]$$

For an electronic state which obeys Hund's case (a) basis, the non zero matrix elements of this Hamiltonian are represented by

$$\langle S,\Sigma | H_{ss} | S,\Sigma \rangle = (2/3)\lambda[3\Sigma^2 - S(S+1)]. \qquad [3.51]$$

The spin splitting of the Σ states with $S>1/2$ ($^3\Sigma$ states) is due to the spin-spin effect and is given by

$$E(^3\Sigma_{\pm}) - E(^3\Sigma_0) = 2\lambda \qquad [3.52]$$

3.4 Energy Matrix and Fitting Procedure:

The first numerical treatment of the appropriate Hamiltonian describing the interactions between $a^3\Pi$, and $A^1\Pi$ states and the perturbing $a'^3\Sigma^+$, $d^1\Delta$, $e^3\Sigma^-$, $I^1\Sigma^-$, and $D^1\Delta$ states of CO was carried out by Field (1971). Later Bergeman and Cossart (1981) in an exhaustive study of the valence states of the CS molecule have discussed in detail the Hamiltonian matrix elements of the relevant singlet and triplet states and their mutual

electrostatic interactions (spin-orbit and rotation-electronic). In the present work, we have used their expressions for the Hamiltonian matrix elements and these are presented in Tables 3.1 and 3.2 for e and f parity respectively. From the analysis of the perturbations of $^{12}C^{16}O$ $a^3\Pi$ and $A^1\Pi$ states, Field et al. (1971, 1972) have concluded that the perturbation matrix elements (α, β) are the product of a vibrational factor and a constant electronic perturbation parameter (a, b), where the parameters a and b are characteristic of the relevant electronic configurations within the single configuration approximation. The effective perturbation parameters α and β are defined in the e/f basis set as

$$\alpha_{A,e} = \langle A\ ^1\Pi, v_A \mid H_{SO} \mid e\ ^3\Sigma^-, v_e \rangle = -(1/4)\, a \langle v_A | v_e \rangle$$

$$\alpha_{A,a} = \langle A\ ^1\Pi, v_A \mid H_{SO} \mid a'\ ^3\Sigma^+, v_{a'} \rangle = (1/4)\, a \langle v_A | v_{a'} \rangle$$

$$\alpha_{A,d} = \langle A\ ^1\Pi, v_A \mid H_{SO} \mid d\ ^3\Delta, {}_A v_d \rangle = -(\sqrt{2}/4)\, a \langle v_A | v_d \rangle$$

$$2\beta_{AI}\sqrt{x} = \langle A\ ^1\Pi, v_A \mid H_{RE} \mid I\ ^1\Sigma^-, v_I \rangle = -\sqrt{x}\ b \langle v_A | B | v_I \rangle$$

$$\beta_{AD}\sqrt{(x-2)} = \langle A\ ^1\Pi, v_A \mid H_{RE} \mid D\ ^1\Delta, v_D \rangle = \sqrt{(x-2)}\ b \langle v_A | B | v_D \rangle\ , \qquad [3.53]$$

where $x = J(J+1)$, $a = \langle 2\pi | a^+ | 2\sigma \rangle$, and $b = \langle 2\pi | I^+ | 2\sigma \rangle$. From the known vibrational wavefunctions, the initial values of the coupling terms α and β for any pair of levels can be calculated.

The effective Hamiltonian for the $^2\Pi$ state which is the upper state of the comet-tail ($A^2\Pi_i - X^2\Sigma^+$) system of CO^+, was discussed in detail by Brown et al. (1979) and the

TABLE 3.1 Matrix elements for the e parity levels of the Hamiltonian for the A $^1\Pi$ and the perturbing I $^1\Sigma^-$, D$^1\Delta$, a$'$ $^3\Sigma^+$, e $^3\Sigma^-$, and d $^3\Delta$ states (adopted from Le Floch, 1989).

e LEVELS		A$^1\Pi$	I$^1\Sigma^{-f}$	D$^1\Delta$	d$'^3\Sigma^+$			e$^3\Sigma^-$			d$^3\Delta$		
					F_2^e $(N=J)$ $^3\Sigma_1^+$	F_3^f $(N=J+1)$ $^3\Sigma_0^-$	F_1^f $(N=J-1)$ $^3\Sigma_1^+$	F_1^e $(N=J-1)$ $^3\Sigma_1^-$	F_3^e $(N=J+1)$ $^3\Sigma_0^-$	F_2^f $(N=J)$ $^3\Sigma_1^-$	$^3\Delta_1$	$^3\Delta_2$	$^3\Delta_3$
A$^1\Pi$		$T+B(x-1)$ $-D(x-0)^2$ $+\frac{1}{2}\gamma x$	0	$A_{02}\sqrt{x-2}$	A_{10}^+	0	0	A_{10}^-	0	0	A_{02}	0	0
I$^1\Sigma^{-f}$			$T+Bx$ $-Dx^2$	0	0	0	0	0	0	0	0	0	0
D$^1\Delta$				$T+B(x-4)$ $-D(x-4)^2$	0	0	0	0	0	0	0	(A_{22})	0
d$'^3\Sigma^+$	F_2^e $(N=J)$ $^3\Sigma_1^+$				$T+Bx$ $-Dx^2$ $+\frac{2}{3}\lambda-\gamma$	0	0	(A_{00})	0	0		0	0
	F_3^f $(N=J+1)$ $^3\Sigma_0^-$					$T+B(x-2)$ $-D(x^2-x-4)$ $-\frac{2}{3}\lambda-2\gamma$	$0+2\alpha\sqrt{x}\,\alpha$ $(B-D(2x+2)$ $+8B-\frac{7}{2}\gamma)$	0	0	0	0	0	0
	F_1^f $(N=J-1)$ $^3\Sigma_1^+$						$T+Bx$ $-D(x^2+4x)$ $+\frac{2}{3}\lambda-\gamma$	0	0	0	0	0	0
e$^3\Sigma^-$	F_1^e $(N=J-1)$ $^3\Sigma_1^-$							$T+Bx$ $-D(x^2+4x)$ $+\frac{2}{3}\lambda-\gamma$	$2\sqrt{x}\left\{\frac{B}{D(2x-2)}\right.$ $+8B$ $\left.-\frac{7}{2}\gamma\right\}$	0		0	0
	F_3^e $(N=J-1)$ $^3\Sigma_0^-$								$T+B(x+2)$ $-D(x^2+x+4)$ $-\frac{2}{3}\lambda-2\gamma$	0	0	0	0
	F_2^f $(N=J)$ $^3\Sigma_1^-$									$T+Bx$ $-Dx^2$ $+\frac{2}{3}\lambda-\gamma$	0	0	0
d$^3\Delta$	$^3\Delta_1$										$T-2A+Bx$ $-D(x^2-2x-4)$ $-2x\Lambda_D-\frac{2}{3}\lambda-\gamma$	$\sqrt{2x-4}\left\{\frac{B-A_D}{D(2x-2)}\right.$ $\left.-\frac{7}{2}\right\}$	$-2D\sqrt{(x-2)(x-6)}$
	$^3\Delta_2$											$T+B(x-2)$ $-D(x^2-12)$ $-\frac{2}{3}\lambda-2\gamma$	$\sqrt{2x-12}\left\{\frac{B+A_D}{D(2x+10)}\right.$ $\left.-\frac{7}{2}\right\}$
	$^3\Delta_3$												$T+2A+B(x-6)$ $-D(x^2-14x+52)$ $+A(2x-16)-\frac{2}{3}\lambda-\gamma$

Asterisks(*) identify the corresponding matrix elements are not included in the energy matrix becaues they belong to a different parity. (This is only for Σ states)

Matrix elements in parantheses are considered zero in the present study, becaues they concern perturbations of the $^3\Pi$ state.

TABLE 3.2 Matrix elements for the f parity levels of the Hamiltonian for the A $^1\Pi$ and the perturbing I $^1\Sigma^-$, D $^1\Delta$, a' $^3\Sigma^+$, e $^3\Sigma^-$, and d $^3\Delta$ states (adopted from Le Floch, 1989)

f LEVELS	$A^1\Pi$	$I^1\Sigma^{-f}$	$D^1\Delta$	$a'^3\Sigma^+$			$e^3\Sigma^-$			$d^3\Delta$		
				F_2^e $(N=J)$ $^3\Sigma_1^+$	F_3^f $(N=J-1)$ $^3\Sigma_0^+$	F_1^f $(N=J-1)$ $^3\Sigma_1^+$	F_1^e $(N=J-1)$ $^3\Sigma_1^-$	F_3^e $(N=J+1)$ $^3\Sigma_0^-$	F_2^f $(N=J)$ $^3\Sigma_1^-$	$^3\Delta_1$	$^3\Delta_2$	$^3\Delta_3$
$A^1\Pi$	$T+B(x-1)$ $-D(x-1)^2$ $-\frac{1}{2}q_x$	$-2A_0\sqrt{x}$	$\beta_{xz}\sqrt{x-2}$	0	0	A^*_{10}	0	0	A^*_{10}	A_{xz}	0	0
$I^1\Sigma^{-f}$		$T+Bx$ $-Dx^2$	0	0	(A^*_{00})	0	0	0	0	0	0	0
$D^1\Delta$			$T+B(x-4)$ $-D(x-4)^2$	0	0	0	0	0	0	0	(A_{zz})	0
$a'^3\Sigma^+$ F_2^e $(N=J)$ $^3\Sigma_1^+$				$T+Bx$ $-Dx^2+\frac{2}{3}\lambda$ $-\gamma$	0	0	0	0	0	0	0	0
$a'^3\Sigma^+$ F_3^f $(N=J+1)$ $^3\Sigma_0^+$					$T+B(x-2)$ $-D(x^2-x+4)$ $-\frac{1}{3}\lambda-2\gamma$	$2\sqrt{x}\left\{\begin{matrix}B\\-D(2x-2)\\+88-7\gamma_2\end{matrix}\right.$	0	0	0	0	0	0
$a'^3\Sigma^+$ F_1^f $(N=J-1)$ $^3\Sigma_1^+$						$T+Bx$ $-D(x^2+4x)$ $-\frac{4}{3}\lambda-2\gamma$	0	0	(A^*_{00})		0	0
$e^3\Sigma^-$ F_1^e $(N=J-1)$ $^3\Sigma_1^-$							$T+Bx$ $-D(x^2+4x)$ $+\frac{2}{3}\lambda-\gamma$	$0\ast(-2\sqrt{x})\ast\left\{\begin{matrix}B\\-D(2x+2)\\+88-7\gamma_2\end{matrix}\right.$	0	0	0	0
$e^3\Sigma^-$ F_3^e $(N=J+1)$ $^3\Sigma_0^-$								$T+B(x+2)$ $-D(x^2+x+4)$ $-\frac{1}{3}\lambda-2\gamma$	0	0	0	0
$e^3\Sigma^-$ F_2^f $(N=J)$ $^3\Sigma_1^-$									$T+Bx$ $-Dx^2$ $+\frac{2}{3}\lambda-\gamma$		0	0
$d^3\Delta$ $^3\Delta_1$										T_1 $T-2A+Bx$ $-D(x^2+2x-4)$ $-2xA_0+\frac{2}{3}\lambda-\gamma$	$\sqrt{2x-4}\left\{\begin{matrix}B\\-D(2x-2)\\-A_0-3\gamma_2\end{matrix}\right.$	$-2D$ $\sqrt{(x-2)(x-6)}$
$d^3\Delta$ $^3\Delta_2$											T_2 $T+B(x-2)$ $-D(x^2-12)$ $-\frac{1}{3}\lambda-2\gamma$	$\sqrt{2x-12}\left\{\begin{matrix}B\\-D(2x-10)\\+A_0-3\gamma_2\end{matrix}\right.$
$d^3\Delta$ $^3\Delta_3$												T_3 $T+2A+B(x-8)$ $-D(x^2-14x+52)$ $+2(x-8)A_0+\frac{2}{3}\lambda-\gamma$

Asterisks(*) identify the corresponding matrix elements are not included in the energy matrix becaues they belong to a different parity. (This is only for Σ states)

Matrix elements in parantheses are considered zero in the present study, becaues they concern perturbations of the $^3\Pi$ state.

corresponding matrix elements were also given by them. Later Amiot et al. (1981) listed the matrix elements of the complete Hamiltonian for the $^2\Pi$ and $^2\Sigma^+$ states, and Douay (1988) made some corrections for the matrix elements of the parameters γ, γ_0, and γ_{01} given by Amiot et al. The matrix elements of the Hamiltonian which are relevant to the present work are given in Table 3.3.

A computational procedure for fitting the parameters appearing in the Hamiltonian described in Section 3.3 will be implemented. This fitting routine is a weighted nonlinear, least-squares procedure which combines the Hellmann-Feynman theorem (Hellmann, 1937; Feynman, 1939) and Marquardt's iterative algorithm (Marquardt, 1963). The program accepts either transition frequencies (F_i) or term energies as input data, along with the initial guesses of the molecular parameters and estimated experimental uncertainty for each datum (σ_i). The Hamiltonian matrix is evaluated by using the initial parameters, and then diagonalized. The calculated transition frequencies are obtained from the term energies (resulting eigenvalues) and compared to the experimentally observed frequencies. Corrections to the parameters are computed and a new set of term energies is generated using the adjusted parameter value. This procedure is repeated until convergence is achieved.

Using Marquardt's algorithm the correction vector δ which is subtracted from the fitted parameters, is obtained by solving the equation

$$(\mathbf{A} - \lambda \mathbf{I})\delta = \mathbf{g} , \qquad [3.54]$$

where the normal equation matrix **A** has dimensions m x m where m is the number of fitted parameters, and **g** is the gradient or error vector. The elements a_{jk} of the matrix are

TABLE 3.3 Matrix elements of the Hamiltonian for $^2\Pi$ and $^2\Sigma^+$ states (Brown et al.,1979)

Molecular Constant	Labelling[a]	Matrix element[b,c]
T_v	1,1	1
	2,2	1
	3,3	1
B_v	1,1	$x(x \mp 1)$
	2,2	$x^2 - 1$
	3,3	$x^2 + 1$
	2,3	$-(x^2 - 1)^{1/2}$
D_v	1,1	$x^2(x \mp 1)^2$
	2,2	$-x^2(x^2 - 1)$
	3,3	$-x^2(x^2 + 3)$
	2,3	$2x^2(x^2 - 1)^{1/2}$
γ_v	1,1	$\pm 0.5(x \mp 1)$
A_v	2,2	0.5
	3,3	-0.5
A_{Dv}	2,2	$0.5(x^2 - 1)$
	3,3	$-0.5(x^2 + 1)$
p_v	3,3	$\mp 0.5x$
q_v	3,3	$\mp x$
	2,3	$\pm 0.5x(x^2 - 1)^{1/2}$

[a]Lables 1, 2, and 3 refer to states $^2\Sigma^+$, $^2\Pi_{3/2}$, and $^2\Pi_{1/2}$, respectively.

[b]$x = J + 0.5$.

[c]The upper and lower signs of notation $\pm$ and $\mp$ refer to the e and f levels respectively.

given by

$$a_{jk} = \sum_{i=1}^{N} w_i \left(\partial f_i/\partial b_j\right)\left(\partial f_i/\partial b_k\right); \quad j=1....m;\ k=1,...m, \qquad [3.55]$$

where N is the number of input data, b_j and b_k are the parameters to be fitted, f_i is the calculated value of the transitions or term energies being evaluated at the current value of the parameters, w_i $(=1/\sigma^2)$ is the corresponding weight computed as the reciprocal of the square of the estimated experimental uncertainties. The error vector **g** has elements given by

$$g_j = \sum_{I=1}^{N} w_i (f_i - F_i)\left(\partial f_i/\partial b_j\right), \quad j=1 \ldots m, \qquad [3.56]$$

where F_i is the experimental value of the i^{th} datum. In solving Eq. [3.54], the initial value of the Marquardt's parameter λ was fixed as 10^{-1} and was divided by 10 at each subsequent iteration. The Hellmann-Feynman theorem was used to calculate the first order derivatives appearing in the normal equation matrix [Eq. [3.55] and error vector [Eq. 3.56]. The procedure is as follows: The eignvector $|\psi\rangle$ of the Hamiltonian H, associated with the eigenvalue f_i may be written in terms of the Hund's case (a) basis set function $|\phi_k\rangle$ as

$$|\psi_i\rangle = \sum_{K=1}^{N} C_{ik} |\phi_k\rangle, \qquad [3.57]$$

where N is the dimension of the Hamiltonian matrix. The Hamiltonian H may be expressed as a linear combination of the molecular parameters as

$$H = \sum_{j=1}^{m} b_j H_j \,. \qquad [3.58]$$

From the Hellmann-Feynman theorem we obtain

$$(\partial f_i/\partial b_j) = \langle \psi_i | (\partial \boldsymbol{H}/\partial b_j) | \psi_i \rangle = \sum_{k=1}^{n} \sum_{l=1}^{n} C_{ik}^{*} C_{il} \langle \phi_k | \boldsymbol{H}_j | \phi_l \rangle \qquad [3.59]$$

The advantage of using the Hellmann-Feynman theorem is that it provides all of $(\partial f_i/\partial b_j)$ after single diagonalization of H rather than n+1 diagonalizations that would otherwise be needed to compute the derivatives by finite differences (Lefebvre-Brion and Field 1986). The first order derivatives $(\partial f_i/\partial b_j)$ are computed from the knowledge of the coefficients C_{ik} of the eigenvectors in the standard basis and of the matrix elements $\langle \phi_k |$ H_j $| \phi_l \rangle$.

REFERENCES

Amiot, C., Maillard, J. P., and Chauville, J. *J. Mol. Spectrosc.* **87**, 196 (1981).

Bergeman, T., and Cossart, J. *J. Mol. Spectrosc.* **87**, 119 (1981).

Brown, J. M., Hougen, J. T., Huber, K. P., Johns, J. W. C., Kopp, I., Lefebvre-Brion, H., Merer, A. J., Ramsay, D. A., Rostas, J., and Zare, R. N., *J. Mol. Spectrosc.* **55**, 500 (1975).

Brown, J. M., and Watson, J. K. G., *J. Mol. Spectrosc.* **65**, 65 (1977).

Brown, J. M., Kaise, M., Kerr, C. M. L., and Milton, D. J., Mol. Phys. **36**, 553, (1978).

Brown, J. M., Colbourn, E. A., Watson, J. K. G., and Wayne, F. D., *J. Mol. Spectrosc.* **74**, 294 (1979).

Douay, M., Rogers, S. A., and Bernath, P. F., *Mol. Phys.* **64**, 425 (1988).

Dunham, J. L., *Phys. Rev.* **41**, 721 (1932).

Feynman, R. P., *Phys. Rev.* **56**, 340 (1939).

Field, R. W., Ph.D thesis, Harvard University, 1971.

Field, R. W., Wicke, B. G., Simmons, J. D., and Tilford, S. G., *J. Mol. Spectrosc.* **44**, 383 (1972).

Field, R. W., Tilford, S. G., Howard, R. A., and Simmons, J. D., *J. Mol. Spectrosc.* **44**, 347 (1972).

Green, S., and Zare, R. N., *J. Mol. Spectrosc.* **64**, 217 (1977).

Hellmann, H., "Einfuhrung in die Quantenchemie," Franz Deuticke, Vienna, (1937).

Herzberg, G., "Molecular Spectra and Molecular Structure. I. Spectra of Diatomic Molecules." Krieger, Malabar, FL, (1991).

Hougen, J. T., "The Calculation of Rotational Energy Levels and Rotational Line Intensities in Diatomic Molecules," Nat. Bur. Stand. (U.S), monograph 115, (1970).

Kayama, K., and Baird, J. C., *J. Chem. Phys.* **46**, 2604 (1967).

Kopp, I., and Hougen, J. T., *Can. J. Phys.* **45**, 2581 (1967).

Kratzer, A., *Z. fur. Physik.* **3**, 289 (1920).

Lefebvre-Brion, H., and Field, R. W., "Perturbations in the Spectra of Diatomic Molecules," Academic Press, New York, 1986.

Marquardt, D. W., *J. Soc. Indust. Appl. Math.* **11**, 431 (1963).

Mullikan, R.S., *Rev. Mod. Phys.* **3**, 89 (1931).

Mullikan, R.S., *Rev. Mod. Phys.* **4**, 1 (1932).

Pekeris, C. L., *Phys. Rev.* **45**, 98 (1934).

Van Vleck, J. H., *Rev. Mod. Phys.* **23**, 213 (1951).

Veseth, L., *Theor. Chim. Acta.* **18**, 368 (1970).

Wang, D.X., Haridass, C., and Reddy, S. P., *J. Mol. Spectrosc.* **175**, 73 (1996).

CHAPTER 4

THE FOURTH POSITIVE (A $^1\Pi$-X $^1\Sigma^+$) SYSTEM OF $^{12}C^{18}O$ AND $^{13}C^{18}O$, EXCITED IN A HOLLOW CATHODE DISCHARGE

4.1 Introduction

Neutral CO and its ion CO^+ are important constituents of the solar atmosphere, stellar atmospheres, comet tails, interstellar space, and planetary atmospheres, and CO is by far the most abundant molecule in interstellar space (see Haridass et al., 1992 and the references therein). CO is also, after H_2, the most abundant molecule in the universe. Spectroscopic studies of these objects by rockets and satellites in recent times extending the spectral range to the vacuum-ultraviolet region have increased their importance in astrophysics. It is essential to have accurate laboratory data of the spectra of various isotopomers of CO and CO^+ in order to estimate abundance ratios of isotopes $^{12}C/^{13}C$ and $^{16}O/^{18}O$ on celestial objects such as comets, meteorites, stars, planetary nebulae and interstellar space. This chapter is concerned with experimental investigation of the fourth positive (A $^1\Pi$-X $^1\Sigma^+$) system of the isotopomers $^{12}C\,^{18}O$ and $^{13}C^{18}O$, in which the upper state A is perturbed by states a′ $^3\Sigma^+$, d $^3\Delta_i$, e $^3\Sigma^-$, I $^1\Sigma^-$, D $^1\Delta$, and D′ $^1\Sigma^+$. The relevant electronic configurations are

K K $(z\sigma)^2$ $(y\sigma)^2$ $(w\pi)^4$ $(x\sigma)^2$: X $^1\Sigma^+$

- - - - $(w\pi)^4$ $(x\sigma)$ $(v\pi)$: a $^3\Pi$, A $^1\Pi$

- - - - $(w\pi)^3$ $(x\sigma)^2$ $(v\pi)$: a′ $^3\Sigma^+$, d $^3\Delta_i$, e $^3\Sigma^-$, I $^1\Sigma^-$, D $^1\Delta$, D′ $^1\Sigma^+$.

Deslandres (1888) was the first to study the emission spectrum of CO and in particular its fourth positive system. Over the years a large number of investigations have

been carried out on the spectra of CO in the microwave, infrared, visible, ultraviolet and vacuum-ultraviolet regions. For the previous work on the fourth positive system of $^{12}C^{16}O$, the reader is referred to the reviews by Krupenie (1966), and Tilford and Simmons (1972) and the compilation by Huber and Herzberg (1979). More recent references on this system are given by Le Floch et al. (1987). Even though the fourth positive system of $^{12}C^{16}O$ was investigated extensively both in emission and absorption, the work done on this system for the corresponding less-abundant isotopomers is fragmentary or non-existent. Tilford and Simmons (1972) reported band head measurements of the absorption spectrum of $A(v')\leftarrow X(v''=0)$ of $^{13}C^{16}O$ from $v'=2$ to 16 at wavelengths shorter than 2000 Å. Domin (1986) provided rotational analyses of 28 emission bands of the A-X system of $^{13}C^{16}O$ at wavelengths longer than 2000 Å. Studies on the fourth positive system of $^{12}C^{18}O$ and $^{13}C^{18}O$ are almost non existent but for the study of the A-X system of $^{12}C^{18}O$ in laser-excited fluorescence by Vikis (1978a,b).

The A $^1\Pi$ state of CO is extensively perturbed by its other electronic states a' $^3\Sigma^+$, d $^1\Delta$, e $^3\Sigma^-$, I $^1\Sigma^-$, and D $^1\Delta$ because of their proximity to the former. Perturbations of the rotational structure can be observed at almost all vibrational levels of state A. For $^{12}C^{16}O$ many perturbations have been reported. Krupenie (1966) classified the perturbations in the A $^1\Pi$ state in his review paper. Simmons et al. (1969) carried out a critical analysis of the perturbations in the A state from the absorption spectra of the A-X system. Field (1971) and Field et al. (1972a, 1972b) performed a deperturbation calculation for the A $^1\Pi$ state. Le Floch and Amiot (1985) studied the Fourier Transform spectrum of the Ångström (B $^1\Sigma^+$ - A $^1\Pi$) system of CO and revised the previous perturber assignments.

Le Floch et al. (1987) made an extensive study of perturbations in the A $^1\Pi$, v=0 state of CO. Le Floch (1989) performed perturbation calculations for the A $^1\Pi$, v=0 to 4 states of CO. Further Le Floch (1992) tabulated accurate energy levels for the A $^1\Pi$, v=0 to 8 for CO. A quantitative analysis of the perturbations in the A $^1\Pi$, v=0, 3 and 5 levels of $^{13}C^{18}O$ was performed by Prasad et al. (1984) from its observed B - A system. Malak et al. (1984) reported observations of perturbations in the A $^1\Pi$, v=0 to 5 of $^{13}C^{18}O$ through the same system. Kepa (1988) studied the Herzberg (C $^1\Sigma^+$ -A $^1\Pi$) system of $^{13}C^{18}O$ and performed a preliminary quantitative analysis of perturbations in the A $^1\Pi$, v=0 state caused by the e $^3\Sigma^-$, v=1 state. From a study of the E $^1\Pi$ - A $^1\Pi$ and B - A systems of $^{12}C^{18}O$, Kepa (1986) partially analyzed the perturbations in the A state. Haridass and Huber (1994) (see Chapter 7) observed perturbations in the A $^1\Pi$, v=0, 1, 2, 5 and 6 states of $^{13}C^{16}O$ from the A-X system.

In the present chapter we report the high resolution vacuum ultraviolet study of the fourth positive system of $^{12}C^{18}O$ and $^{13}C^{18}O$ in emission in the spectral region 1710 - 1935 Å. The spectra were excited in the anode glow of a hollow-cathode discharge tube and eight bands of $^{12}C^{18}O$ with v′=0 to 2 and v″=2 to 6, and three bands of $^{13}C^{18}O$ with v′=0 to 1 and v″=4 and 5 were recorded. The rotational structure of five bands (1-4, 1-5, 2-2, 2-5, and 2-6) of $^{12}C^{18}O$ and two bands (1-4 and 1-5) of $^{13}C^{18}O$ was analyzed. Strong perturbations of the order of 2 cm^{-1} in the A, v=1 level, and weak perturbations in the A, v=2 level, of $^{12}C^{18}O$ were observed. Also, weak perturbations were observed in the A, v=1 level of $^{13}C^{18}O$. The deperturbed molecular constants were obtained for the A state of both isotopomers. Spectroscopic information was also obtained for the perturbing

vibrational states of a′ $^1\Sigma^+$, d $^3\Delta$, e $^3\Sigma^-$, D $^1\Delta$ and I $^1\Sigma^-$. Mixing coefficients and electronic perturbation parameters which characterize each perturbation were also derived.

4.2 Experimental Details

The bands of the fourth positive system of $^{12}C^{18}O$ and $^{13}C^{18}O$ were excited in the anode column of a hollow-cathode discharge tube of special design (Reddy and Prasad, 1989). Carbon-12 and oxygen-18 gas with a specified purity of 97.6% of ^{18}O and carbon-13 and oxygen-18 gas with specified purities of 98% ^{13}C and 95.7% of ^{18}O, both supplied by Merck Sharpe and Dohme Canada Limited were used in the experiments. A d.c voltage of 1300 V applied between the electrodes of the discharge tube maintained the discharge in each gas, at a current of ~ 90 mA where the pressure inside the discharge tube was ~ 0.8 Torr. The spectra were photographed on a 10.6 m vacuum spectrograph at the Herzberg Institute of Astrophysics, National Research Council of Canada in the 6th and 7th orders of a normal incidence concave grating with 600 grooves mm^{-1} blazed at 12000 Å. The slit width of the spectrograph was maintained at 20 μm. The spectra were photographed on Kodak SWR plates. A lithium fluoride prism/cylinder combination (Huber etal., 1987, Huber etal., 1992) was used to predisperse the light entering the spectrograph, thus eliminating overlapping orders of the spectra. The exposure time was 3 hrs to record each of the $^{12}C^{18}O$ and $^{13}C^{18}O$ emission spectra. An Fe-Ne hollow-cathode lamp was used as a source for the reference spectra whose wavelengths were taken from Crosswhite (1975). The measurements, made at Memorial University of Newfoundland on a Gaertner Optical Company comparator (Model M 1205 C), have accuracies of ~

±.001 Å for sharp lines.

4.3 Rotational Analysis

(a) Rotational structure of the bands

The rotational structure of a band arising from a $^1\Pi$ - $^1\Sigma'$ transition gives rise to P_{ee}, Q_{fe}, and R_{ee} branches corresponding to the rotational selection rule $\Delta J = -1, 0$, and $+1$ and is schematically shown in Fig. 4.1. The notation for e/f parity levels adopted here is according to Brown et al. (1975). The measured wavenumber ν of the rotational levels of a band in a $^1\Pi$ - $^1\Sigma^+$ transition free from perturbations can be represented by

$$\nu = \nu_0 + B_v' (x'-1) - D_v' (x'-1)^2 - (B_v'' x'' - D_v'' x''^2), \qquad |4.1|$$

where ν_0 is the band origin, $x' = J'(J'+1)$, $x'' = J''(J''+1)$, B_v' and D_v' are the molecular constants of the upper state $^1\Pi$, and B_v'' and D_v'' are those of the lower $^1\Sigma'$. It can also be represented by

$$\nu = T'(v',J') - T''(v'',J'')$$

$$= T_v' + B_v' (x'-1) - D_v' (x'-1)^2 - [G_0''(v'') + B_v'' x'' - D_v'' x''^2]. \qquad |4.2|$$

In Eq.|4.2|, T_v' is the vibrational term of the upper state A $^1\Pi$, and the term in the square bracket represents the vibration-rotation term $T''(v'',J'')$ of the lower X $^1\Sigma'$ relative to $X^1\Sigma^+$, $v''=0$, $J''=0$.

Authier et al. (1993) estimated precisely the mass-independent Dunham coefficients for the ground state X $^1\Sigma^+$ of CO. Making use of these coefficients the ground state term values $T''(v'',J'')$ are estimated in the present work for $^{12}C^{18}O$ and $^{13}C^{18}O$. The rotational analysis of the band is straight forward and the assignment of J values to the rotational

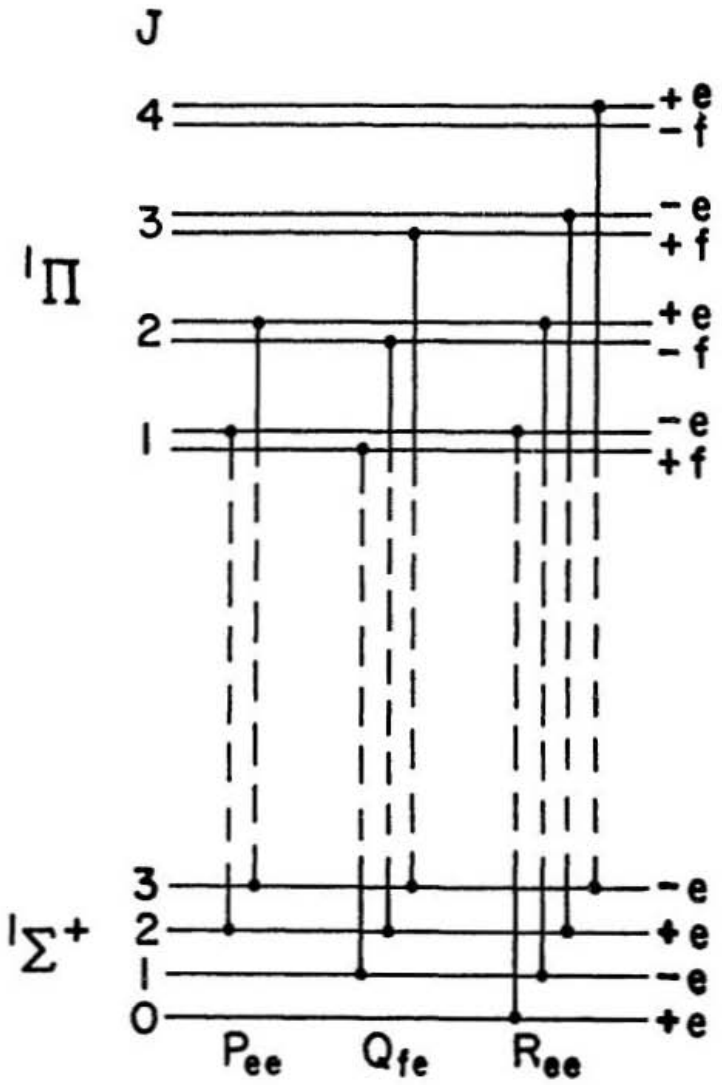

Figure 4.1. A Schematic energy level diagram showing the first few rotational transitions of the three branches of a band of a $^1\Pi$ - $^1\Sigma^+$ transition.

structure including those with perturbations was done with the help of precisely known combination differences $\Delta_2F''(J)$ (Herzberg, 1950). The rotational structures of the 1-4, 1-5, 2-2, 2-5, and 2-6 bands of $^{12}C^{18}O$ and of the 1-4, 1-5 bands of $^{13}C^{18}O$ are analyzed. The rotational structures of the 1-5 bands of $^{12}C^{18}O$ and $^{13}C^{18}O$ are shown in Fig. 4.1 (a). The rotational quantum numbers and the vacuum wavenumbers (in cm^{-1}) of the spectral lines of these bands are listed in Tables 4.1 and 4.2 for $^{12}C^{18}O$ and $^{13}C^{18}O$ respectively.

(b) Interactions between the levels of A $^1\Pi$ and the nearby levels

Many crossings occur between the vibrational levels of the A $^1\Pi$ state of CO and those of its nearby states a' $^3\Sigma^+$, d $^1\Delta$, e $^3\Sigma^-$, I $^1\Sigma^-$, and D $^1\Delta$. The appropriate matrix elements of the singlet and triplet states and their mutual electronic interactions are given by Field (1971), Bergeman and Cossart (1981) and Lefebvre-Brion and Field (1986). Numerous perturbations can be observed near the crossings. These arise mainly from the rotation-electronic H_{RE} (**L**-uncoupling operator, see Eq. [3.30] in section 3.3(a)) and spin-orbit H_{SO} (see Chapter 3, Eq. [3.40]) Hamiltonian operators, which can be represented by

$$H_{RE} = -(1/2\mu R^2)\ (J^+ L^- + J^- L^+), \qquad [4.3]$$

$$H_{SO} = \sum_i \frac{1}{2} \hat{a}_i\ (l_i^+ s_i^- + l_i^- s_i^+) + \hat{a}\ l_{iz}\ s_{iz}. \qquad [4.4]$$

In these equations μ is the reduced mass of the molecule, R is its internuclear separation, **J** and **L** are the total and orbital angular momentum operators, $\hat{a}$ is the spin orbit coupling constant, **l** and **s** are the orbital and spin angular momentum operators of the individual electrons.

Garetz et al. (1991) constructed a perturbation diagram for $^{12}C^{16}O$ locating the

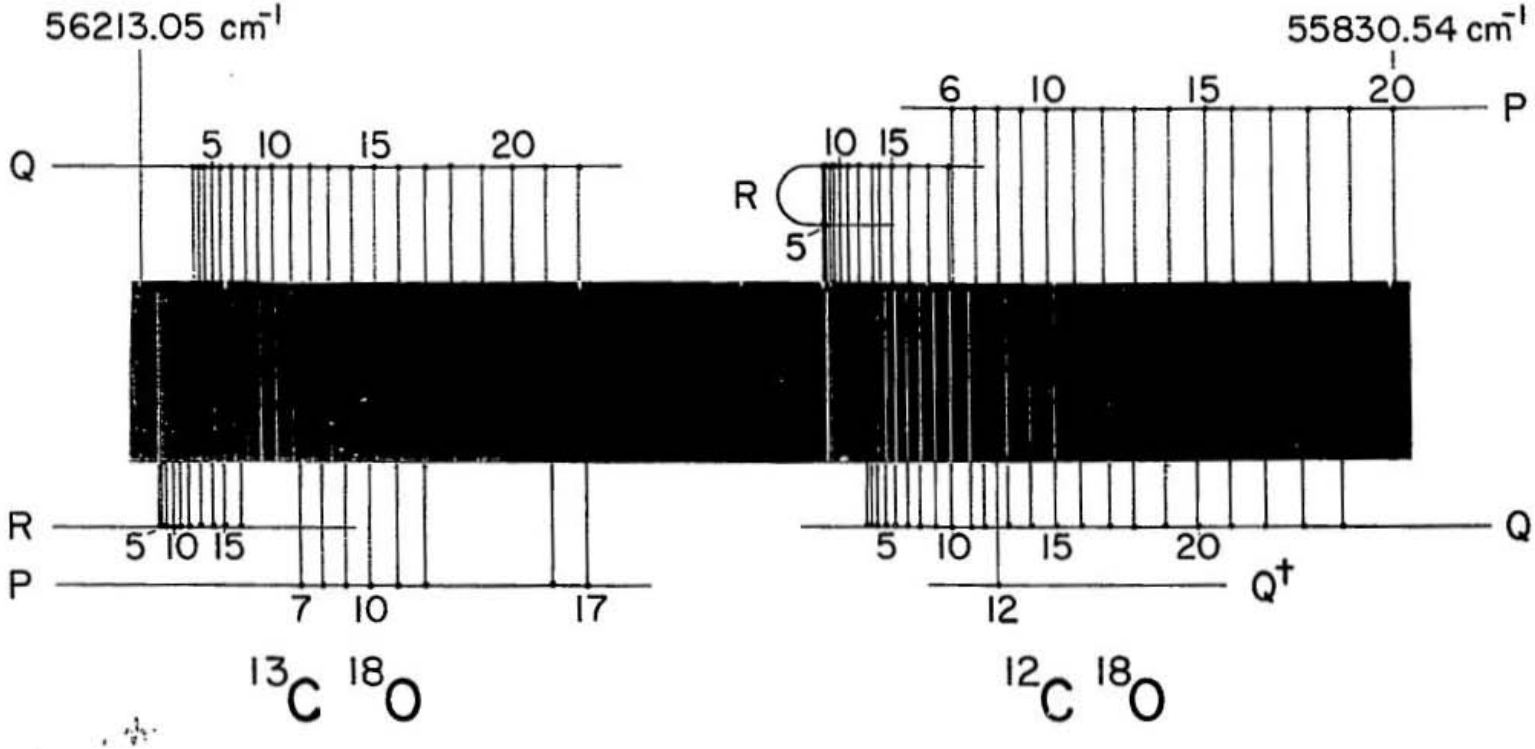

Figure 4.1(a) Rotational structure of the 1-5 bands of the A $^1\Pi$ - X $^1\Sigma^+$ system of $^{13}C^{18}O$ and $^{12}C^{18}O$, photographed on the 10.6 m vacuum grating spectrograph: the extra line $Q^{\dagger}(12)$ in $^{12}C^{18}O$ arises from the perturbation of the A, v=1 level by the a′ $^3\Sigma^+$, v=10 level.

TABLE 4.1 Vacuum wavenumbers (in cm^{-1}) of the rotational lines of five bands of the fourth positive (A-X) system of $^{12}C^{18}O$[a]

Band	1-4			1-5		
J	R(J)	Q(J)	P(J)	R(J)	Q(J)	P(J)
0	57987.90(7)					
1	90.25(-6)	57984.30(0)				
2	92.33(6)	83.31(6)			55991.72(0)	
3	93.76(6)	81.66(-2)			90.21(-4)	
4	94.7 (1)	79.57(0)	57967.58(4)	56003.40(9)	88.26(-2)	
5	95.00(2)	76.98(3)	61.89(-2)	03.86(1)	85.80(-1)	
6	94.85(0)	73.80(0)	55.9 (1)	03.86(-4)	82.90(4)	55964.80(-2)
7	94.16(-1)	70.12(1)	49.03(-6)	03.40(-6)	79.40(-1)	58.36(-1)
8	93.01(4)	65.93(2)	41.88(-1)	02.44(-8)	75.44(-2)	51.44(0)
9	91.27(2)	61.16(-1)	34.11(-5)	01.09(0)	70.98(-3)	43.98(-2)
10	89.00(3)	55.88(1)	25.91(0)	56999.15(1)	66.06(2)	36.09(1)
11	86.13(-1)	49.89(-1)	17.10(-3)	96.65(-1)	60.41(-2)	27.67(2)
12	82.66(2)	45.63(3)	07.81(1)	93.57(2)	56.46(-6)	18.73(0)
12		41.14(4)			52.02(0)	
13	77.65(-3)	37.58(0)	57897.90(-2)	88.93(-9)	48.88(-4)	09.31(4)
14	76.04(4)	30.0 (-1)	87.40(1)	87.78(-2)	41.87(-3)	55899.19(1)
15	70.63(-4)	22.16(-2)	75.41(2)	83.04(8)	34.51(4)	87.71(3)
16	65.14(-3)	13.74(2)	66.66(-2)	77.92(-5)	26.54(1)	79.49(1)
17	59.20(-1)	04.52(0)	54.32(-1)	72.56(-1)	17.81(-6)	67.69(2)
18	52.77(0)	57896.36(2)	41.79(0)	66.64(-7)	10.30(2)	55.79(5)
19	45.75(-6)	85.97(3)	28.81(-1)		00.53(2)	43.35(-3)
20	38.2 (-1)	75.41(1)	15.29(-7)		55890.61(0)	30.54(-3)
21	30.40(7)	64.40(1)			80.25(-4)	
22		52.90(2)	57787.0 (1)		69.54(5)	
23	12.69(-3)	40.90(5)	71.97(7)		58.21(1)	
24		28.24(-4)	56.39(2)		46.34(-7)	
25		15.1 (-1)				
26		01.44(-1)				
27		57786.16(1)				
28		73.25(-3)				

TABLE 4.1 (Continued)

Band	2-2			2-5		
J	R(J)	Q(J)	P(J)	R(J)	Q(J)	P(J)
0	63458.95(-6)					
1	61.30(-6)			57411.8 (4)		
2	63.12(5)	63454.14(0)		13.6 (2)	57404.36(-8)	57398.0 (-5)
3		52.29(3)	63442.9 (-5)		02.89(5)	94.8 (9)
4	64.63(1)	49.80(0)	38.3 (4)	15.56(-1)	00.66(-6)	88.7 (-1)
5	64.43(-2)	46.65(1)	31.73(-6)	15.8 (-1)	57398.01(-6)	83.27(4)
6	63.67(2)	42.86(2)	24.98(-8)	15.66(-2)	94.82(-5)	76.9 (-2)
7	62.20(-2)	38.34(-1)	17.67(-3)	14.88(-6)	91.02(-3)	70.46(5)
8	60.17(0)	33.60(1)	09.64(-7)	13.59(-6)	87.07(-3)	63.18(-3)
9	57.48(0)	28.0 (-1)	01.09(-1)	11.77(-7)	82.24(-1)	55.46(-1)
10	54.14(-2)	21.54(-3)	63392.0 (1)	09.45(-6)	76.87(-6)	47.18(-2)
11	50.19(-2)	14.70(0)	81.99(0)	06.60(-3)	71.05(-3)	38.39(-2)
12	45.62(0)	07.12(-1)	71.48(-1)	03.13(-8)	64.67(-3)	29.01(-8)
13	40.37(-4)	63398.95(-2)	60.32(-5)	57399.25(	57.75(-6)	19.15(-8)
14	34.50(-5)	90.15(2)	48.58(-3)	94.82(4)	50.32(-5)	08.77(-7)
15	28.10(4)	80.72(0)	36.4(2)	89.73(-2)	42.35(-5)	57297.86(-6)
16	21.00(7)	70.64(2)	23.27(6)	84.12(-7)	33.84(-6)	86.43(-3)
17	13.25(9)	60.01(3)	09.59(3)		24.82(3)	74.49(1)
18	04.70(-6)	48.58(1)	63295.34(6)	71.0 (-4)	15.24(-3)	61.90(-5)
19	63395.70(1)	36.5 (1)	80.42(5)	64.21(0)	05.13(-2)	48.82(-6)
20	86.1 (1)	23.3 (2)	64.84(4)		57294.43(-5)	35.2 (-1)
21	75.44(-9)	10.75(0)	48.41(-9)		83.22(-5)	
22	64.28(-3)	63296.81(-3)	31.82(9)		71.42(-8)	06.45(5)
23		82.22(-4)			59.09(-9)	
24		67.00(0)			46.27(1)	
25					32.71(1)	
26					18.0 (-4)	

TABLE 4.1 (Continued)

Band	2-6		
J	R(J)	Q(J)	P(J)
0			
1	55444.75(-6)		
2	46.75(-4)	55437.89(2)	55431.98(4)
3	48.27(0)	36.48(9)	
4	49.25(1)	34.39(0)	
5	49.76(3)	31.98(8)	17.11(4)
6	49.76(5)	28.93(4)	11.2 (1)
7	49.25(7)	25.32(2)	04.69(2)
8	48.3 (1)	21.64(3)	55397.77(5)
9	46.8 (1)	17.11(6)	90.32(4)
10	44.8 (1)	12.12(7)	82.35(1)
11	42.2 (1)	06.62(5)	73.90(0)
12	39.07(-3)	00.62(3)	65.03(7)
13	35.54(-2)	55394.2 (1)	55.53(0)
14	31.8 (2)	87.18(5)	45.60(0)
15	27.2 (1)	79.68(3)	35.15(-1)
16		71.72(6)	24.22(-2)
17	16.42(3)	63.24(7)	12.9 (1)
18		54.21(4)	
19	03.9 (2)	44.75(8)	
20		34.69(4)	
21		24.22(9)	

[a]The number in parentheses represents (ν_{obs}-ν_{cal}) in the last digit.

TABLE 4.2 Vacuum wavenumbers (in cm^{-1}) of the rotational lines of 1-4 and 1-5 bands of the fourth positive (A-X) system of $^{13}C^{18}O$[a]

Band	1-4			1-5		
J	R(J)	Q(J)	P(J)	R(J)	Q(J)	P(J)
0						
1	58150.69(-3)					
2	52.61(2)				56196.24(1)	
3	53.93(-3)	58142.47(0)			94.87(4)	
4		40.3 (-1)			92.95(0)	
5		37.94(-5)		56207.90(5)	90.59(-2)	
6	55.11(1)	34.96(-3)		07.90(-1)	87.76(-4)	
7	54.51(4)	31.47(-3)	58111.42(3)		84.49(-3)	56164.47(5)
8	53.31(-4)	27.46(-5)	04.48(-6)	06.65(4)	80.76(-2)	57.86(6)
9	51.81(8)	22.8 (-2)	58097.13(-5)	05.27(0)	76.52(-4)	50.73(1)
10	49.57(-4)	17.95(-8)	89.27(-6)	03.47(2)	71.88(1)	43.19(3)
11	47.2 (2)	12.54(-1)	80.91(-6)	01.15(-1)	66.74(2)	35.09(-5)
12	43.87(1)	06.55(-1)	72.11(-1)	56198.39(0)	61.11(2)	26.61(-5)
13	40.3 (1)	00.03(-5)	62.74(-4)	95.17(1)	55.01(1)	
14	36.14(3)	58093.07(-2)	52.87(-6)	91.51(5)	48.44(0)	
15	31.47(-1)	85.60(0)	42.61(3)	87.32(3)	41.42(1)	
16	26.35(1)	77.61(-1)	31.75(1)	82.71(7)	33.89(-2)	56088.06(3)
17	20.68(-3)	69.12(-1)	20.39(-1)		25.90(-4)	77.19(-1)
18	14.55(-3)	60.13(-1)	08.53(-3)		17.56(7)	
19	07.83(-9)	50.63(-1)	57996.26(4)		08.61(4)	
20	00.72(-5)	40.67(2)			56099.22(4)	
21		30.16(1)			89.31(-1)	
22		19.3 (1)			78.97(-1)	
23		07.8 (1)				
24		57995.54(-8)				

[a]The number in parentheses represents $(\nu_{obs}-\nu_{cal})$ in the last digit.

crossings of the A $^1\Pi$, v=0 to 13 levels with the nearby states. We have now obtained similar perturbation diagrams for the A $^1\Pi$, v=0 to 5 levels of $^{12}C^{18}O$ and $^{13}C^{18}O$ using the data of Field (1971) and the isotopic relations (Dunham, 1932). These diagrams are presented in Figs. 4.2 and 4.3 for $^{12}C^{18}O$ and $^{13}C^{18}O$, respectively. It is evident from these figures that the calculated values for the corresponding energy levels can be obtained from the eigenvalues of a specific energy matrix which includes the perturbed state and the perturbing states. The eigenvectors of the appropriate energy matrix are obtained from the wavefunctions which are expressed as a linear combination of several wavefunctions of interacting states. The coefficients C_a that appear in the linear combinations are called the mixing coefficients (see Chapter 3). Accurate values of the mixing coefficients are very useful to analyze the life time measurements of short-lived ($^1\Pi$) and long-lived triplet (a′ $^3\Sigma^+$, d $^3\Delta_i$, e $^3\Sigma^-$) levels.

In the present work, the occurrence of perturbations are mainly due to the interconfigurational interactions. For these interactions the operators H_{RE} and H_{SO} play a very important role. The selection rules for H_{RE} (Lefebvre-Brion and Field, 1986) are

$$\Delta S = 0, \quad \Delta\Sigma = 0, \quad \Delta\Lambda = \Delta\Omega = \pm 1, \qquad [4.5]$$

where S is the spin angular momentum quantum number, Σ, Λ, and Ω are respectively the projection quantum numbers of the spin, orbital and total electronic angular momenta onto the internuclear axis. For the operator H_{SO}, the first term in Eq. [4.4] contributes to the interconfigurational interactions. The selection rules for H_{SO} (Lefebvre-Brion and Field, 1986) are

$$\Delta S = 0, \pm 1: \quad \Delta\Lambda = -\Delta\Sigma = \pm 1; \quad \Lambda\Omega = 0. \qquad [4.6]$$

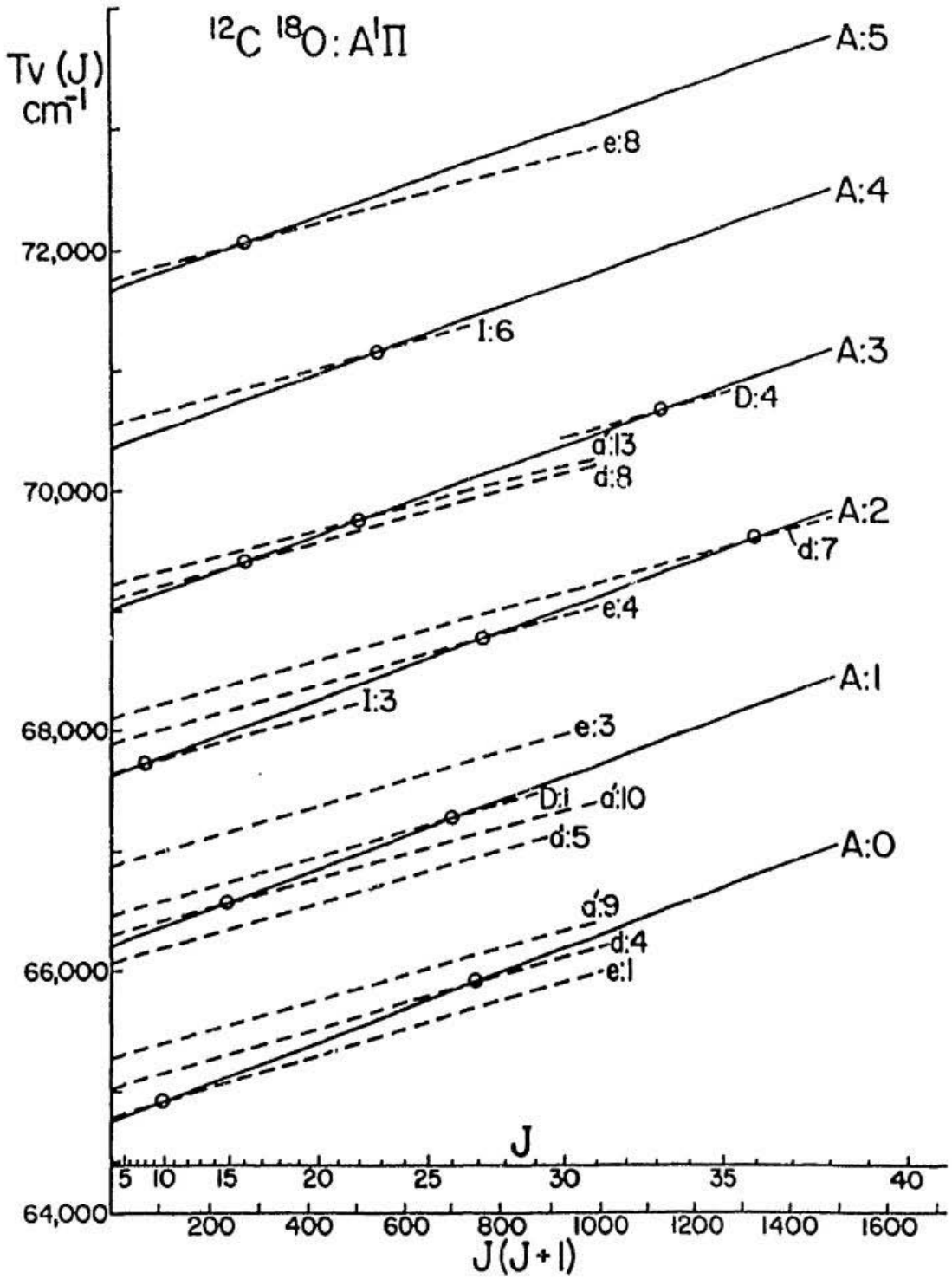

Figure 4.2 Perturbation diagram of $^{12}C^{18}O$ for A $^1\Pi$, v=0 to 5. The term values $T_v(J)$ are relative to X $^1\Sigma^+$, v=0 and J=0.

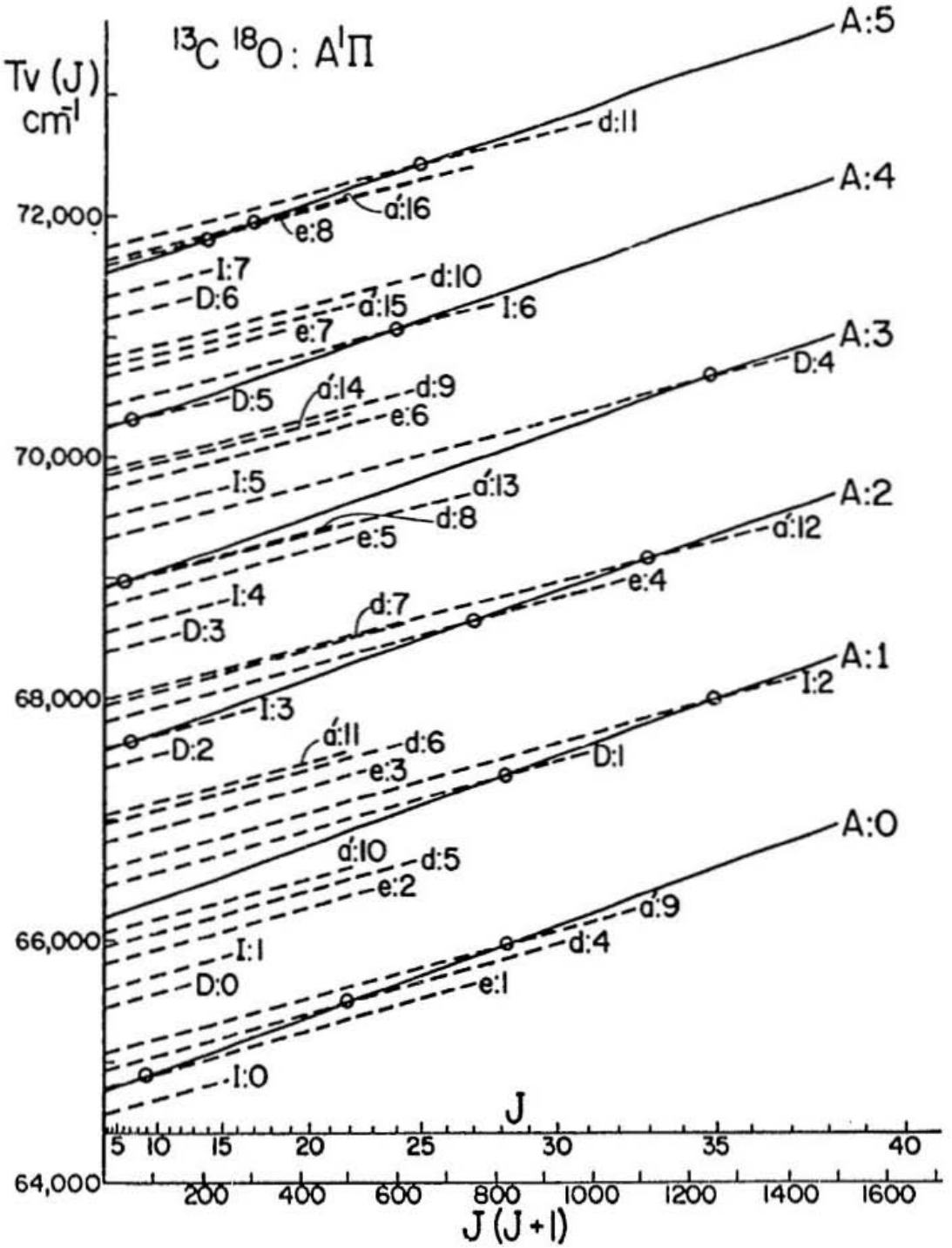

Figure 4.3 Perturbation diagram of $^{13}C^{18}O$ for A $^1\Pi$, v=0 to 5. The term values $T_v(J)$ are relative to X $^1\Sigma^+$, v=0 and J=0.

Field (1971) and Field et al. (1972 a,b) have concluded from the analysis of the perturbations in the a $^3\Pi$ and A $^1\Pi$ states of $^{12}C^{16}O$ that the perturbation matrix element (α, β) is the product of a vibrational factor and a constant electronic perturbation parameter (**a**, **b**). The parameters **a** and **b** are characteristic of the relevant electronic configurations within the single configuration approximation. Hall et al. (1973) from the *ab initio* calculations have shown that the constants (**a**, **b**) are strongly dependent on the internuclear separation of the molecule. The effective perturbation parameters α and β that are fitted to the present set of experimental data are defined in the e/f basis set by the following set of equations (Lefebvre-Brion and Field, 1986) (same as Eq.[3.53]):

$$\alpha_{A,e} = \langle A\ ^1\Pi,\ v_A \,|\, H_{SO} \,|\, e\ ^3\Sigma^-,\ v_e \rangle = -(1/4)\ \mathbf{a}\ \langle v_A \,|\, v_e \rangle$$

$$\alpha_{A,a'} = \langle A\ ^1\Pi,\ v_A \,|\, H_{SO} \,|\, a'\ ^3\Sigma^+,\ v_{a'} \rangle = (1/4)\ \mathbf{a}\ \langle v_A \,|\, v_{a'} \rangle$$

$$\alpha_{A,d} = \langle A\ ^1\Pi,\ v_A \,|\, H_{SO} \,|\, d\ ^3\Delta,\ v_d \rangle = -(\sqrt{2}/4)\ \mathbf{a}\ \langle v_A \,|\, v_d \rangle$$

$$2\ \beta_{A,I}\sqrt{x} = \langle A\ ^1\Pi,\ v_A \,|\, H_{RE} \,|\, I\ ^1\Sigma^-,\ v_I \rangle = -\sqrt{x}\ \mathbf{b}\ \langle v_A \,|\, B \,|\, v_I \rangle$$

$$\beta_{A,D}\sqrt{x-2} = \langle A\ ^1\Pi,\ v_A \,|\, H_{RE} \,|\, D\ ^1\Delta,\ v_D \rangle = \sqrt{x-2}\ \mathbf{b}\ \langle v_A \,|\, B \,|\, v_D \rangle, \qquad [4.7]$$

where $x = J(J+1)$, $\mathbf{a} = \langle 2\pi \,|\, al^+ \,|\, 2\sigma \rangle$, and $\mathbf{b} = \langle 2\pi \,|\, l^+ \,|\, 2\sigma \rangle$. From the known vibrational wavefunctions, the initial values of the coupling terms α and β for any pair of levels can be calculated.

(c) Fitting procedure

The neighbouring levels which cross with the A $^1\Pi$, v=1 and 2 levels of $^{12}C^{18}O$ and those with the A $^1\Pi$, v=1 of $^{13}C^{18}O$ are shown with circles in Fig. 4.2 and 4.3, respectively. These are summarized below.

$^{12}C^{18}O$, $A\ ^1\Pi$, v=1; $a'\ ^3\Sigma^+$, v=10; $D\ ^1\Delta$, v=1;

$A^1\Pi$, v=2; $I\ ^1\Sigma^-$, v=3; $e\ ^3\Sigma^-$, v=4; $d\ ^3\Delta$, v=7.

$^{13}C^{18}O$, $A\ ^1\Pi$, v=1; $D\ ^1\Delta$, v=1; $I\ ^1\Sigma^-$, v=2.

The perturbing levels interact with the vibrational levels of the A state at different J values and the dimension of the appropriate energy matrix depends on the J range considered. The Hamiltonian matrix used in the present analysis contains not only the perturbing levels which cross the A state levels but also those which interact strongly with them. The present experimental data for the A, v=1 level of $^{12}C^{18}O$ and $^{13}C^{18}O$ which involve four vibrational levels for the former and three vibrational levels for the latter were fitted satisfactorily to the eigen values of a 31 × 31 energy matrix. Also our data for the A, v=2 level of $^{12}C^{18}O$ which involve one perturbed and seven perturbing levels were fitted successfully to the eigenvalues of a 33 × 33 energy matrix. In these fittings, the observed wavenumbers were fitted to the energy matrix by an appropriate weighted nonlinear least-squares method with the help of a computer program (see Appendix A of Ref. (Le Floch et al., 1987 for details). This program, which includes an iterative process, combines Marquardt's algorithm with the Helmann-Feymann theorem. In this program the following main steps are adopted: initial values of the matrix were calculated and the matrix is then diagonalized; the eigenvalues or the differences between them are compared with the experimental measurements of the wavenumbers of the rotational structure; corrections to the molecular parameters are calculated; and the final iteration is carried out until the convergence of the parameters is obtained. At the last stage of this procedure, the wavenumbers (ν_{cal}) from Eq. [4.1] and the mixing coefficients are

calculated. The (ν_{obs}-ν_{cal}) values of the rotational structure of the analyzed bands thus obtained are listed in parentheses in Tables 4.1 and 4.2. The final values of the dimensionless variance σ^2 are 1.3 for v=1, and 0.8 for v=2, of $^{12}C^{18}O$, and 2.7 for v=1 of $^{13}C^{18}O$.

4.4 Results and Discussion

(a) Perturbations in $^{12}C^{18}O$

A $^1\Pi$, **v=1**:

The occurrence of perturbations in the observed rotational structure of bands is visually exhibited by a plot of the deviation $|T(v,J)_{obs} - T(v,J)_{cal}|$ versus the rotational quantum number J. Such a plot for the A, v=1 level of $^{12}C^{18}O$ is shown in Fig. 4.4. In this figure strong discontinuities are noted at J=12/13, 14/15, and 17/18 and these are characteristic of strong spin-orbit interaction H_{SO} between the A $^1\Pi$, v=1 level and the a′ $^3\Sigma^+$, v=10 level. It should be noted that for $^3\Sigma^+$ states the J-crossing (J_c) occurs for the F_2 (parity e) components whereas the F_1 and F_2 (both of parity f) components have lower and higher J_c′s, respectively. This mixing has yielded an extra line |Q(12) 57 941.14 cm^{-1}| (see Table 4.1) which belongs to the intercombination band a′ $^3\Sigma^+$ (v=10) -X $^1\Sigma^+$ (v=5). Apart from the strong a′ $^3\Sigma^+$ - A $^1\Pi$ perturbation, the interaction between D $^1\Delta$, v=1 and A $^1\Pi$, v=1 gives rise to an additional perturbation near J=27, which characterizes rotation-electronic interaction H_{RE}. The fitted values of the vibrational terms T_v for the A $^1\Pi$, v=1, a′ $^3\Sigma^+$, v=10 and D $^1\Delta$, v=1 levels and the rotational constants B for the A, v=1 and a′, v=10 level are given in Table 4.3. Also listed in this table are the fitted perturbation parameters $\alpha^{a'}_{1,10}$ and $\beta^{D}_{1,1}$, which are determined for the first time. The values of the

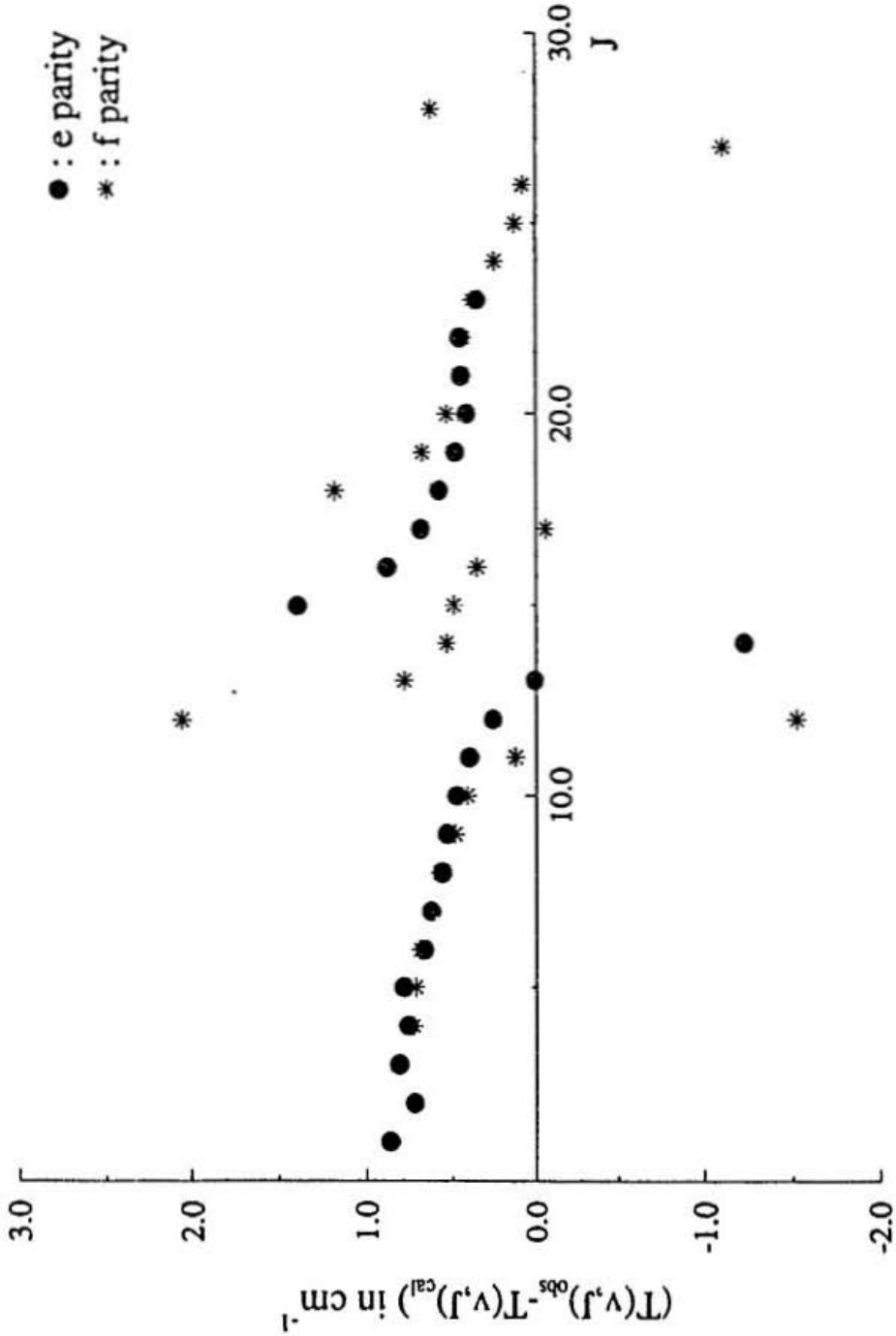

Figure 4.4 Plot of deviations [$T(v,J)_{obs}$ - $T(v,J)_{cal}$] of the rotational levels versus J in A $^1\Pi$, v=1 of $^{12}C^{18}O$.

TABLE 4.3 Molecular parameters[a] (in cm^{-1}) of the A $^1\Pi$, v=1 state and the perturbing states D $^1\Delta$, a′ $^3\Sigma^+$ and d $^3\Delta$ of $^{12}C^{18}O$.

Molecular Parameter	A $^1\Pi$ v=1	D $^1\Delta$ v=1	a′ $^3\Sigma^+$ v=10	d $^3\Delta$ v=5
T	66202.946(6)	66461.2(9)		-
T_1	-	-	66288.2(1)	66029.71[b]
T_2	-	-	-	66063.18[b]
T_3	-	-	-	66096.65[b]
B	1.50658(3)	1.17241[b]	1.1140(7)	1.16052[b]
$D \times 10^6$	6.8[b]	6.3[b]	5.7[b]	5.8[b]
α	-	-	2.91(1)	-9.8[b]
β	-	-0.085(9)	-	-
$\gamma \times 10^3$	-	-	-7.2[b]	-8.3[b]
λ	-	-	-1.1[b]	1.2[b]
$A_D \times 10^4$	-	-	-	-1.0[b]

[a]The number in parentheses indicates the uncertainty in the last digit and corresponds to one standard deviation.
[b]Fixed constants in the least squares fit are taken from Field (1971).

fixed parameters which were used in the least squares fit are also given in Table 4.3.

Perturbations occurring in the A $^1\Pi$, v=1 level are also represented in Fig. 4.5. In this figure the percentage $^1\Pi$ character of each rotational level is plotted against J for both e and f parities for the A $^1\Pi$, v=1 level as well as for the a′ $^3\Sigma^+$, v=10 state. These quantities are equal to 100 C_{ik}^2, where C_{ik} (= $\langle\phi_k | \psi_i\rangle$) is the mixing coefficient extracted from the eigenvectors of the energy matrix from the final diagonalization which uses the values of the fitted parameters. In Fig. 4.5 the percentage $^1\Pi$ character greater than 50 is concerned with the levels having dominant $^1\Pi$ character whereas it is less than 50 for the perturbing a′ $^3\Sigma^+$, v=10 level. The $^1\Pi$ character of A, v=1 drops to 65% for J=12, and for a′, v=10 it reaches 34% for the F_1(f) component. The dips at J=14 and J=18 are due to the crossing of the F_2(e) component and F_3(f) component of the perturbing a′, v=10 level (see Herzberg, 1991). A weak perturbation occurs between the D, v=1 and A, v=1 levels at J=27 for which the $^1\Pi$ character of the A state drops to 73% with no extra lines. For the A $^1\Pi$, v=1 rotational levels, the percentages of singlet and triplet character are presented in Table 4.4. These values are of importance for the determination of life-times of the A $^1\Pi$ state.

A $^1\Pi$, v=2:

As seen in Fig. 4.2, the I, v=3, e, v=4, and d, v=7 levels cross the A, v=2 level at J=7/8, 27/28, and 36/37, repectively. A plot of deviation $[T(v,J)_{obs} - T(v,J)_{cal}]$ versus J for A, v=2 level is given in Fig. 4.6. It is seen from this figure the deviation is largest for J=26 and is due to the perturbing e, v=4 level. The fitted values T_v and B of A, v=2, T_v of I, v=3 are given in Table 4.5. Also given in this table are the fitted perturbation

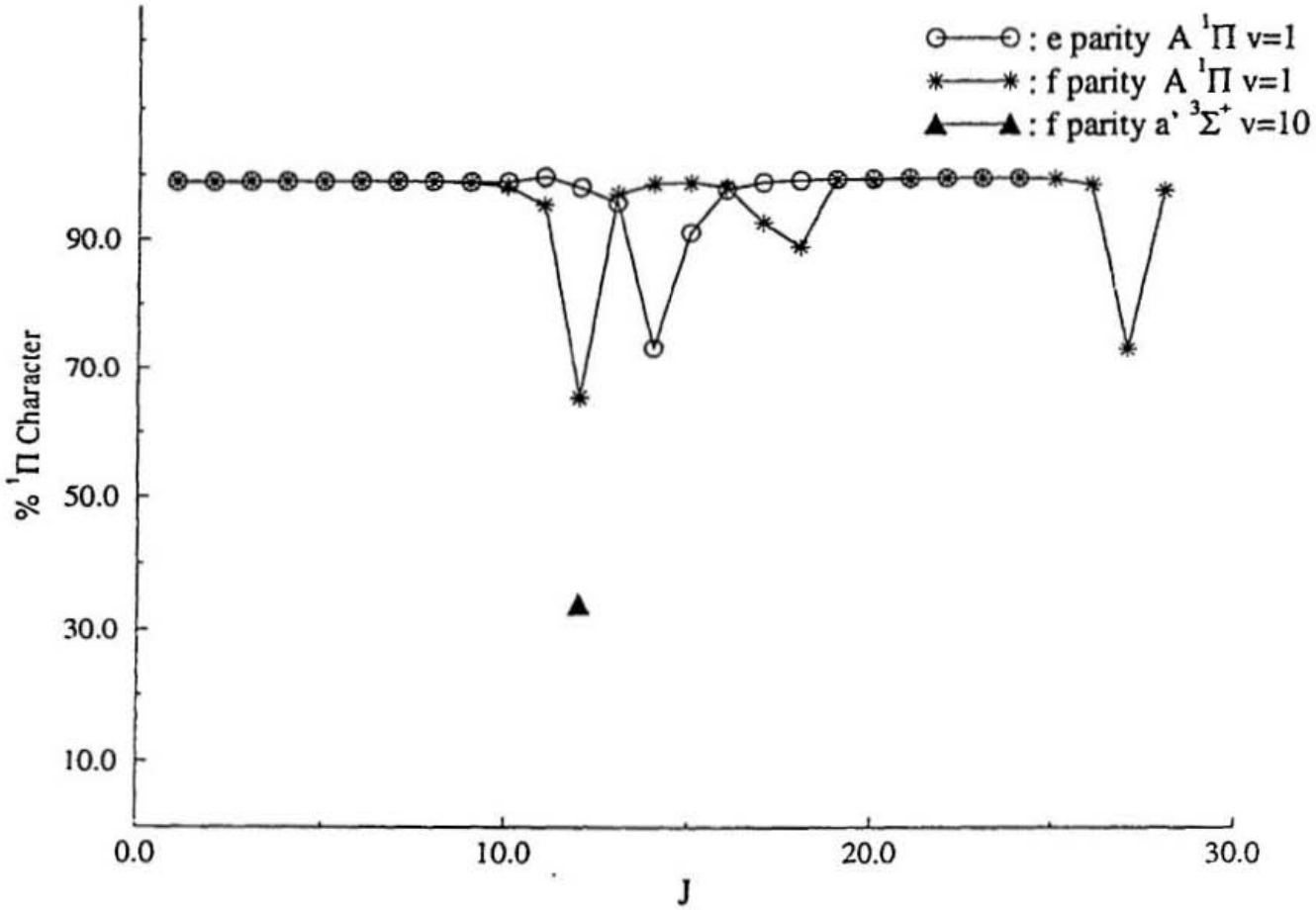

Figure 4.5 Percentage $^{1}\Pi$ character versus J for the e and f parity levels of A $^{1}\Pi$, v=1 and the f parity level of a' $^{3}\Sigma^{+}$, v=10 of $^{12}C^{18}O$

TABLE 4.4 Percentage of the squares of mixing coefficients of A $^1\Pi$, v=1 and 2 and a′ $^3\Sigma^+$, v=10 of $^{12}C^{18}O$ and A $^1\Pi$, v=1 of $^{13}C^{18}O$

	$^{12}C^{18}O$					$^{13}C^{18}O$	
	A $^1\Pi$		a′ $^3\Sigma^+$	A $^1\Pi$		A $^1\Pi$	
	v=1		v=10	v=2		v=1	
J	e	f	f	e	f	e	f
1	99.0	99.0		99.9			
2	99.1	99.1		99.9	99.9	99.7	99.7
3	99.1	99.1		99.9	99.9	99.7	99.7
4	99.1	99.1		99.9	99.8	99.7	99.7
5	99.1	99.1		99.9	99.7		99.7
6	99.1	99.1		99.9	99.3	99.7	99.7
7	99.2	99.1		99.9	94.1	99.7	99.7
8	99.2	99.1		99.9	95.7	99.7	99.7
9	99.1	98.9		99.9	99.2	99.8	99.8
10	99.1	98.4		99.9	99.6	99.8	99.8
11	98.8	95.6		99.9	99.7	99.8	99.8
12	98.2	65.4	34.1	99.9	99.8	99.8	99.8
13	95.9	97.3		99.8	99.8	99.8	99.8
14	73.3	98.8		99.8	99.8	99.8	99.8
15	91.2	99.0		99.8	99.8	99.8	99.8
16	98.0	98.4		99.8	99.8	99.9	99.9
17	99.0	92.8		99.7	99.7	99.9	99.9
18	99.4	89.0		99.7	99.7	99.9	99.9
19	99.6	98.5		99.6	99.7	99.9	99.9
20	99.7	99.4		99.5	99.6	99.9	99.9
21	99.7	99.6		99.3	99.5	99.9	99.9
22	99.8	99.7		98.8	99.4		99.9
23	99.8	99.7		97.3	99.2		99.9
24	99.7	99.7			98.8		99.9
25		99.5			98.0		
26		98.7			95.9		
27		73.2					
28		97.8					

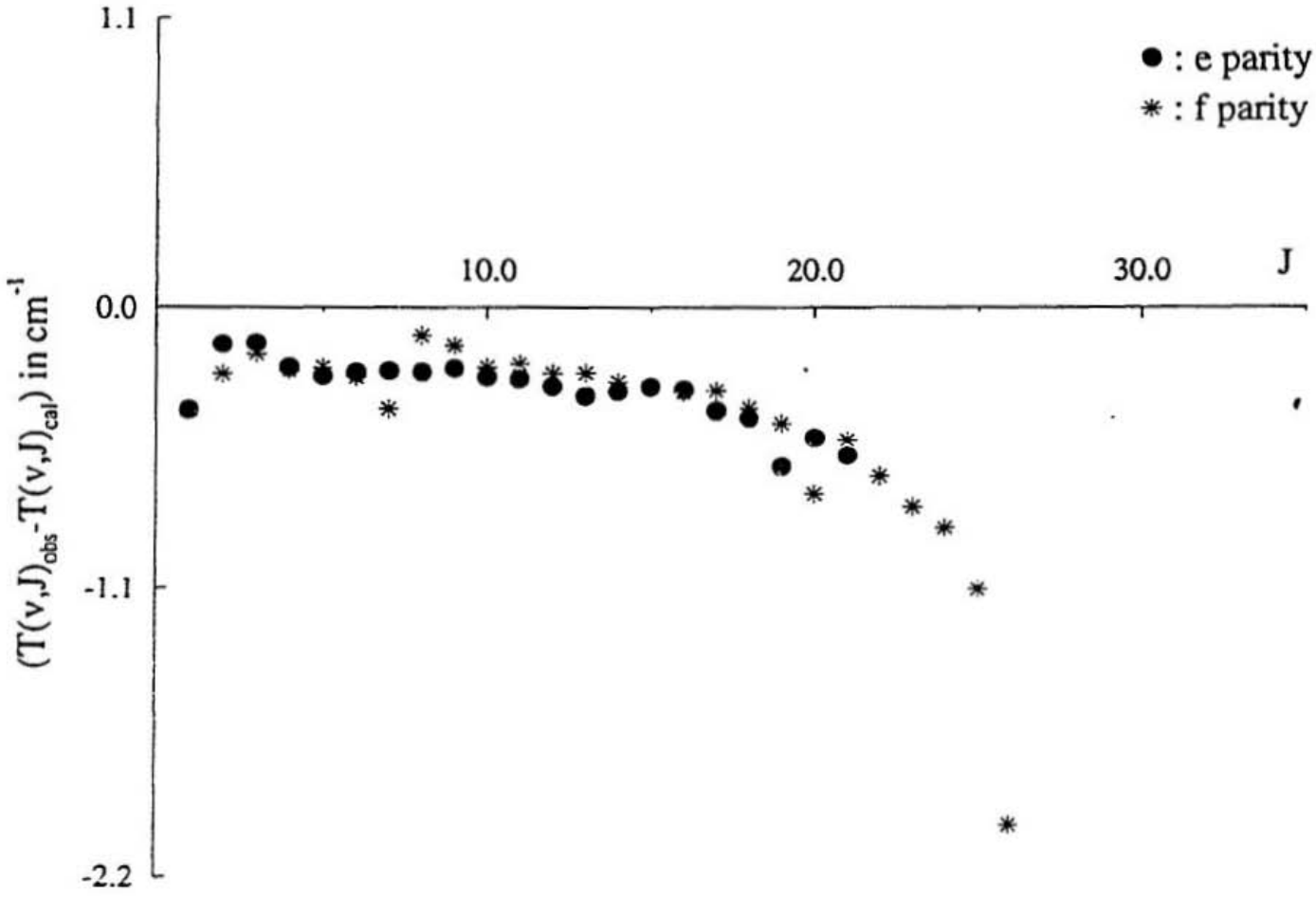

Figure 4.6 Plot of deviations $[T(v,J)_{obs} - T(v,J)_{cal}]$ of the rotational levels versus J in A $^1\Pi$, v=2 of $^{12}C^{18}O$.

TABLE 4.5 Molecular parameters[a] (in cm^{-1}) of the A $^1\Pi$, v=2 state and the perturbing states I $^1\Sigma^-$, D $^1\Delta$, a' $^3\Sigma^-$, e $^3\Sigma^-$ and d $^3\Delta$ of $^{12}C^{16}O$

Molecular Parameter	A $^1\Pi$ v=2	I $^1\Sigma^-$ v=3	D $^1\Delta$ v=3	a' $^3\Sigma^+$ v=11	a' $^3\Sigma^+$ v=12	e $^3\Sigma^-$ v=4	d $^3\Delta$ v=7	d $^3\Delta$ v=8
T	67616.78(1)	67636.0(6)	68431.42[b]	-	-	-	-	-
T_1	-	-	-	-	-	-	68068.63[b]	67058.23[b]
T_2	-	-	-	67277.87[b]	68249.47[b]	67884.44[b]	68102.72[b]	67092.05[b]
T_3	-	-	-	-	-	-	68136.81[b]	67125.87[b]
B	1.48522(6)	1.15147[b]	1.13967[b]	1.09856[b]	1.08361[b]	1.14897[b]	1.12927[b]	1.14482[b]
$D \times 10^6$	6.9[b]	6.3[b]	6.3[b]	5.7[b]	5.7[b]	6.3[b]	5.7[b]	5.8[b]
α	-	-	-	3.9[b]	-3.2[b]	7.3(3)	6.2[b]	-8.3[b]
β	-	0.040(3)	-0.04[b]	-	-	-	-	-
$\gamma \times 10^1$	-	-	-	-	-	-3.4[b]	-8.3[b]	-8.3[b]
λ	-	-	-	-1.1[b]	-1.1[b]	0.7[b]	1.2[b]	1.3[b]

[a]The number in parentheses indicates the uncertainty in the last digit and corresponds to one standard deviation.
[b]Fixed constants in the least squares fit are taken from Field (1971).

parameters $\alpha^{e}_{2,4}$ and $\beta^{i}_{2,3}$ which are determined for the first time. The values of the fixed parameters used in the least-squares fit are also listed in Table 4.5. Even though the I, v=3 level crosses the A, v=2 level at the low value of J=7/8, the corresponding $|T(v,J)_{obs} - T(v,J)_{cal}|$ is significant (Fig. 4.6). The dip corresponding to this perturbation is seen clearly in Fig. 4.7 in which the percentage $^1\Pi$ character is plotted against J. In Fig. 4.7 additional dips at J=24 and 26 are also seen, arising from the interaction between the A, v=2 and e, v=4 levels. The values of the percentage $^1\Pi$ character for the rotational level of A, v=2 for both e and f parities are given in Table 4.4.

(b) Perturbations in $^{13}C^{18}O$

A $^1\Pi$, v=1:

The perturbation diagram given in Fig. 4.3 for $^{13}C^{18}O$ shows the location of the crossings of the A $^1\Pi$ v=0 to 5 levels. It is clear from this figure that the A, v=1 level is perturbed by the D, v=1 level at J=28 and the I, v=2 level at J=35/36. Unlike the 1-4 and 1-5 bands of $^{12}C^{18}O$ which are strongly perturbed by the a′, v=10 level, the corresponding bands of $^{13}C^{18}O$ do not show any perturbation by the a′, v=10 level because of the large difference in their energies. The trend appearing in Fig. 4.8 characterizes the interaction due to the nearby levels of a′,v=10 and d $^3\Delta$, v=5, located just below the A, v=1 level. The corresponding drop appears also in Fig. 4.9 where the percentage $^1\Pi$ character of the e and f levels is shown. The fitted values of T_v, B and D of A, v=1 and the values of the fixed parameters are given in Table 4.6. The values of the percentage $^1\Pi$ character for the rotational levels of A, v=1 are listed in Table 4.4.

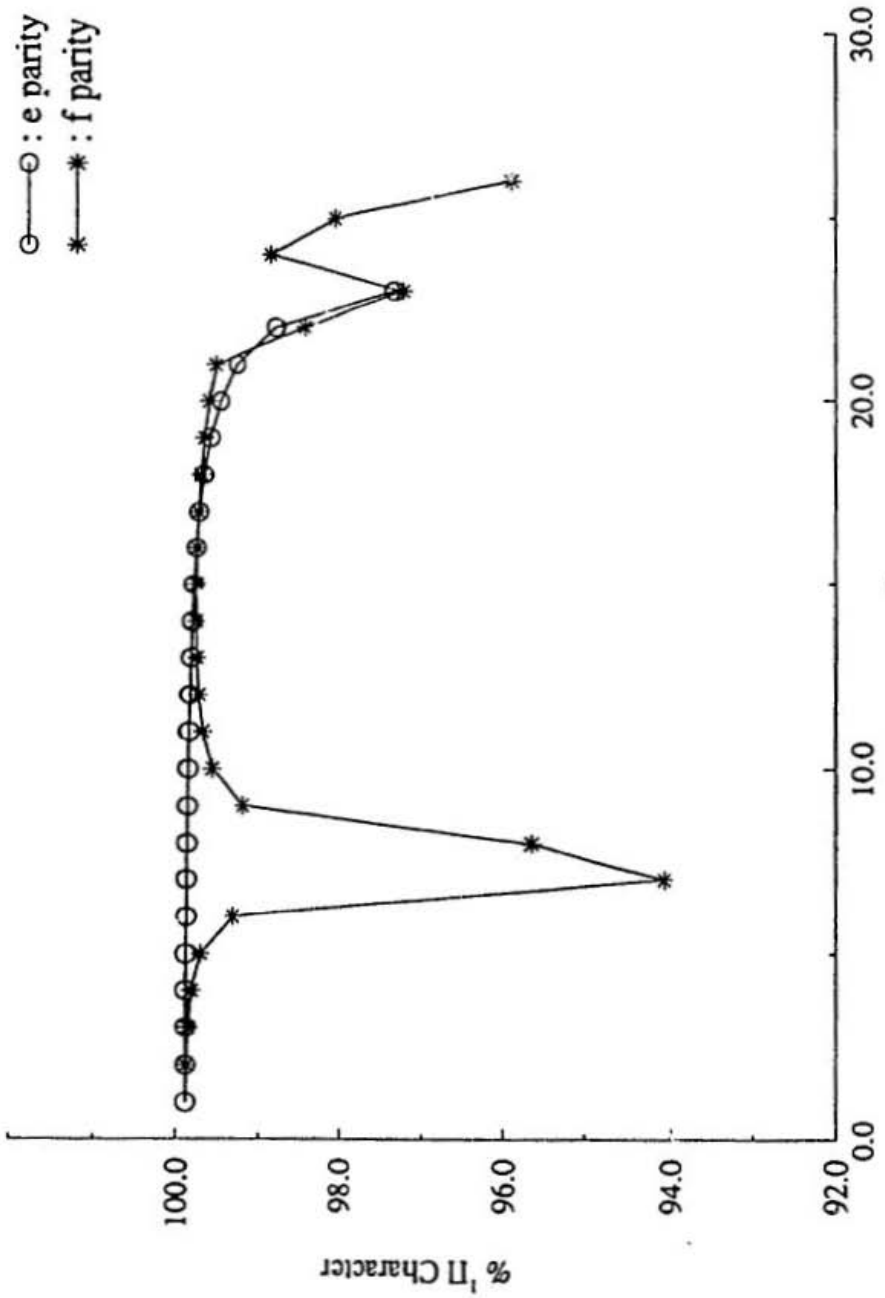

Figure 4.7 Percentage $^1\Pi$ character versus J for the e and f parity levels of A $^1\Pi$, v=2 of $^{12}C^{18}O$

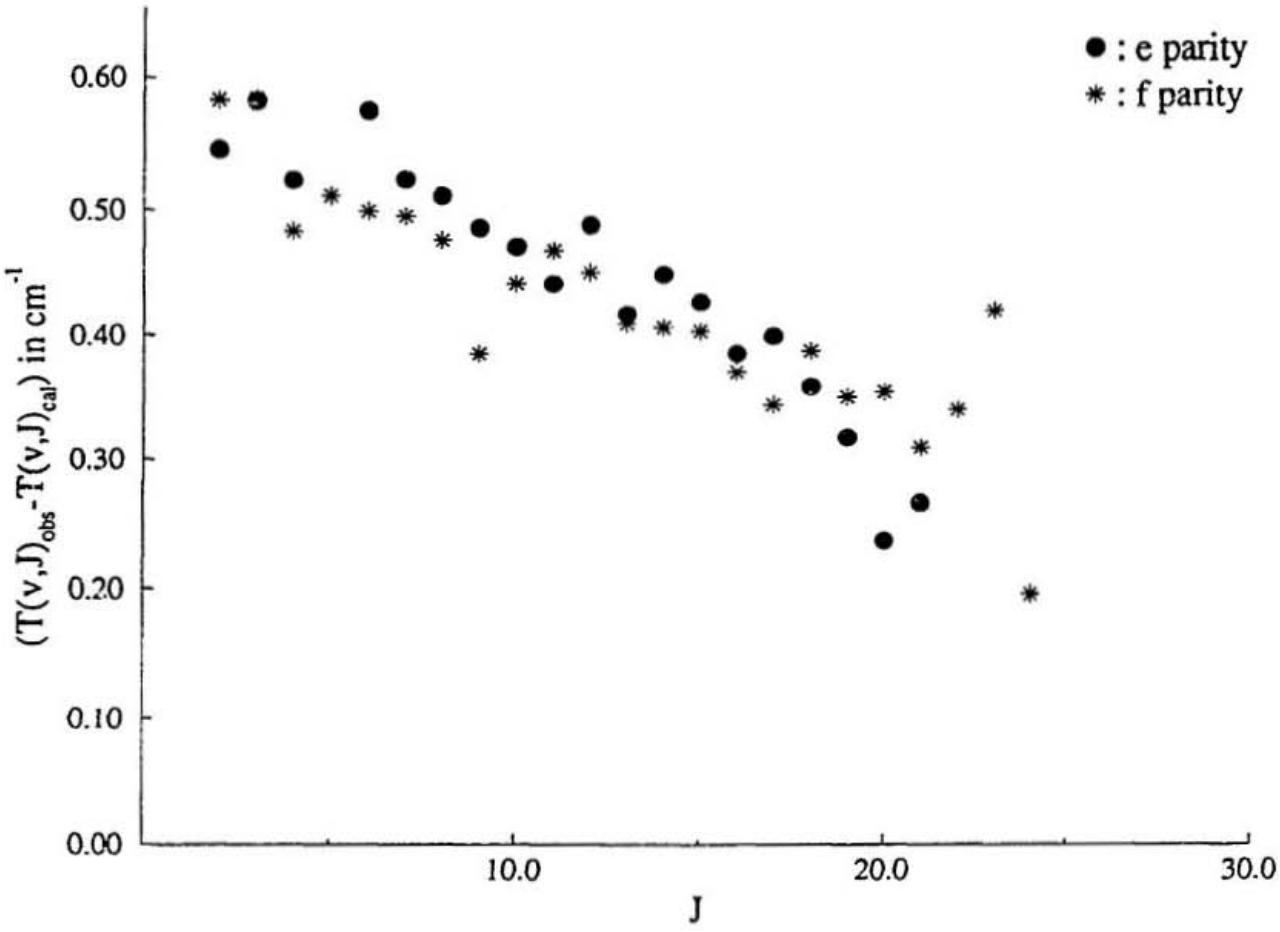

Figure 4.8 Plot of deviations $[T(v,J)_{obs} - T(v,J)_{cal}]$ of the rotational levels versus J in A $^1\Pi$, v=1 of $^{13}C^{18}O$.

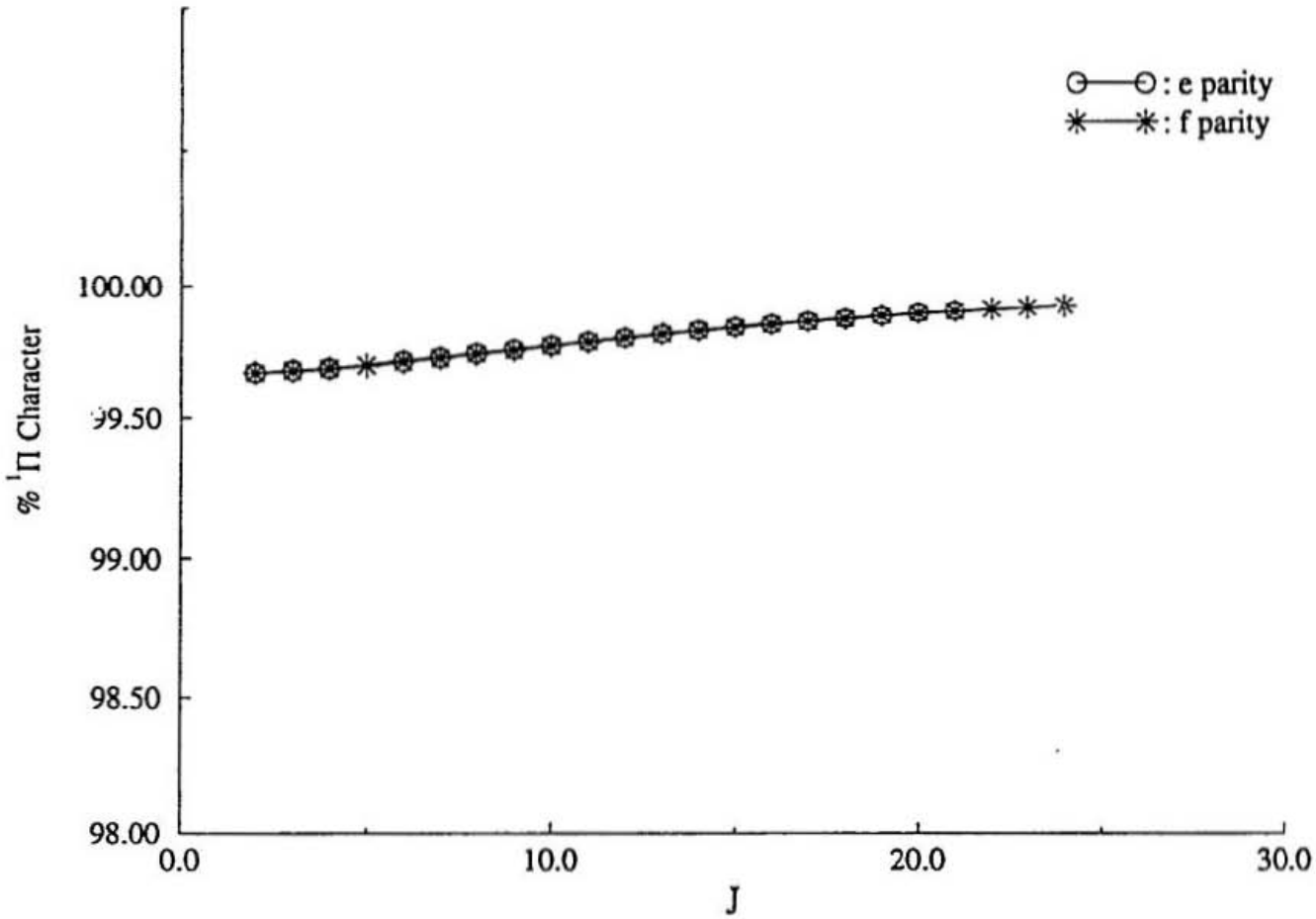

Figure 4.9 Percentage $^{1}\Pi$ character versus J for the e and f parity levels of A $^{1}\Pi$, v=1 of $^{13}C^{18}O$

TABLE 4.6 Molecular parameters[a] (in cm^{-1}) of the A $^1\Pi$, v=1 state and the perturbing states a′ $^3\Sigma^+$ and d $^3\Delta$ of $^{13}C^{18}O$.

Molecular Parameter	A $^1\Pi$ v=1	a′ $^1\Sigma^+$ v=10	d $^3\Delta$ v=5
T	66177.045(6)	-	-
T_1	-	-	65920.490[b]
T_2	-	66066.930[b]	65953.960[b]
T_3	-	-	65987.430[b]
B	1.43748(4)	1.06557[b]	1.11087[b]
$D \times 10^6$	6.6(1)	5.2[b]	5.3[b]
α	-	2.8[b]	-9.8[b]
$\gamma \times 10^3$	-	-7.2[b]	-8.3[b]
λ	-	-1.1[b]	1.2[b]
$A_D \times 10^4$	-	-	-1.0[b]

[a]The number in parentheses indicates the uncertainty in the last digit and corresponds to one standared deviation.

[b]Fixed constants in the least squares fit are taken from Field (1971).

(c) Electronic perturbation parameters

The electronic perturbation parameters **a** and **b** (Eq. |4.7|) were extracted from the fitted spin-orbit parameter α and the rotation-electronic parameter β, and are presented in Table 4.7. The overlap integrals $\langle v_\Lambda \mid v_p \rangle$, and $\langle v_\Lambda \mid B \mid v_p \rangle$ calculated by Field and quoted by Le Floch (1989) for $^{12}C^{16}O$ were used in the present work because the overlap integrals are the same for all isotopomers in the first approximation. Table 4.7 shows that the present results are consistent with those obtained previously. For example, the spin orbit parameter **a** = 88.6(3) cm^{-1} for the a′-A interaction is in agreement with the values given by Field (1972b) and LeFloch (1989). As expected, we note that this value is smaller than the one obtained for the e-A interaction (98(4) cm^{-1}). For the rotation-electronic parameter **b** our value 0.212(16) cm^{-1} for the I-A interaction is very similar to the results of Field and Le Floch. Finally, for the D-A interaction, our value of **b** = 0.137(15) cm^{-1} confirms the smaller value (about a half of the one for the I-A or I-a) previously obtained by Le Floch et al. (1987).

4.5 Conclusions

High resolution measurements of five bands of $^{12}C^{18}O$ and two bands of $^{13}C^{18}O$ of their Fourth Positive System have been carried out. With these data it was possible to extend the analysis up to J=28 for A $^1\Pi$, v=1, and J=26 for v=2, of $^{12}C^{18}O$ and J=26 for v=1 of $^{13}C^{18}O$. The present analysis provides accurate deperturbed constants for the state A. Mixing coefficients C_{ik} and electronic perturbation parameters **a** and **b** have also been

TABLE 4.7 Spin-orbit and rotation-electronic parameters obtained from perturbations of the A $^1\Pi$, v=1 and 2 levels of $^{12}C^{18}O$ and v=1 level of $^{13}C^{18}O$

Perturber	v_p	$\langle v_A \vert v_p \rangle$[a]	α (cm^{-1})	a (cm^{-1})	$\langle v_A \vert B \vert v_p \rangle$[a]	β (cm^{-1})	b (unitless)
$^{12}C^{18}O$							
				A $^1\Pi$, v=1			
a' $^3\Sigma^+$	10	-0.1314	2.91(1)	88.6(3)			
d $^3\Delta$	5	0.2882	-9.75[b]	95.7			
D $^1\Delta$	1				-0.6223	-0.085(9)	0.137(15)
				A $^1\Pi$, v=2			
a' $^3\Sigma^+$	11	-0.1907	3.9[b]	82.4			
	12	0.1539	-3.2[b]	84.0			
e $^3\Sigma^-$	4	-0.2976	7.3(3)	98(4)			
d $^3\Delta$	7	-0.1880	6.2[b]	93.3			
	8	0.2460	-8.3[b]	95.7			
I $^1\Sigma^-$	3				0.3775	0.040(3)	0.212(16)
D $^1\Delta$	3				-0.3748	-0.042[b]	0.11
$^{13}C^{18}O$							
				A $^1\Pi$, v=1			
a' $^3\Sigma^+$	10	-0.1341	2.8[b]	84.6			
d $^3\Delta$	5	0.2882	-9.7[b]	95.7			

[a]Calculated by Field (private communication) and taken from Le Floch (1989)
[b]Fixed constants in the least-squares fit are taken from Field (1971).

estimated. The molecular parameters obtained in the present work are useful for the study of the abundance ratio of the CO isotopomers in several astrophysical objects and in interstellar space. The accurate term values of the A state obtained from the present work when combined with the data on the Ångström ($B\ ^1\Sigma^+ - A\ ^1\Pi$), the Herzberg ($C\ ^1\Sigma^+ - A\ ^1\Pi$) and ($E\ ^1\Pi - A\ ^1\Pi$) systems of $^{12}C^{18}O$ and $^{13}C^{18}O$, it will make it possible to estimate accurate term values and molecular constants for the Rydberg states B, C, and E. The results presented in this chapter have appeared in a publication (Haridass, C., Reddy, S.P., and Le Floch, A. C., *J. Mol. Spectrosc.*, **167**, 334 (1994)). A reprint of this paper is included in the Appendix.

REFERENCES

Authier, N., Bagland, N., and Le Floch, A. C., *J. Mol. Spectrosc.* **160**, 590 (1993).

Bergman, T., and Cossart, D., *J. Mol. Spectrosc.* **87**, 119 (1981).

Brown, J. M., Hougen, J. T., Huber, K. P., Johns, J. W. C., Kopp, I., Lefebvre-Brion, H., Merer, A. J., Ramsay, D. A., Rostas, J., and Zare, R.N., *J. Mol. Spectrosc.* **55**, 500 (1975).

Crosswhite, H. M., *J. Res. Nat. Bur. Stand.* **79** A, 17 (1975).

Deslandres, *C. R. Acad. Sci. (Paris)* **106**, 842 (1888).

Domin, J., *Acta. Phys. Hung.* **60**, 43 (1986).

Dunham, J L., *Phys. Rev.* **41**, 721 (1932).

Field, R. W., Ph.D thesis, Harvard University, 1971.

Field, R. W., Wicke, B. G., Simmons, J. D., and Tilford, S. G., *J. Mol. Spectrosc.* **44**, 383 (1972a).

Field, R. W., Tilford, S. G., Howard, R. A., and Simmons, J. D., *J. Mol. Spectrosc.* **44**, 347 (1972b).

Field, R. W., Unpublished vibrational integrals and r-centroids of CO: M. I. T, Cambridge, Massachusetts.

Garetz, B. A., Kittrell, C., and Le Floch, A. C., *J. Chem. Phys.* **94**, 843 (1991).

Haridass, C., and Huber, K. P., *Astrophys. J.* **420**, 433 (1994).

Haridass, C., Prasad, C. V. V., and Reddy, S. P., *Astrophys. J.* **388**, 669 (1992).

Hall, J. A., Schamps, J., Robbe, J. M., and Lefebvre-Brion, H., *J. Chem. Phys.* **59**, 3271

(1973).

Herzberg, G., "Molecular Spectra and Molecular Structure, I. Spectra of Diatomic Molecules," Krieger, Malabar, FL, (1991).

Huber, K. P., and Herzberg, G., "Molecular Spectra and Molecular Structure," IV. "Constants of Diatomic Molecules," van Nostrand-Reinhold, Princeton. N.J., 1979.

Huber, K. P., Klug, C. A., and Alberti, F., *J. Mol. Spectrosc.* **124**, 407 (1987).

Huber, K. P., Holland, F., and Coxon, J. A., *J. Chem. Phys.* **96**, 1005 (1992).

Kepa, R., *Acta Phys. Hung.* 60, 227 (1986).

Kepa, R., *Can. J. Phys.* **66**, 1012 (1988).

Krupenie, P. H., "The Band Spectum of Carbon Monoxide," Nat. Bur. Stand., NBS 5, Washington, D. C., 1966.

Lefebvre-Brion, H., and Field, R. W., "Perturbations in the Spectra of Diatonic Molecules," Academic Press, New York, 1986.

Le Floch, A. C., and Amiot, C., *Chem. Phys.* 97, 379 (1985).

Le Floch, A. C., Launay, F., Rostas, J., Field, R. W., Brown, C. M., and Yoshino, K., *J. Mol. Spectrosc.* **121**, 337 (1987).

Le Floch, A. C., Ph.D thesis, University Paris-Sud, Orsay, 1989.

Le Floch, A. C., *J. Mol. Spectrosc.* **155**, 177 (1992).

Malak, Z., Rytel, M., Janjić, J. D., and Pešić, D. S., *Acta. Phys. Hung.* **55**, 85 (1984).

Prasad, C. V. V., Bhale, G. L., and Reddy, S. P., *J. Mol. Spectrosc.* **104**, 165 (1984).

Reddy, S. P., and Prasad, C. V. V., *J. Phys. E.* **22**, 305 (1989).

Simmons, J. D., Bass, A. M., and Tilford, S. G., *Astrophys. J.* **155**, 345 (1969).

Tilford, S. G., and Simmons, J. D., *J. Phys. Chem. Ref. Data* **1**, 147 (1972).

Vikis, A. C., *J. Chem. Phys.* **69**, 697 (1978a).

Vikis, A. C., *Chem. Phys. Lett.* **57**, 522 (1978b).

CHAPTER 5

DEPERTURBATION ANALYSIS OF THE A $^1\Pi$ - X $^1\Sigma^+$ SYSTEM OF $^{13}C^{18}O$ EXCITED IN A JET DISCHARGE

5.1 Introduction

Carbon monoxide occurs in the atmospheres of the sun, stars, and planets, including earth and in the products of hydrocarbon combustion. The infrared fundamental band of CO plays an important role in the propagation of radiation, particularly of the monochromatic and quasi-monochromatic radiation of lasers. Observations of the upper atmosphere of Mars by the Mariner 6, 7, and 9 spacecraft have shown that the fourth positive (A $^1\Pi$ - X $^1\Sigma^+$) system of CO is the strongest molecular emission feature of the day glow in the vacuum ultraviolet (VUV) region between 1100 Å to 2000 Å (Barth et al., 1969, 1971, and 1972). This process is due to the resonant fluorescent scattering of solar radiation in the vacuum ultraviolet by the fourth positive system of CO. This system of CO is one of the most important band systems occurring in the VUV region because it has been extensively used to detect the CO in astrophysical objects, to probe their physical conditions to understand the physical and chemical processes taking place, and to develop new sources of coherent radiation. From recorded high resolution stellar spectra, the existence of ^{13}C, ^{17}O, and ^{18}O isotopes was established in the atmosphere of Alpha Herculis by Maillard (1973, 1974). Similarly Hall et al. (1972, 1973) identifed the same isotopes in the recorded high resolution sunspot spectra. In the solar system, the ratio of ^{12}C and ^{13}C was found to be 11.0 : 0.122 and that of ^{16}O, ^{17}O, and ^{18}O was found to be 23.7 : 9.04×10^{-3} : 4.76×10^{-2}, all relative to Si (Grevesse et al., 1991 and Anders

and Grevesse, 1989). All isotopomers of CO except $^{13}C^{17}O$ have been detected in the radio frequency emission from dense galactic gas clouds, which shows the effects of nuclear processing and isotopic fractionation. The information on the A-X system of the rarer isotopomers of CO should enable astronomers to detect them in the directions of highest CO column density.

The A $^1\Pi$ state of CO is extensively perturbed by its nearby electronic states a′ $^3\Sigma^+$, d $^3\Delta_i$, e $^3\Sigma^-$, I $^1\Sigma^-$, and D $^1\Delta$. Because of such perturbations, it is not possible to predict accurately the term value of the A-X transitions for isotopic species by means of standard isotope relations. For the isotopomer $^{13}C^{18}O$, the information on the A $^1\Pi$ state is obtained from the Ångström (B $^1\Sigma^+$ - A $^1\Pi$), Herzberg (C $^1\Sigma^+$ - A $^1\Pi$), and (E $^1\Pi$ -A $^1\Pi$) systems. In all these systems, only quantitative information of the perturbations in the A $^1\Pi$ state is known. For complete information on the literature for this isotopomer the reader is referred to Chapter 4 and the references therein. A literature survey reveals that no measurements of the bands of the A-X system of $^{13}C^{18}O$ are available (see for example, Morton and Noreau, 1994). We have therefore undertaken the study of the high-resolution VUV emission spectrum of this system of $^{13}C^{18}O$ in the spectral region 1460-1670 Å for the first time. The spectra were generated in emission from a d.c. discharge in supersonically expanding argon gas containing trace amounts of $^{13}C^{18}O_2$. Thirty bands with $v' = 0$ to 9 and $v'' = 0$ to 5 were recorded. In this chapter, the rotational analysis of nineteen bands (0-0, 0-1, 0-2, 1-0, 1-1, 2-0, 2-1, 2-2, 2-3, 4-0, 4-3, 4-4, 6-1, 6-3, 7-1, 7-2, 7-3, 9-2, and 9-5) of the A-X system of $^{13}C^{18}O$ will be reported. Strong perturbations of the order of 10 cm^{-1} in the A, v=0 level, and weak perturbations

in the A, v=4, 6, 7, and 9 levels are observed. The deperturbed molecular constants are obtained for the A,v=0, 1, 2, 4, 6, 7, and 9 levels. Spectroscopic information was also obtained for the perturbing vibrational states of $a'\,^3\Sigma^+$, $d\,^3\Delta$, $e\,^3\Sigma^-$, $I\,^1\Sigma^-$, and $D\,^1\Delta$. Mixing coefficients and electronic perturbation parameters which characterize each perturbation are also derived.

5.2 Experimental Details

The A-X system of $^{13}C^{18}O$ was excited from a d.c discharge in a supersonically expanding jet of argon gas containing trace amounts of $^{13}C^{18}O_2$. The $^{13}C^{18}O_2$ gas with a purity of 99.1 atom % of ^{13}C and 99.9 atom % of ^{18}O was supplied by Isotech, Ohio. A detailed description of the experimental procedure to record the A-X spectra is given in Chapter 2. The jet emission spectra were photographed on the 10.6 m vacuum spectrograph of the National Research Council, Ottawa in the 7th and 8th orders of a normal-incidence concave grating with 600 grooves/mm and blazed at 12,000 Å, which gave reciprocal dispersions 0.21 Å/mm and 0.18 Å/mm, respectively. In addition to the fourth positive bands of $^{13}C^{18}O$, the jet spectra contain a number of atomic emission lines which are attributed to ^{13}C. The final wavelength calibration was made with the help of $^{13}C_I$ emission lines at 1561 Å and 1657 Å in the 7th order and at 1450 Å in the 8th order.

5.3 Rotational Analysis

The rotational structures of the 0-0 band of the A-X system of $^{13}C^{18}O$ and that of the 1-0 band of its $e\,^3\Sigma^- - X\,^1\Sigma^+$ system are shown in Fig. 5.0. The rotational analysis of the A-X bands is straight forward, and the assignment of J values in the perturbed region is unambiguously achieved with the help of precisely known ground state combination

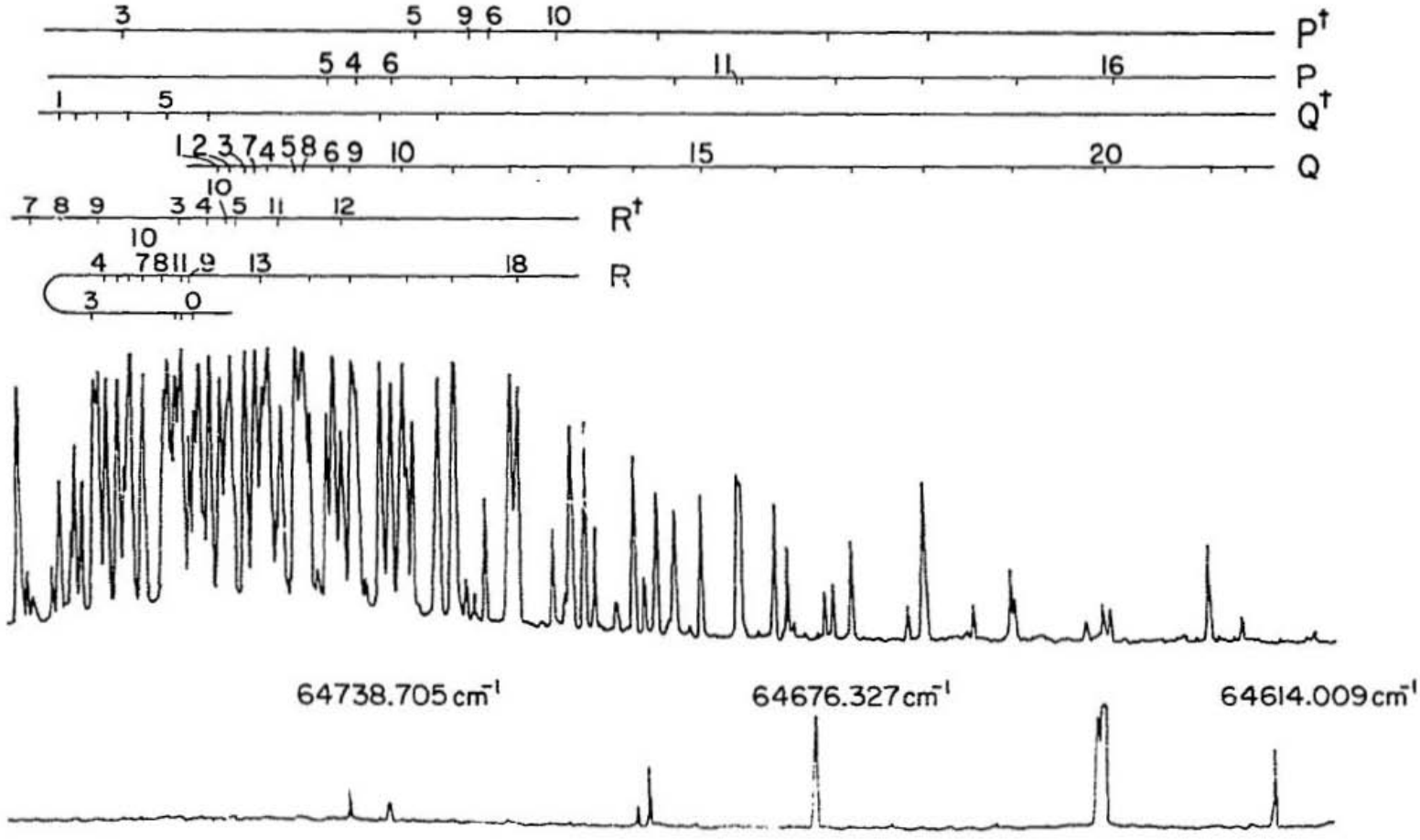

Figure 5.0 Rotational structure of the 0-0 band of the A $^1\Pi$ - X $^1\Sigma^+$ system of $^{13}C^{16}O$, photographed on the 10.6 m vacuum grating spectrograph in the seventh order along with the Fe lines in the third and fourth orders. Extra branches denoted by $R^e(J)$, $Q^e(J)$, and $P^e(J)$ in the 0-0 band arise from perturbations of the A, v=0 level by the e $^3\Sigma^-$, v=1 level.

differences. These combination differences were obtained by calculating the ground state term values T″(v″,J″) by making use of the precisely estimated mass-independent Dunham coefficients reported by Authier et al. (1993). The rotational quantum numbers and the absolute vacuum wavenumbers (in cm^{-1}) of the rotational lines of the nineteen analyzed bands are listed in Table 5.1. The procedure adopted for the deperturbation analysis of the A-X bands of $^{13}C^{18}O$ is the same as the one discussed in Chapter 4. In this chapter a brief discussion of the results obtained are outlined. Many crossings occur between the vibrational levels of the A $^1\Pi$ state and those of its neighbouring states a′ $^3\Sigma^+$, d $^3\Delta_i$, e $^3\Sigma^-$, I $^1\Sigma^-$, and D $^1\Delta$. A perturbation diagram locating the crossings of the A $^1\Pi$, v=0 to 13 levels with the nearby states for $^{12}C^{16}O$ was constructed by Garetz et al. (1991). Similar perturbation diagrams for the A $^1\Pi$, v=0 to 5 levels of $^{12}C^{18}O$ and $^{13}C^{18}O$ are given in Figs. 4.2 and 4.3. Perturbation diagrams for $^{13}C^{18}O$ are now extended for levels up to v=9 and are given in Figs. 5.1 and 5.2. It is evident from these figures that the calculated values for the corresponding energy levels can be obtained from the eigenvalues of a specific energy matrix which includes the perturbed states and the perturbing states. The occurrence of perturbations is mainly due to the interconfigurational interactions. These perturbations arise mainly from the rotation-electronic and spin-orbit Hamiltonian operators H_{RE} and H_{SO}. The selection rules (Lefebvre-Brion and Field, 1986) for these operators are

$$H_{RE}: \quad \Delta S = 0;\ \Delta\Sigma = 0;\ \Delta\Lambda = \Delta\Omega = \pm 1 \qquad [5.1]$$

$$H_{SO}: \quad \Delta S = 0\ \pm 1;\ \Delta\Lambda = -\Delta\Sigma = \pm;\ \Delta\Omega = 0. \qquad [5.2]$$

Here S is the spin angular momentum quantum number, and Σ, Λ, and Ω are the quantum

TABLE 5.1 Vacuum wavenumbers[a] (in cm^{-1}) of the rotational lines of the bands of the $A\ ^1\Pi - X\ ^1\Sigma^+$ system and of the related intercombination bands of $^{13}C^{18}O$

Band	A-X (0 - 0)			e - X (1 - 0)		
J	R(J)	Q(J)	P(J)	$R^f(J)$	$Q^f(J)$	$P^f(J)$
0	64759.57(2)					
1	761.43(4)	64756.16(1)		64786.56(-6)[b]	64777.88(-6)[c]	
2	762.18(1)	754.77(1)		788.73(-1)[b]	775.78(2)[c]	
3	773.14(3)	752.62(0)	64743.96(3)	761.43(-6)[b]	772.50(-2)[c]	64769.14(-2)[b]
4	771.49(4)	749.68(0)	737.79(7)	758.86(1)[b]	768.36(5)[c]	
5	770.02(3)	745.81(0)	741.68(-1)	754.18(4)[b]	763.24(-0)[c]	730.07(1)[b]
6	768.37(-6)	740.80(-2)	733.07(3)		757.50(0)[c]	720.44(1)[b]
7	766.50(4)	751.32(0)	724.60(0)	782.20(2)[d]	734.48(1)[c]	
8	763.78(-4)	744.93(2)	716.11(5)	777.71(4)[d]	726.60(3)[c]	
9	760.26(3)	738.32(-4)	707.12(2)	772.50(9)[d]		722.86(3)[d]
10	766.5 (-3)	731.68(7)	697.54(5)	755.18(-9)[d]		711.40(6)[d]
11	761.4 (2)	724.59(5)	686.92(-1)	748.46(1)[d]		699.14(3)[d]
12		717.03(-3)	686.60(9)	739.74(3)[d]		675.04(6)[d]
13	750.39(7)	709.11(-1)	674.02(3)			661.4 (2)[d]
14	744.44(-4)	700.63(-1)	661.8 (1)			645.56(6)[d]
15	738.3 (2)	691.63(1)	649.24(9)			628.19(9)[d]
16	731.03(-3)	682.02(4)	636.40(4)			609.1 (-1)[d]
17	724.59(-7)	671.51(-1)	623.04(-3)			588.8 (-2)[d]
18	716.13(-4)	661.76(2)	609.07(4)			
19	707.09(2)	649.85(5)	595.9 (2)			
20	696.20(-8)	637.33(7)	580.34(8)			
21	695.24(-8)	623.05(1)	564.26(6)			
22	682.02(-3)	618.61(-4)	546.46(-3)			
23	669.3 (-4)	602.1 (2)	538.60(-1)			
24	656.18(-3)	586.18(7)	518.46(5)			
25		569.16(0)	499.4 (2)			
26			478.78(3)			
27		546.5 (-3)				

TABLE 5.1 (Continued)

Band	A - X (0 - 1)			e - X (1 - 1)		
J	R(J)	Q(J)	P(J)	$R^{\dagger}(J)$	$Q^{\dagger}(J)$	$P^{\dagger}(J)$
0	62715.87(2)					
1	717.9 (2)	62712.52(3)		62742.8 (-1)[b]	62734.31(3)[c]	
2	718.52(-5)	711.17(2)	62705.51(4)	745.07(-7)[b]	732.18(3)[c]	
3	729.60(-1)	709.12(1)	700.43(1)	717.90(-8)[b]	729.02(0)[c]	62725.4 (-3)[b]
4	728.10(4)	706.27(-1)	694.29(-5)	715.45(-1)[b]	724.92(-1)[c]	
5	726.78(3)	702.5 (-1)	698.42(-3)	711.1 (2)[b]	720.00(-1)[c]	686.84(1)[b]
6	725.39(1)	697.75(-2)	689.93(-5)		714.46(2)[c]	677.39(0)[b]
7	723.62(1)	708.49(2)	681.77(2)	739.42(8)[d]	691.63(-1)[c]	
8	721.22(-0)	702.39(7)	673.46(1)	735.11(4)[d]	683.98(1)[c]	
9	717.88(-3)	696.05(1)	664.76(-1)	730.03(-6)[d]		680.52(2)[d]
10	724.9 (1)	689.60(1)	655.48(1)	713.17(-7)[d]		669.32(-0)[d]
11	719.52(-3)	682.86(2)	645.22(-2)			657.44(2)[d]
12	714.47(-3)	675.72(-1)	645.22(3)	698.40(2)[d]		633.68(2)[d]
13		668.15(-3)	633.04(-2)			620.30(3)[d]
14		660.13(-0)	621.13(1)			604.96(-3)[d]
15		651.54(-2)	609.11(1)			588.09(4)[d]
16		642.42(1)	596.79(0)			
17		632.45(-2)				
18		623.4 (1)				

TABLE 5.1 (Continued)

Band	A - X (0 - 2)			e - X (1 - 2)		
J	R(J)	Q(J)	P(J)	$R^{f}(J)$	$Q^{f}(J)$	$P^{f}(J)$
0	60696.1 (-1)					
1	698.11(-1)	60692.85(-3)		60723.33(-1)[b]	60714.63(-4)[c]	
2	698.99(-4)	691.60(-0)	60685.87(-5)	725.65(6)[b]	712.58(-3)[c]	
3	710.11(-4)	689.63(-3)	681.01(5)	698.48(-5)[b]	709.53(-3)[c]	60706.3 (2)[b]
4	708.69(-4)	686.94(-1)	674.99(-1)	696.10(-2)[b]	705.55(-4)[c]	701.52(-5)[b]
5	707.55(-2)	683.38(-1)	679.20(-6)	691.6 (-1)[b]	700.79(-4)[c]	667.60(-4)[b]
6	706.33(-4)	678.74(-2)	670.93(-4)	685.5 (-1)[b]	695.39(-5)[c]	658.37(-1)[b]
7	704.80(-3)	689.63(-6)	662.92(-4)	720.51(-3)[d]	672.82(-2)[c]	647.07(-4)[b]
8	702.64(-3)	683.7 (-1)	654.88(-3)	716.52(-1)[d]	665.3 (-1)[c]	634.07(-6)[b]
8						672.15(-4)[d]
9	699.58(-4)	677.74(-2)	646.46(-4)	711.75(-6)[d]	656.37(-4)[c]	662.22(0)[d]
10	706.77(-2)	671.56(-6)	637.47(-3)	695.4 (1)[d]	645.83(-3)[c]	651.28(-7)[d]
11	701.86(-5)	665.29(8)	627.61(1)	689.09(-3)[d]		639.75(-3)[d]
12	697.16(-7)	658.37(-9)	627.82(-9)	681.0 (-1)[d]		616.3 (-1)[d]
13		651.28(-2)	616.3 (1)	671.6 (1)[d]		603.39(-0)[d]
14	687.55(4)	643.63(-4)				
15		635.52(-3)				
16		626.85(-4)				
17		617.42(-4)				

TABLE 5.1 (Continued)

Band	1-0			1-1		
J	R(J)	Q(J)	P(J)	R(J)	Q(J)	P(J)
0	66178.99(3)			64135.21(-5)		
1	181.24(3)	66175.46(-1)		137.50(-5)		
2	183.0 (1)	174.21(-2)	66168.49(1)	139.16(-8)	64130.61(-1)	64124.83(-4)
3	184.0 (2)	172.37(0)	163.69(-6)	140.27(-8)	128.84(-1)	120.0 (-2)
4	184.1 (-2)	169.83(-6)	158.44(5)	140.82(-4)	126.48(-2)	114.98(-2)
5	184.05(3)	166.83(4)	152.44(1)	140.82(4)	123.55(0)	109.18(-1)
6	183.11(-6)	163.11(4)	145.83(-1)	140.2 (1)	120.03(2)	102.76(-1)
7	181.67(-4)	158.69(-4)	138.63(1)	138.89(4)	115.87(-1)	095.77(-1)
8	179.61(-1)	153.81(4)	130.80(0)	137.01(0)	111.16(-1)	088.18(-2)
9	176.90(-0)	148.18(-1)	122.38(3)	134.57(-1)	105.84(-2)	080.02(-0)
10	173.62(4)	142.02(3)	113.30(2)	131.61(6)	099.95(-1)	071.23(-3)
11	169.65(3)	135.19(2)	103.61(1)	127.91(-2)	093.50(2)	061.84(-7)
12	165.02(-3)	127.74(1)	093.32(2)	123.6 (-2)	086.41(0)	051.92(-6)
13	159.88(3)	119.71(3)	082.39(1)	118.89(-3)	078.74(-0)	041.43(-2)
14	154.2 (1)	111.03(3)	070.85(1)	113.50(-2)	070.49(-0)	030.31(-2)
15	147.8 (2)	101.73(2)	058.62(-6)	107.52(-2)	061.64(-0)	018.63(-0)
16	140.53(0)	091.82(4)	045.92(1)	100.9 (-1)		006.32(-1)
17	132.86(2)	081.27(3)	032.6 (1)		042.23(5)	63993.47(2)
18	124.56(3)	070.13(5)	018.53(3)	086.01(-0)	031.56(0)	979.93(-6)
19	115.62(3)	058.33(4)	003.89(2)	077.62(-4)	020.37(1)	965.89(-4)
20	106.05(3)	045.91(4)	65988.60(-1)		008.57(2)	951.23(-5)
21	095.87(4)	032.84(0)	972.74(0)	059.14(0)	63996.18(3)	936.02(-1)
22	085.07(6)	019.18(-0)	956.23(-0)		983.15(-0)	920.15(-6)
23	073.53(-4)	004.91(2)	939.07(-5)	038.19(-4)	969.56(-0)	903.78(-1)
24	061.47(-1)	65990.01(3)	921.38(0)		955.36(-1)	886.77(-0)
25	048.72(-3)	974.45(2)	903.00(-1)		940.57(-2)	869.13(-4)
26	035.31(-5)	958.4 (1)	883.99(-2)		925.17(-3)	
27	021.12(-1)	941.44(4)	864.35(-4)		909.17(1)	
28	007.38(2)	923.77(6)	844.13(3)		892.35(3)	
29	65991.85(-1)	906.46(-2)	822.88(-9)		875.96(-1)	
30	975.92(-2)	887.57(4)	802.31(-1)		857.93(0)	
31	959.34(-8)	868.16(1)	779.93(-1)			
32	941.9 (-4)	848.16(1)	757.23(7)			
33	924.42(-6)	827.50(0)	733.79(3)			
34	906.5 (4)	806.15(2)	709.76(-0)			

TABLE 5.1 (Continued)

Band	1-0 (Continued)		
J	R(J)	Q(J)	P(J)
35	887.03(5)	783.65(0)	685.13(0)
36	867.28(1)	763.64(-1)	660.0 (1)
37	846.86(-4)	739.56(-0)	633.96(-1)
38	825.82(-4)	715.65(5)	607.48(4)
39	803.99(-4)	691.09(-2)	580.1 (-2)
40	782.36(5)	666.04(5)	552.35(-6)
41	759.04(-4)	640.27(4)	523.75(-3)
42	735.30(1)	613.76(1)	495.4 (1)
43		586.44(6)	465.29(0)
44	686.47(6)	558.17(0)	434.70(-3)
45		531.7 (1)	401.76(-5)

TABLE 5.1 (Continued)

Ban	2-0			2-1		
J	R(J)	Q(J)	P(J)	R(J)	Q(J)	P(J)
0	67560.44(1)			65516.79(4)		
1	562.57(-4)	67556.91(-3)		519.00(5)	65513.28(-0)	
2	564.16(4)	555.65(3)	67549.99(3)	520.55(2)	512.05(3)	65506.39(3)
3	565.01(3)	553.66(2)	545.15(0)	521.52(5)	510.14(1)	501.8 (2)
4	565.24(6)	551.02(1)	539.6 (-1)	521.74(-5)	507.62(-0)	496.26(-3)
5	564.8 (1)	547.77(6)	533.61(6)	521.52(4)	504.46(-1)	490.36(4)
6	563.65(5)	543.74(0)	526.79(3)	520.55(1)	500.69(0)	483.79(8)
7	561.83(2)	539.07(-1)	519.36(3)	519.00(2)	496.26(2)	476.48(0)
8	559.39(2)	534.08(-4)	511.24(2)	516.79(1)	491.43(-9)	468.64(2)
9	556.26(-1)	528.03(1)	502.49(3)	513.93(-1)	485.71(2)	460.3 (1)
10	552.52(2)	521.43(2)	493.07(3)	510.49(1)	479.40(2)	451.09(7)
11		514.17(3)	482.99(3)	506.39(1)	472.51(6)	441.35(7)
12	543.1 (2)	506.25(2)	472.26(3)		465.0 (2)	
13	537.24(2)	497.71(6)	460.85(2)		456.67(-4)	
14	530.89(9)	488.44(3)	448.79(2)		448.0 (1)	
15	523.71(-1)	478.53(1)	436.07(1)		438.48(3)	
16	515.94(-2)	467.99(4)	422.70(2)			
17	507.47(-6)	456.72(-0)	408.62(-1)			
18	498.2 (-3)	444.83(0)	393.91(-2)			
19	488.4 (-2)	432.25(-1)	378.49(-6)			
20	478.5 (3)	419.00(-3)	362.4 (-1)			
21	467.1 (2)	405.17(6)	345.1 (-7)			
22	454.84(8)	390.49(-2)	328.6 (2)			
23	440.9 (4)	375.13(-7)	310.3 (1)			
23	452.7 (-2)					
24	432.2 (1)	359.0 (-1)	291.2 (1)			
25	417.30(3)	342.1 (-2)	270.3 (4)			
25			282.1 (-2)			
26	402.40(-7)	323.8 (-3)	254.8 (2)			
27	386.9 (-1)	302.20(-1)	232.95(4)			
27		317.08(-3)	211.16(-5)			
28	370.5 (-2)	292.9 (3)	188.85(-5)			
29		272.2 (2)				
30		251.9 (-1)				
31		231.89(-2)				
32		209.8 (1)				

TABLE 5.1 (Continued)

Band	2-2			2-3		
J	R(J)	Q(J)	P(J)	R(J)	Q(J)	P(J)
0	63497.08(-2)			61501.39(-7)		
1	499.35(1)	63493.65(-2		503.66(-7)	61498.02(-4)	
2	500.97(-0)	492.49(1)	63486.75(-6)	505.36(-6)	496.87(-5)	61491.19(-6
3	502.05(3)	490.69(1)	482.13(-4)	506.53(-2)	495.15(-7)	486.63(-9)
4	502.4 (-1)	488.29(1)	476.99(4)	507.08(-4)	492.91(-4)	481.56(-5)
5	502.34(5)	485.28(-0)	471.13(-0)	507.08(-3)	490.06(-4)	475.88(-6)
6	501.56(2)	481.69(1)	464.72(1)	506.53(-0)	486.63(-5)	469.66(-5)
7	500.17(-1)	477.40(-4)	457.70(1)	505.36(-2)	482.59(-6)	462.85(-4)
8	498.22(-0)	472.88(-9)	450.10(3)	503.66(-1)	478.3 (-1)	455.47(-5)
9	495.63(-3)	467.42(1)	441.84(-2)		473.09(-4)	447.55(-3)
10	492.49(-2)	461.42(1)	433.04(-1)		467.40(-3)	439.03(-3)
11	488.6 (-2)	454.84(3)	423.63(-1)		461.16(-1)	
12	484.39(1)	447.61(-1)	413.64(2)		454.2 (-1)	420.26(-9)
13	479.40(-0)	439.84(1)	402.99(-3)		446.99(4)	
14		431.45(1)	391.84(3)		439.03(5)	
15		422.46(1)				
16		412.87(1)			421.30(-4)	
17		402.72(6)				
18		391.84(-2)				

TABLE 5.1 (Continued)

Band	4-0			4-3		
J	R(J)	Q(J)	P(J)	R(J)	Q(J)	P(J)
0	70230.62(1)			64171.60(-4)		
1	232.64(1)	70227.11(-1)		173.71(-4)	64168.18(-6)	
2	234.0 (1)	225.68(3)		175.25(5)	166.92(-3)	64161.45(1)
3		223.44(1)	70215.16(-1)	176.02(1)	165.01(1)	161.66(-7)
4		220.45(-1)	209.51(5)	176.0 (-2)	162.39(-1)	151.40(0)
5	233.34(3)	216.79(-0)	202.99(-1)	175.72(2)	159.13(-5)	145.48(9)
6	231.64(1)	212.37(1)	195.85(1)	174.61(4)	155.29(-1)	138.9 (1)
7	229.23(1)	207.20(1)	187.93(2)	172.76(-2)	150.75(-1)	131.6 (1)
8	225.99(-7)	201.30(2)	179.24(-2)	170.30(-6)	145.51(-7)	123.55(-1)
9	222.16(1)	194.65(2)	169.94(8)			114.99(1)
10	217.51(0)	187.25(0)	159.73(1)	163.50(-4)	133.24(-4)	105.83(8)
11	212.3 (2)	179.16(4)	148.85(0)	159.13(-2)	126.12(-2)	095.8 (-1)
12	206.02(1)	170.21(-4)	137.25(1)	154.13(1)	118.38(1)	085.37(1)
13	199.16(2)	160.65(0)	124.90(1)	148.35(-9)	109.86(-8)	
14	191.56(3)	150.30(1)	111.78(-1)		100.85(-1)	
15	183.16(-1)	139.21(1)	097.96(-1)			
16	174.01(-6)	127.38(1)	083.38(-2)		080.6 (-2)	
17	164.26(4)	114.79(-1)	068.13(4)		069.71(-2)	
18	153.61(-2)	101.50(3)	052.04(1)			
19	142.28(-1)	087.43(3)	035.25(0)			
20	130.19(-1)	072.65(5)	017.70(-1)		032.8 (1)	
21	117.43(6)	057.09(4)	69999.41(-3)		019.10(4)	
22		040.73(-1)			004.69(-7)	
23		023.65(-5)				
24		006.3 (4)				
25		69987.42(7)				
26		968.00(-5)				

TABLE 5.1 (Continued)

Band	4-4		
J	R(J)	Q(J)	P(J)
0	62199.8 (-2)		
1	202.0 (-1)	62196.51(-5)	
2	203.55(-4)	195.28(-6)	
3	204.50(2)	193.49(1)	
4		190.99(-1)	62179.92(-7)
5	204.50(5)	187.89(-4)	174.13(-1)
6	203.55(5)	184.21(-1)	167.70(-0)
7	201.97(4)	179.92(2)	160.64(1)
8	199.77(4)	174.92(-4)	152.96(2)
9	196.8 (-1)	169.37(-4)	
10	193.49(-1)	163.21(-2)	

TABLE 5.1 (Continued)

Band	6-1			6-3		
J	R(J)	Q(J)	P(J)	R(J)	Q(J)	P(J)
0	70731.1 (-1)			66715.91(4)		
1	732.95(-8)			717.85(4)	66712.42(-5)	
2	734.13(2)	70726.11(0)	70720.6 (-2)		717.85(4)	
3		723.79(7)	715.73(2)		708.79(-2)	66700.82(2)
4		720.58(3)	709.87(-1)	719.22(0)	705.85(-3)	695.22(1)
5	732.63(3)	716.59(1)	703.26(2)	718.17(-6)	702.20(-2)	688.79(-7)
6	730.53(2)	711.84(1)	695.82(1)	716.47(-3)	697.80(-2)	681.7 (-1)
7	727.65(2)	706.27(-0)	687.61(1)	713.97(-8)	692.65(-4)	673.98(-3)
8	723.9 (-1)	699.94(1)	678.60(1)	710.93(8)	686.80(-4)	665.49(0)
9	719.49(2)	692.79(-1)	668.81(2)	706.93(1)	680.17(-7)	656.1 (-1)
10	714.23(1)	684.89(2)	658.22(2)	702.20(-7)	672.90(-2)	646.4 (2)
11	708.16(0)	676.17(1)	646.82(1)	696.87(-1)	664.86(-1)	635.54(0)
12	701.32(1)	666.65(1)	634.65(1)		656.14(5)	624.10(1)
13	693.62(-5)	656.34(0)	621.66(-2)		646.4 (-2)	
14	685.18(-4)	645.24(0)	607.88(-4)		636.29(-3)	
15	676.2 (2)	633.36(0)	593.29(-8)		625.34(-0)	
16	666.01(6)	620.67(0)	577.95(-9)			
17	655.18(6)	607.17(-1)	561.98(8)			
18	643.5 (-1)	592.92(1)				
19	631.15(7)	577.95(3)	527.31(5)			
20		561.98(-0)	508.7 (-1)			
21	603.82(-1)	545.24(-7)	489.50(4)			
22		527.81(-5)	469.38(2)			
23		509.64(4)				
24		490.49(-4)				
25		470.68(1)				

TABLE 5.1 (Continued)

Band	7-1			7-2		
J	R(J)	Q(J)	P(J)	R(J)	Q(J)	P(J)
0				69935.74(-2)		
1		71951.88(-6)		937.58(-1)	69932.29(-4)	
2	71958.22(6)	950.4 (1)		938.67(5)	930.72(-1)	
3	958.22(-8)	947.78(0)	71939.90(2)	938.7 (-1)	928.30(-2)	69920.44(1)
4	957.60(-0)	944.47(1)	933.95(2)	938.32(6)	925.11(-0)	914.60(1)
5	956.05(-1)	940.30(1)	927.06(-8)	936.87(-1)	921.10(-1)	907.95(-1)
6	953.71(1)	935.34(4)	919.52(0)	934.70(0)	916.28(-2)	900.53(1)
7	950.4 (-1)	929.46(-1)	911.14(7)	931.69(-1)	910.69(1)	892.26(-1)
8	946.46(0)	922.83(2)	901.79(2)	927.93(2)	904.28(1)	883.23(0)
9	941.57(-2)	915.36(4)	891.68(2)	923.34(3)	897.02(-3)	873.38(0)
10	935.7 (-2)	907.04(5)	880.70(-1)	917.91(-0)	889.02(1	862.74(0)
11	929.5 (1)	897.86(4)	868.94(2)	911.70(-0)	880.18(-1)	851.30(2)
12	921.95(-0)	887.88(5)	856.34(4)	904.6 (-1)	870.54(-1)	839.04(1)
13		877.03(4)	842.86(0)		860.12(1)	826.00(3)
14		865.36(5)	828.54(-3)		848.86(1)	812.05(-6)
15		852.84(4)			836.77(-2)	797.40(-4)
16		839.47(3)			823.98(6)	781.97(2)
17		825.24(1)			810.21(-2)	
18		810.17(2)			795.63(-6)	
19					780.23(-2)	
20					763.23(4)	
21						
22					730.0 (-1)	

TABLE 5.1 (Continued)

Band	7-4		
J	R(J)	Q(J)	P(J)
0	65968.8 (2)		
1	970.38(8)	65965.04(-1)	
2	971.55(9)	963.56(-0)	65958.36(6)
3	971.78(-7)	961.32(-2)	953.52(7)
4	971.52(0)	958.35(-3)	947.94(9)
5	970.38(-6)	954.65(-2)	941.44(-7)
6	968.57(-5)	950.22(-0)	934.44(-0)
7	966.05(-0)	945.01(-2)	926.60(-2)
8	962.74(-0)	939.08(-2)	918.05(-1)
9	958.9 (-3)	932.40(-2)	908.74(-2)
10	953.85(-4)	924.55(-6)	898.6 (-1)
11	948.2 (-1)	916.82(-2)	887.8 (-2)
12	941.9 (-2)	907.93(0)	876.41(0)
13	934.9 (-2)	898.33(5)	851.12(-0)
14	927.1 (-1)	887.8 (-1)	837.43(6)
15	918.5 (-1)	876.6 (-1)	822.88(3)
16		864.7 (-1)	807.7 (1)
17		852.20(6)	
18		838.71(1)	

TABLE 5.1 (Continued)

Band	9-2			9-5		
J	R(J)	Q(J)	P(J)	R(J)	Q(J)	P(J)
0						
1		72289.06(3)		66379.07(3)	66373.91(-4)	
2		287.16(-9)		380.1 (1)	372.36(1)	
3				380.11(-4)	369.97(0)	
4		281.01(-4)		379.57(5)	366.80(2)	66356.63(2)
5		276.63(0)		378.08(-1)	362.79(-3)	350.11(2)
6		271.29(-2)		375.81(-6)	358.06(1)	342.82(5)
7		265.08(-4)		372.78(-7)	352.52(3)	334.70(4)
8		258.03(-0)		369.08(4)	346.09(-3)	325.78(1)
9		250.02(-4)		364.42(0)	338.96(-1)	316.08(1)
10		241.14(-6)		359.00(-1)	330.99(-2)	305.67(8)
11		231.45(0)			322.27(0)	
12					312.71(0)	
13					302.32(3)	
14					291.36(3)	

[a]Number in parantheses indicates the $(\nu_{obs} - \nu_{cal}) \times 10^2$ in units of cm^{-1}.
[b]Rotational lines correspond to F_1 levels: $R^1(J)={}^{Q}R(J)$; $P^1(J)={}^{Q}P(J)$.
[c]Rotational lines correspond to F_2 levels: $Q^1(J)={}^{Q}Q(J)$.
[d]Rotational lines correspond to F_3 levels: $R^1(J)={}^{S}R(J)$; $P^1(J)={}^{Q}P(J)$.

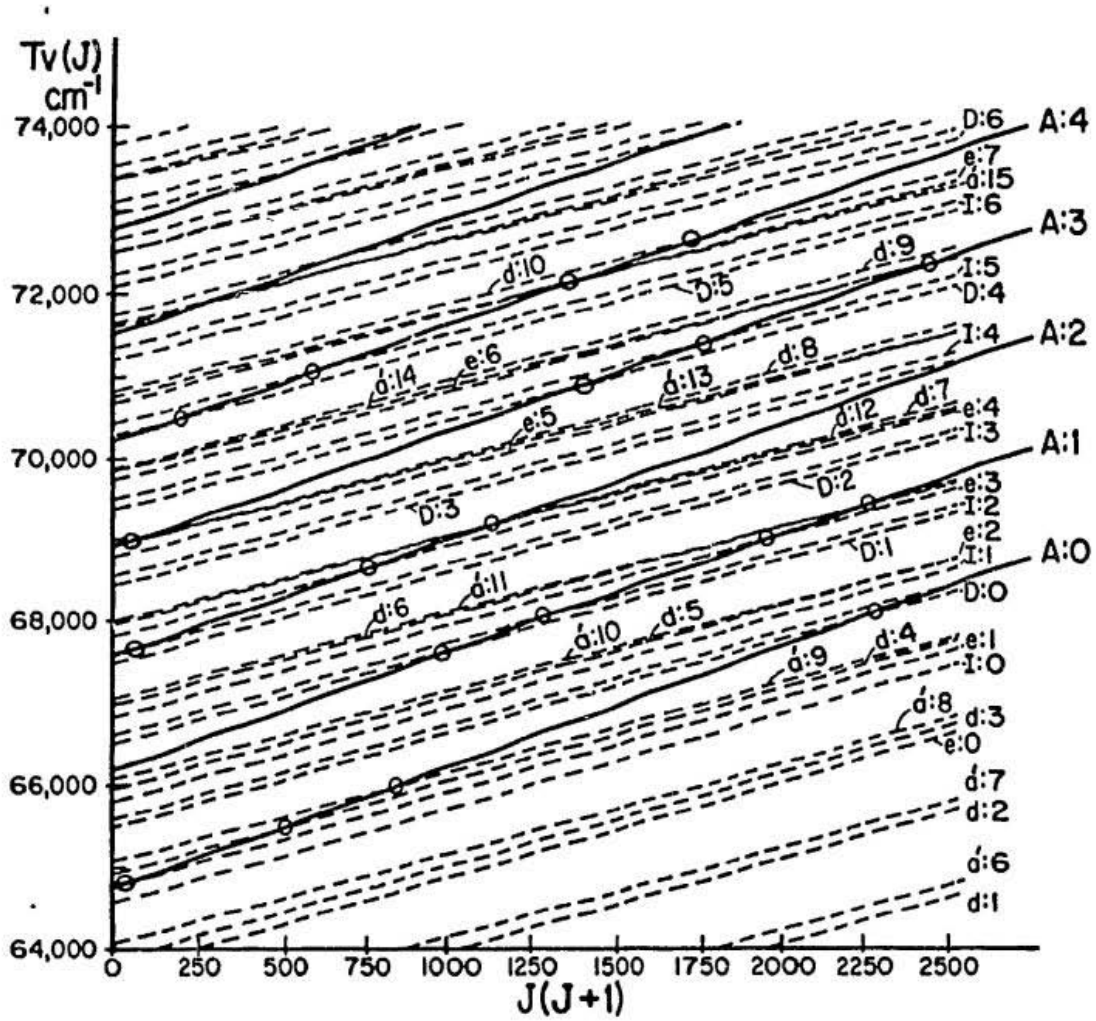

Figure 5.1 Perturbation diagram of $^{13}C^{18}O$ for A $^1\Pi$, v=0 to 4. The term values $T_v(J)$ are relative to X $^1\Sigma^+$, v=0 and J=0

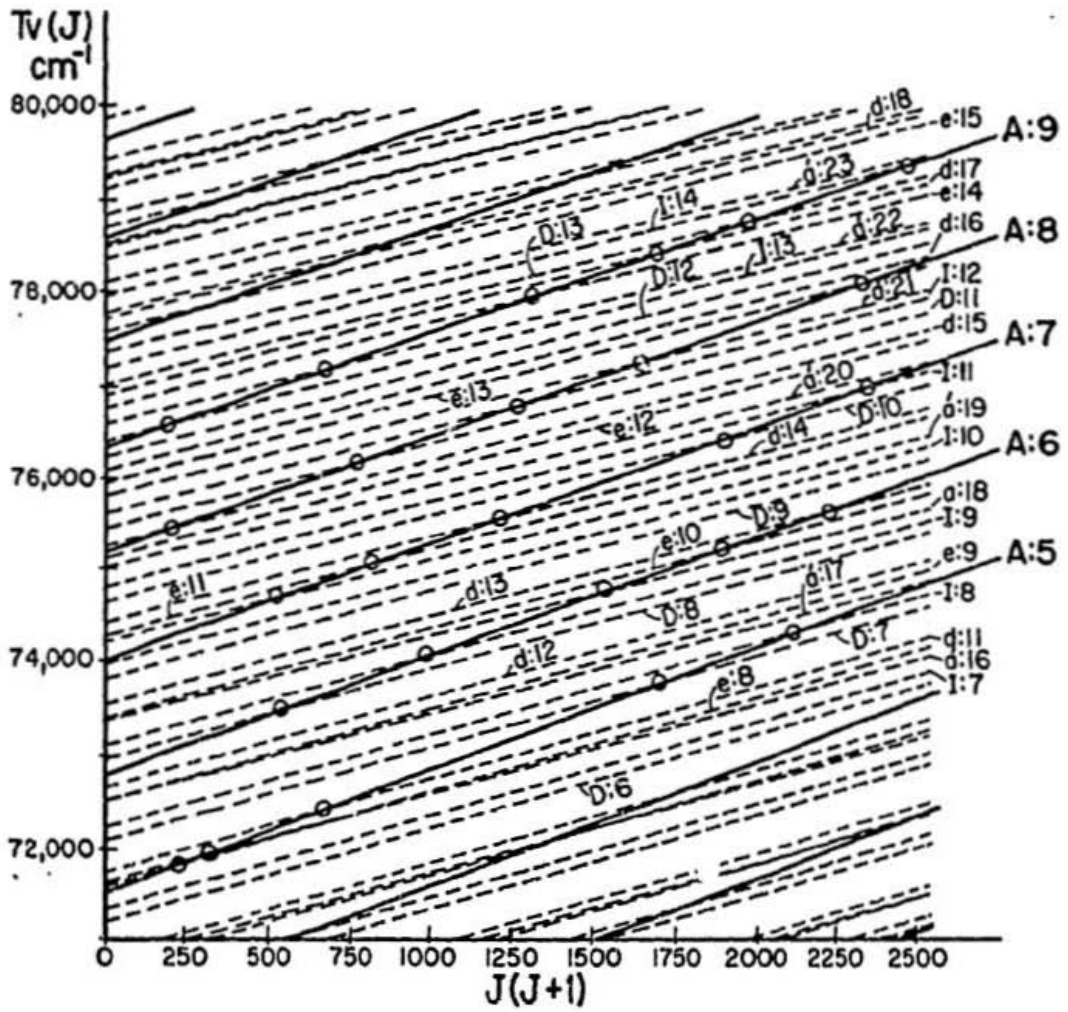

Figure 5.2 Perturbation diagram of $^{13}C^{18}O$ for A $^1\Pi$, v=5 to 9. The term values $T_v(J)$ are relative to X $^1\Sigma^+$, v=0 and J=0

numbers of the components of angular momentum along the internuclear axis of the spin, orbital and electronic angular momenta, respectively. From the deperturbation analysis of the a $^3\Pi$ and A $^1\Pi$ states of $^{12}C^{16}O$, Field et al. (1971, 1972a, and 1972b) have shown that each perturbation matrix element (α, β), between levels of a given pair of states belonging to $\sigma\pi$ and $\pi^3\pi$ configurations, is the product of a vibrational factor and a constant electronic perturbation parameter (**a**, **b**). Expressions for the relevant interaction matrix elements are given in Tables 3.1 and 3.2 and also in Eq. [4.7]. These expressions have been used in constructing the energy matrix for $^{13}C^{18}O$.

In Figs. 5.1 and 5.2, the circles denote the crossing of the neighbouring levels with the A $^1\Pi$, v=0 to 9 levels. The crossings of the perturbing levels with the A state for which the perturbation analysis has been carried out are summarized below:

A $^1\Pi$,v=0: e $^3\Sigma^-$, v=1; d $^3\Delta$, v=4; a′ $^3\Sigma^+$, v=9; D $^1\Delta$, v=0;

v=1: D $^1\Delta$, v=1; I $^1\Sigma^-$, v=2; e $^3\Sigma^-$, v=3; a′ $^3\Sigma^+$, v=11; d $^3\Delta$, v=6;

v=2: I $^1\Sigma^-$, v=3; e $^3\Sigma^-$, v=4; a′ $^3\Sigma^+$, v=12; d $^3\Delta$, v=7;

v=4: D $^1\Delta$, v=5; I $^1\Sigma^-$, v=6; a′ $^3\Sigma^+$, v=15; e $^3\Sigma^-$, v=7; d $^3\Delta$, v=10;

v=6: D $^1\Delta$, v=8; I $^1\Sigma^-$, v=9; a′ $^3\Sigma^+$, v=18; e $^3\Sigma^-$, v=10; d $^3\Delta$, v=13;

v=7: a′ $^3\Sigma^+$, v=19; e $^3\Sigma^-$, v=11; d $^3\Delta$, v=14, D $^1\Delta$, v=10; I $^1\Sigma^-$, v=11;

v=9: I $^1\Sigma^-$, v=13; a′ $^3\Sigma^+$, v=22; e $^3\Sigma^-$, v=14; d $^3\Delta$, v=17; D $^1\Delta$, v=13; I $^1\Sigma^-$, v=14.

The Hamiltonian matrix used in the present analysis contains not only the perturbing levels which cross a level of the A state but also those which interact strongly with them. A weighted nonlinear least-squares method (Le Floch, 1989) was used to fit the observed wavenumbers to the energy matrix. This method necessarily uses an iterative approach

which combines Marquardt's algorithm (Marquardt, 1963) with the Hellmann-Feynman (Hellmann, 1937) theorem. The (ν_{obs} - ν_{cal}) values of the analyzed bands are also listed in parantheses in Table 5.1.

5.4 Results and Discussion

(a) Perturbations in the A $^1\Pi$ levels of $^{13}C^{18}O$:

A $^1\Pi$, v=0:

For this level, three bands (0-0, 0-1 and 0-2) have been used in the deperturbation analysis. A plot of deviation $|T(v,J)_{obs} - T(v,J)_{cal}|$ versus J that characterizes the occurrence of perturbations in the observed rotational structure of these bands is shown in Fig. 5.3. The most important feature of this figure is the strong discontinuities associated with the A $^1\Pi$ rotational levels at J=3/4, J=6/7, and J=10/11, and these are characteristic of strong spin-orbit interaction H_{SO} between the A $^1\Pi$, v=0 level and the e $^3\Sigma^-$, v=1 level. It should be noted that for the $^3\Sigma^-$ state the J crossing (J_c) occurs for the F_2 (f parity) component, whereas the components F_1 and F_3 (both of parity e) have lower and higher J_c's respectively. The mixing between A $^1\Pi$, v=0 and e $^3\Sigma^-$, v=1 is so strong, that it has yielded a total of 94 extra lines (31 belonging to the intercombination band e $^3\Sigma^-$ (v=1) - X $^1\Sigma^+$ (v=0); 28 belonging to e $^3\Sigma^-$ (v=1) - X $^1\Sigma^+$ (v=1); and 35 belonging to e $^3\Sigma^-$ (v=1) - X $^1\Sigma^+$ (v=2)) which are given in Table 5.1. Apart from the strong e $^3\Sigma^-$ - A $^1\Pi$ perturbation, the spin-orbit interaction between d $^1\Delta$, v=4 and A $^1\Pi$, v=0 gives rise to an additional perturbation at J=21/22 and near J=25. No extra lines are observed because of this interaction. The fitted values of the vibrational terms T_v for the A $^1\Pi$, v=0, e $^3\Sigma^-$,

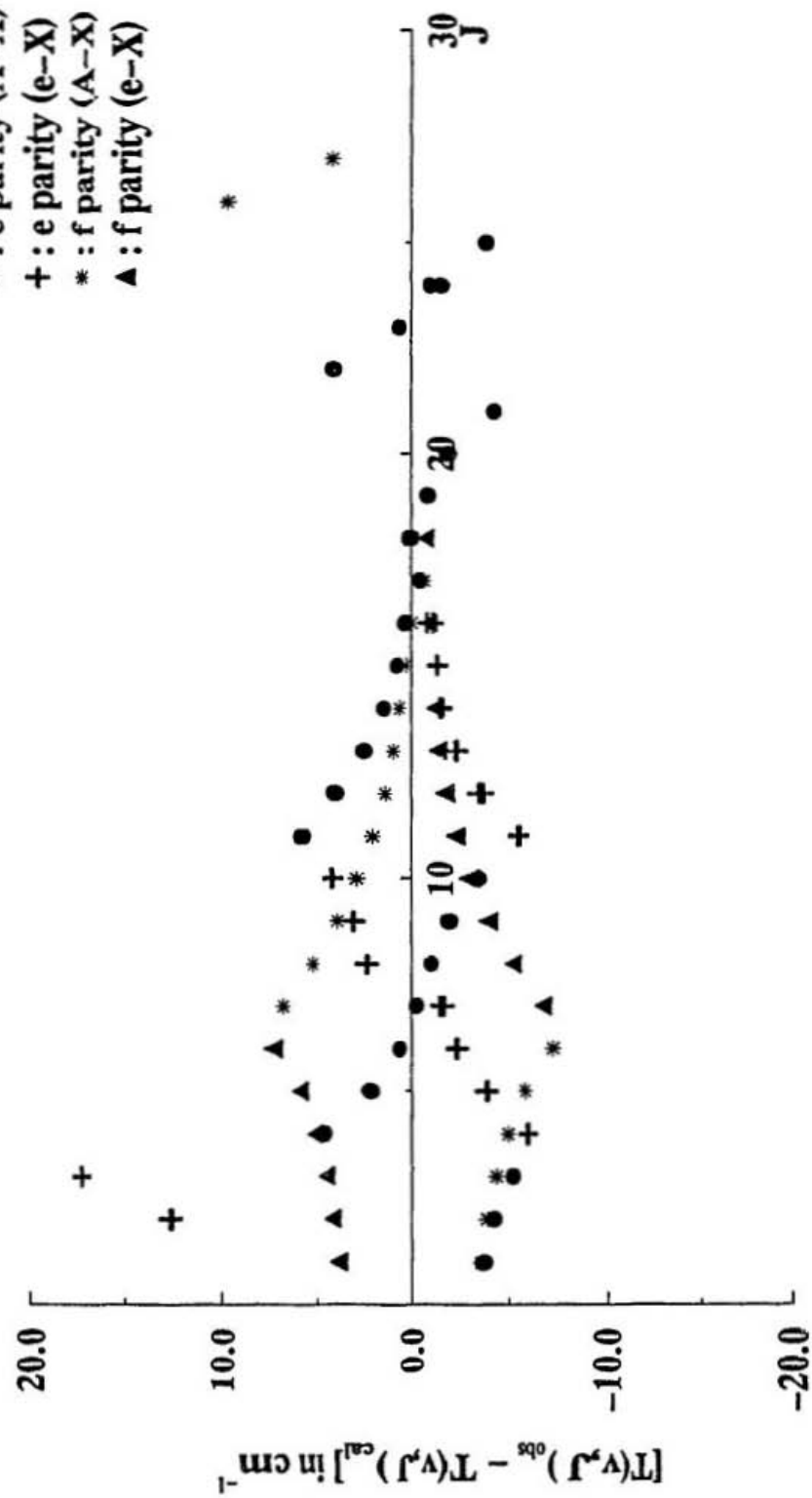

Figure 5.3 Plot of deviations $[T(v,J)_{obs} - T(v,J)_{cal}]$ of the rotational levels versus J in A $^1\Pi$, v=0 of $^{13}C^{18}O$.

v=1, and d $^3\Delta$, v=4 levels, the rotational constants B′s for the A, v=0, e, v=1, and d, v=4 levels and the centrifugal distortion constant D for the A state are given in Table 5.2. Also listed in this table are the fitted spin - orbit parameter $\alpha^e_{0,1}$ and $\alpha^d_{0,4}$ which are determined for the first time. The spin - spin parameter (λ) of the e $^1\Sigma$, v=1 level was also detemined in the present analysis. The values of the fixed parameters which were used in the least - squares fit are also given in Table 5.2. The perturbing levels interact with the A, v=4 level at different J values and the dimension of the appropriate energy matrix depends on the J - range considered. The Hamiltonian matrix used in the present work contains not only the perturbing levels which cross the A state but also those which interact strongly with them. The present experimental data for the A, v=0 level were fitted satisfactorily to the eigenvalues of a 33 x 33 energy matrix for J_{max}=27. In this fit, the value of the dimensionless variance σ^2 is 5.1.

Perturbations occurring in the A $^1\Pi$, v=0 level are also presented in Fig. 5.4. In this figure the percentage $^1\Pi$ character of each rotational level is plotted against J for both e and f parities for the A, v=0, e, v=1 and d, v=4 levels. In Fig. 5.4 the % $^1\Pi$ character greater than 50 corresponds to the level having a dominant $^1\Pi$ character, whereas it is less than 50 for the perturbing (e $^1\Sigma^-$, v=1) level. This figure clearly shows the effects of a strong perturbation that occurs between the e $^1\Sigma^-$ and A $^1\Pi$ states. The percentage $^1\Pi$ character of A, v=0 drops to 43% for J=4 and for e $^1\Sigma^-$, v=1 it reaches 49% for the F_1 (e) component. The dips at J=6 and J=11 for A, v=0 are due to the crossing of the F_2 (f) and F_1 (e) components of the perturbing e, v=1 level. At these J values the % $^1\Pi$ character for e, v=1 reaches 45 and 47. The decrease in the values of the percentage $^1\Pi$ character

TABLE 5.2

Molecular parameters[a] (in cm^{-1}) of the A $^1\Pi$, v=0 state and the perturbing states I $^1\Sigma^-$, D $^1\Delta$, a′ $^3\Sigma^-$, e $^3\Sigma^-$ and d $^3\Delta$ of $^{13}C^{18}O$

Molecular	A $^1\Pi$	I $^1\Sigma^-$		D $^1\Delta$		
Parameter	v=0	v=0	v=1	v=0		
T	64762.899(17)	64571.85[b]	65993.16[b]	65448.57[b]		
B	1.45747(21)	1.14543[b]	1.13202[b]	1.13393[b]		
$D \times 10^5$	7.23(42)	5.7[b]	5.7[b]	5.8[b]		
β	-	0.03[b]	-0.05[b]	2.48[b]		
	a′ $^3\Sigma^+$			e $^3\Sigma^-$		d $^3\Delta$
	v=8	v=9	v=10	v=1	v=2	v=4
T_1	-	-	-	-	-	64895.25(58)
T_2	64073.36[b]	65079.75[b]	66069.93[b]	64774.938(16)	65802.43[b]	64928.3(1.3)
T_3	-	-	-	-	-	64961.9(1.2)
B	1.09386[b]	1.07966[b]	1.06557[b]	1.14273(13)	1.12738[b]	1.1230(20)
$D \times 10^6$	5.2[b]	5.2[b]	5.2[b]	5.6[b]	5.6[b]	5.6[b]
α	2.0[b]	1.4[b]	-1.0[b]	8.3221(82)	-10.2[b]	-12.432(50)
$\gamma \times 10^3$	-	0.7[b]	-0.7[b]	-	-	-8.5[b]
λ	-1.2[b]	-1.2[b]	-1.2[b]	0.549(19)	0.5[b]	-
$A_D \times 10^4$	-	-	-	-	-	-0.5[b]

[a]The number in parentheses indicates the uncertainty in the last digit and corresponds to one standard deviation.
[b]Fixed constants in the least squares fit are taken from Field (1971).

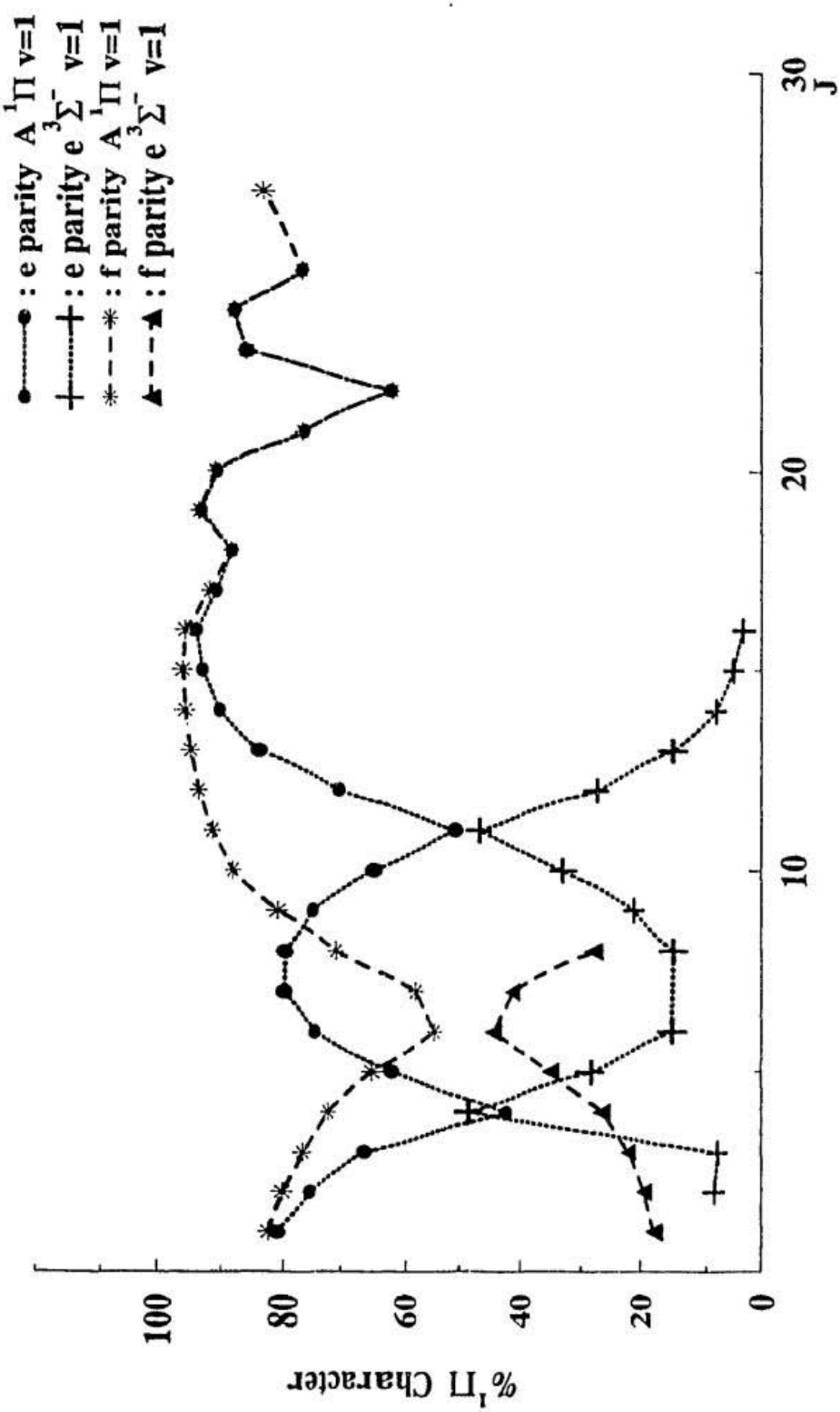

Figure 5.4 Percentage $^1\Pi$ character versus J for the e and f parity levels of $A\,^1\Pi$, v=0 of $^{13}C^{18}O$.

to 62% and 77% at J=22 and 25 for both e and f parities are due to the crossing of the F_1 and F_2 components of the d $^3\Delta$, v=4 level. The percentage $^1\Pi$ character of the singlet(A $^1\Pi$) and triplet (e $^3\Sigma^-$) states are presented in Table 5.3. These quantities will have fundamental importance for the determination of the intrinsic lifetimes of the A $^1\Pi$ (v) and the perturbing states.

***A* $^1\Pi$ v=1:**

The perturbation analysis for A $^1\Pi$, v=1 was carried out by using 1-0 and 1-1 bands. For this level it was possible to observe the crossing of the perturbing levels D $^1\Delta$ v=1, I $^1\Sigma^-$, v=2, e $^1\Sigma^-$, v=3, and d $^3\Delta$, v=6 with the A $^1\Pi$, v=1 level at J=28/29, J=36, J=43 and 44 respectively (see Fig. 1.1). A plot of deviations $|T(v,J)_{obs} - T(v,J)_{cal}|$ versus J is given in Fig. 5.5. In this figure the largest deviation at J=44 is due to the crossing of the d $^3\Delta$, v=6 level. It is also seen that at J=28/29 the deviation in both e and f parity levels characterizes the crossing of the $^1\Delta$, v=1 level and at J=36, the deviation in the f level corresponds to the crossing of the I $^1\Sigma^-$, v=2 level. A total of 11 parameters (T_v for A, v=1, B_v for A, I, D, e, and d, D_v for A, rotation-electronic perturbation parameter β for I and D, and spin-orbit interaction parameter α for e and d) were estimated and are given in Table 5.4. The values of the fixed parameters used in the least - squares fit are also listed in Table 5.4. The Hamiltonian matrix used in the analysis of the data of the A, v=1 level contains three more additional perturbing levels a' $^3\Sigma^+$, v=11, e $^3\Sigma^+$, v=2 and d $^3\Delta$, v=5 which do not cross but interact with the A $^1\Pi$, v=1 level. The experimental data of the A, v=1 level were fitted satisfactorily to the eigenvalues of a 31 x 31 energy matrix. The value of the dimensionless variance σ^2 obtained is 1.5, which indicates that

TABLE 5.3 Percentage of the squares of mixing coefficients of A $^1\Pi$, v=0, 1, 2, 4, 6, 7, and 9, and e $^3\Sigma^-$, v=1 and 4 of $^{13}C^{18}O$.

	A $^1\Pi$		e $^3\Sigma^-$		A $^1\Pi$	
	v=0		v=1		v=1	
J	e	f	e	f	e	f
1	80.9	82.0		17.6[c]	99.6	99.6
2	76.0	80.3	8.6[a]	19.3[c]	99.6	99.6
3	66.1	77.3	8.0[a]	22.3[c]	99.6	99.6
4	42.8	72.4	48.9[a]	27.2[c]	99.6	99.6
5	62.3	65.0	28.8[a]	34.6[c]	99.7	99.7
6	75.0	54.5	15.0[a]	45.1[c]	99.7	99.7
7	80.1	58.0	8.0[a]	41.5[c]	99.7	99.7
8	80.0	70.9	14.9[b]	28.6[c]	99.7	99.7
9	75.4	81.0	21.2[b]	18.5[c]	99.7	99.7
10	64.9	87.7	32.7[b]	11.7[c]	99.7	99.7
11	50.8	91.8	47.3[b]		99.7	99.7
12	70.3	94.2	28.0[b]		99.8	99.8
13	83.5	95.7	14.9[b]		99.8	99.8
14	90.3	96.5	8.1[b]		99.8	99.8
15	93.5	96.8	4.7[b]		99.8	99.8
16	94.7	96.6	2.9[b]		99.8	99.8
17	90.8	92.2			99.8	99.8
18	88.0	88.1			99.8	99.8
19	93.8	94.2			99.8	99.8
20	90.8	91.2			99.8	99.8
21	77.0	77.3			99.8	99.8
22	62.5	62.3			99.8	99.8
23	85.5	85.6			99.8	99.8
24	87.4	87.5			99.8	99.8
25	77.4	77.4			99.8	99.8
26					99.7	99.7
27		83.1			99.4	99.4
28					95.7	95.7
29					95.7	95.6

TABLE 5.3 (Continued)

	$A\ ^1\Pi$ v=0		$e\ ^3\Sigma^-$ v=1		$A\ ^1\Pi$ v=1	
J	e	f	e	f	e	f
30					99.4	99.3
31					99.7	99.6
32					99.8	99.6
33					99.8	99.4
34					99.8	98.8
35					99.8	93.3
36					99.8	88.1
37					99.8	98.4
38					99.7	99.3
39					99.6	99.5
40					98.0	99.5
41					97.3	99.4
42					99.3	99.1
43					98.8	97.1
44					67.2	46.0
45					97.9	97.2

TABLE 5.3 (Continued)

	$A\ ^1\Pi$		$e\ ^3\Sigma^-$		$A\ ^1\Pi$	
	v=2		v=4		v=4	
J	e	f	e	f	e	f
1	99.9	99.9			100.0	100.0
2	99.9	99.9			100.0	100.0
3	99.9	99.9			99.9	99.9
4	99.9	99.8			95.7	95.7
5	99.9	99.8			99.9	99.9
6	99.9	99.6			100.0	100.0
7	99.9	98.0			100.0	100.0
8	99.9	86.6			100.0	100.0
9	99.9	99.0			100.0	100.0
10	99.9	99.5			100.0	100.0
11	99.8	99.7			100.0	100.0
12	99.8	99.7			100.0	100.0
13	99.8	99.8			100.0	100.0
14	99.8	99.8			100.0	100.0
15	99.8	99.8			100.0	100.0
16	99.7	99.7			100.0	100.0
17	99.7	99.7			100.0	100.0
18	99.6	99.7			100.0	100.0
19	99.6	99.6			100.0	100.0
20	99.4	99.5			100.0	100.0
21	99.1	99.4			100.0	100.0
22	98.4	99.3			100.0	100.0
23	96.1	98.9				100.0
24	76.6	98.3	23.1[a]			99.9
25	88.7	96.7				99.9
26	97.1	91.0				99.9
27	98.2	57.5		42.2[c]		
28	97.8	87.9				
29	94.8	95.3				
30		90.3				
31		88.7				
32		96.8				

TABLE 5.3 (Continued)

	$A\ ^1\Pi$		$A\ ^1\Pi$		$A\ ^1\Pi$	
	v=6		v=7		v=9	
J	e	f	e	f	e	f
1	99.5		99.9	99.9		99.9
2	99.5	99.5	99.9	99.9	99.9	99.9
3	99.5	99.5	99.9	99.9	99.9	99.9
4	99.5	99.5	99.9	99.9	99.9	99.9
5	99.6	99.6	99.9	99.9	99.9	99.9
6	99.6	99.6	99.9	99.9	99.9	99.9
7	99.6	99.6	99.9	99.9	99.9	99.9
8	99.7	99.7	99.9	99.9	99.9	99.9
9	99.7	99.7	99.9	99.9	99.9	99.9
10	99.7	99.7	99.9	99.9	99.9	99.9
11	99.7	99.7	99.9	99.9	99.9	99.9
12	99.8	99.8	99.9	99.9		99.7
13	99.8	99.8	99.9	99.8		96.9
14	99.8	99.8	99.8	99.8		98.7
15	99.8	99.8	99.8	99.8		
16	99.8	99.8		99.7		
17	99.9	99.8		99.6		
18	99.8	99.8		99.3		
19	93.0	93.0		98.2		
20	99.9	99.9		82.1		
21	99.9	99.9				
22	99.9	99.9		98.8		

[a]percentage character correspond to F_1 level.
[b]percentage character correspond to F_3 level.
[c]percentage character correspond to F_2 level.

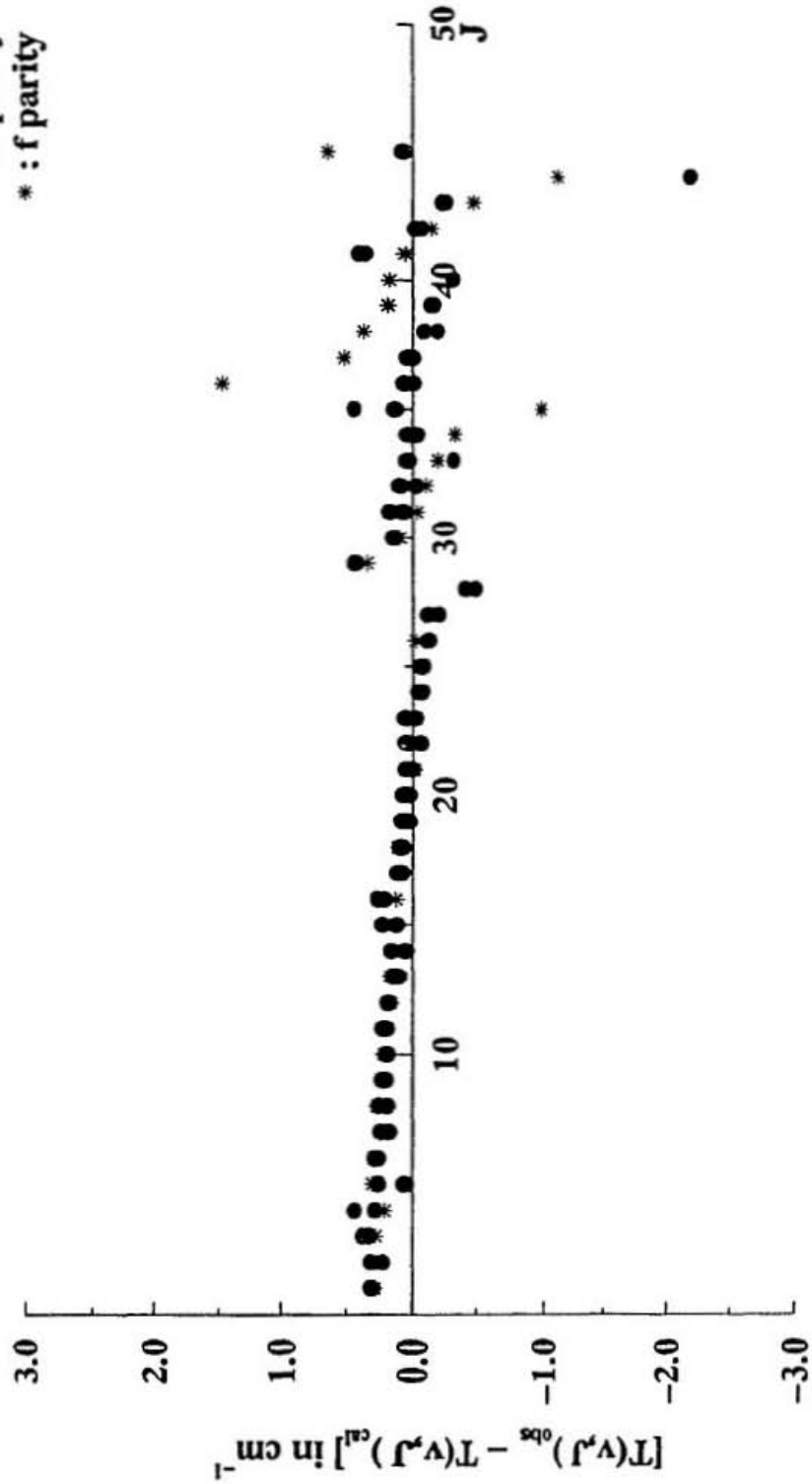

Figure 5.5 Plot of deviations [$T(v,J)_{obs}$ - $T(v,J)_{cal}$] of the rotational levels versus J in A $^1\Pi$, v=1 of $^{12}C^{18}O$.

TABLE 5.4

Molecular parameters[a] (in cm^{-1}) of the A $^1\Pi$, v=1 state and the perturbing states I $^1\Sigma^-$, D $^1\Delta$, a′ $^3\Sigma^-$, e $^3\Sigma^-$ and d $^3\Delta$ of $^{13}C^{18}O$

Molecular Parameter	A $^1\Pi$ v=1	I $^1\Sigma^-$ v=2	D $^1\Delta$ v=1			
T	66176.942(13)	66595.51[b]	66442.44[b]			
B	1.437699(20)	1.11453(23)	1.12519(46)			
D $\times 10^6$	6.220(17)	5.7[b]	5.8[b]			
β	-	0.05468(61)	-0.0682(12)			
	a′ $^3\Sigma^+$		e $^3\Sigma^-$		d $^3\Delta$	
	v=10	v=11	v=2	v=3	v=5	v=6
T_1	-	-	-	-	65920.49[b]	66929.47[b]
T_2	66066.93[b]	67037.77[b]	65802.43[b]	66811.69[b]	65953.96[b]	66963.25[b]
T_3	-	-	-	-	65987.43[b]	66997.03[b]
B	1.06557[b]	1.05115[b]	1.12738[b]	1.11157(43)	1.10873[b]	1.09312(28)
D $\times 10^6$	5.2[b]	5.2[b]	5.6[b]	5.6[b]	5.4[b]	5.4[b]
α	2.8[b]	-2.1[b]	-7.1[b]	2.98(10)	-9.8[b]	9.60(46)
$\gamma \times 10^3$	-0.7[b]	4.5[b]	-	-	-8.3[b]	-8.3[b]
λ	-1.2[b]	-1.1[b]	0.6[b]	0.6[b]	1.2[b]	1.3[b]
$A_D \times 10^4$	-	-	-	-	-1.0[b]	-1.0[b]

[a]The number in parentheses indicates the uncertainty in the last digit and corresponds to one standard deviation.
[b]Fixed constants in the least squares fit are taken from Field (1971).

the experimental data of the 1-0 and 1-1 band are well represented by the energy matrix.

A plot of percentage $^1\Pi$ character versus J is shown in Fig. 5.6. In this figure, the value of the % $^1\Pi$ character for both e and f parities of the A, v=1 level at J=28/29 decreases to 96, corresponding to the crossing of the perturbing D $^1\Delta$, v=1 level. A dip at J=36 to 88% for the f parity level is due to the interaction of the I $^1\Sigma^-$, v=2 level with the A, v=1 level. Though the e $^3\Sigma^-$, v=3 level crosses A, v=1 at J=43, the plot of percentage $^1\Pi$ character versus J in Fig. 5.6 shows a weak interaction compared to the interaction between d $^3\Delta$, v=6 and A $^1\Pi$, v=1 at J=44. This is due to the large value of the interaction parameter $\alpha^f_{1,4}$ = 9.60(46) cm^{-1} estimated from the d - A interaction, which is three times the value of the parameter $\alpha^e_{1,3}$ = 2.98(10) cm^{-1} estimated from the e - A interaction. The values of the percentage $^1\Pi$ character for the rotational levels of A, v=1 for both e and f parities are given in Table 5.3.

A $^1\Pi$**, v=2:**

Perturbation analysis of the A, v=2 level was carried out from four observed bands with v′=2 and v″=0 to 3. Even though the perturbation diagram (Fig. 5.1) predicts three crossings: I $^1\Sigma^-$, v=3 at J=8, e $^3\Sigma^-$, v=4 at J=27, and d $^3\Delta$, v=7 at J=33, for the observed J (J_{max}=33) it was possible to see only two well defined crossings due to I and e states. A plot of $|T(v,J)_{obs} - T(v,J)_{cal}|$ versus J for the A, v=2 level is shown in Fig. 5.7. In this figure, the discontinuity in the f parity level at J=8 due to the crossing of I$^1\Sigma^-$, v=3 is barely seen. This discontinuity is due to the crossing of the I, v=3 level with the A v=2 level and characterizes rotation-electronic interaction. The strong discontinuities at J=24/25 and at J=27/28 are characteristic of strong spin-orbit interaction between the

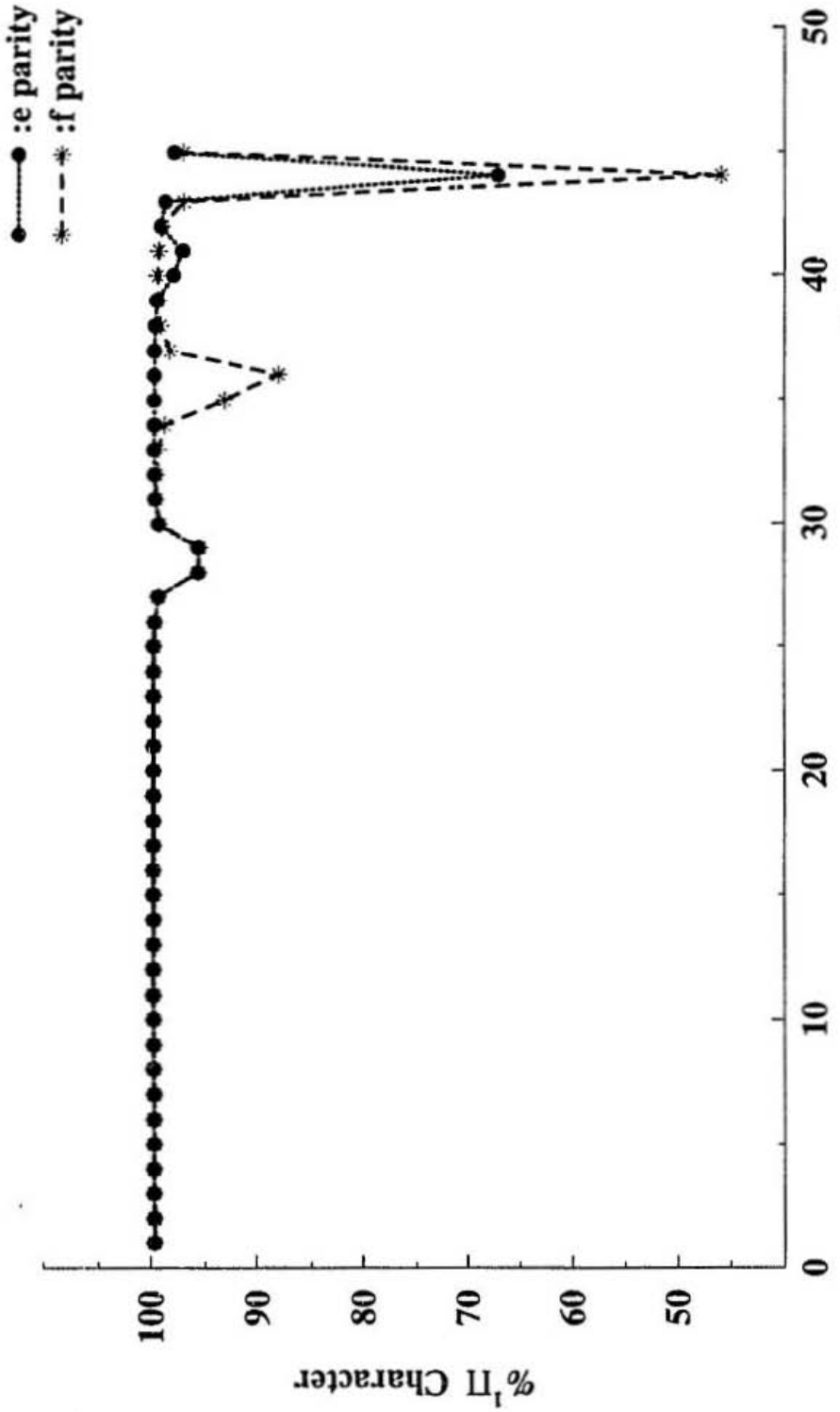

Figure 5.6 Percentage $^1\Pi$ character versus J for the e and f parity levels of A $^1\Pi$, v=1 of $^{13}C^{18}O$.

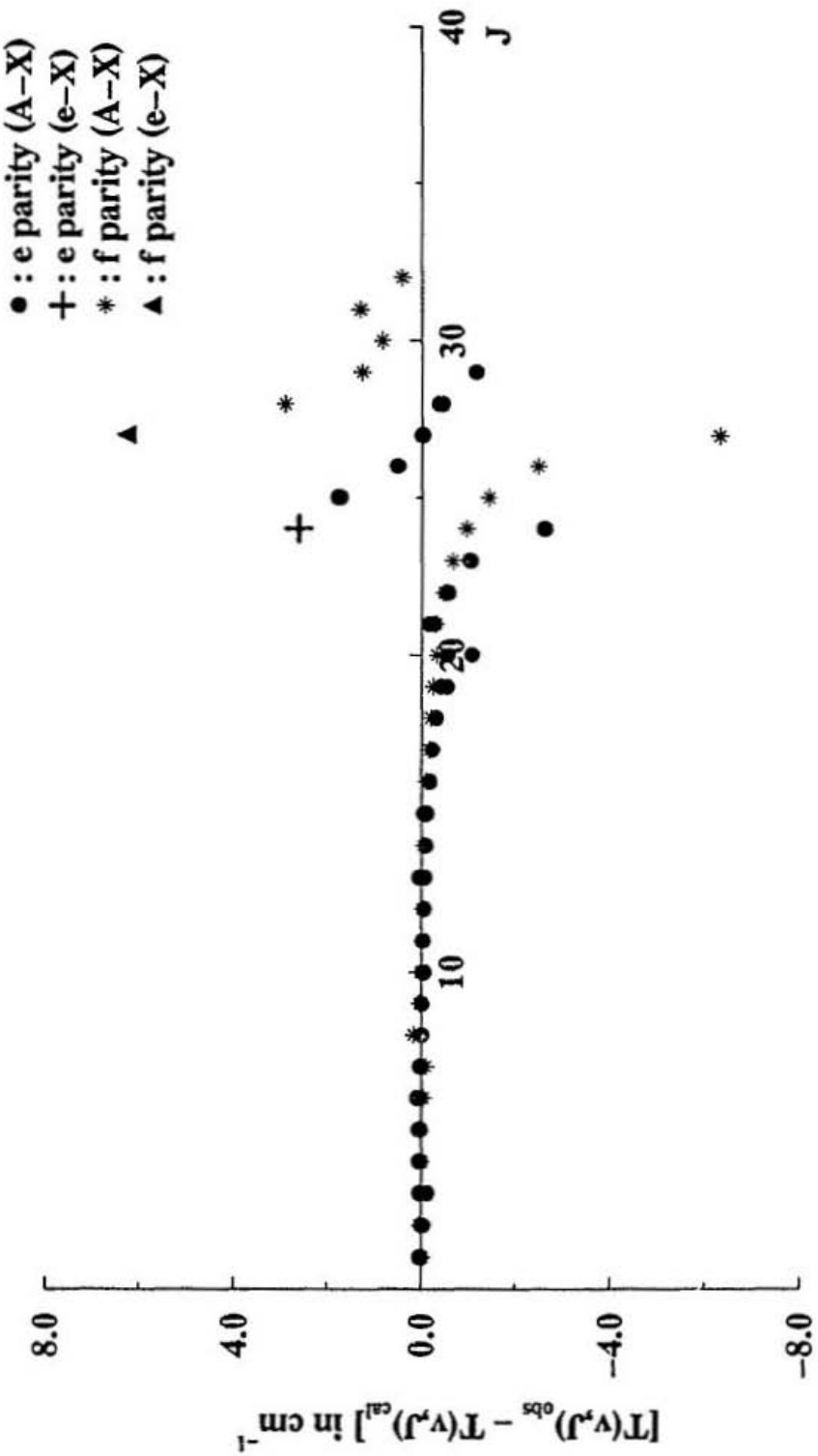

Figure 5.7 Plot of deviations [$T(v,J)_{obs}$ - $T(v,J)_{cal}$] of the rotational levels versus J in A $^1\Pi$, v=2 of $^{13}C^{18}O$.

A, v=2 level and the e, v=4 level. It should be noted that for $^3\Sigma^-$ state the J crossing (J_c) occurs for the F_2 (parity f) component, whereas the F_1 and F_3 (both of parity e) components have lower and higher J_c's, respectively. For the recorded spectra, it was possible to observe the crossing of F_1(e) and F_2(f) components since the observed J_{max} in P and R branches is 29 and it is 32 in the Q branch. This mixing has yielded 3 extra lines [R(23), 67452.662 cm^{-1}, Q(27), 67317.080 cm^{-1}, and P(25), 67282.119 cm^{-1}] (see Table 5.1) which belong to the intercombination band e $^3\Sigma^-$(v=4) - X $^1\Sigma^+$(v=0). The fitted values of the vibrational terms T_v for the A $^1\Pi$, v=2 and e $^3\Sigma^-$, v=4 levels, the rotational constants B_v for the A, v=2, and e, v=4 and the D_v for A, v=2 are given in Table 5.5. Also listed in this table are the fitted perturbation parameters $\beta^l_{2,3}$ and $\alpha^c_{2,4}$, which are determined for the first time. The values of the fixed parameters which were used in the least - squares fit are also given in Table 5.5. The experimental data for the A, v=2 level were fitted satisfactorily to the eigenvalues of a 33 × 33 energy matrix which contains not only the perturbing levels which cross the A, v=2 level but also the D $^1\Delta$, v=3 and a' $^3\Sigma^+$, v=11 levels which interact with the former. The dimensionless variance σ^2 obtained in the fit is 8.3. This large value is due to the difficulty in predicting the crossing of F_1 and F_3 components of the e $^3\Sigma^-$, v=4 level. At higher J values (J > 28) the rotational lines of the P branch of the 2-0 band are overlapped by the 8-4 band. At low J values the A, v=8 level is strongly perturbed by the d $^3\Delta$, v=15 level. Therefore, the fit of the expermental data of the A, v=2 level shows a large variance. Perturbations occurring in the A, v=2 level are also presented in Fig. 5.8, in which the percentage $^1\Pi$ character is plotted against J for both e and f parities for the A $^1\Pi$, v=2 level and the

e $^3\Sigma^-$, v=4 level. Even though the I, v=3 level crosses at the low value of J=7/8, the

TABLE 5.5

Molecular parameters[a] (in cm^{-1}) of the A $^1\Pi$, v=2 state and the perturbing states I $^1\Sigma^-$, D $^1\Delta$, a′ $^3\Sigma^-$, e $^3\Sigma^-$ and d $^3\Delta$ of $^{13}C^{18}O$

Molecular	A $^1\Pi$	I $^1\Sigma^-$	D $^1\Delta$	
Parameter	v=2	v=3	v=2	v=3
T	67559.307(10)	67579.15[b]	67418.41[b]	68376.47[b]
B	1.417460(94)	1.09946[b]	1.10344[b]	1.08819[b]
D $\times 10^6$	5.73(11)	5.7[b]	5.8[b]	5.8[b]
β	-	0.0358(47)	-0.01[b]	-0.03[b]
	a′ $^3\Sigma^+$		e $^3\Sigma^-$	d $^3\Delta$
	v=11	v=12	v=4	v=7
T_1	-	-	-	67912.05[b]
T_2	67037.77[b]	67991.51[b]	67827.83(49)	67946.15[b]
T_3	-	-	-	67980.25[b]
B	1.05155[b]	1.03761[b]	1.06324(76)	1.07958[b]
D $\times 10^5$	5.2[b]	5.2[b]	6.6[b]	5.4[b]
α	4.0[b]	-3.2[b]	7.370(41)	6.4[b]
$\gamma \times 10^3$	-	-	-3.4	-8.3[b]
λ	-1.1[b]	-1.1[b]	0.5[b]	1.2[b]
$A_D \times 10^4$	-	-	-	-1.0[b]

[a]The number in parentheses indicates the uncertainty in the last digit and corresponds to one standard deviation.
[b]Fixed constants in the least squares fit are taken from Field (1971).

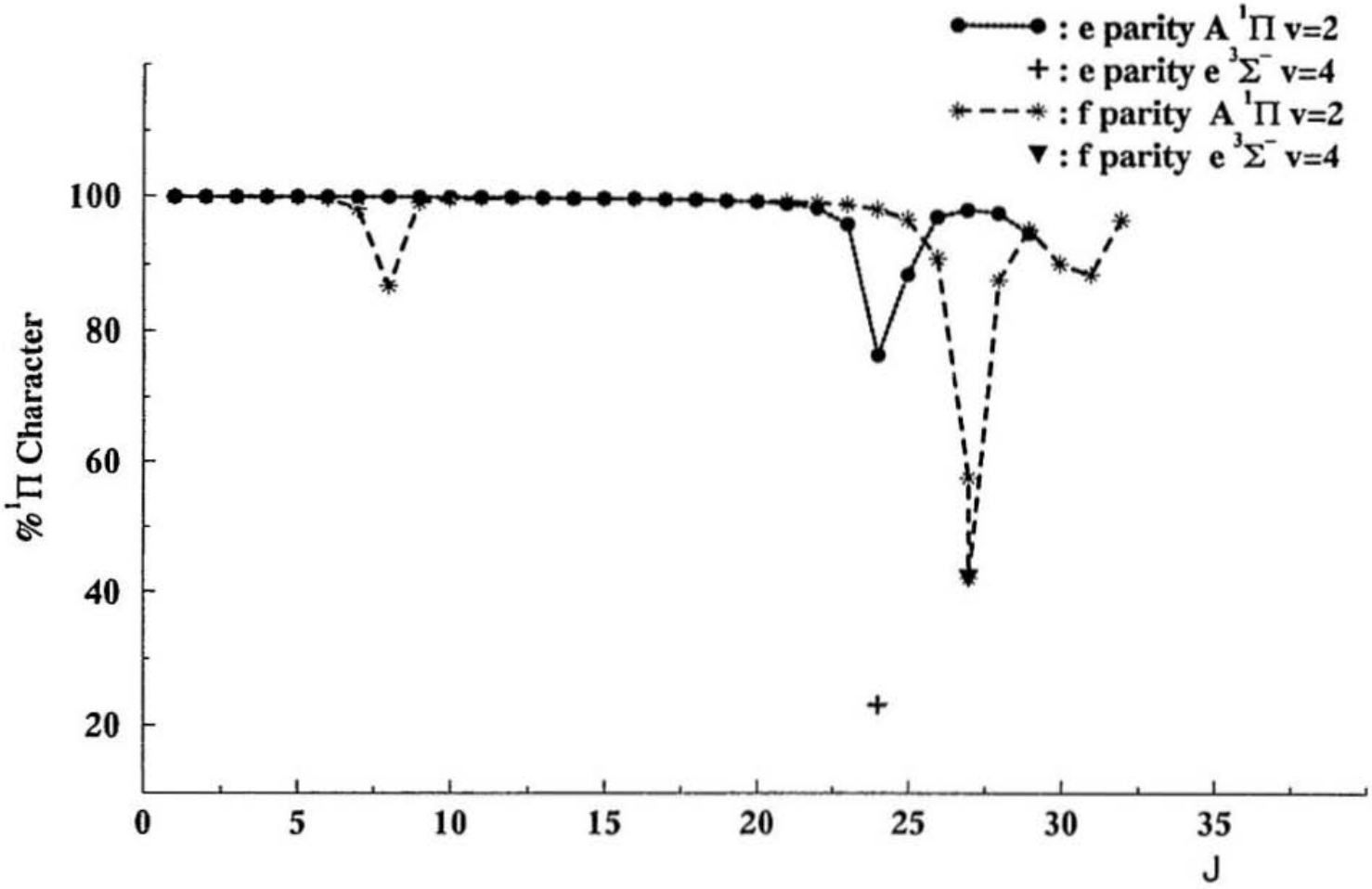

Figure 5.8 Percentage $^1\Pi$ character versus J for the e and f parity levels of A $^1\Pi$, v=2 of $^{13}C^{18}O$.

corresponding deviation $|T(v,J)_{obs} - T(v,J)_{cal}|$ is small and is masked by a large deviation of – 2.2 cm^{-1} due to the crossing of the e $^1\Sigma^-$, v=4 level. But the dip at J=8 of the f parity level in Fig. 5.8 clearly indicates the crossing of the I, v=3 level. At J=24 the percentage $^1\Pi$ character of A, v=2 decreases to 77% and it reaches 23% for the F_1(e) component of the e, v=4 level. The percentage $^1\Pi$ character reaches 42% for the F_2(f) component of e,v=4 and it drops to 58% for A, v=2 at J=27. This mixing is due to the strong spin-orbit interaction between the e $^1\Sigma^-$ and A $^1\Pi$ states. The percentages of the singlet and triplet characters of the rotational levels for both e and f parities are given in Table 5.3.

A $^1\Pi$, v=4:

The 4-0, 4-3, and 4-4 bands were used in the analysis of the perturbed A $^1\Pi$, v=4 level. Of the predicted five crossings of the perturbing D, I, a′, e, d states with A, v=4 only one perturbation due to D $^1\Delta$, v=5 at J=4 was observed as the maxium value of J=26 in the recorded 4-0 band. A plot of $|T(v,J)_{obs} - T(v,J)_{cal}|$ versus J for the A, v=4 level is given in Fig. 5.9. In this figure, the discontinuity associated with the A $^1\Pi$ rotational level at J=4 due to the crossing of the D state is not clearly seen due to a large scattering of the observed data. The fitted values T_v and B_v of A, v=4 and the perturbation parameter $\beta^{D}_{4,5}$ are listed in Table 5.6. In the same table the values of the fixed parameters used in the least - squares fit are also listed. The experimental data for the A, v=4 level of $^{13}C^{18}O$ are fitted satisfactorily to the eigenvalues of a 33 × 33 energy matrix. In this fit, the final value of the dimensionless variance σ^2 is 0.9.

Perturbation occurring in the A, v=4 level is also represented in Fig. 5.10. In this figure the dip at J=4 for both e and f parities is due to the crossing of the D $^1\Delta$, v=5 level

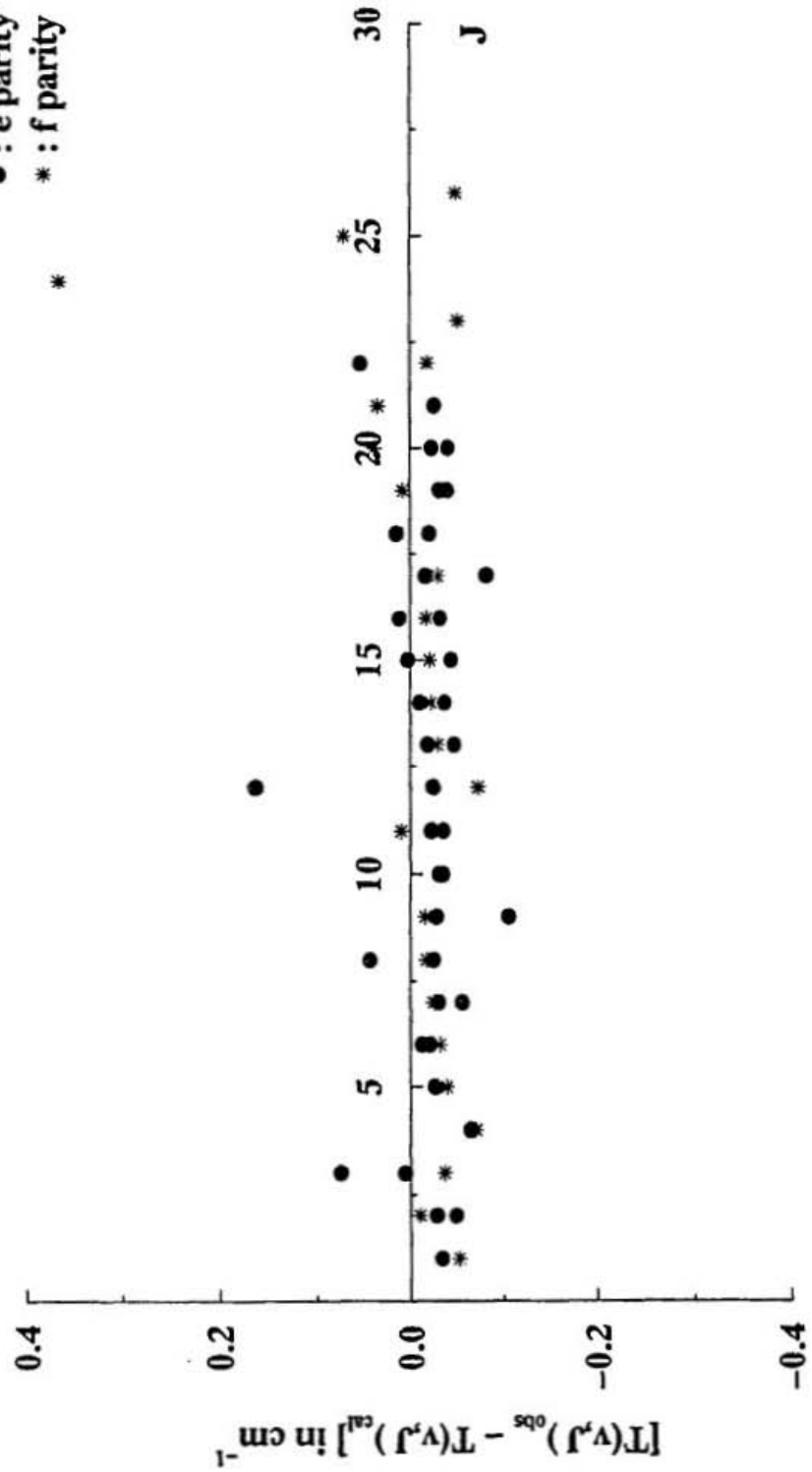

Figure 5.9 Plot of deviations $[T(v,J)_{obs} - T(v,J)_{cal}]$ of the rotational levels versus J in A $^1\Pi$, v=4 of $^{13}C^{18}O$.

TABLE 5.6
Molecular parameters[a] (in cm^{-1}) of the A $^1\Pi$, v=4 state and the perturbing states I $^1\Sigma^-$, D $^1\Delta$, a' $^3\Sigma^-$, e $^3\Sigma^-$ and d $^3\Delta$ of $^{13}C^{18}O$

Molecular	A $^1\Pi$	I $^1\Sigma^-$	D $^1\Delta$	a' $^3\Sigma^+$	e $^3\Sigma^-$	d $^3\Delta$
Parameter	v=0	v=6	v=5	v=15	v=7	v=10
T	70229.3130(39)	70419.65[b]	70238.85[b]	-	-	-
T_1	-	-	-	-	-	70782.84[b]
T_2	-	-	-	70751.15[b]	70672.91[b]	70818.00[b]
T_3	-	-	-	-	-	70853.16[b]
B	1.377367(21)	1.05338[b]	1.05770[b]	0.99605[b]	1.05348[b]	1.03698[b]
$D \times 10^6$	6.4[b]	5.7[b]	5.8[b]	5.1[b]	5.6[b]	5.4[b]
α	-	-	-	4.0[b]	-4.5[b]	0.53[b]
β	-	0.01[b]	0.0192(60)	-	-	-
$\gamma \times 10^3$	-	-	-	-6.9[b]	-8.5[b]	-8.0[b]
λ	-	-	-	-1.1[b]	-0.8[b]	1.2[b]
$A_D \times 10^4$	-	-	-	-	-	-1.0[b]

[a]The number in parentheses indicates the uncertainty in the last digit and corresponds to one standard deviation.
[b]Fixed constants in the least squares fit are taken from Field (1971).

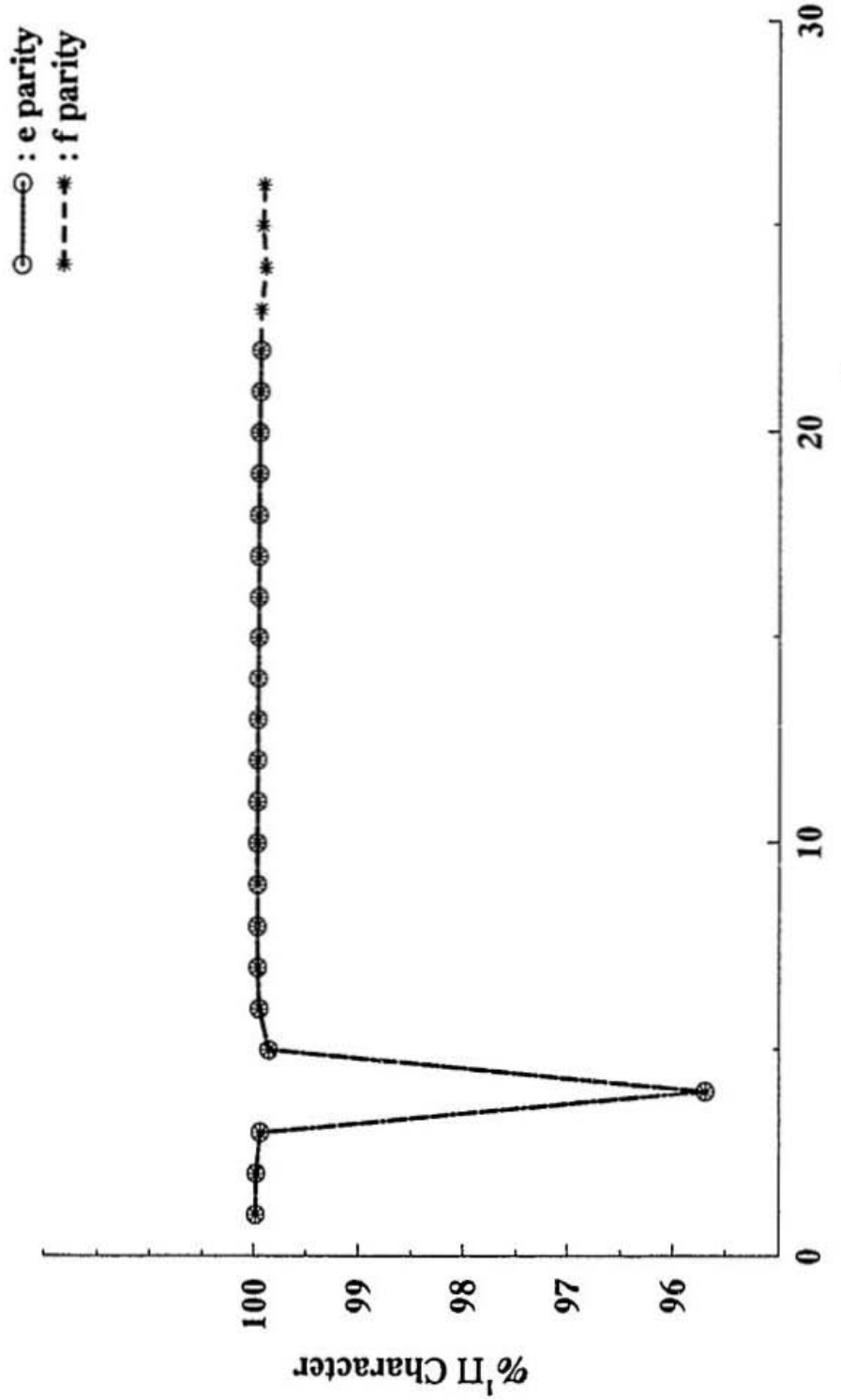

Figure 5.10 Percentage $^{1}\Pi$ character versus J for the e and f parity levels of A $^{1}\Pi$, v=4 of $^{13}C^{18}O$.

with the A, v=4 level and characterizes the rotation-electronic interaction. The values of the % $^1\Pi$ character for the rotational levels of A, v=4 of both e and f parities are given in Table 5.3.

A $^1\Pi$, **v=6:**

The perturbation diagram (Fig. 5.2) shows the location of the crossings of the A $^1\Pi$, v=5 to 9 levels. It is clear from this figure that the perturbing levels D, v=8, I, v=8 and a′, v=18 cross the A, v=6 level at J=19, J=31, and J=39. As the observed J_{max} in the 6-1 and 6-3 bands is 26, only one perturbation due to the D $^1\Delta$, v=8 level is observed. A plot of $|T(v,J)_{obs} - T(v,J)_{cal}|$ versus J is shown in Fig. 5.11. The fitted values T_v and B_v of the A, v=6 level and the perturbation parameter $\beta^{D}_{6,8}$ are given in Table 5.7. The values of the fixed parameters are also listed in the same table. In Fig. 5.11 a discontinuity should be seen in both e and f parity levels due to the crossing of the D, v=8 level with A, v=6 at J=19. However, it is obscured because of large scattering in the observed data. A dip in the plot of percentage $^1\Pi$ character of the rotational levels for both e and f parity levels shown in Fig. 5.12 is due to the rotation-electronic interaction between the D, v=8 level and the A, v=6 level. The values of the % $^1\Pi$ character for the rotational levels of A, v=6 for both the parities are given in Table 5.3. The dimension of the energy matrix used in fittng the data of the 6-1 and 6-3 bands is 31 × 31 and the dimensionless variance σ^2 for this fit is 1.3.

A $^1\Pi$, **v=7:**

In the present deperturbation analysis for the A, v=7 level of $^{13}C^{18}O$, the rotational lines of the 7-1, 7-2, and 7-4 bands have been used. For the maximum value of J

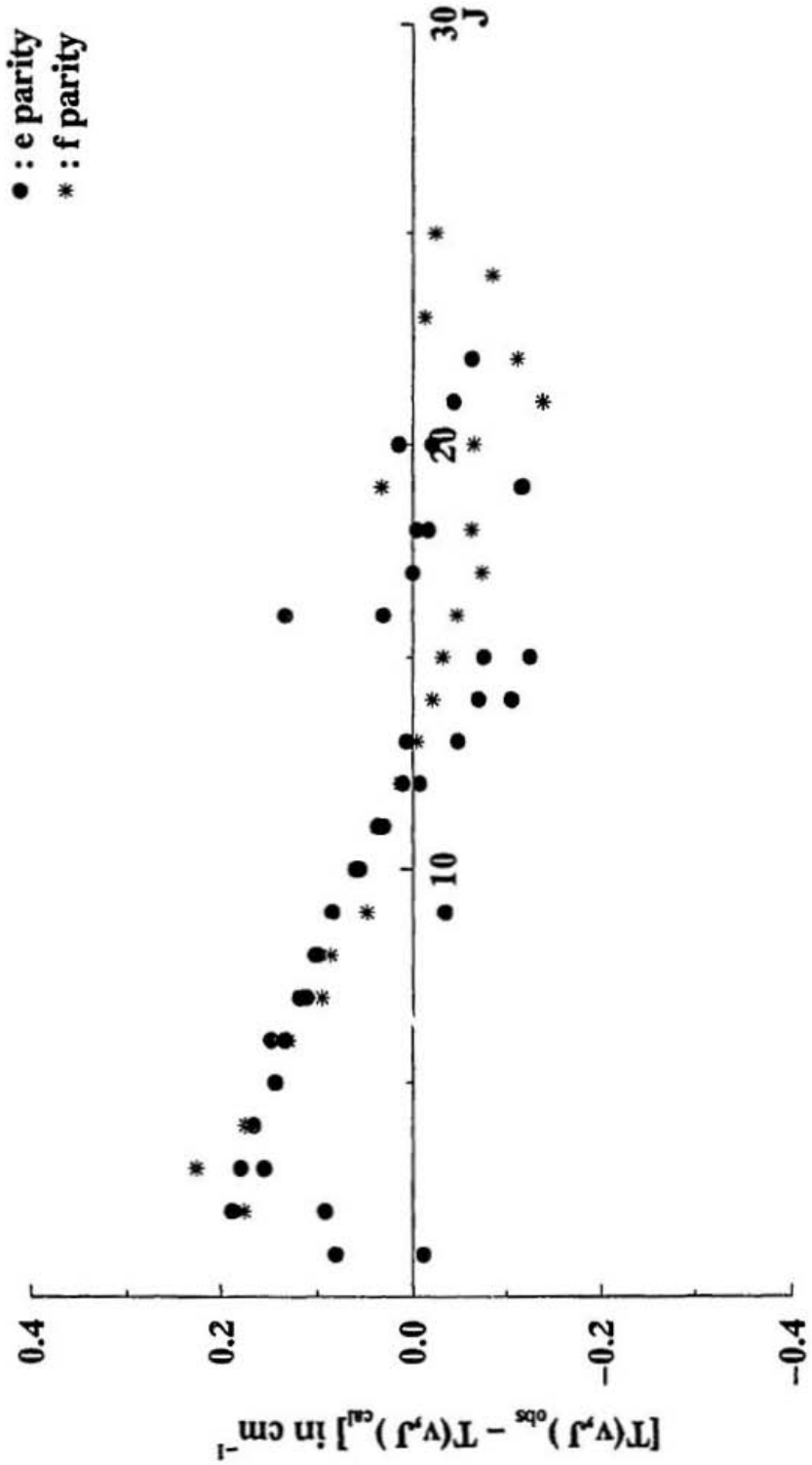

Figure 5.11 Plot of deviations $[T(v,J)_{obs} - T(v,J)_{cal}]$ of the rotational levels versus J in A $^1\Pi$, v=6 of $^{13}C^{18}O$.

TABLE 5.7

Molecular parameters[a] (in cm^{-1}) of the A $^1\Pi$, v=6 state and the perturbing states I $^1\Sigma^-$, D $^1\Delta$, a′ $^3\Sigma^-$, e $^3\Sigma^-$ and d $^3\Delta$ of $^{13}C^{18}O$

Molecular	A $^1\Pi$	I $^1\Sigma^-$		D $^1\Delta$	
Parameter	v=6	v=8	v=9	v=8	
T	72773.0196(52)	72222.68[b]	72898.11[b]	72898.11[b]	
B	1.336165(25)	1.02297[b]	1.01196[b]	1.01196[b]	
$D \times 10^6$	6.6[b]	5.7[b]	5.8[b]	5.8[b]	
β	-	0.04[b]	0.01[b]	0.0137(32)	
	a′ $^3\Sigma^+$		e $^3\Sigma^-$		d $^3\Delta$
	v=17	v=18	v=9	v=10	v=12
T_1	-	-	-	-	72608.65[b]
T_2	72506.87[b]	73359.54[b]	72500.51[b]	73388.92[b]	72644.59[b]
T_3	-	-	-	-	72680.53[b]
B	0.96844[b]	0.95464[b]	1.02457[b]	1.01015[b]	1.00923[b]
$D \times 10^5$	5.1[b]	5.1[b]	5.6[b]	5.6[b]	5.4[b]
α	4.0[b]	-3.9[b]	2.7[b]	0.7[b]	6.3[b]
$\gamma \times 10^3$	-7.0[b]	-7.0[b]	-	-	-8.0[b]
λ	-1.1[b]	-1.1[b]	0.7[b]	0.7[b]	1.2[b]
$A_D \times 10^4$	-	-	-	-	-1.0[b]

[a]The number in parentheses indicates the uncertainty in the last digit and corresponds to one standard deviation.
[b]Fixed constants in the least squares fit are taken from Field (1971).

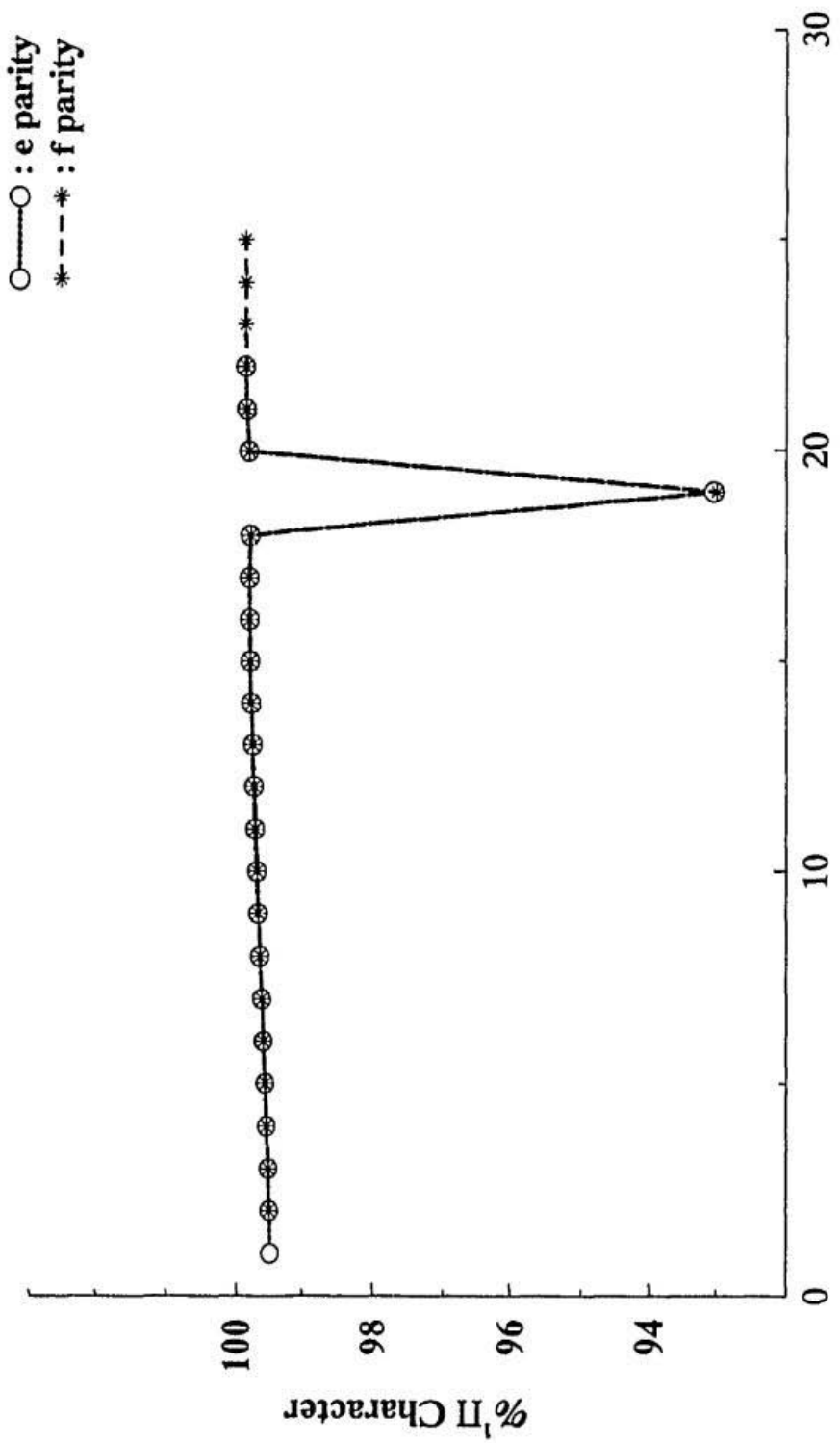

Figure 5.12 Percentage $^{1}\Pi$ character versus J for the e and f parity levels of A $^{1}\Pi$, v=6 of $^{13}C^{18}O$.

(J_{max}=22 for both 7-1 and 7-2 bands), only one perturbation due to a′ $^3\Sigma^+$, v=19 at J=20 is observed even though it is expected to observe five different crossings from in Fig. 5.2. A plot of $|T(v,J)_{obs} - T(v,J)_{cal}|$ versus J for A, v=7 is given in Fig. 5.13. In this figure the discontinuity at J=20 in the f parity level of A, v=7 is due to the crossing of the F_1(f) component of the a′ $^3\Sigma^+$, v=17 level. For the maxium value of J=22 observed in the 7-2 band the crossing of the F_2(e) and F_3(f) at higher J values could not be seen. The fitted values of the vibrational term T_v for A, v=7 and the rotational constants B_v for A, v=7 and a′, v=19 are given in Table 5.8. In this table, the fitted spin-orbit perturbation parameter $\alpha^{a'}_{7,19}$ and the fixed parameters used in the fit are also listed. An energy matrix of dimension 33 × 33 is used in the simultaneous fit of the experimental data of the 7-1, 7-2, and 7-4 bands. The dimensionless variance σ^2 obtained in the fit is 0.9. The crossing of the F_1(f) component of a′ $^3\Sigma^+$, v=19 with A, v=7 is seen in Fig. 5.14 as a drop in the value of the % $^1\Pi$ character of the f parity level of A, v=7 at J=20. This is characteristic of the spin-orbit interaction bewteen a′ $^3\Sigma^+$ and A $^1\Pi$ states. The values of the percentage $^1\Pi$ character for the rotational levels of the A, v=7 level for both e and f parities are listed in Table 5.3.

***A* $^1\Pi$, v=9:**

The deperturbation analysis of the A, v=9 level was carried out from data of the 9-2 and 9-4 bands. In the weak 9-2 band, it is possible to assign only a few rotational lines of the Q branch (see Table. 5.1). All the three (R, Q, and P) branches are identified for the 9-5 band. A plot of $|T(v,J)_{obs} - T(v,J)_{cal}|$ versus J is displayed in Fig. 5.15. In this figure the discontinuity at J=13/14 for the f parity level characterizes

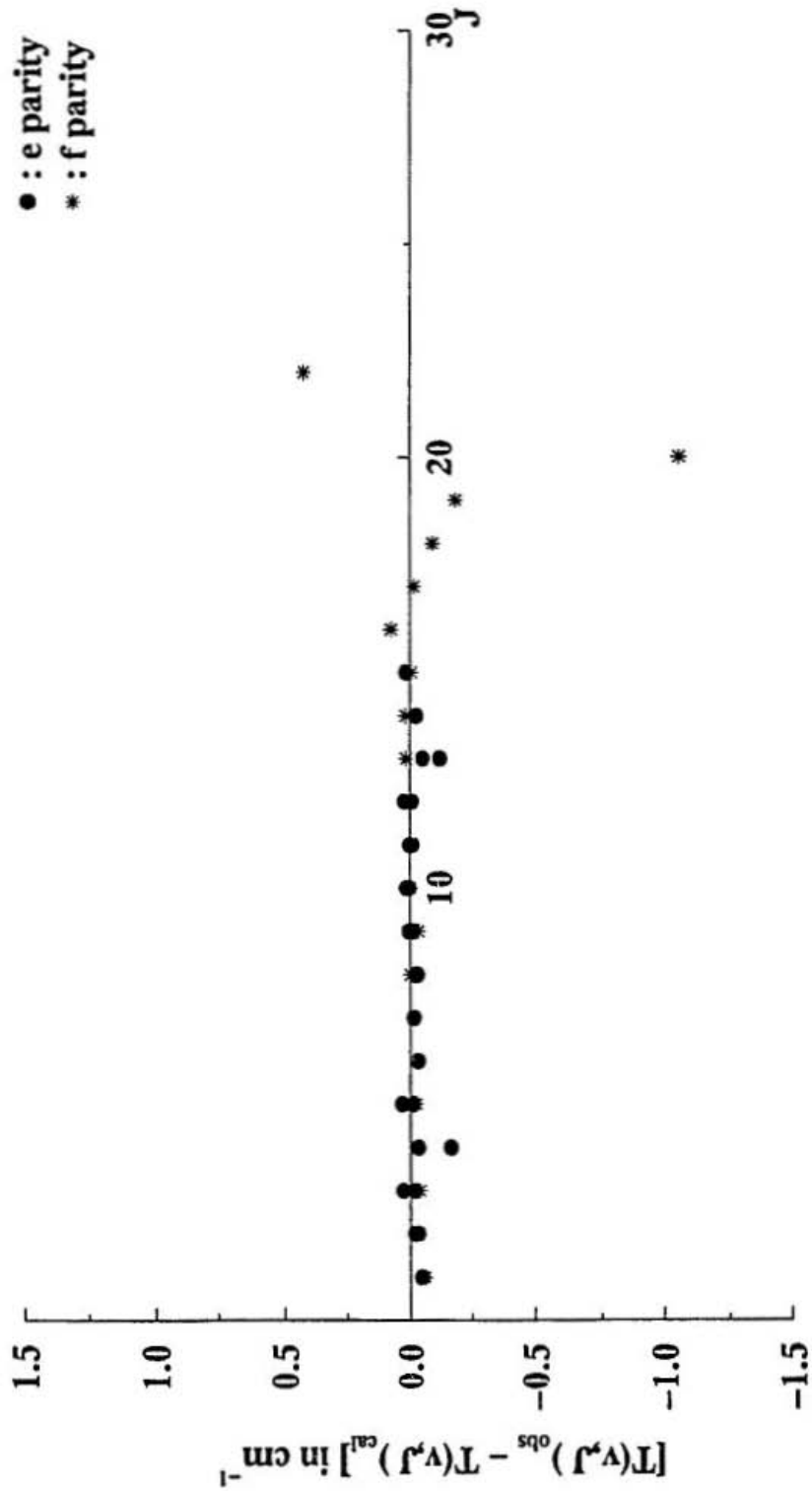

Figure 5.13 Plot of deviations $[T(v,J)_{obs} - T(v,J)_{cal}]$ of the rotational lines versus J in $A\ ^1\Pi$, v=7 of $^{13}C^{18}O$.

TABLE 5.8

Molecular parameters[a] (in cm^{-1}) of the A $^1\Pi$, v=7 state and the perturbing states I $^1\Sigma^-$, D $^1\Delta$, a′ $^3\Sigma^-$, e $^3\Sigma^-$ and d $^3\Delta$ of $^{13}C^{18}O$

Molecular Parameter	A $^1\Pi$ v=7	I $^1\Sigma^-$ v=10	D $^1\Delta$ v=9	
T	73997.8523(87)	73953.90[b]	73748.72[b]	
B	1.315522(56)	0.99275[b]	0.99672[b]	
D $\times 10^6$	6.6[b]	5.7[b]	5.8[b]	
β	-	-0.03[b]	0.03[b]	
	a′ $^3\Sigma^+$ v=19	e $^3\Sigma^-$ v=11	d $^3\Delta$ v=13	d $^3\Delta$ v=14
T_1	-	-	75221.30[b]	74367.22[b]
T_2	74195.35[b]	74260.48[b]	73532.68[b]	74404.00[b]
T_3	-	-	73569.04[b]	74440.78[b]
B	0.9411(24)	0.99574[b]	0.99545[b]	0.98169[b]
D $\times 10^6$	5.1[b]	5.6[b]	5.4[b]	5.4[b]
α	-3.96(23)	-2.2[b]	6.6[b]	-5.8[b]
γ $\times 10^3$	0.01[b]	-	-8.0[b]	-8.0[b]
λ	-1.1[b]	0.7[b]	1.2[b]	1.2[b]
$A_D \times 10^4$	-	-	-1.0[b]	-1.0[b]

[a]The number in parentheses indicates the uncertainty in the last digit and corresponds to one standard deviation.
[b]Fixed constants in the least squares fit are taken from Field (1971).

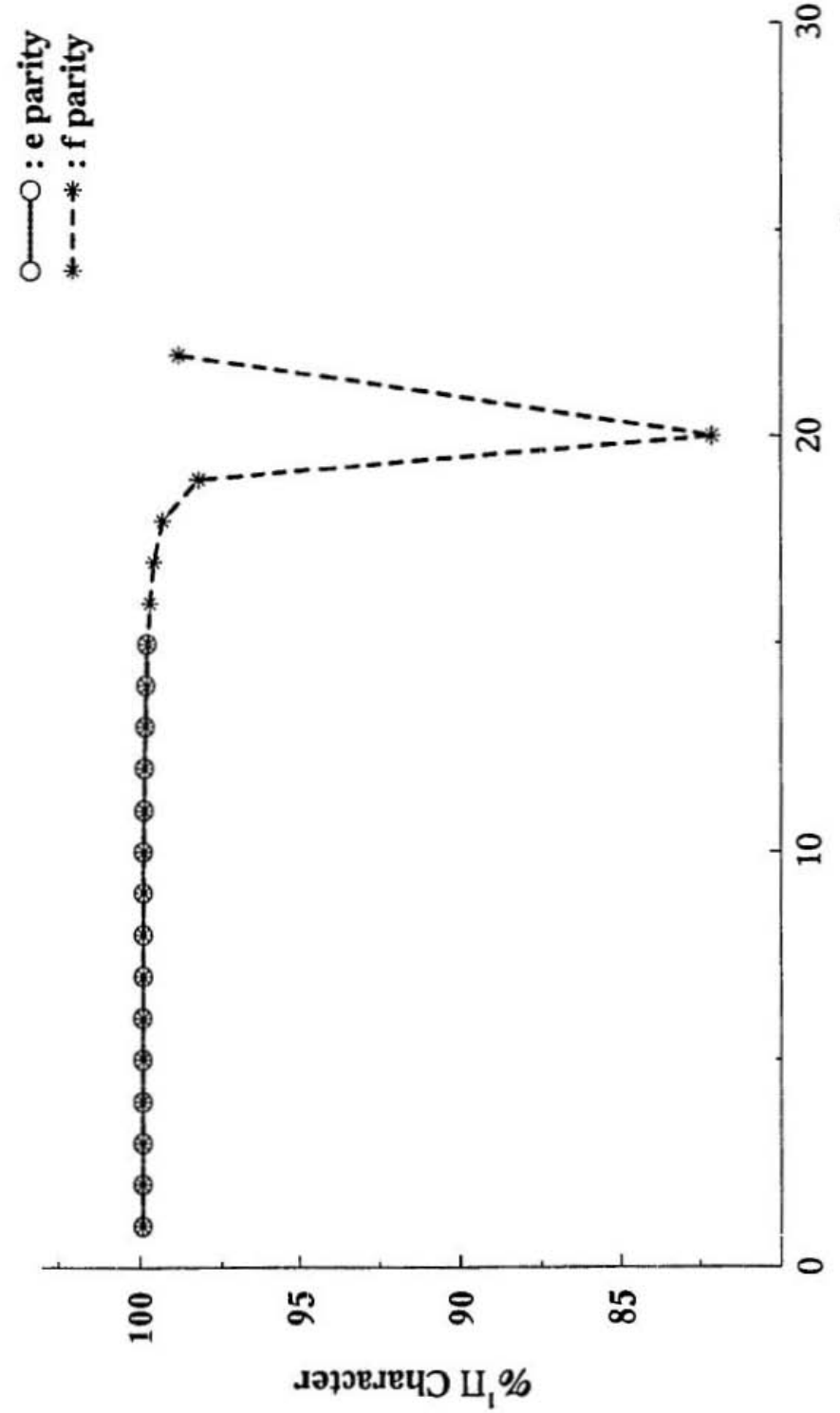

Figure 5.14 Percentage $^{1}\Pi$ character versus J for the e and f parity levels of A $^{1}\Pi$, v=7 of $^{13}C^{18}O$.

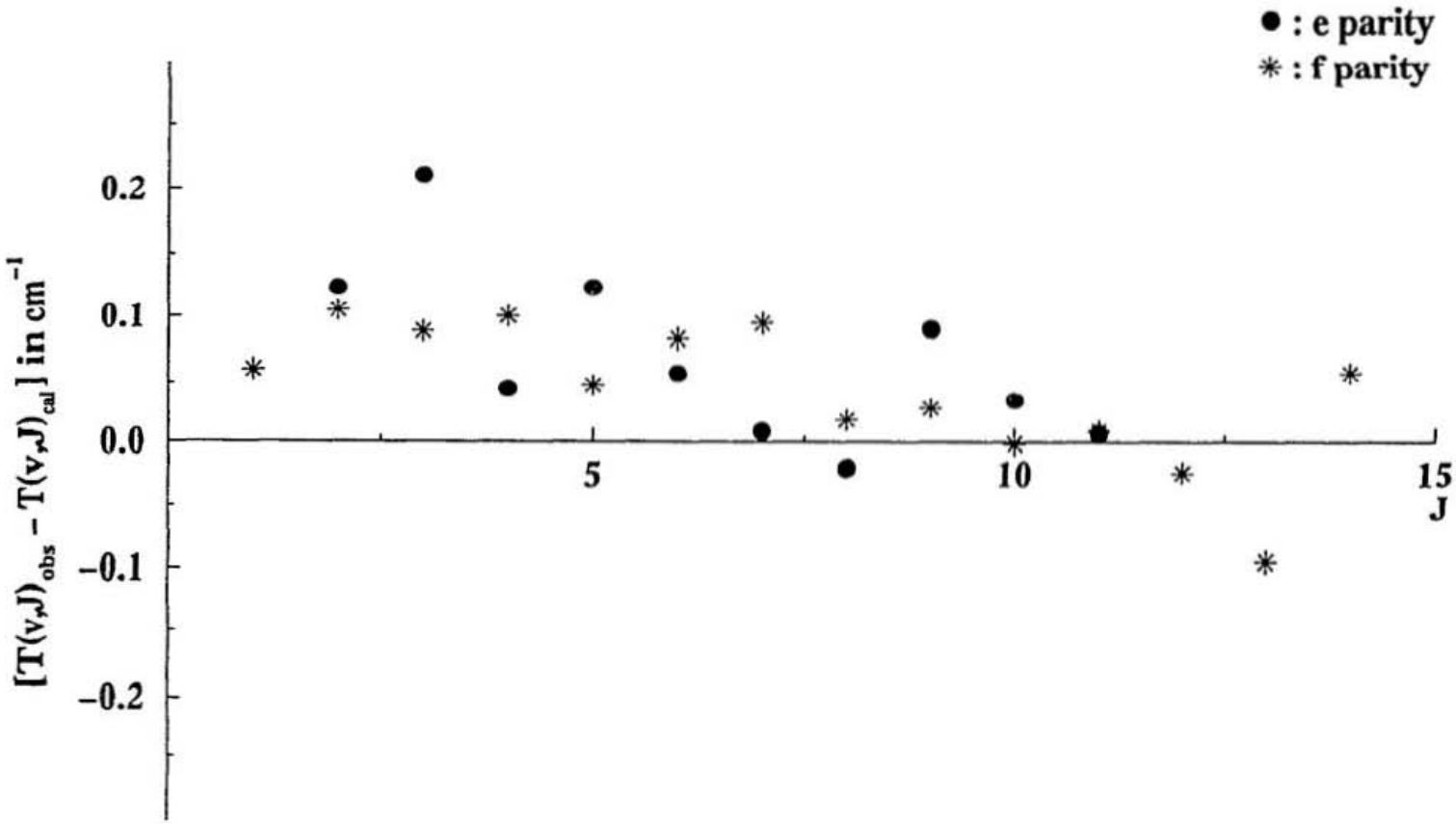

Figure 5.15 Plot of deviations $[T(v,J)_{obs} - T(v,J)_{cal}]$ of the rotational levels versus J in A $^1\Pi$, v=9 of $^{13}C^{18}O$

the weak rotation-electronic interaction between the A $^1\Pi$, v=9 level and the I $^1\Sigma^-$, v=13. The fitted values of T_v and B_v for A, v=9, the perturbation parameter $\beta^I_{9,13}$ and the fixed parameters used in the fit are given in Table 5.9. The value of the dimensionless variance σ^2=1.4 confirms that the experimental data for the A, v=9 level were fitted satisfactorily to the eigenvalues of a 31 x 31 energy matrix. A plot of the percentage $^1\Pi$ character versus J for both e and f parities for A, v=9 is given in Fig. 5.16. In this figure, the dip at J=13 of the f parity level corresponds to the the rotation-electronic interaction between the $^1\Sigma^-$ and $^1\Pi$ states. The values of the percentage $^1\Pi$ character for the A, v=9 level for both e and f parities are listed in Table 5.3.

b) Electronic perturbation parameters

The electronic perturbation parameters a (spin-orbit interaction) and **b** (rotation-electronic interaction) (Eqs. |3.53| and |4.7|) extracted from the fitted coupling terms α (spin-orbit interaction parameter) and β (rotation-electronic interaction parameter) are presented in Table 5.10. These parameters **a** and **b** are calculated by dividing α and β by the vibrational overlap integral $\langle v_A|v_p\rangle$ and the rotational overlap integral $\langle v_A|B|v_p\rangle$ respectively. These integrals calculated by Field and quoted by Le Floch (1989) for $^{12}C^{16}O$ are also given in Table 5.10 and were used in the present analysis for $^{13}C^{18}O$ because in the first approximation the overlap integrals are the same for all the isotopomers of CO. Most of the values of **a** and **b** obtained in the present work are consistent with those obtained by Field (1972a) and Le Floch (1989). For example, the value of **a** = 99.07(55) cm^{-1} for the e(v=4) - A(v=2) interaction is in agreement with the value **a** = 98.9 cm^{-1} given by Field (1972) and **a** = 99.05 cm^{-1} given by Le Floch

TABLE 5.9

Molecular parameters[a] (in cm^{-1}) of the A $^1\Pi$, v=9 state and the perturbing states I $^1\Sigma^-$, D $^1\Delta$, a′ $^3\Sigma^-$, e $^3\Sigma^-$ and d $^3\Delta$ of $^{13}C^{18}O$

Molecular	A $^1\Pi$	I $^1\Sigma^-$	D $^1\Delta$		
Parameter	v=9	v=13	v=12		
T	76354.3629(90)	76415.89[b]	76193.06[b]		
B	1.27379(11)	0.94728[b]	0.95098[b]		
D $\times 10^6$	6.8[b]	5.7[b]	5.8[b]		
β	-	0.0223(31)	-		
	a′ $^3\Sigma^+$		e $^3\Sigma^-$	d $^3\Delta$	
	v=21	v=22	v=13	v=16	
T_1	-	-	-	76058.52[b]	
T_2	75816.10[b]	76600.80[b]	75952.95[b]	76096.19[b]	
T_3	-	-	-	76133.87[b]	
B	0.91314[b]	0.89929[b]	0.96688[b]	0.95397[b]	
D $\times 10^6$	5.1[b]	5.1[b]	5.6[b]	5.4[b]	
α	-2.3[b]	2.8[b]	-4.7[b]	-5.3[b]	
$\gamma \times 10^3$	0.01[b]	0.01[b]	-	-8.0[b]	
λ	-1.1[b]	-1.1[b]	0.7[b]	-	
$A_D \times 10^4$	-	-	-	-1.0[b]	

[a]The number in parentheses indicates the uncertainty in the last digit and corresponds to one standard deviation.
[b]Fixed constants in the least squares fit are taken from Field (1971).

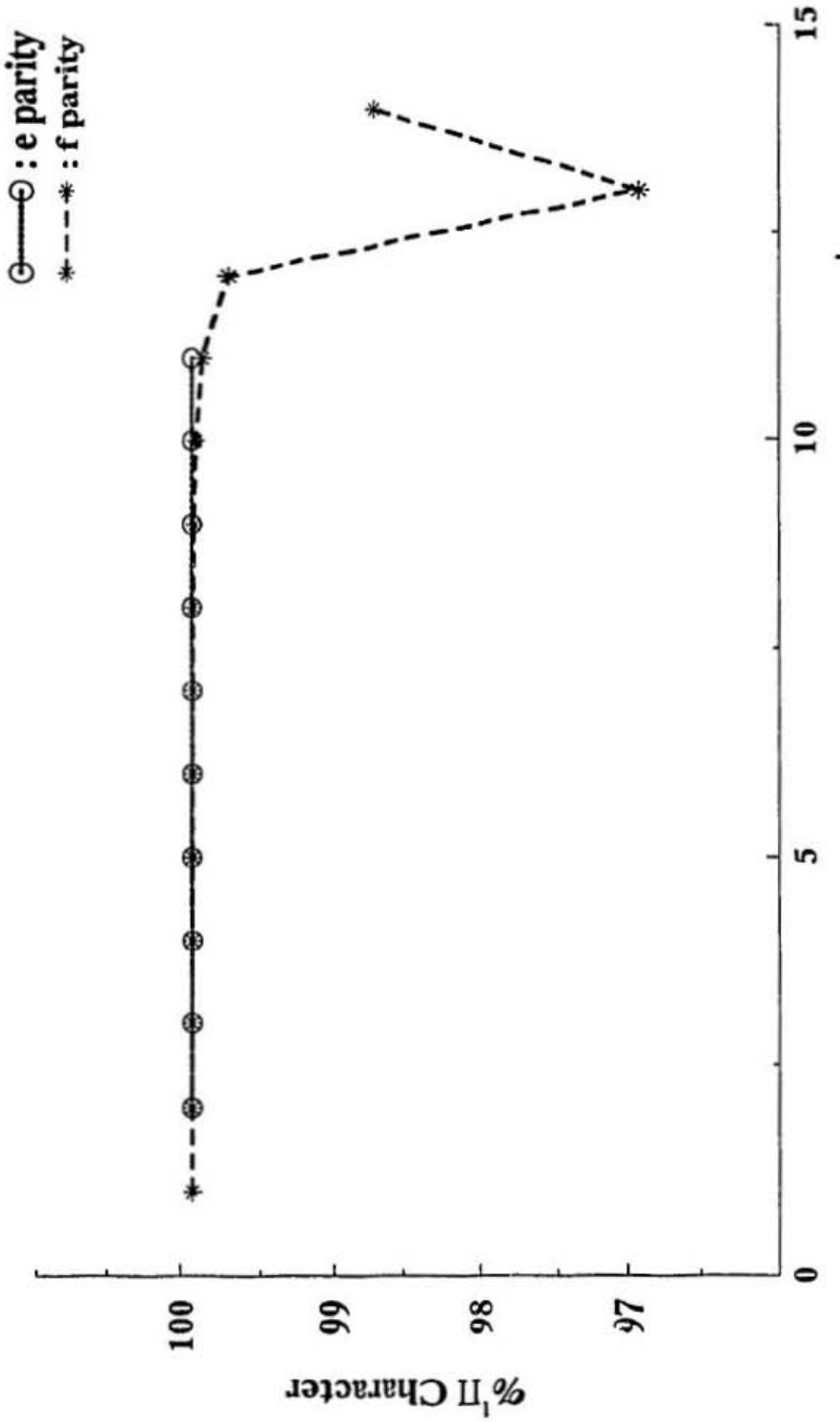

Figure 5.16 Percentage $^1\Pi$ character versus J for the e and f parity levels of $A\,^1\Pi$, v=9 of $^{13}C^{18}O$.

TABLE 5.10 Spin-orbit and rotation-electronic parameters obtained from perturbations of the A $^1\Pi$, v=0, 1, 2, 4, 6, 7, and 9 levels of $^{13}C^{18}O$

Perturber	v_p	$\langle v_A \vert v_p \rangle^a$	α (cm^{-1})	a (cm^{-1})	$\langle v_A \vert B \vert v_p \rangle^a$	β (cm^{-1})	b (unitless)
				A $^1\Pi$, v=0			
a′ $^3\Sigma^+$	8	0.0965	2.0[b]	83.34			
	9	-0.0682	1.4[b]	83.04			
	10	0.0479	-1.0[b]	83.04			
e $^3\Sigma^-$	1	-0.3522	8.3221(82)	94.527(93)			
	2	0.4116	-10.2[b]	98.95			
d $^3\Delta$	4	0.3691	-12.432(50)	95.25(38)			
I $^1\Sigma^-$	0				0.2867	0.033[b]	0.23
	1				-0.4743	0.055[b]	0.23
D $^1\Delta$	0				0.2723	0.025[b]	0.09
				A $^1\Pi$, v=1			
a′ $^3\Sigma^+$	10	-0.1341	2.8[b]	83.04			
	11	0.1009	2.1[b]	83.04			
e $^3\Sigma^-$	2	0.2860	7.1[b]	98.95[b]			
	3	-0.0845	2.98(10)	141(5)			
d $^1\Delta$	5	0.2882	9.8[b]	95.75[b]			
	6	-0.3139	9.60(46)	86(4)			
I $^1\Sigma^-$	2				0.4686	0.05468(61)	0.2334(26)
D $^1\Delta$	1				-0.6224	-0.0682(12)	0.1096(19)
				A $^1\Pi$, v=2			
a′ $^3\Sigma^+$	11	-0.1907	4.0[b]	83.04			
	12	0.1539	3.2[b]	83.04			
e $^1\Sigma^-$	4	0.2976	7.370(41)	99.07(55)			
d $^3\Delta$	7	-0.1880	6.4[b]	95.75			
I $^1\Sigma^-$	3				0.3775	0.0358(47)	0.190(25)
D $^1\Delta$	2				0.0694	0.01[b]	0.09

TABLE 5.10 (Continued)

Perturber	v_p	$\langle v_A \mid v_p \rangle^a$	α (cm^{-1})	a (cm^{-1})	$\langle v_A \mid B \mid v_p \rangle^a$	β (cm^{-1})	b (unitless)
				A $^1\Pi$, v=4			
a′ $^3\Sigma^+$	15	-0.1917	3.9[b]	83.04			
e $^3\Sigma^-$	7	0.1801	4.5[b]	98.95			
d $^3\Delta$	10	-0.0156	0.5[b]	95.74			
I $^1\Sigma^-$	6				0.0754	0.009[b]	0.23
D $^1\Delta$	5				0.2943	0.0192(60)	0.065(20)
				A $^1\Pi$, v=6			
a′ $^3\Sigma^+$	17	-0.1915	4.0[b]	83.02			
	18	0.1895	3.9[b]	83.05			
e $^3\Sigma^-$	9	0.2860	7.1[b]	98.95			
	10	-0.0263	0.7[b]	98.96			
d $^1\Delta$	12	-0.1853	6.3[b]	95.74			
I $^1\Sigma^-$	8				0.3258	0.038[b]	0.23
	9				-0.2617	0.030[b]	0.23
D $^1\Delta$	8				0.3188	0.0137(32)	0.043(10)
				A $^1\Pi$, v=7			
a′ $^3\Sigma^+$	19	0.1765	3.94(13)	89(3)			
e $^3\Sigma^-$	11	0.0899	2.2[b]	98.94			
d $^1\Delta$	13	-0.1941	6.6[b]	95.75			
	14	0.1727	-5.8[b]	95.75			
I $^1\Sigma^-$	10				-0.3016	-0.03[b]	0.23
D $^1\Delta$	9				0.2775	0.03[b]	0.09
				A $^1\Pi$, v=9			
a $^3\Sigma^+$	21	0.1117	-2.3[b]	83.04			
	22	-0.1369	2.8[b]	83.07			
e $^3\Sigma^-$	13	0.1881	4.7[b]	98.95			
d $^1\Delta$	16	0.1561	-5.3[b]	95.75			
I $^1\Sigma^-$	13				0.2318	0.0222(31)	0.192(27)

[a]Calculated by Field (private communication).
[b]Fixed constants in the least-squares fit and are taken from Field (1971).

(1989). However the new value for **a** (e,v=3 - A,v=1) is 141(5) cm^{-1} which is 42% larger than the one obtained earlier. The value of **a** for the a′-A, and d-A interactions (89(3) cm^{-1} and 95.25(38) cm^{-1}) are in agreement with the results of Field and Le Floch (85 cm^{-1} and 82 cm^{-1}). The values of the rotation-electronic interaction parameter **b** (0.2334(26), 0.190(25), and 0.192(27)) for the I-A interaction obtained in the present analysis are very similar to the results of Le Floch and Field (0.2290(24) and 0.2273(38)). The **b** value (0.1096(19)) for the A-D interaction is in agreement with the value 0.11 obtained by Le Floch et al. (1987). It is much smaller than the value 0.47 expected from ab initio calculations by Hall et al. (1973). This illustrates the limited validity of the single configuration approximation and the difficulty of ab initio calculations to estimate a value for **b**.

The values of the molecular parameters T and B given in Tables 5.2 to 5.9 are the effective values which depend on the choice of a particular Hamiltonian matrix used in the analysis of rotational levels of the A $^1\Pi$ state. For example, in the deperturbation analysis of the A $^1\Pi$, v=0 level, a 33 × 33 energy matrix was constructed by including its nine nearest neighbouring levels (see Table 5.2), and the $X^1\Sigma^+$, v″=0, 1 and 2 levels. A complete set of deperturbed molecular constants T′ and B′ of A $^1\Pi$, v=0 can be obtained by considering the contributions arising from the nine nearest neighbouring levels to first order and subtracting the second order contributions arising from remote levels. The second order corrections are estimated through Van Vleck transformation. The completely deperturbed molecular constants T′ and B′ are represented by

$$T' = T^{eff} - \sum_{\Lambda^3} O(\Lambda^3) \qquad [5.3]$$

and

$$B' = B^{eff} - \sum_{\Lambda^3} O_D(\Lambda^3) - q(D\ ^1\Delta). \qquad [5.4]$$

Here the second-order correction parameters O, O_D, and q are defined as (Bergmann and Cossart, 1981, and Zare et al., 1973):

$$O(\Lambda^3) = \sum_{v} |W_v|^2/\Delta T_v \qquad [5.5]$$

$$O_D(\Lambda^3) = -\sum_{v} |W_v|^2 \Delta B_v/(\Delta T_v)^2 \qquad [5.6]$$

and

$$q(D\ ^1\Delta) = \mathbf{b}^2 \sum_{v_D} |\langle v_A|B|v_D\rangle|^2/(T_{vA} - T_{vD}), \qquad [5.7]$$

where

$$W_v = \langle A\ ^1\Pi|\mathbf{H}_{SO}|\Lambda^3\rangle$$

$$\Delta T_v = T(A\ ^1\Pi) - T(\Lambda^3)$$

and

$$\Delta B_v = B(A\ ^1\Pi) - B(\Lambda^3). \qquad [5.8]$$

Here the Λ^3 represents each of the triplet a' $^3\Sigma^+$, e $^3\Sigma^-$, d $^3\Delta$, and a $^3\Pi$ states and $\langle A\ ^1\Pi|H_{SO}|\Lambda^3\rangle$ is given in Eqs. [3.53]. The second order corrections are calculated, considering only those levels which are excluded in the least-squares fit (18 to 20 remote

levels of the perturbing triplet states and 8 to 9 vibrational levels of the $^1\Delta$ state) by using the appropriate electronic perturbation parameters **a** and **b** (given in Table 5.10), the values of the overlap integrals given by Field and Eqs.[5.3 - 5.8]. These corrections $O(A^3)$, $O_D(A^3)$ and $q(D\ ^1\Delta)$ are presented in Tables 5.11 and 5.12. In the deperturbation analysis for the A $^1\Pi$ levels the matrix, elements concerning the a $^3\Pi$ state are not taken into account because states A $^1\Pi$ and a $^3\Pi$ are farther apart. However, to calculate completely deperturbed constants for the A $^1\Pi$ levels, the contribution from the a $^3\Pi$ state is accounted for by calculating the second order corrections due to a $^3\Pi$ levels. The values of the correction parameters O(a $^3\Pi$) and O_D, (a $^3\Pi$) given in Tables 5.11 and 5.12 are 0.110 cm^{-1} and 0.05×10^{-5} cm^{-1} (Le Floch, 1989) respectively. The large constant value of O can be attributed to the fact that A $^1\Pi$ and a $^3\Pi$ are from the same configuration and hence the potential curves are similar (Fig. 1.1). Both A $^1\Pi$ and a $^3\Pi$ have the same equilibrium internuclear distance and hence the overlap integrals are significant only when $\Delta v=0$. The same argument holds for the constant value of 0.05×10^{-5} cm^{-1} for the parameter O_D(a $^3\Pi$) given in Table 5.12. The T'_v values given in Table 5.11 were fitted to the expression

$$T'_v = T_e + \omega_e(v+1/2) - \omega_e x_e(v+1/2)^2 + \omega_e y_e(v+1/2)^3, \qquad [5.9]$$

and the equilibrium vibrational constants T_e, ω_e, $\omega_e x_e$, and $\omega_e y_e$ along with their standard deviations are given in Table 5.13. The B′ values given in Table 5.12 thus obtained were fitted to the relation

$$B'_v = B_e - \alpha_e(v+1/2) + \gamma_e(v+1/2)^2 + \delta_e(v+1/2)^3, \qquad [5.10]$$

TABLE 5.11 Deperturbed T'_v values for the A $^1\Pi$ levels of $^{13}C^{18}O$.

A $^1\Pi$	T^{eff}	$O(\Lambda^3)$ (cm^{-1})				T'_v
v	(cm^{-1})	a′ $^3\Sigma^+$	e $^3\Sigma^-$	d $^3\Delta$	a $^3\Pi$	(cm^{-1})
0	64762.899(17)	0.070	-0.083	0.298	0.110	64762.504(62)
1	66176.942(13)	0.078	0.138	0.022	0.110	66176.594(54)
2	67559.307(10)	0.064	0.084	0.002	0.110	67559.047(40)
4	70229.3130(39)	0.095	0.023	0.139	0.110	70228.946(55)
6	72773.0196(52)	0.027	0.053	0.098	0.110	72772.732(44)
7	73997.8523(87)	0.032	0.086	0.086	0.110	73997.538(48)
9	76354.3629(90)	0.031	0.021	0.015	0.110	76354.186(28)

Number in parantheses indicates uncertainty in the last digit and corresponds to one standard deviation

TABLE 5.12 Deperturbed B'_v values for the A $^1\Pi$ levels of $^{13}C^{18}O$.

A $^1\Pi$	B^{eff}	$O_v(\Lambda^3) \times 10^5$ (cm^{-1})				$q \times 10^5$ (cm^{-1})	B′
v	(cm^{-1})	a′ $^3\Sigma^+$	e $^3\Sigma^-$	d $^3\Delta$	a $^3\Pi$	D $^1\Delta$	(cm^{-1})
0	1.45747(21)	-0.45	-2.22	-14.40	0.05	-0.51	1.45765(21)
1	1.437699(20)	-0.92	-6.11	-2.85	0.05	0.03	1.437797(25)
2	1.417460(94)	-0.91	-4.37	-4.02	0.05	0.13	1.417551(95)
4	1.377367(21)	-6.04	-1.76	-7.08	0.05	0.13	1.377514(30)
6	1.336165(25)	-0.97	-1.51	-3.33	0.05	0.04	1.336222(26)
7	1.315522(56)	-2.22	-2.72	-1.36	0.05	0.13	1.315583(57)
9	1.27379(11)	-0.12	-2.95	-4.78	0.05	0.10	1.27387(11)

Number in parantheses indicates the uncertainty in the last digit and correspond to one standard deviation

TABLE 5.13 Equilibrium molecular constants[a] of the A $^1\Pi$ state of $^{13}C^{18}O$

Molecular Constant	Value (cm^{-1})
T_e	64043.352(83)
ω_e	1446.157(70)
$\omega_e x_e$	15.994(15)
$\omega_e y_e \times 10^2$	1.841(93)
B_e	1.46699(11)
$\alpha_e \times 10^2$	1.920(10)
$\gamma_e \times 10^4$	-1.87(22)
$\delta_e \times 10^6$	7.1(1.5)

Number in parantheses indicates uncertainty in the last digit and corresponds to one standard deviation.

and the equilibrium rotational constants B_e, α_e, γ_e and δ_e estimated for the A $^1\Pi$ state along with their standard deviations are listed in Table 5.13.

5.5 Conclusions

High resolution spectra of nineteen bands of the fourth positive system of $^{13}C^{18}O$ excited in a jet discharge were photographed on the 10.6 m vacuum grating spectrograph. Perturbations in levels v=0, 1, 2, 4, 6, 7, and 9 of the A $^1\Pi$ state have been studied in detail and the deperturbed constants were obtained. Mixing coefficients and electronic perturbation parameters have also been estimated. The derived molecular constants are useful to the astronomers to predict the abundance ratio of the isotopomers of CO in the interstellar space. When term values of the A $^1\Pi$ state are calculated from the data of the present work and combined with the data of the Ångström (b $^1\Sigma^+$ - A $^1\Pi$), Herzberg (C $^1\Sigma^+$ - A $^1\Pi$), and (E $^1\Pi$ - A $^1\Pi$) systems of $^{13}C^{18}O$, accurate spectroscopic information for the Rydberg states B, C, and E states can be obtained.

REFERENCES

Anders, E., and Grevesse, N., *Geochim. Cosmochim. Acta.* **53**, 197 (1989).

Authier, N., Bagland, N., and Le Floch, A. C., *J. Mol. Spectrosc.* **169**, 590 (1993).

Barth, C. A., Fastie, W. G., Hord, C. W., Pearce, J. B., Kelly, K. K., Stewart, A. I., Thomas, G. E., Anderson, G. P., and Raper, O. F., Mariner 6: Ultraviolet of Mars upper atmosphere, *Science* **165**, 1004 (1969).

Barth, C. A., Hord, C. W., Pearce, J. B., Kelly, K. K., Anderson, G. P., and Stewart, A. I., Mariner 6 and 7 spectrometer experiment: Upper atmosphere data, *J. Geophys. Res.* **76**, 2213 (1971).

Barth, C. W., Hord, C. W., Stewart, A. I., and Lane, A. L., Mariner 9, Ultraviolet spectrometer experiment: Initial results, *Science* **175**, 309 (1972).

Field, R. W., Ph. D. thesis, Harvard University, (1971).

Field, R. W., Wicke, B. G., Simmons, J. D., and Tilford, S. G., *J. Mol. Spectrosc.* **44**, 383 (1972a).

Field, R. W., Tilford, S. G., Howard, R. A., and Simmons, J. D., *J. Mol. Spectrosc.* **44**, 347 (1972b).

Field, R. W., Unpublished vibrational integrals and r-centroids of CO: M. I. T., Cambridge Massachusetts.

Garetz, B. A., Kittrell, C., and Le Floch, A. C., *J. Chem. Phys.* **94**, 843 (1991).

Grevesse, N., Lambert, D. L., Sauval, A. J., van Dishoeck, E. F., Farmer, C. B., and Norton, R. H., *Astronomy and Astrophysics* **242**, 488 (1991).

Hall, D. N. B., Noyes, R. W., and Ayres, T. R., *Astrophys. J.* **171**, 615 (1972).

Hall, D. N. B., *Astrophys. J.* **182**, 977 (1973).

Hall, J. A., Schamps, J., Robbe, J. M., and Lefebvre-Brion, H., *J. Chem. Phys.* **59**, 3271 (1973).

Haridass, C., Reddy, S. P., and Le Floch, A. C., *J. Mol. Spectrosc.* **167**, 334 (1994).

Le Floch, A. C., Ph. D. Thesis, University Paris-Sud, Orsay (1989).

Maillard, J. P., Thèse, Doctorat d'Etat ès Sciences Physiques, No. 1157, Faculté des Sciences d'Orsay (1973).

Maillard, J. P., "Highlights of Astronomy" (G. Contopoulos, Ed.), 313, D. Reidel, Dordrecht, Holland (1974).

Morton, D. C., and Noreau, L., *Astrophys. J.* **95**, 301 (1994).

CHAPTER 6

PRECISE ROVIBRONIC TERM VALUES OF SOME VIBRATIONAL LEVELS OF THE A $^1\Pi$, B $^1\Sigma^+$, C $^1\Sigma^+$ AND E $^1\Pi$ STATES OF $^{12}C^{18}O$ AND $^{13}C^{18}O$.

6.1 Introduction

After molecular hydrogen, carbon monoxide is the most abundant molecule in the universe and is used in millimeter radioastronomy to map the density of molecules in the interstellar medium. The spectra of the CO isotopomers are studied in interstellar space, stellar atmospheres, comet-tails, and planetary atmospheres. In all these media the CO abundance with respect to H_2 is determined by the rate of its predissociation under the influence of the UV radiation field. It has been suggested by Bally and Langer (1982) that the photodestruction rate of CO through predissociation of discrete states could be larger than that due to continuum absorption and that this effect explains the observed anomalous isotope ratios of various isotopomers of CO in interstellar molecular clouds. Predissociation in discrete absorption lines of CO is also influenced by coincidence with the rotational structure of H_2 and other molecular lines. Interstellar CO has been the subject of several studies through its ultraviolet electronic transitons A $^1\Pi$-X $^1\Sigma^+$, B $^1\Sigma^+$-X $^1\Sigma^+$, and C $^1\Sigma^+$-X$^1\Sigma^+$ that are based on the spectra of ζ OPHIUCHI acquired with the *Copernicus* satellite and the *Hubble* Space Telescope. For details on these studies the reader is referred to Scheffer et al. (1992) and the references therein.

To identify the absorption and emission spectra of the astrophysical objects and predict the presence of the CO isotopomers, accurate laboratory spectral data are

necessary. Moreover the A $^1\Pi$ state is perturbed by its nearby electronic states a' $^3\Sigma^+$, d $^1\Delta$, e $^3\Sigma^-$, I $^1\Sigma^-$, D $^1\Delta$ and D' $^1\Sigma^+$ and hence one cannot assume the extrapolation of the data of $^{12}C^{16}O$ for its other isotopomers. In Chapter 4 the rotational anlaysis of several bands of the fourth positive (A $^1\Pi$-X $^1\Sigma^+$) system of $^{12}C^{18}O$ and $^{13}C^{18}O$, recorded in the spectral region 1710-1935 Å on a 10.6 m vacuum grating spectrograph has been reported. Several perturbations observed in the A $^1\Pi$ state of these isotopomers have been analyzed and these include A, v=1 and 2 states of $^{12}C^{18}O$ and A, v=1 state of $^{13}C^{18}O$. Deperturbed molecular constants for the A $^1\Pi$ state have been obtained for $^{12}C^{18}O$ and $^{13}C^{18}O$.

Accurate term values of the B $^1\Sigma^+$, v=0 and 1 levels of $^{12}C^{16}O$ were first determined by Le Floch and Amiot (1985) by combining the data obtained from the Fourier Transform spectroscopy and the conventional data of the B $^1\Sigma^+$-A $^1\Pi$ system. Later Eidelsberg et al. (1987) obtained the term values of the B $^1\Sigma^+$, v=0, 1 and 2 levels from the study of the B $^1\Sigma^+$-X $^1\Sigma^+$ system. Le Floch (1992) reported the term values of the A $^1\Pi$, v=0 to 8 states of $^{12}C^{16}O$ and computed accurate term values for the C $^1\Sigma^+$, v=0 and E $^1\Pi$, v=0 levels, from the measurements of the C $^1\Sigma^+$-A $^1\Pi$, E $^1\Pi$-A $^1\Pi$ and A $^1\Pi$-X $^1\Sigma^+$ systems. As far as the isotopomers are concerned, the term values were obtained for the B $^1\Sigma^+$, v=0, 1 and 2 levels of $^{13}C^{16}O$, $^{12}C^{18}O$ and $^{13}C^{18}O$, and the B, v=0 and 1 levels of $^{14}C^{18}O$ (1987). All the reported term values are with reference to X $^1\Sigma^+$, v=0 and J=0. The information on the C $^1\Sigma^+$ state of the CO isotopomers is obtained through the study of the C $^1\Sigma^+$-X $^1\Sigma^+$ system by Eidelsberg et al. (1990, 1991, 1992) and of the Herzberg (C $^1\Sigma^+$- A $^1\Pi$) system by Janjić et al. (1978), Prasad et al. (1985) and Kepa (1988). Roncin et al. (1993) recorded the 0-0 band of C $^1\Sigma^+$-B $^1\Sigma^+$ sytem in the infrared region

for the four isotopomers of CO on a Fourier Transform interferometer and have reported band origins and molecular constants of the excited state C $^1\Sigma^+$. Recently Baker et al. (1993) have tabulated the experimental term values for the E $^1\Pi$, v=0 and 1 levels of the isotopomers $^{12}C^{16}O$, $^{13}C^{16}O$, $^{12}C^{18}O$ and $^{13}C^{18}O$, obtained from a study of the 2+1 resonance enhanced multiphoton spectra of the E-X system.

The purpose of the present work is to obtain accurate term values for the A $^1\Pi$, v=1 and 2, B $^1\Sigma^+$, v=0 and 1, C $^1\Sigma^+$, v=0 and E $^1\Pi$, v=0 states of $^{12}C^{18}O$ by combining our data of the A-X system (Haridass et al., 1994) with those of its B-A (Kepa (1986) and Rytel (1970)), C-A (Janjić et al. (1978)) and E-A (Kepa et al. (1978) and Kepa (1986)) systems. It is also the aim of this work to calculate the precise term values for the A, v=1, B, v=0 and 1, C, v=0 and E, v=0 states of $^{13}C^{16}O$ by combining our data of the A-X system with those of the B-A (Prasad et al., 1984, and Malak et al., 1984), C-A (Prasad et al., 1985, and Kepa, 1988) and E-A (Kepa, 1988) systems.

Section 6.2 describes the determination of the rovibronic levels of A $^1\Pi$, v=1 and 2 of $^{12}C^{18}O$ and v=1 of $^{13}C^{18}O$, as well as B $^1\Sigma^+$, v=0 and 1, C $^1\Sigma^+$, v=0 and E $^1\Pi$, v=0 of both isotopomers. The molecular parameters of their B, C and E states determined from the calculated term values are given in Section 6.3. Conclusions are summarized in Section 6.4.

6.2 Determination of Rovibronic Term Values

$^{12}C^{18}O$:

(i) The A $^1\Pi$, v=1 and 2 levels

Rotational analysis of the 1-4, 1-5, 2-2, 2-5 and 2-6 bands of the A $^1\Pi$-X $^1\Sigma^+$ system of $^{12}C^{18}O$ recorded on a 10.6 m vacuum grating spectrograph at Ottawa was performed and the wavenumbers of the rotational lines are listed in Chapter 4. The term values T(v,J) of the X $^1\Sigma^+$ state can be obtained from the Dunham expression,

$$T(v,J) = \sum_{lm} Y_{lm} (v+1/2)^l [J(J+1)]^m \qquad |6.1|$$

where

$$Y_{lm} = U_{lm} \mu^{-(l+2m)/2} [1+m_e(\Delta_{lm}^C/m_C + \Delta_{lm}^O/m_O]$$

and

$$(1/\mu) = (1/m_C) + (1/m_O).$$

Here U_{lm} are the mass-independent Dunham parameters, Δ_{lm}^C and Δ_{lm}^O are the mass-scaling parameters for CO, and m_C and m_O are the masses of carbon and oxygen atoms. The T(v,J) values for v=2, 4, 5 and 6 of X $^1\Sigma^+$ state of $^{12}C^{18}O$ are calculated from Eq. |6.1| using the numerical values of U_{lm}, Δ_{lm}^C and Δ_{lm}^O calculated by Authier et al. (1993). The rovibrational term values of the A $^1\Pi$, v=1 state are then obtained, by adding the observed wavenumbers of the 1-4 and 1-5 bands of the A-X system to the corresponding values for v=4 and 5 of X $^1\Sigma^+$. By this procedure we have obtained 124 term values, 73 of e parity and 51 of f parity, with J=1 to 28 for A $^1\Pi$, v=1. Each vibrational term value is obtained from several independently determined weighted average values. Each weight

is taken as the reciprocal of the square of the relevant total error. Finally the term values of A $^1\Pi$, v=1 with reference to X $^1\Sigma^+$, v=0 and J=0 are listed in Table 6.1. For further clarification, we mention here as an example that the value 66310.46(2) cm^{-1} for the e parity level of J=8 is the weighted average value obtained from the P and R branches of the 1-4 and 1-5 bands (see Table 6.1). It should be noted that in Table 6.1, the value 66433.90(2) cm^{-1} for J=12 level of the f parity belongs to the perturbing a' $^1\Sigma^+$, v=10 level which appears as an extra line in each of the 1-4 and 1-5 bands of the A-X system. Because this perturbation is strong, the rotational levels of A, v=1 are severely affected. A plot of the Λ-doubling, i.e., the $T_f - T_e$ values, against J for A $^1\Pi$, v=1, given in Fig. 6.1 shows large anomalous behaviour of the Λ doubling at J=12/13, 14/15 and 17/18.

Using a similar procedure we have calculated the rovibronic term values of the A $^1\Pi$, v=2 level, by adding the wavenumbers of the 2-2, 2-5 and 2-6 bands of the A-X system to the corresponding term values of the X $^1\Sigma^+$, v=2, 5 and 6, as mentioned above, and these are presented in Table 6.1. For the v=2 level, the term values for J=1 to 26 are obtained from a total of 192 values, of which 121 belong to the e parity and 71 belong to the f parity. A plot of the Λ doubling against J shown in Fig. 6.2 indicates perturbations at J=7/8 and 22/23 and these are caused by the I $^1\Sigma^-$, v=3 and e $^1\Sigma$, v=4 levels. The term values of the rovibronic levels of the A $^1\Pi$, v=1 and 2 of $^{12}C^{18}O$ are reported for the first time.

(ii) The B $^1\Sigma^+$, v=0 and 1 levels

Among the observed Rydberg states of CO, the B $^1\Sigma^+$ (.... $2p^4$ $2p\sigma$ $3s\sigma$) state is the first member of the nsσ series which converges to the ground state X $^2\Sigma^+$ of the molecular

TABLE 6.1 Rovibronic term values[a] (in cm^{-1}) of the A $^1\Pi$ (v=1 and 2), B $^1\Sigma^+$ (v=0 and 1), C $^1\Sigma^+$ (v=0) and E $^1\Pi$(v=0) states of $^{12}C^{18}O$

	A $^1\Pi$			
	v=1		v=2	
J	e level	f level	e level	f level
1	66205.3 (2)	66205.25(3)	67618.1 (1)	
2	66211.2 (2)	66211.26(3)	67623.9 (1)	67623.97(5)
3	66220.33(3)	66220.27(3)	67632.9 (1)	67632.91(4)
4	66232.30(8)	66232.31(3)	67644.77(3)	67644.76(3)
5	66247.33(7)	66247.33(4)	67659.61(2)	67659.61(8)
6	66265.38(2)	66265.38(3)	67677.42(4)	67677.40(5)
7	66286.42(1)	66286.41(2)	67698.20(4)	67698.06(2)
8	66310.46(2)	66310.45(6)	67621.93(2)	67622.09(3)
9	66337.52(2)	66337.47(2)	67748.65(2)	67748.71(3)
10	66367.56(2)	66367.49(1)	67778.31(1)	67778.34(8)
11	66400.59(1)	66400.32(1)	67810.93(2)	67810.98(8)
12	66436.55(2)	66438.4 (1)	67846.52(2)	67846.56(3)
12		66433.90(2)		
13	66475.42(1)	66476.22(3)	67885.06(2)	67885.11(3)
14	66516.33(5)	66518.09(6)	67926.54(2)	67926.60(3)
15	66564.02(3)	66563.10(8)	67971.00(4)	67971.05(6)
16	66611.60(3)	66611.08(0)	68018.41(3)	68018.44(3)
17	66662.51(3)	66661.79(3)	68068.7 (1)	68068.77(9)
18	66716.48(1)	66717.08(1)	68122.02(7)	68122.04(5)
19	66773.48(3)	66773.64(1)	68178.2 (1)	68178.25(6)
20	66833.4 (2)	66833.54(2)	68237.33(2)	68237.4 (1)
21	66896.4 (3)	66896.49(3)	68299.42(4)	68299.48(3)
22	66962.49(0)	66962.46(3)	68364.2 (3)	68364.43(5)
23	67031.37(6)	67031.38(2)	68431.90(9)	68432.31(5)
24	67103.21(9)	67103.21(4)		68503.11(2)
25		67178.0 (3)		68576.69(3)
26		67255.81(3)		68652 (1)
27		67335.45(3)		
28		67420.95(9)		

TABLE 6.1 (Continued)

	$B\ ^1\Sigma^+$		$C\ ^1\Sigma^+$	$E\ ^1\Pi$	
	v=0	v=1	v=0	v=0	
J	e level	e level	e level	e level	f level
0	86916.6 (3)		91918.6 (2)		
1	86920.4 (2)	88953.9 (2)	91922.3 (3)	92933.1 (3)	92933.35(7)
2	86927.8 (1)	88961.29(9)	91930.00(8)	92940.77(8)	92940.79(1)
3	86938.94(6)	88972.28(3)	91941.06(6)	92951.9 (1)	92951.97(4)
4	86953.83(4)	88986.9 (1)	91955.90(7)	92966.97(7)	92966.77(4)
5	86972.37(2)	89005.42(6)	91974.41(4)	92985.64(4)	92985.36(5)
6	86994.67(4)	89027.29(5)	91996.61(5)	93008.15(5)	93007.67(5)
7	87020.61(3)	89052.80(4)	92022.51(4)	93034.29(4)	93033.70(6)
8	87050.27(3)	89082.10(4)	92052.15(4)	93064.22(3)	93063.43(4)
9	87083.63(2)	89115.01(3)	92085.43(4)	93097.86(3)	93096.90(6)
10	87120.74(3)	89151.71(3)	92122.6 (3)	93135.26(4)	93134.07(3)
11	87161.51(2)	89191.89(4)	92163.15(4)	93176.38(3)	93174.95(6)
12	87206.00(3)	89235.82(3)	92207.54(4)	93221.23(4)	93219.54(4)
13	87254.19(3)	89283.32(4)	92255.61(5)	93269.77(4)	93267.81(4)
14	87306.09(3)	89334.6 (1)	92307.38(5)	93322.13(4)	93319.88(5)
15	87361.66(3)		92362.85(3)	93378.13(4)	93375.56(6)
16	87420.95(3)		92422.03(6)	93437.95(4)	93434.99(5)
17	87483.93(2)		92484.87(4)	93501.42(3)	93498.15(7)
18	87550.57(3)		92551.38(5)	93568.62(5)	93565.0 (1)
19	87620.90(3)		92621.57(5)	93639.55(5)	93635.40(9)
20	87694.95(4)		92695.45(8)	93714.12(9)	93709.8 (2)
21	87772.61(4)		92772.99(7)		
22	87854.02(5)		92854.2 (1)		
23	87839.10(7)				
24	88027.78(4)				
25	88120.17(3)				
26	88216.25(5)				
27	88316.25(2)				
28	88419.55(2)				

[a]These are the weighted average values and the number in the parentheses indicates the statistical error and corresponds to 3 standard deviations.

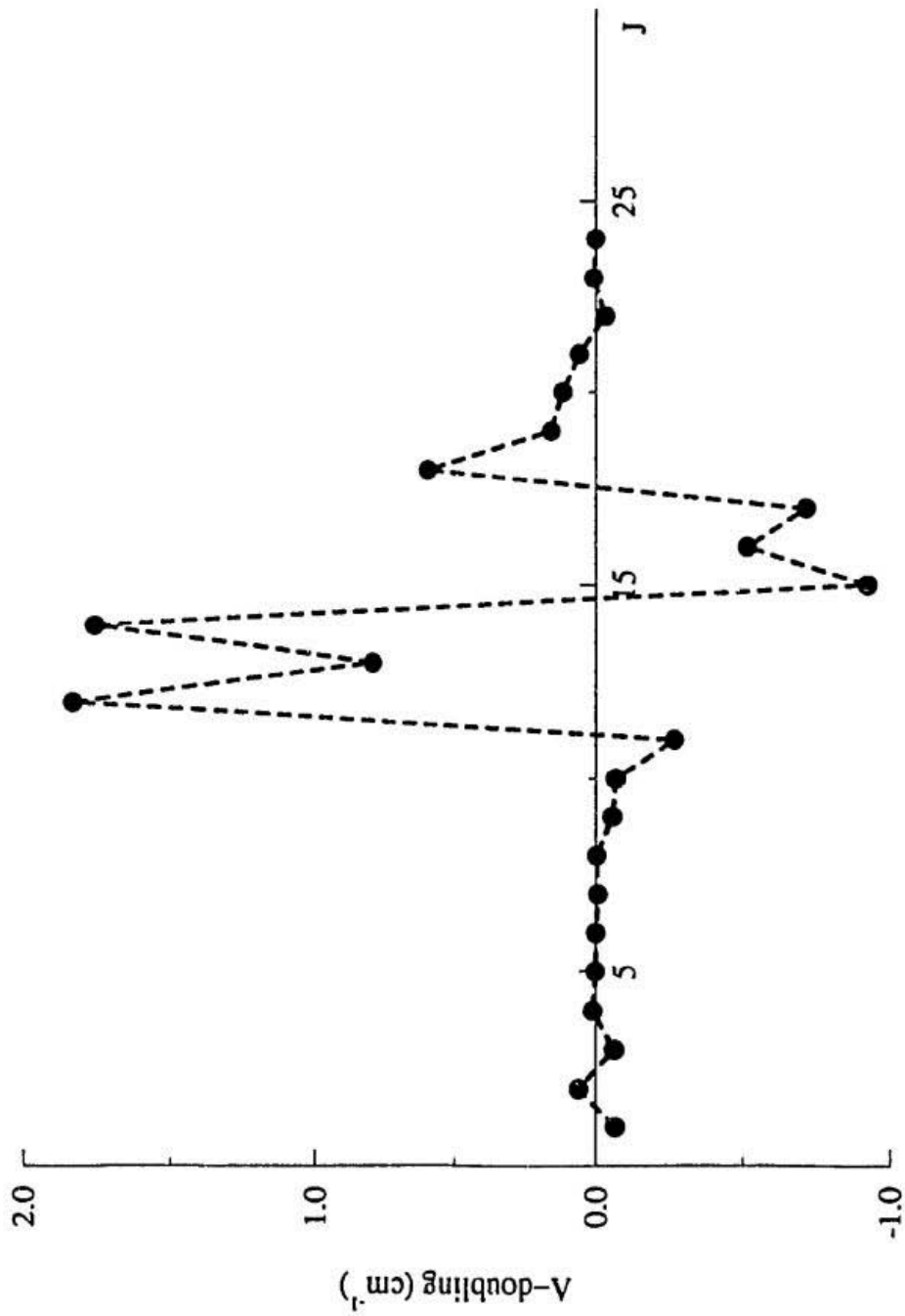

Figure 6.1 A plot of Λ-doubling (T_f - T_e) versus J for the A $^1\Pi$, v=1 level of $^{12}C^{18}O$. The large anomalous behaviour of Λ due to a' $^3\Sigma^+$ (v=10) is clearly seen at J = 12/13, 14/15, and 17/18.

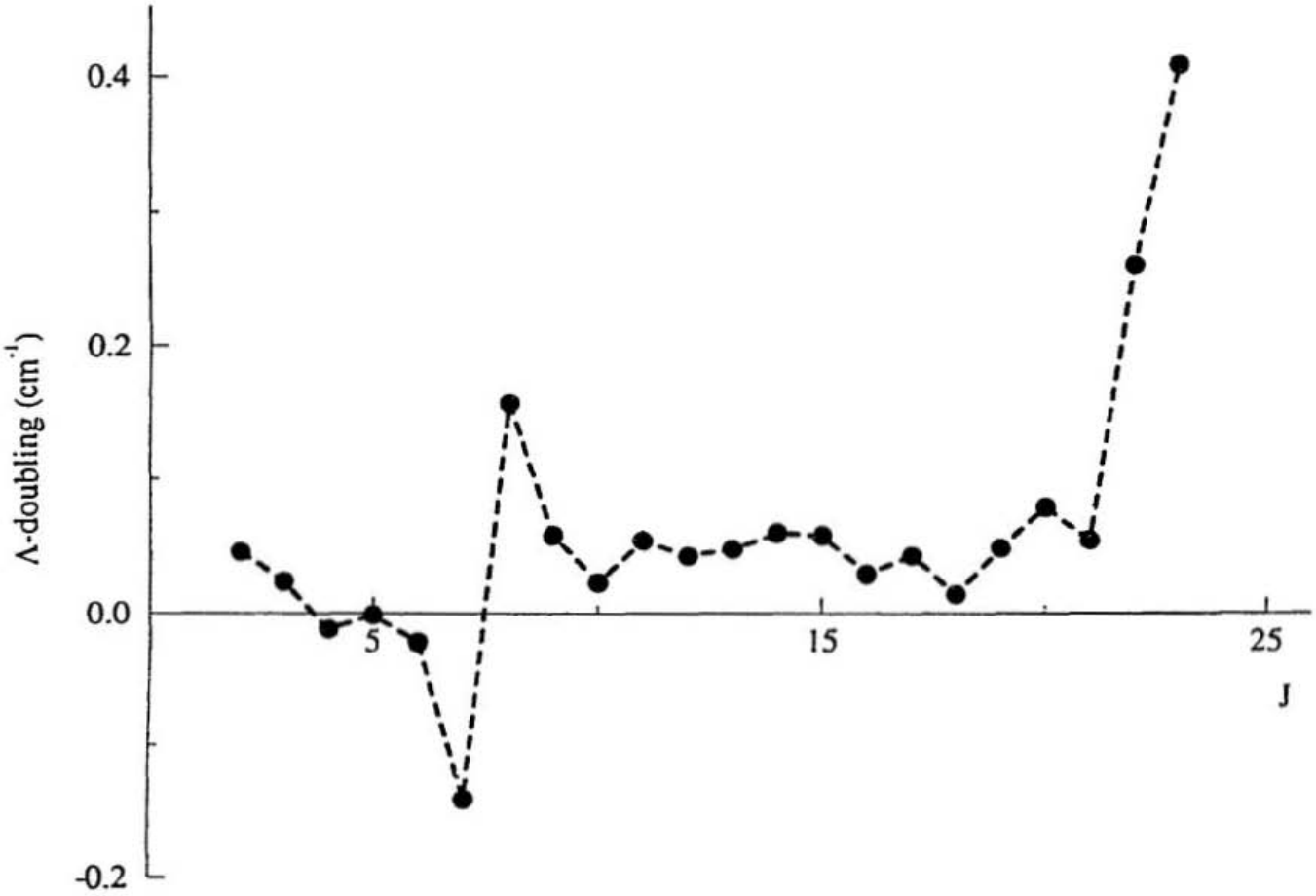

Figure 6.2 A plot of Λ-doubling (T_f - T_e) versus J for the A $^1\Pi$, v=2 level of $^{12}C^{18}O$. Note the anomalous behaviour of Λ at J = 7/8 and 22/23, due to I $^1\Sigma^-$ (v=3) and e $^3\Sigma^-$ (v=10) respectively.

ion CO^+. Eidelsberg et al. (1987) obtained the rovibrational term values of B $^1\Sigma^+$, v=0,1 and 2 of four isotopomers of CO including those of $^{12}C^{18}O$, directly from the analysis of the Hopefield-Birge B $^1\Sigma^+$-X $^1\Sigma^+$ system. In the present work, we obtain the term values of the B $^1\Sigma^+$, v=0 and 1 levels of $^{12}C^{18}O$ by adding the wave numbers of the 0-1 and 0-2 bands by Kepa (1986) and of the 0-1, 0-2 and 1-1 bands by Rytel (1970) of the Ångström (B $^1\Sigma^+$-A $^1\Pi$) system, with those of our data on five bands of the A-X system and the corresponding term values of X $^1\Sigma^+$, v=2, 4, 5 and 6 calculated from the mass-independent Dunham coefficients, as mentioned above. A total of 940 term values with J=0 to 28 for B,v=0, and 59 term values with J=1 to 14 (all of e parity) for B, v=1 have been estimated. Finally the weighted average term values for v=0 and 1 are presented in Table 6.1. The motivation for reporting the new term values for B, v=0 of $^{12}C^{18}O$ is that the values reported by Eidelsberg et al. (1987) have shifts of about +0.3 cm^{-1} and our term values are in good agreement with the values obtained by Drabbels (1993a). The term value 87160.58 cm^{-1} of B, v=0, J=11 reported in (Eidelsberg etal., 1987) seems to be a misprint. The new term values for B, v=1 except for J=5 and 6 are in good agreement with the values reported by Eidelsberg et al. (1987).

(iii) The C $^1\Sigma^+$, v=0 level

The term values of the Rydberg state C $^1\Sigma^+$ (.... $2p\pi^4$ $2p\sigma$ $3p\sigma$) can be obtained from the analysis of the bands of the Hopefield-Birge system (C $^1\Sigma^+$-X $^1\Sigma^+$), the Knauss system (C $^1\Sigma^+$-a′ $^3\Sigma^+$), C $^1\Sigma^+$-B $^1\Sigma^+$ transition or C $^1\Sigma^+$-d $^3\Delta_i$ system. We report here for the first time the rovibrational term values of the C $^1\Sigma^+$, v=0 level of $^{12}C^{18}O$ by combining our experimental data of the A-X system with those of the Herzberg (C-A) system by Janjić

et al. (1978) and the X $^1\Sigma^+$ state (see above). In all 440 term values for C $^1\Sigma^+$, v=0, J=0 to 22 have been estimated. The weighted average term values are presented in Table 6.1.

(iv) The E $^1\Pi$, v=0 level

Most of the information on the Rydberg state E $^1\Pi$ (.... $2p\pi^2$ $2p\sigma$ $3p\pi$) of the CO isotopomers has been obtained from the emission spectra of the E $^1\Pi$-A $^1\Pi$ transitions by Kepa (1986, 1988b) and Kepa et al. (1978). Eidelsberg et al. (1990, 1991, 1992) have carried out one photon absorption studies of the E $^1\Pi$ (v=0, 1 and 2) - X $^1\Sigma^+$ (v=0) transitions in four isotopomers of CO, with ^{12}C, ^{13}C, ^{16}O and ^{18}O. Baker et al. (1993) performed the rotational analysis of the 0-0 and 1-0 bands of the E-X system of the isotopomers of CO from their 2+1 resonance enhanced multiphoton spectra and observed perturbations in both the e and f levels of the E $^1\Pi$, v=1 state. The authors have also tabulated the term values for the f parity levels of E, v=0 and 1. We have now obtained the rovibrational term values of both the e and f parity levels of E, v=0 of $^{12}C^{18}O$ by combining the wavenumbers of the 0-1 and 0-2 bands of the E-A system obtained by Kepa (1986) and 0-1 band by Kepa et al. (1978), with those of the five bands of the A-X system and the term values of the X $^1\Sigma^+$ system (see above). In all 675 term values of the E, v=0, J=1 to 20 levels are calculated. Of these, 440 are e levels and 235 are f levels. Finally the weighted average term values are listed in Table 6.1. It is noted from this table that except for J=1, the e levels have higher term values than the corresponding f levels, and the magnitude of Λ-doubling ($|T_f - T_e|$) increases with J and it is 4.25 cm^{-1} for J=20. It was shown by Hines et al. (1990) and Lefebvre-Brion and Field (1986) that this Λ-doubling for the E $^1\Pi$ state of CO is due to the mutual rotation-electronic

interaction between the C $^1\Sigma^+$, v=0 and E $^1\Pi$, v=0 levels which are the σ and π components of the 3p Rydberg complex. A plot of the Λ-doubling versus J(J+1) for E $^1\Pi$, v=0 of $^{12}C^{18}O$ is shown in Fig. 6.3 and it gives a straight line which can be represented by the relation (Brown and Merer, 1979)

$$T_f - T_e = -q_0\, J(J+1). \qquad [6.2]$$

The value obtained for the Λ-doubling parameter from Fig. 6.3 is q_0 = 0.01065(10) cm^{-1}. This value is less than 0.01148(29) cm^{-1} obtained from the $\Delta_2F(J)$ differences, and also less than 0.01107 (17) cm^{-1}, obtained by Jenkins-McKellar method, by Kepa (1986) and Kepa et al. (1978). However the present value is in better agreement with the value 0.01062(10) cm^{-1}, reported by Baker et al. (1993).

$^{13}C^{18}O$:

(i) The A $^1\Pi$, v=1 level

The term values of the A $^1\Pi$, v=1 state of $^{13}C^{18}O$ are calculated from the wavenumbers of the 1-4 and 1-5 bands of the A-X system and the term values of the X $^1\Sigma^+$, v=4 and 5. A total of 93 term values for A, v=0, J=2 to 24 are calculated. Of these, 50 are e levels and 43 are f levels. The resulting weighted average term values are given in Table 6.2. Table 6.2 shows that there is no significant Λ-doubling in the v_A=1 level of $^{13}C^{18}O$ unlike $^{12}C^{18}O$ as discussed before.

(ii) The B $^1\Sigma^+$, v=0 and 1 levels

The term values of the B, v=0 and 1 of $^{13}C^{18}O$ are calculated by combining the wavenumber data of the 0-1 and 1-1 bands of the Ångström (B-A) system (Prasad et al., 1984 and Malak et al., 1984), with the term values of A $^1\Pi$, v=1 obtained from the

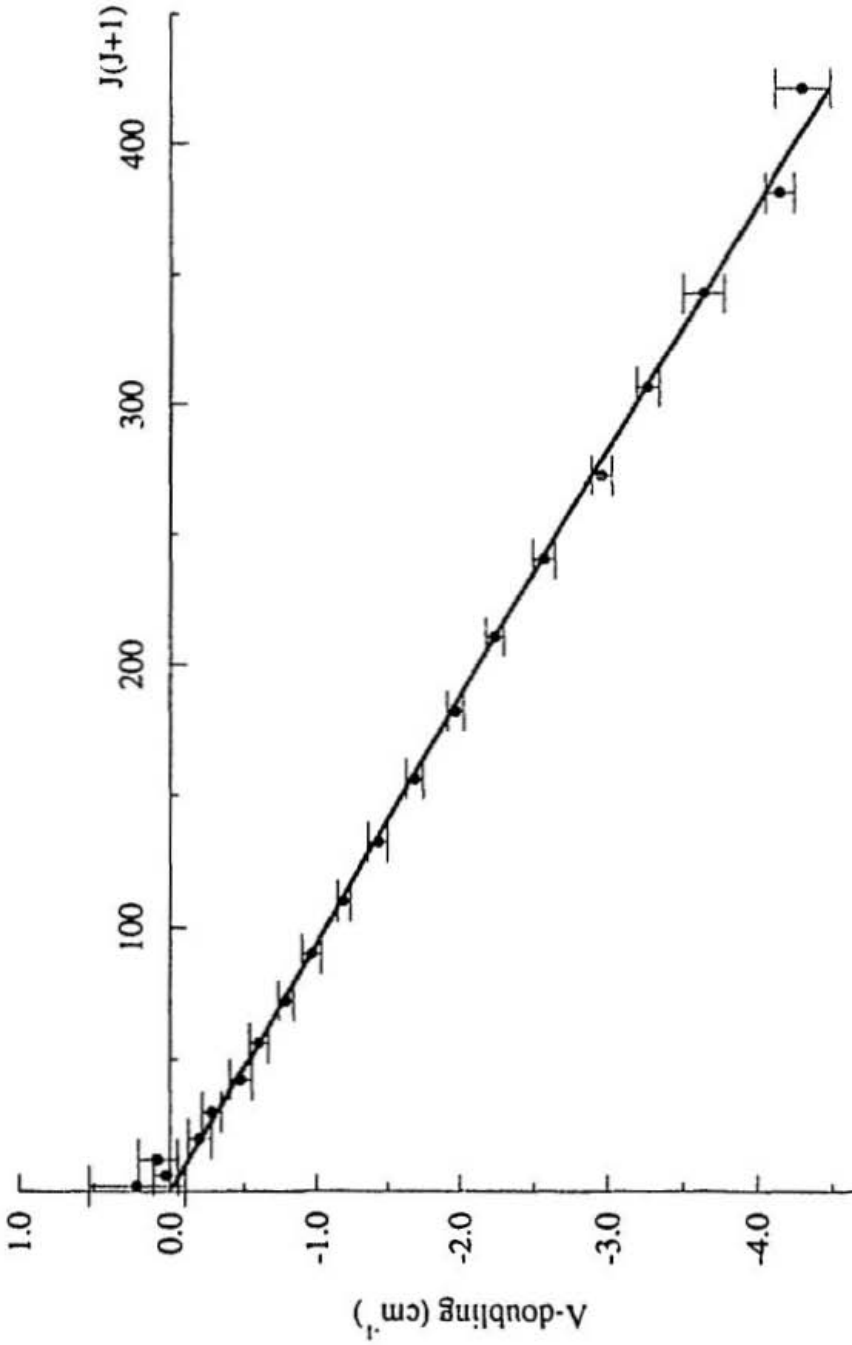

Figure 6.3 A plot of Λ-doubling (T_f - T_e) versus J(J+1) for the E $^1\Pi$, v=0 level of $^{12}C^{18}O$. The slope of the straight-line graph gives the parameter q_0

TABLE 6.2 Rovibronic term values[a] (in cm^{-1}) of the A $^1\Pi$ (v=1), B $^1\Sigma^+$ (v=0 and 1), C $^1\Sigma^+$ (v=0) and E $^1\Pi$ (v=0) states of $^{13}C^{18}O$

	A $^1\Pi$		B $^1\Sigma^+$		C $^1\Sigma^+$	E $^1\Pi$	
	v=1		v=0	v=1	v=0	v=0	
J	e level	f level	e level	e level	e level	e level	f level
1			86921.0 (1)	88908.1 (3)	91922.6 (1)		
2	66184.76(9)	66184.79(3)	86928.10(4)	88915.1 (2)	91929.6 (1)		
3	66193.41(6)	66193.41(7)	86938.69(6)	88925.6 (1)	91940.13(8)	92950.71(2)	92950.6 (3)
4	66204.85(9)	66204.89(3)	86952.85(7)	88939.6 (1)	91954.31(9)	92965.14(7)	92964.92(3)
5		66219.23(3)	86970.56(5)	88957.08(9)	91971.93(6)	92982.97(8)	92982.66(6)
6	66236.52(3)	66236.45(1)	86991.76(2)	88978.1 (1)	91993.10(4)	93004.34(3)	93003.90(3)
7	66256.59(2)	66256.56(1)	87016.56(3)	89002.5 (1)	92017.87(5)	93029.32(4)	93028.74(2)
8	66279.57(3)	66279.54(3)	87044.84(3)	89030.47(8)	92046.14(4)	93057.85(2)	93057.08(3)
9	66305.41(7)	66305.35(9)	87076.69(4)	89061.9 (1)	92077.93(5)	93089.93(3)	93089.01(3)
10	66334.11(3)	66334.12(4)	87112.05(3)	89096.81(8)	92113.19(4)	93125.57(3)	93124.49(5)
11	66365.67(3)	66365.68(4)	87150.96(4)	89135.19(9)	92152.01(4)	93164.78(3)	93163.49(3)
12	66400.11(3)	66400.11(4)	87193.38(2)	89177.12(8)	92194.37(5)	93207.55(2)	93206.03(3)
13	66437.42(2)	66437.42(3)	87239.39(4)	89222.53(9)	92240.25(5)	93253.90(2)	93252.10(3)
14	66477.59(2)	66477.58(3)	87288.83(1)	89271.38(7)	92289.66(5)	93303.80(3)	93301.72(3)
15	66520.61(2)	66520.60(1)	87341.90(3)	89323.73(7)	92342.57(4)	93357.21(2)	93354.83(3)
16	66566.47(2)	66566.46(1)	87398.39(3)	89379.5 (1)	92399.00(5)	93414.17(4)	93411.51(5)
17	66615.20(3)	66615.19(2)	87458.37(2)	89438.8 (1)	92458.91(3)	93474.70(2)	93471.70(2)
18	66666.8 (1)	66666.78(4)	87521.99(3)	89501.5 (1)	92522.37(4)	93538.79(5)	93535.3 (2)
19	66721.19(6)	66721.20(4)	87589.09(4)	89567.7 (2)	92589.36(6)	93606.3 (2)	93602.49(5)
20	66778.4 (3)	66778.51(3)	87659.69(5)	89637.4 (1)	92659.85(7)		
21	66838.6 (2)	66838.60(3)	87733.80(2)	89710.7 (2)	92733.81(6)		
22		66901.55(3)	87811.38(6)	89787.6 (7)	92811.35(8)		
23		66961.5 (4)	87892.65(9)	89868.3 (3)	92892.43(5)		
24		67035.9 (2)	87977.0 (3)		92976.7 (4)		

[a]These are the weighted average values and the number in the parentheses indicates the statistical error and corresponds to 3 standard deviations.

analysis of the 1-4 and 1-5 bands of the A-X systm, and the term values of the X $^1\Sigma^+$, v=4 and 5 calculated as mentioned earlier. For B, v=0, 288 term values with J=1 to 24 and for B, v=1, 275 term values with J=1 to 23 are calculated. The resulting weighted average term values are presented in Table 6.2. For B, v=0, 50% of our term values show shifts in the range 0.1 to 0.2 cm^{-1} (except for J=7) from those reported by Eidelsberg et al. (1987) and the remaining 50% agree with latter within the range 0.01 to 0.09 cm^{-1}. For B, v=1, 73% of our term values show shifts of -0.1 to -0.4 cm^{-1} from those of Eidelsberg et al. (1987) and the remaining 27% agree within -0.04 to -0.09 cm^{-1}.

(iii) The C $^1\Sigma^+$, v=0 level

By using the procedure similar to the B $^1\Sigma^+$ state, 440 term values of the C $^1\Sigma^+$, v=0 level of $^{13}C^{18}O$ are obtained for J=1 to 24 by combining the wavenumbers of the 0-1 band of Herzberg (C-A) system (Kepa, 1988a and Prasad et al., 1985), with the term values obtained for the A, v=1 level from the analysis of the A-X system along with the term values of the ground state X $^1\Sigma^+$. The weighted average term values of the C $^1\Sigma^+$, v=0 are listed in Table 6.2.

(iv) The E $^1\Pi$, v=0 level

The term values of E, v=0 of $^{13}C^{18}O$ are calculated by combining the wavenumbers of the 0-1 band of the E-A system (Kepa, 1988b), with those of the 1-4 and 1-5 bands of the A-X system and the term values of the X, v=4 and 5 from Eq. [6.1]. A total of 161 term values for E, v=0, J=3 to 19 are calculated. Of these, 94 are e levels and 67 are the f levels. Finally the weighted term values for E, v=0 of $^{13}C^{18}O$ are listed in Table 6.2. Just as in the case of $^{12}C^{18}O$, the term values of the e levels for E, v=0 are higher

than those of the corresponding f levels. The magnitude of the Λ-doubling, i.e., $(T_f - T_e)$ increases with J and has a value of 3.77 cm^{-1} for J=19. As in the case of E, v=0 of $^{12}C^{18}O$, the Λ-doubling in E(v=0) of $^{13}C^{18}O$ is caused by the interaction between the C $^1\Sigma^+$, v=0 and the E $^1\Pi$, v=0 levels. A plot of the Λ-doubling versus J(J+1) is shown in Fig. 6.4 and the slope of the graph gives q_0=0.009957(50) cm^{-1}. This value is in agreement with the values 0.00989(19) cm^{-1} reported by Kepa (1988b) and 0.00973(10) cm^{-1} given by Baker et al. (1993).

6.3 Molecular Parameters

The term values thus obtained in Section 6.2 and presented in Tables 6.1 and 6.2 were fitted to the appropriate energy matrix of one dimension for the B $^1\Sigma^+$ state and of 2 × 2 dimension for the C $^1\Sigma^+$ and E $^1\Pi$ states. The energy matrix for the B state is represented by

$$T(B^1\Sigma^+, v=0 \text{ and } 1, J) = T_v^B + B_v^B x - D_v^B x^2 \qquad [6.3]$$

and the diagonal elements of the 2 × 2 matrix are given by

$$T(C\ ^1\Sigma^+, v=0, J) = T_0^C + B_0^C x - D_0^C x^2$$

$$T(E\ ^1\Pi, v=0, J) = T_0^E + B_0^E (x-1) - D_0^E (x-1)^2, \qquad [6.4]$$

where x=J(J+1). The observed Λ-doubling of the E $^1\Pi$ state for both $^{12}C^{18}O$ and $^{13}C^{18}O$ is mainly due to the interaction with the neighbouring C $^1\Sigma^+$ Rydberg state. Since the levels of C state have e parity, only the e levels of the E state will be perturbed. The off-diagonal rotation-electronic interaction element for the e parity levels in the 2 × 2 matrix is represented by

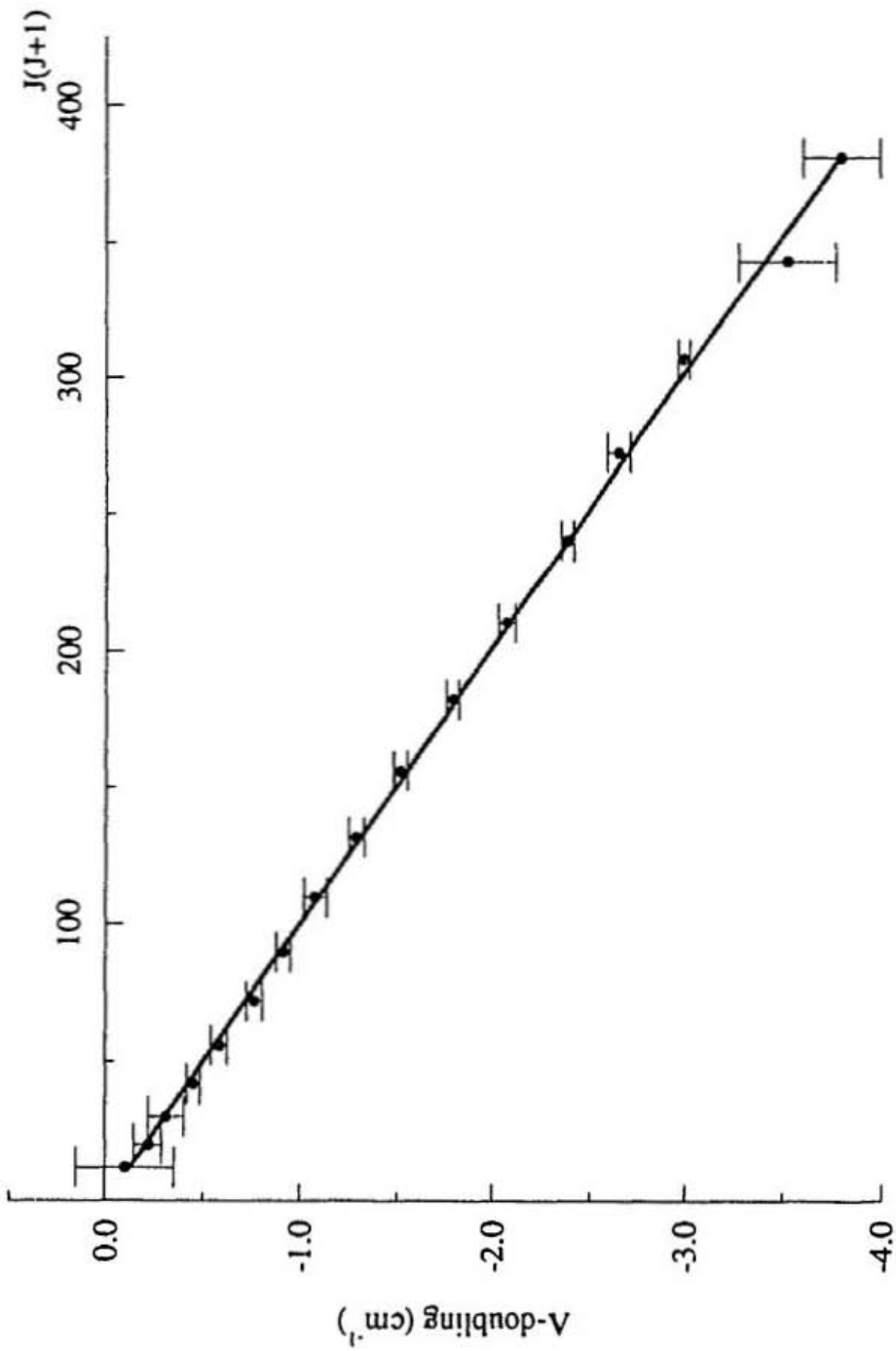

Figure 6.4 A plot of Λ-doubling (T_f - T_e) versus J(J+1) for the E $^1\Pi$, v=0 level of $^{13}C^{18}O$. The slope of the straight-line graph gives the parameter q_0

$$\langle T(C\ ^1\Sigma^+, v=0, J) | H_{RE} | T(E\ ^1\Pi, v=0, J)\rangle = 2\ \beta\ (x)^{1/2}. \qquad [6.5]$$

For the analysis of the data of both C and E states of $^{12}C^{18}O$ and $^{13}C^{18}O$ a nonlinear fitting procedure described by Le Floch et al. (1987) (also see Chapter 3, section 3.4) is used. For the B state a nonlinear fitting procedure, described by Haridass et al. (1992) and modified for the singlet states is used. The value of the dimensionless variance obtained (σ^2=1.5 for B,v=0, 1.5 for B,v=1 and 0.70 for C and E, v=0) for $^{12}C^{18}O$ indicates that all the term values for B, C and E states are well represented by the energy matrix given above. Similarly the dimensionless variance obtained (σ^2=1.2 for B,v=0, 1.5 for B, v=1 and 0.74 for C and E, v=0) for $^{13}C^{18}O$ indicates the term values for B, C and E states are also well represented by the energy matrix. The corresponding results appear in Table 6.3 and 6.4, along with the previous results for comparison.

$^{12}C^{18}O$:

(i) The B $^1\Sigma^+$ State

The molecular parameters T, B and D are presented in Table 6.3. It should be noted that the value 86916.705 (6) cm^{-1} obtained for T_0^B from the new term values of the B, v=0 state is more accurate than the value 86916.42(4) cm^{-1} reported by Eidelsberg et al. (1987) and is in good agreement with the value 86916.7047(19) cm^{-1} reported by Drabbels et al. (1993). The present rotational constants B and D obtained are in agreement with those reported by Eidelsberg et al. (1987) within the error limits. For v=1, the values of the molecular parameters T and B are in good agreement with those in Eidelsberg et al. (1987).

TABLE 6.3 Molecular constants[a] (in cm^{-1}) of the B $^1\Sigma^+$, C $^1\Sigma^+$, and E $^1\Pi$ states of $^{12}C^{18}O$

v	T_v	B_v	$D_v \times 10^6$	q_v	β	Ref.
			E $^1\Pi$			
0	92931.466(7)	1.85960(7)	6.01[b]	0.01065(10)	1.654(6)	1
	92929.74 (5)		5.9(1)	0.01062(10)		2
	92929.61 (8)	1.8705 (25)	6.0(2)			3
			4.86(47)[c]	0.01148(29)		4
		1.87087(16)	6.50(29)[d]			4
			C $^1\Sigma^+$			
0	91918.86(2)	1.8622(1)	5.72[b]			1
	91918.1 (2)	1.85354(55)	6.9(4)			3
		1.85125(7)	5.5(1)			5
		1.85179(21)	6.9(6)[e]			6
			B $^1\Sigma^+$			
0	86916.705(6)	1.85549(5)	6.09(7)			1
	86916.7047(	1.85553	6.2			7
	86916.42(4)	1.85553(23)	6.257(26)			8
	86916.42(4)	1.85553(23)	6.2(1)			3
		1.855597(6	6.142(65)			4
		1.855533(1	6.11(12)			9
1	88950.303(9)	1.83123(6)	6.3[b]			1
	88950.24(6)	1.83100(42)	6.35(54)			8
	88950.24(6)	1.83100(42)	6.3(5)			3

[a]The number in parentheses indicates the uncertainty in the last digit and corresponds to one standard deviation.
[b]Fixed constant in the least squares fit (from data of Eidelsberg et al., 1987).
[c]Obtained from f parity term values.
[d]Obtained from e parity term values.
[e]The uncertainty corresponds to 3 standard deviations.
1:Present Work, **2**:Baker et al. (1993), **3**:Eidelsberg and Rostas (1990), **4**:Kepa (1986), **5**:Janjić et al. (1978), **6**:Roncin et al. (1993), **7**:Drabbels (1993a), **8**:Eidelsberg et al. (1987), **9**:Rytel (1970).

TABLE 6.4 Molecular constants[a] (in cm^{-1}) of the B $^1\Sigma^+$, C $^1\Sigma^+$, and E $^1\Pi$ states of $^{13}C^{18}O$

v	T_v	B_v	$D_v \times 10^6$	q_v	β	Ref.
			E $^1\Pi$			
0	92931.216(9)	1.77371(5)	5.47[b]	0.009957(50)	1.584(4)	1
	92929.43(5)	1.77412(14)[c]	5.5(1)	0.00973(10)		2
	92929.37(3)	1.78423(23)	5.9(2)			3
		1.77896(13)	5.70(25)	0.00989(19)		4
			C $^1\Sigma^+$			
0	91918.97(2)	1.77612(8)	5.20[b]			1
	91919.06(5)	1.76517(56)	4.2(1)			3
		1.7670 (3)	6.9(5)			5
		1.766512(70)	5.302(80)			6
		1.76623(50)[d]	4.4(1.4)[d]			7
		1.7665(1)	5.6(2)			8
			B $^1\Sigma^+$			
0	86917.455(5)	1.76977(6)	6.1(1)			1
	86917.34(8)	1.76980(42)	5.6[b]			9
	86917.34 (8)	1.76980(42)	5.6(1.0)			3
		1.7694 (1)	4.8(3)			10
		1.769653(48)	5.49(34)			11
		1.7697(1)	5.8(2)			8
1	88904.663(7)	1.74757(5)	6.3(2)			1
	88904.81(8)	1.74733(33)	6.0[b]			9
	88904.81(8)	1.74733(33)	6.0(5)			3
		1.7476 (6)	7.0(1.1)			10
		1.74709(11)	5.66(22)			11
		1.7473(2)	6.2(4)			8

[a]The number in parentheses indicates the uncertainty in the last digit and corresponds to one standard deviation.

[b]Fixed constant in the least squares fit (from data of Eidelsberg etal., 1987).

[c]Obtained from f parity term values.

[d]The uncetainty corresponds to 3 standard deviations.

1:Present Work, **2**:Baker et al. (1993), **3**:Eidelsberg and Rostas (1990), **4**:Kepa (1988b), **5**:Prasad et al. (1985), **6**:Kepa (1988a), **7**:Roncin et al. (1993), **8**:Prasad and Reddy (1988), **9**:Eidelsberg et al. (1987), **10**:Prasad et al. (1984), **11**:Malak et al. (1984).

(ii) The C $^1\Sigma^+$ State

The molecular parameters T and B for v=0 of C $^1\Sigma^+$ are presented in Table 6.3. The value 91918.86(2) cm^{-1} for T_0^C obtained from the term values of C $^1\Sigma^+$, v=0 is 0.76 cm^{-1} greater than the value reported by Eidelsberg and Rostas (1970), but is in good agreement with the value 91918.780(8) cm^{-1} obtained by combining the band origin (5002.075(15) cm^{-1}) of the C-B (0-0) band reported by Roncin et al. (1993) and the present T_0^B value of 86916.705(6) cm^{-1} listed in Table 6.3. The value 1.8622(1) cm^{-1} of the deperturbed rotational constant B_0^C is significantly greater (see Table 6.3) than the *effective* values reported in the literature (Eidelsberg and Rostas, 1990, Janjić et al., 1978, and Roncin et al., 1993) due to strong C – E interaction. The value of the difference (ΔB_0^C) in the range 0.0087(6) to 0.0110(1) cm^{-1} thus obtained is in harmony with the value of the observed Λ-doubling parameter q_0=0.01065(10) cm^{-1} and with the correction term $\Delta B_0^C = 4\ \beta^2/(T_0^E - T_0^C) = 0.01081(8)$ cm^{-1} obtained from the perturbation theory.

(iii) The E $^1\Pi$ State

Table 6.3 gives the molecular parameters T and B of the E $^1\Pi$, v=0 level. The value of T_0^E obtained in the present work is more accurate than the effective value (T_0^E - B_0^E) reported by Baker et al. (1993) and Eidelsberg and Rostas (1990). The value of B_0^E = 1.85960(7) cm^{-1} is in good agreement with the values reported in the literature (Baker et al., 1993, Kepa, 1986) within the error limits. The value 1.8705(25) cm^{-1} reported by Eidelsberg and Rostas (1990) for B of E $^1\Pi$, v=0 is B_0^f, pertaining to the Q branch. From the experimental result of the perturbation parameter β represented by

$$\beta = \langle v' \mid B \mid v'' \rangle\ |J(J+1)/2|^{1/2}, \qquad [6.6]$$

it is possible to obtain the value of $l(l+1)$ for the p Rydberg orbital. Using the value of β = 1.654 cm^{-1} and B_0 = 1.8609 cm^{-1} (the average of B_0^C and B_0^B) obtained from the present work, $l(l+1)$ is found to be 1.580, which is smaller than the "pure precession" value of 2 for the p Rydberg orbitals.

' ***$C^{18}O$***:

(i) The B $^1\Sigma^+$ State

The values of the molecular parameters T, B and D for $B^1\Sigma^+$, v=0 and 1 of $^{12}C^{18}O$ obtained in the present work are listed in Table 6.4. These values agree with those reported in the literature (Eidelsberg and Rostas, 1990, Prasad et al., 1984, Malak et al., 1984, and Prasad and Reddy, 1988).

(ii) The C $^1\Sigma^+$ State

Table 6.4 gives the molecular parameters for C, v=0 of $^{12}C^{18}O$ obtained from the deperturbation analysis. The value 91918.97(2) cm^{-1} for T_0^C is more accurate than 91919.06(5) cm^{-1} reported by Eidelsberg and Rostas (1990), but it is 0.087 cm^{-1} greater than the value 91918.883(11) cm^{-1} obtained by combining the band origin for the 0-0 band of the C-B system (5001.428(30) cm^{-1}) reported by Roncin et al. (1993) and the present value 86917.455(5) cm^{-1} obtained for T_0^B from the analysis of the term values of the B $^1\Sigma^+$, v=0 state. The deperturbed rotational constant B_0^C (due to strong C ~ E interaction) is significantly greater than the effective value reported in the literature (Eidelsberg and Rostas, 1990, Prasad et al., 1985, Kepa, 1988a, Roncin et al., 1993, and Prasad and Reddy, 1988) (see Table 6.4). This difference ΔB_0^C between the value of B

obtained in the present work and those reported in the literature is obviously due to the effect of the C -- E coupling. This difference is in the range 0.00912(31) to 0.01095(57) cm^{-1} and is in harmony with the observed value of the Λ-doubling parameter q_0=0.009957(50) cm^{-1} for the E $^1\Pi$, v=0 level and the value for the correction term $\Delta B_0'$ = 0.00990(5) cm^{-1} obtained from the perturbation theory.

(iii) The E $^1\Pi$ State

The deduced molecular parameters T and B of the E $^1\Pi$, v=0 level of $^{13}C^{18}O$ are presented in Table 6.4. The value of T_0^E obtained in the present work is more accurate than the effective value (T_0^E - B_0^E) reported by Baker et al.(1993) and Eidelsberg and Rostas (1990). The rotational constant B_0^E = 1.77371(5) cm^{-1} obtained from the simultaneously-fitted term values of the C and E states is less than the value reported in the literature (Eidelsberg and Rostas, 1990, Kepa, 1988b). The value of B_0= 1.77412(14) cm^{-1} reported by Baker et al. (1993) is obtained from the fit of the f parity term values. The value of $J(J+1)$ calculated from the experimental values of β (1.583 cm^{-1}) and B_0 (1.77492 cm^{-1}, average value of B_0^C and B_0^E) is 1.591 which is smaller than the pure precession value of 2.

6.4 Conclusions

Accurate rovibronic term values for the A $^1\Pi$, v=1 and 2, B $^1\Sigma^+$, v=0 and 1, C $^1\Sigma^+$, v=0 and E $^1\Pi$, v=0 levels of $^{12}C^{18}O$ and A $^1\Pi$, v=1, B $^1\Sigma^+$, v=0 and 1, C $^1\Sigma^+$, v=0 and E $^1\Pi$, v=0 levels of $^{13}C^{18}O$ with reference to X $^1\Sigma^+$, v=0, J=0 are determined by combining the available wavenumber data of the B-A, C-A, E-A and A-X systems and the accurate

term values of the ground state X $^1\Sigma^+$. These term values show a good internal consistency of the Rydberg B, C and E states via the B-A, C-A, E-A and A-X transitions. From these term values it will be possible to obtain wavenumbers for the transitions E $^1\Pi$(v=0) - B$^1\Sigma^+$(v=0 and 1) and those of the transitions between the highly excited Rydberg states to the lower B$^1\Sigma^+$, C$^1\Sigma^+$ and E$^1\Pi$ states. The term values deduced in the present chapter should be useful for the astronomers who are interested in the determination of the abundances of the CO isotopomers in interstellar molecular clouds. The results presented in this chapter have appeared in a publication (Haridass, C., Reddy, S. P., and Le Floch, A. C., *J. Mol. Spectrosc.* **168**, 429 (1994)). A reprint is included in the Appendix.

REFERENCES

Authier, N., Bagland, N., and Le Floch, A. C., *J. Mol. Spectrosc.*, **169**, 590 (1993).

Baker, J., Lemaire, J. L., Couris, S., Vient, A., Malmasson, D., and Rostas, F., *Chem. Phys.* **178**, 569 (1993).

Bally J., and Langer, W. D., *Astrophys. J.* **255**, 143 (1982).

Brown, J. M., and Merer, A. J., *J. Mol. Spectrosc.* **74**, 488 (1979).

Drabbels, M., Meerts, W. L., and Meulen, J. J. T., *J. Chem. Phys.* **99**, 2352 (1993).

Drabbels, M., Heinze, J., Meulen, J. J. T., and Meerts, W. L., *J. Chem. Phys.* **99**, 5701 (1993).

Drabbels, M., Ph. D. Thesis, chapter 8, Katholieke Universiteit Nijmegen (1993).

Eidelsberg, M., and Rostas, F., *Astron. Astrophys.* **235**, 472 (1990).

Eidelsberg, M., Roncin, J. -Y, Le Floch, A. C., Launay, F., Letzelter, C., and Rostas, J., *J. Mol. Spectrosc.* **121**, 309 (1987).

Eidelsberg, M., Benayoun, J. J., Viala, Y., and Rostas, F., *Astron. Astrophys. Suppl.* **90**, 231 (1991).

Eidelsberg, M., Benayoun, J. J., Viala, Y., Rostas, F., Smith, P. L., Yoshino, K., Stark, G., and Shettle, C. A., *Astron. Astrophys.* **265**, 839 (1992).

Haridass, C., Prasad, C. V. V., and Reddy, S. P., *Astrophys. J.* **388**, 669 (1992).

Haridass, C., Reddy, S. P., and Le Floch, A. C., *J. Mol. Spectrosc.* **167**, 334 (1994).

Hines, M. A., Michelsen, H. A., and Zare, R. N., *J. Chem. Phys.* **93**, 8557 (1990).

Janjić, J. D., Čonkić, LJ. U., Pešić, D. S., Kepa, R., and Rytel, M., *J. Mol. Spectrosc.* **72**, 297 (1978).

Kepa, R., *Acta. Phys. Hung.* **60**, 227 (1986).

Kepa, R., *J. Mol. Spectrosc.* **132**, 545 (1988).

Kepa, R., *Can. J. Phys.* **66**, 1012 (1988).

Kepa, R., Rytel, M., and Rzeszut, Z., *Acta. Phys. Pol.* **A56**, 355 (1978).

Le Floch, A. C., *J. Mol. Spectrosc.* **155**, 177 (1992).

Le Floch, A. C., Launay, F., Rostas, J., Field, R. W., Brown, C. M. and Yoshino, K., *J. Mol. Spectrosc.* **121**, 337 (1987).

Le Lloch, A. C., and Amiot, C., *Chem. Phys.* **97**, 379 (1985).

Lefebvre-Brion, H., and Field, R. W., "Perturbations in the Spectra of Diatomic Molecules," Academic Press, New York, 1986.

Malak, Z., Rytel, M., Janjić, J. D., and Pešić, D. D., *Acta. Phys. Hung.* **55**, 85 (1984).

Prasad C. V. V., and Reddy, S. P., *J. Mol. Spectrosc.* **130**, 62 (1988).

Prasad, C. V. V., Bhale, G. L., and Reddy, S. P., *J. Mol. Spectrosc.* **104**, 165 (1984).

Prasad, C. V. V., Reddy, S. P., and Sandys-wunsch, M., *J. Mol. Spectrosc.* **114**, 436 (1985).

Roncin, J. -Y., Ross, A., and Boursey, E., *J. Mol. Spectrosc.* **162**, 353 (1993).

Rytel, M., *Acta. Phys. Pol.* **A38**, 299 (1970).

Scheffer, Y., Fererman, S. R., Lambert, D. L., and Cardelli, J. A., *Astrophys. J.* **397**, 482 (1992).

CHAPTER 7

HIGH-RESOLUTION SPECTRA OF THE A $^1\Pi \rightarrow$ X $^1\Sigma^+$ SYSTEM OF $^{13}C^{16}O$ AND THE ATOMIC LINES OF $^{13}C_I$, AND $^{13}C_{II}$ IN THE VUV REGION

7.1 Introduction

Laboratory investigations of the CO molecule have created a very detailed picture of its rovibronic structure from the ground state up to energies that come close to the first ionization potential at 14.014 eV. This is particularly true for the most abundant isotopomer, $^{12}C^{16}O$, where the identification and modelling of interstellar transitions can now rely on a solid base of observed rovibronic energies instead of having to resort to sometimes uncertain extrapolations, especially at wavelengths in the vacuum ultraviolet (VUV) region of the spectrum. The X $^1\Sigma^+$ ground state levels have been reduced by Farrenq et al. (1991) to an exhaustive set of Dunham coefficients; LeFloch (1992) has tabulated term values for A $^1\Pi$; and Eidelsberg et al. (1987, 1991, 1992) have provided term values and transition wavenumbers relevant to many of the higher excited states reached in dipole-allowed transitions from X $^1\Sigma^+$.

The picture is less complete for the isotopomers of lower abundances. For wavelengths shorter than 2000 Å no high-resolution measurements have been published for the rotational structure of the bands of the fourth positive system (A $^1\Pi$ - X $^1\Sigma^+$), although Tilford and Simmons (1972) have reported band head measurements in the A(v′) ← X(v″ =0) progression of $^{13}C^{16}O$ from v′ =2 to 16. At wavelengths longer than 2000 Å, Domin (1986) has carried out the rotational analyses of 28 emission

bands of the A-X transition of $^{13}C^{16}O$, the transitions involving A levels with $v' = 3$ to 11 and ground state $^1\Sigma^+$ levels with $v'' = 12$ to 22. These authors provide no information on the three lowest vibrational levels in A $^1\Pi$, and fail to report the measured wavenumbers of individual lines which could be reduced to upper-state term values with the help of the very extensive and precise ground state data of Farrenq et al. (1991).

As a first step in an effort to close this information gap, the results of a high-resolution study of $^{13}C^{16}O$ at wavelengths between 1600 Å and 1370 Å, which include transitions from the A $^1\Pi$ levels with $v' = 0,..9$ to X $^1\Sigma^+$ levels with $v'' = 0, ..5$, are presented in this chapter. Similar results might be obtained from a wide-ranging absorption study of the $v' \leftarrow 0$ upper-state progression. However, considering the high costs of pure isotopes, it seems more economical to take advantage not only of the high sensitivity of an emission experiment, but also of the sequence structure of the emission spectra which makes it possible to derive the same upper-state information from measurements over a much narrower range of wavelengths by simultaneously recording bands with $v'' > 0$. Again, for the reduction of the line measurements to upper-state term values the ground state levels are reliably calculated from the Dunham coefficients of Farrenq et al. (1991).

The A $^1\Pi$ state of $^{13}C^{16}O$ is also accessible through the transitions from higher-lying Rydberg states. Rytel (1970) reported wavenumbers of the six bands in the $v'=0 \rightarrow v''=0$ to 5 lower state progression, and the 1-0 and 1-1 bands of the B $^1\Sigma^+ \rightarrow$ A $^1\Pi$ Ångström system. Janjić et al. (1972) extended these studies to the 1-4, 1-5, and 1-6 bands. Kepa (1978) and Kepa, Para, and Rytel (1990) observed the same A state levels together with the $v'' = 7$ in the Herzberg system from $v' = 0$ of C $^1\Sigma^+$. In addition,

Kepa, Rytel and Rzeszut (1978) contributed measurements for the 0-1 and 0-2 bands of the E $^1\Pi \rightarrow$ A $^1\Pi$ transition. Since all three Rydberg states have been observed in absorption from X $^1\Sigma^+$ (Eidelsberg and Rostas (1990); Eidelsberg et al. (1991, 1992)) it is, in principle, feasible to derive the A state energy levels from appropriate combinations of emission and absorption data. However, the A $\rightarrow$ X transitions in the 1500 Å region can be measured at nearly twice the resolution that was available for the B $\leftarrow$ X, C $\leftarrow$ X, and E $\leftarrow$ X bands recorded at wavelengths shorter than 1210 Å (Eidelsberg et al. (1987)). It is primarily for this reason that we prefer the more direct route outlined above which closes the cycles of observations and leads to a stringent test on the reliablilty of present and previous measurements.

In the absence of published wavenumbers it has been suggested by Hanson, Snow, and Black (1992) that the A-X transitions for isotopic species can be predicted with the help of vibrational and rotational constants that have been derived from those of $^{12}C^{16}O$ (Tilford and Simmons (1972)) by means of standard isotope relations. However, the results of such calculations are often misleading since they fail to account for the many perturbations of A $^1\Pi$ by a number of overlapping singlet and triplet Σ and Δ states (Simmons, Bass, and Tilford (1969); Field (1971); Field et al. (1972); Le Floch et al. (1987); Le Floch, Rostas and Schamps (1988); and Le Floch (1989)) interactions which may shift the affected A $^1\Pi$ rovibronic levels by several cm^{-1} from their anticipated positions. The location, though not the strength, of a perturbation can be predicted fairly well from diagrams of the sort shown in Figure 1 of a recent publication of Garetz, Kittrell, and Le Floch (1991). However, it is hoped that the energy levels presented here

will, to a large extent, eliminate the need for uncertain extrapolations.

7.2 Experimental Details and Data Reduction

The A $\rightarrow$ X spectra of $^{13}C^{16}O$ were generated in emission from a dc discharge in supersonically expanding Ar containing trace amounts of $^{13}C^{16}O_2$ (Matheson, 99.1 atom% ^{13}C, 5.1 atom% ^{18}O). The use of CO_2 rather than CO is known to result in a "clean" discharge where any carbon deposited in the source is continuously burnt up by the oxygen freed in the reaction producing CO, making it possible to carry out preliminary experiments with CO_2 with carbon 13 present in natural abundance without the danger of contaminating the system before turning to the final experiments with enriched ^{13}C isotopes.

The preference of a jet discharge over more conventional sources stems from the fact that the former, in contrast to the latter, produces spectra of comparatively low temperature where low-J lines are clearly visible and are relatively free from overlaps by the returning R or P branch lines of strongly degraded bands. The rotational temperatures can be as low as 20 K (Huber and Sears (1985); Huber, Klug, and Alberti (1987); and Huber, Holland and Coxon (1992)).

The molecules emerging from a pinhole nozzle may have substantial velocity components along the line of observation. The resulting Doppler effects on line shapes and line positions have been documented by Huber and Sears (1985) and Huber and Vervloet (1992) for spectra in the visible and near infrared regions; at the VUV wavenumbers of the present work they would be proportionately larger and might affect

the peak positions of individual lines by as much as 0.25 cm^{-1}, or by more than five times the expected accuracy of our measurements.

In order to avoid these complications, following recommendations by Veeken and Reuss (1985), the two-dimensional jet expansion from a pinhole nozzle has been replaced by a one-dimensional expansion from a slit nozzle. The slit, 5 mm long and approximately 0.015 mm wide, is formed by two knife edges which are isolated not only from the tungsten anode at the center of the pyrex tube connecting with the nozzle assembly, but also from the grounded booster and rotatory pump combination that doubles as cathode for the dc discharge. The slit construction is a somewhat simplified version of the design shown in Fig. 1 of Comer and Foster (1993). The tip of the anode at 1 mm upstream from the nozzle slit is carefully centered with respect to the latter, both longitudinally and laterally. With the discharge running, a thin sheet of luminous gas expands from the tip of the anode in a plane normal to the direction of the nozzle slit. The line of observation is parallel to the slit direction and passes through the thin emission zone at approximately 2 mm downstream from the nozzle orifice. The gas mixtures expand from a relatively low reservoir pressure of 300 Torr, and a voltage of 600 V applied to the anode is sufficient to maintain a steady discharge of around 60 mA (for other details, see Chapter 2).

The jet emission spectra were photographed on the 10.6 m vacuum spectrograph of the National Research Council in the 7th and 8th orders of a normal-incidence concave grating with 600 grooves mm^{-1}, the reciprocal dispersion being 0.21 and 0.18 Å mm^{-1}, respectively. Predispersion of the light entering into the spectrograph was achieved by

a lithium fluoride prism/cylinder combination in the manner described by Huber etal. (1987, 1992). With a spectrograph slit width of 0.020 mm, exposure times varying from 10 to 90 minutes were needed to record the CO emission of Kodak SWR plates.

The molecular spectra together with a number of atomic emissions were measured against Fe and Ne standards (Crosswhite (1975)) in overlapping orders. The final wavelength calibration was made with the help of O_I and N_I emission lines (Kaufmann and Edlen (1974)) which appear as impurities in the jet discharge at 1493 Å in 7th order and at 1304 Å in the 8th order respectively. Following the completion of the rotational analyses we have checked the compatibility of our results with the B $\leftrightarrow$ X and B $\rightarrow$ A measurements of Eidelsberg etal. (1987) and of Rytel (1970) by comparing the upper-state term values derived from subtracting the B $\leftrightarrow$ A transitions from the B $\rightarrow$ X transitions to obtain the A state energies. The comparision was limited to v=0 of the B $^1\Sigma^+$; for 77% of the results the agreement was better than ± 0.1 cm^{-1}, with only 3% falling outside the ± 0.2 cm^{-1} limits. There is evidence for a small systematic shift of about 0.02 cm^{-1}.

7.3 Results

Of the 23 red-shaded bands recorded between 1370 and 1600 Å 13 bands (0-0, 0-1, 1-0, 2-0, 3-1, 3-2, 4-0, 5-1, 6-1, 7-1, 7-2, 8-2, and 9-5) were selected for rotational analysis, giving preference to bands of low to medium intensity with rotational lines that are not excessively saturated. The rotational structure of the 0-0 band of the A-X system of $^{13}C^{16}O$ and that of the 1-0 band of its $e^3\Sigma^-$ -X $^1\Sigma^+$ system are shown in Fig. 7.0. The intensity of the Q branch lines in unperturbed bands is found to be strongest for J=6, indicating the rotational temperature is somewhat less than 300 K, i.e., very much lower

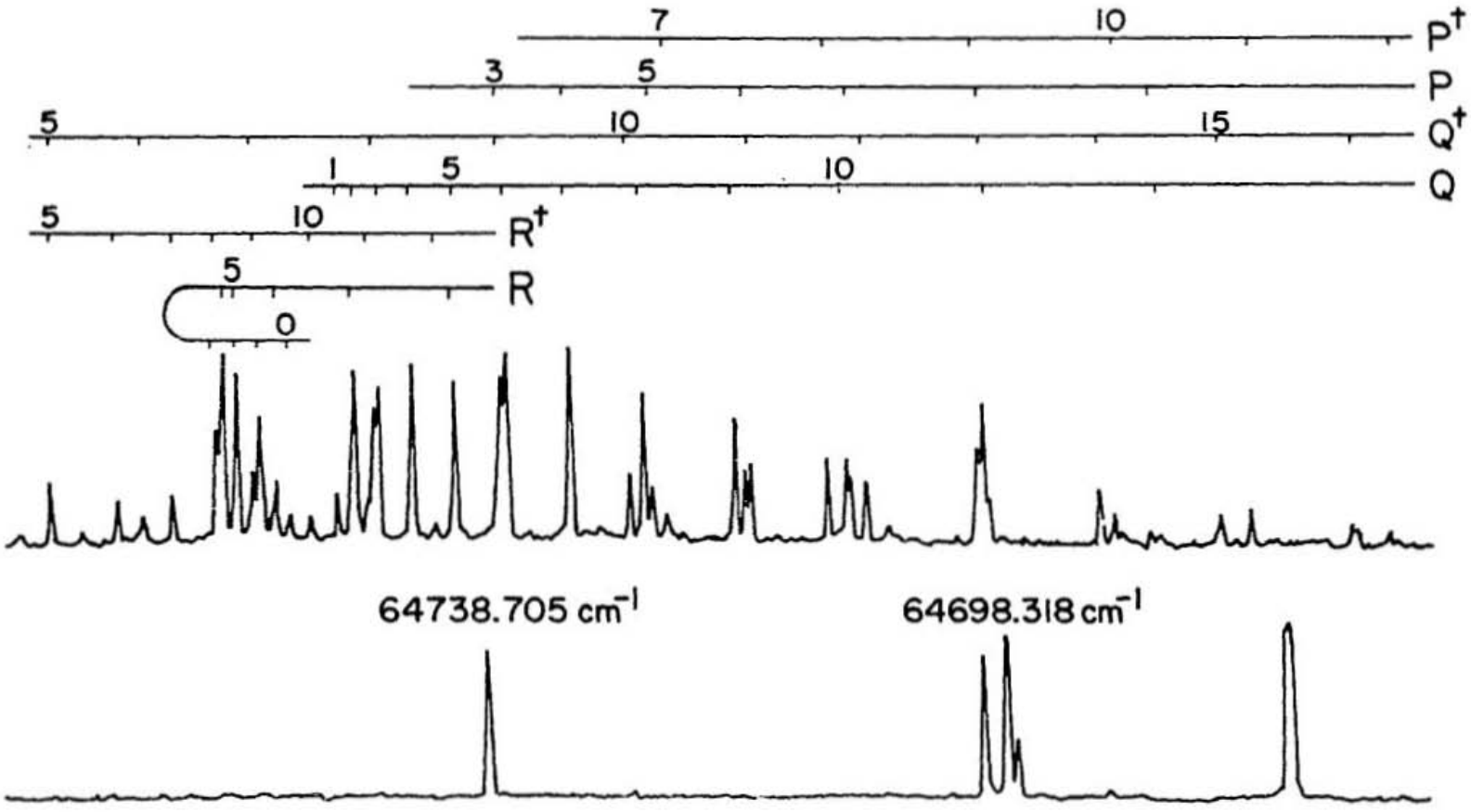

Figure 7.0 Rotational structure of the 0-0 band of the A $^1\Pi$ - X $^1\Sigma^+$ system of $^{13}C^{16}O$, photographed on the 10.6 m vacuum grating spectrograph in the seventh order along with the Fe lines in the third and fourth orders. Extra branches denoted by $R^\dagger(J)$, $Q^\dagger(J)$, and $P^\dagger(J)$ in the 0-0 band arise from perturbations of the A, v=0 level by the e $^3\Sigma^-$, v=1 level.

than in standard dc discharges, but considerably higher than what might be expected from a jet discharge in Ar mixed with CO rather than CO_2. The rotational quantum numbers and the vacuum wavenumbers (in cm^{-1}) of the spectral lines of the above mentioned bands are listed in Table 7.1

The rotational analysis of the bands is straightforward, and even in perturbed structures the J numbering is unambiguously achieved with the help of precisely known ground state combination differences. The upper-state term values, suitably averaged over multiple observations, are collected in Table 7.2 and are displayed in Figure 7.1 after subtraction of the estimated upper-state rotational energies $B'J'(J'+1)$. Unperturbed levels are represented by essentially horizontal lines, strong deviations marking the presence of perturbations by various singlet and triplet states. The e and f levels (Brown et al. (1975)) refer to the rotational energy levels with parity $+(-1)^J$ and $-(-1)^J$, respectively, the former being observed in the R and P branches, the latter in the Q branch transitions.

The perturbations of primary interest in an astrophysical context occur in $v' = 0$, 6, and 8 where they influence the low-J rotational structure seen in absorption from ground state levels populated at the temperature of the interstellar medium. The pattern of three avoided crossings in A $^1\Pi(v = 0)$ at J=7 and 10 in the e and f levels, respectively, observed in this work, and again at J = 14 or 15 in the e levels observed by Rytel (1970) from B $^1\Sigma^+$ is compatible with the perturber being v=1 of e $^1\Sigma^-$. The spin-orbit interaction matrix element is 8.53 cm^{-1}, very similar to the value derived by Lefloch et al. (1987) from the analogous perturbation in $^{12}C^{16}O$ and large enough to shift the

TABLE 7.1 Vacuum wavenumbers (in cm^{-1}) of the rotational lines of the bands of the $A\ ^1\Pi - X\ ^1\Sigma^+$ system of $^{13}C^{16}O$

Band	$0\text{-}0^+$					
J	R(J)		Q(J)		P(J)	
0	64754.089					
1	756.324*		64750.401			
2	758.075*		749.160*			
3	759.065*		747.203		64738.023	
4	759.065*		744.592		732.400*	
5	758.075*	64772.598*	741.274	64772.598*	725.964	
6	755.155	767.327	737.264	765.242	718.648	
7	749.160*	762.993	732.400*	756.871	710.300	64724.913
8		759.562	726.635	747.567	700.057*	712.170
9		756.324*	719.552	737.673	686.835	700.471
10		752.526	710.674	727.744		689.776
11		748.082	699.625	718.198		679.090
12		742.783	686.149	709.091		668.122
13				700.057*		656.369
14				690.875		
15				681.330		
16				671.112		
17				660.463		

TABLE 7.1 (Continued)

Band			0-1†		
J	R(J)		Q(J)		P(J)
0	62658.182				
1	660.426		62654.279		
2	662.146		653.138		
3	663.325		651.320		62642.178
4	663.325		648.846		636.648
5	662.444	62677.040	645.677	62677.040	630.406
6	659.808	671.933	641.893	669.853	623.277
7	654.279	667.853	637.257	661.719	615.156
8		664.730	631.749	652.766	605.133
9		661.719	624.922	643.144	592.606
10		658.182	616.453	633.516	
11		654.279	605.815	624.294	
12			659.606	615.572	
13				606.987	
14				598.282	

TABLE 7.1 (Continued)

Band	1-0			2-0		
J	R(J)	Q(J)	P(J)	R(J)	Q(J)	P(J)
0	66207.319			67622.672		
1	209.688	66203.608		624.968	67618.981	
2	211.485	202.283		626.571	617.645	67611.691
3	212.481	200.308	66191.259	627.579	615.525	606.575
4	212.721	197.672	185.776	627.579	612.753	600.775
5	212.481	194.386	179.332	627.204	609.395	594.468
6	211.485	190.441	172.331	625.996	605.066	587.218
7	209.939	185.776	164.727	624.084	600.113	579.382
8	207.722	180.576	156.440	621.493	594.794	570.847
9	204.853	174.664	147.636	618.168	588.493	561.616
10	201.258	168.066	137.914	614.211	581.525	551.662
11	197.049	160.798	127.676	609.395	573.864	541.061
12	192.090	152.804	116.782	604.144	565.496	529.717
13	186.415	143.167	105.217	598.052	556.450	517.703
14	179.587	135.776	092.968	591.302	546.700	504.990
15	175.034	125.730	079.971	583.757	536.223	491.572
16	166.887	115.179	065.914	575.563	525.089	477.445
17	158.620	103.964	053.995	566.629	513.257	462.638
18		091.970	038.594	556.855	500.666	447.126
19		081.112		546.700	487.295	430.924
20		067.071		535.710	473.414	414.001
21		053.127		523.763	458.729	396.361
22		038.594		511.070	443.318	378.024
23				496.866	427.189	358.852
24					410.293	
25					392.576	
26					373.928	
27					353.705	

TABLE 7.1 (Continued)

Band	3-1			3-2		
J	R(J)	Q(J)	P(J)	R(J)	Q(J)	P(J)
0	66910.112			64839.359		
1	912.396	66906.528		841.614	64835.682	
2	913.900	905.016	66899.314	843.188	834.423	
3	914.766	903.003	894.153	844.163	832.405	64823.598
4	914.766	900.174	888.374	844.163	829.708	817.886
5	914.218	896.621	881.831	844.163	826.349	811.714
6	913.900	892.373	874.768	842.919	822.260	804.687
7	910.912	887.416	866.829	841.083	817.595	797.030
8	908.169	881.830	858.288	838.592	812.156	788.664
9		875.404	848.956	835.492	806.123	779.702
10	900.540	868.296	839.079	831.666	799.364	770.068
11	895.900	860.607	828.261	827.161	791.957	759.551
12	890.268	852.050	816.869	822.260	783.764	
13	883.959	842.893	804.746	816.158	775.135	
14	876.853	833.026	791.907		765.528	
15	869.262	822.339	778.427		755.452	
16	860.607	811.050	764.288		744.615	
17	851.649	799.019			733.102	
18		786.238			720.973	
19		772.680			708.058	

TABLE 7.1 (Continued)

Band	4-0			5-1		
J	R(J)	Q(J)	P(J)	R(J)	Q(J)	P(J)
0	70356.162			69576.732		
1	358.303	70352.485		578.753	69573.049	
2	359.679	351.007		580.144	571.416	
3	359.982	348.565	70339.916	580.396	569.067	560.528
4	359.982	345.438	333.905	580.144	565.891	554.504
5	358.879	341.547	327.075	578.970	561.901	547.667
6	357.065	336.808	319.492	577.082	557.172	540.070
7	354.487	331.343	311.074	574.387	551.616	531.650
8	351.007	325.116	301.768	570.890	545.275	522.477
9	346.960	318.060	292.155	566.522	538.127	512.411
10	341.935	310.239	281.342	561.536	530.182	501.630
11	336.306	301.768	269.838	555.560	521.442	490.179
12	329.764	292.155	257.537	548.862	511.922	477.772
13	322.482	282.029	244.489	541.352	501.630	464.586
14	314.428	271.087	230.641	533.056	490.398	450.618
15	305.539	259.326	216.046	523.949	478.515	435.863
16		246.808	200.638	514.090	465.814	420.313
17		233.461	184.456	503.355	452.329	403.943
18		219.381	167.435	491.836	437.878	386.769
19		204.494		479.559	422.812	368.877
20		188.783		466.368	406.876	350.114
21		172.341		452.329	390.148	330.592
22		155.164		437.878	372.574	310.217
23		136.982		422.177	354.131	289.071
24		118.177		405.669	334.876	267.106
25					313.997	244.297
26					295.167	220.621
27					273.105	
28					250.446	
29					226.175	

TABLE 7.1 (Continued)

Band	6-1			7-1		
J	R(J)	Q(J)	P(J)	R(J)	Q(J)	P(J)
0	70863.782					
1	865.491	70860.094			72107.754	
2	866.337	858.125		72114.265	105.919	
3	866.337	855.407	70847.279	114.265	103.288	
4	865.491	851.741	840.812	113.506	099.761	
5	863.782	847.279	833.548	111.915	095.303	081.643
6	861.321	841.952	825.418	109.390	090.099	073.480
7	858.125	835.833	816.436	105.919	083.823	064.575
8	853.950	828.919	806.684	101.608	076.779	054.762
9	849.057	821.198	796.126	096.402	068.831	044.054
10	843.275	812.633	784.760	090.099	059.990	032.413
11	836.701	803.293	772.589	083.399	050.270	019.929
12	829.310	793.111	759.612	075.477	039.645	006.644
13	821.198	782.102	745.807	066.741	028.147	71992.354
14	812.190	770.281	731.164	057.130	015.799	977.212
15	802.465	757.619			002.499	
16		744.134			71988.365	944.420
17		729.674			973.315	
18					957.342	
19					940.571	
20					922.826	

TABLE 7.1 (Continued)

Band	7-2			8-2		
J	R(J)	Q(J)	P(J)	R(J)	Q(J)	P(J)
0	70040.562			71259.720		
1	042.509	036.939		261.448	71256.469	
2	043.638	035.204	70029.604	262.191	254.558	71248.880
3	043.638	032.695	024.519	262.191	251.810	243.340
4	043.148	029.313	018.231	261.232	248.115	236.857
5	041.631	025.053	011.242	259.318	243.340	229.568
6	039.254	019.964	003.353	256.469	237.795	221.416
7	036.047	014.004	69994.681	252.921	231.389	212.356
8	032.043	007.218	985.130	248.325	224.104	202.390
9	027.065	69999.519	974.698	242.982	215.950	191.603
10	021.324	991.026	963.531	236.857	206.909	179.803
11	014.628	981.669	951.329	229.568	196.979	167.179
12	007.218	971.431	938.468	221.416	186.156	153.643
13	69999.031	960.379	924.541	212.356	174.463	139.265
14	989.725	948.448	909.851	202.390	161.825	123.547
15	979.623	935.627	894.356	191.904	148.302	107.770
16		922.016	877.968	179.803	134.251	090.624
17		907.532	860.704	167.179	118.591	073.027
18				153.278	102.278	053.780
19					084.850	

TABLE 7.1 (Continued)

Band	9-5		
J	R(J)	Q(J)	P(J)
0	66383.467		
1	385.300	66379.920	
2	386.280	378.342	
3	386.280	375.671	
4	385.619	372.353	66361.608
5	384.064	368.060	354.710
6	381.702	363.022	347.017
7	378.342	357.085	338.371
8	374.353	350.353	328.982
9	369.447	342.759	318.731
10	363.498	334.290	307.681
11	357.085	325.025	295.755
12	349.547	314.777	282.957
13		304.013	
14		292.045	
15		279.469	

*indentify strongly bended lines.

†Doubling of columns in the data of the 0-0 and 0-1 bands for each branch denotes the perturbation regions and extra lines.

TABLE 7.2 Rovibronic term values of the A $^1\Pi$ (v=0 to 9) state of $^{13}C^{16}O$

	v=0+				v=1	
J	e	e	f	f	e	f
1	64754.17		64754.08		66207.32	66207.28
2	760.11		760.13		213.34	213.31
3	769.14		769.25		222.52*	222.36
4	781.11		781.35		234.47	234.43
5	795.84		796.40	64827.74*	249.52	249.52
6	813.19	64827.82	814.45	842.42	267.64	267.63
7	832.35	844.50	835.32	859.78	288.75	288.69
8	852.21	865.89	858.94	879.92	312.93	312.88
9		891.89	884.91	903.08	340.03	340.04
10		921.61	912.81	929.87	370.21	370.18
11		954.67	942.19	960.71	403.37	403.31
12		990.66	972.72	995.68	439.55	439.39
13		65029.37		65034.40	478.69	477.49
14				076.62	520.75	521.50
15				122.12	565.37	566.52
16				170.63	615.86	614.69
17				222.36	666.40	665.86
18					720.52	719.90
19						778.73
20						838.03
21						901.08
22						967.18*

TABLE 7.2 (Continued)

	v=2		v=3		v=4	
J	e	f	e	f	e	f
1	67622.70	67622.66	69006.22	69006.18	70356.16	70356.16
2	628.64	628.67	012.08	012.04	361.98	362.04*
3	637.57	637.58	020.85	020.91	370.68	370.62
4	649.60	649.51	032.69	032.65	382.21	382.20
5	664.40	664.53*	047.33	047.33	396.68	396.68
6	682.31	682.25	064.91	064.91	414.00	413.99
7	703.17	703.02	085.48	085.48	434.25	434.25
8	726.99	727.10	108.96	108.93	457.40	457.42
9	753.78	753.87	135.39	135.37	483.45	483.43
10	783.56	783.63	164.71	164.68	512.34	512.35
11	816.31	816.38	196.96	197.00	544.08	544.28*
12	852.03	852.08	232.22	232.11	578.82	578.74*
13	890.73	890.78	270.32	270.32	616.36	616.36
14	932.37	932.43*	311.36	311.29	656.82	656.82
15	977.00	977.01	352.21	355.24	700.15	700.12
16	68024.54	68024.60	402.19	402.12	746.34	746.32
17	075.07	075.15	451.74*	451.81	795.37	795.36
18	128.54	128.60	504.61*	504.59		847.31
19	184.96	184.92*		560.11		902.12
20	244.31	244.38				959.75
21	306.64	306.68				71020.29
22	371.71	371.90				083.75
23	439.65	440.05				149.84
24	509.72	511.06				218.95
25		584.90				
26		661.43				
27		740.02				

TABLE 7.2 (Continued)

	v=5		v=6		v=7	
J	e	f	e	f	e	f
1	71672.80	71672.76	72959.85*	72959.80	74207.38	74207.42
2	678.46	678.41	965.20	965.12*	212.97	212.88*
3	687.00	686.99	973.31	973.33	221.15	221.19
4	698.35	698.39	984.26	984.24	232.28	232.25
5	712.64	712.61	997.98	997.99	246.03	246.02
6	729.70	729.74	73014.50	73014.52	262.61	262.59
7	749.66	749.68	033.88	033.89	281.92	281.89
8	772.41	772.47	056.09	056.11	303.97	303.97
9	798.08	798.09	081.14	081.17	328.82	328.78
10	826.55	826.56	109.02	109.01	356.34	356.36
11	857.89	857.86	139.68	139.72	386.72	386.69
12	891.99	892.02	173.17	173.21	419.74	419.74
13	928.97	929.05*	209.47	209.52	455.56	455.57
14	968.78	968.76	248.61*	248.64	494.14	494.14
15	72011.43	72011.45	290.55	290.55	535.46	535.41
16	056.89	056.95	335.40	335.27	579.40	579.47
17	105.20	105.29		382.63		626.25
18	156.33	156.28*				675.75
19	210.26	210.29				728.04
20	267.04	267.03				782.98
21	326.56	326.61				
22	388.97	388.95				
23	454.13	454.03*				
24	522.06	521.90				
25	592.70	591.75				
26		667.25				
27		743.12				
28		821.98				
29		902.82				

TABLE 7.2 (Continued)

	v=8		v=9	
J	e	f	e	f
1	75426.53	75426.90*	76611.28	76611.24
2	431.88	432.21	616.62	616.69*
3	439.81*	440.29	624.54	624.56
4	450.61*	451.04	635.20	635.29
5	464.15	464.31*	648.56	648.55
6	480.29	480.43	664.53	664.58
7	499.13*	499.29	683.24	683.22
8	520.83	520.87	704.55	704.58
9	545.11	545.20	728.60	728.58
10	572.21	572.24	755.28	755.21
11	601.95	601.99	784.60	784.56
12	634.46	634.46	816.62*	816.42
13	669.62	669.65	851.19	851.27
14	707.53	707.50		888.41
15	748.06	748.06		928.44
16	791.70	791.69		
17	837.34	837.30		
18	885.88*	885.84		
19	936.84	936.86		

[a]Term values are given relative to X $^1\Sigma^+$ (v=0, J=0).
*Identify levels derived from strongly blended lines.
[†]Doubling of columns in the v=0 level for both e and f parities denotes the perturbation regions and extra lines

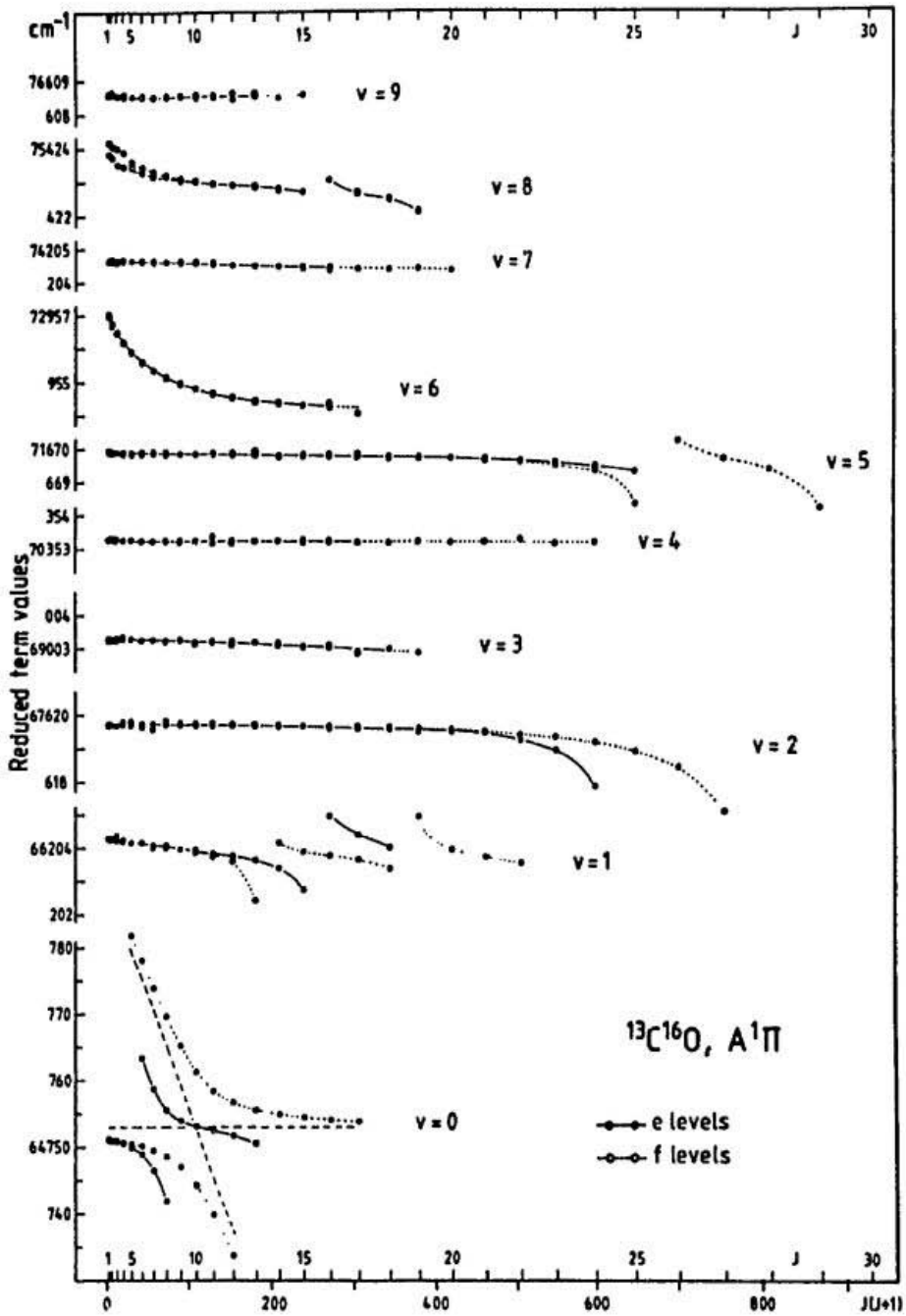

Figure 7.1 Reduced term values T(J) - BJ(J+1) for the v=0 to 9 rovibronic levesl in A $^1\Pi$ of $^{13}C^{16}O$. For v=0, the hypothetical unperturbed and crossing f levels are indicated by dashed lines. Notice, that the wavenumber scale for v=0 differs by a factor of 5 from the scale used for other levels

lowest rotational levels by 2 cm^{-1} more from their unperturbed postions. The percentage $^1\Pi$ character in the mixed A state levels can been seen from Table 7.3; since e $^1\Sigma^-$ makes no significant contribution to the transition moment, the $^1\Pi$ - $^1\Sigma$ Hönl-London factors for transitions to the mixed upper-state levels must be reduced accordingly.

The perturbation in v=6 arises from spin-orbit interaction with the Ω = 1 component of d $^3\Delta_i$ (v=12). Here, the interaction produces no Λ-type splittings in the perturbed levels. A preliminary deperturbation analysis estimates the interaction matrix element at close to 7 cm^{-1}; the calculated A $^1\Pi$ charcter of low-J levels is again shown in Table 7.3 and should be used to reduce the Hönl-London factors that would be appropriate for transitions to the deperturbed upper-state rovibronic levels. The perturbation of low-J levels in v=8 has not yet been analyzed. The occurrence of a sizable Λ-type doubling points to a Σ perturber, possibly v=12 of e $^1\Sigma^-$ and/or v = 20 of a′ $^3\Sigma^+$.

In addition to the fourth positive bands of $^{13}C^{16}O$, the jet spectra contain a number of atomic multiplets that can be attributed to ^{13}C. The wavenumbers of these lines, together with the corresponding transitions of ^{12}C are given in Table 7.4 which compares the observed isotope shifts $\Delta\nu$ with theoretical predictions by Clark (1984) based on multiconfiguration Hartee-Fock calculations of the so-called specific mass shifts $\Delta\nu_s$. The observed shifts represent the sum of the specific shifts $\Delta\nu_s$ and of the more familiar normal mass shifts $\Delta\nu_N$; the latter result from the dependence of the Rydberg constant on the reduced mass of the electrons and always displace the transition of the heavier isotope to higher wavenumbers (positive shift). For the three multiplets at 1329, 1335, and

TABLE 7.3 Percentage $^1\Pi$ character in mixed A state levels of $^{13}C^{16}O$[a]

	A(v=0)[b]		A(v=6)[c]
J	e	f	e,f
1	95%	95%	81%
2	94	94	83
3	93	94	86
4	91	93	89
5	87	92	91
6	76	90	93
7	54	86	95

[a]Obtained from the present work and the results of a deperturbation analysis (Field 1993) for the lower state levels of the B $^1\Sigma^+ \rightarrow$ A $^1\Pi$ (Ångström) system of $^{13}C^{16}O$ (Rytel, 1970; Janjić et al., 1972).

[b]Perturbed by c $^3\Sigma^-$ (v=1).

[c]Perturbed by d $^3\Delta_1$ (v=12).

TABLE 7.4 Wavenumbers and ^{13}C isotope shifts (cm^{-1}) for vacuum ultraviolet transition of C_I and C_{II}

	Observed			Calculated	
Transition	$\nu(^{12}C)^a$	$\nu(^{13}C)^b$	$\Delta\nu$	$\Delta\nu_N{}^c$	$\Delta\nu^d$
C_I, 1329 Å					
$2s^22p^2$, ^3P-$2s2p^3$, $^3P^0$	75253.98	75254.41	+0.43		
	239.72	240.08	+0.36		
	238.86	239.24	+0.38	+0.27	+0.38
	237.56	237.98	+0.42		
	211.86	212.27	+0.41		
	210.56	211.05	+0.49		
C_{II}, 1335 Å					
$2s^22p^3$, $2P^0$-$2s^2p^2$, ^2D	74932.62	74933.37	+0.75		
	869.20	869.97	+0.77	+0.26	+0.86
	866.68	867.57	+0.89		
C_I, 1561 Å					
$2s^22p^2$, ^3P-$2s2p^3$, $^3D^0$	64089.86	64090.55	+0.69		
	074.54		+0.4		
	073.44	074.9[e]	+1.5	+0.23	+0.67
	047.54	048.28	+0.74		
	046.45	047.15	+0.70		
	043.51	044.10	+0.59		
C_I, 1657 Å					
$2s^22p^2$, ^3P-$2s^22p3s$, $^3P^0$	60376.73	60376.57	-0.16		
	352.64	352.50	-0.14		
	349.73	349.59	-0.14	+0.21	
	336.22	336.07	-0.15		
	317.02	316.7[e]	-0.3		
	309.22	[f]			
C_I, 1931 Å					
$2s^22p^2$, ^1D-$2s^22p3s$, $^1P^0$	51789.17	51789.00	-0.17	+0.18	

[a]Kaufman and Edlen (1974); Kelly (1987).

[b]Present work

[c]$\Delta\nu_N = -\nu\Delta(m/M) = -\nu * 5.5\times10^{-4}\ \Delta\{1/M(amu)\}$, where m and M are the electron and nuclear masses respectively. (see Clark,1984).

[d]$\Delta\nu = \Delta\nu_N + \Delta\nu_s$, see Eq. [4] and Table I of Clark (1984); based on Hartee Fock calculations of $\Delta\nu_s$.

[e]Strongly blended lines.

[f]Outside the range of wavelengths recorded in the present work.

1561 Å the observations are in very satisfactory agreement with the calculations which claim an accuracy of 10% - 20%. The negative, rather than positive, shifts of the multiplet at 1657 Å and of the strong singlet line at 1931 Å support Clark's (1984) conclusion that the specific mass shift, although positive if the number of p electrons in the upper state is greater than in the lower state, will be negative if there are more p electrons in the lower state and will tend to reduce, or even reverse the effects of the positive normal shift.

7.4 Conclusions

The consistency of the A state term values in Table 7.2 with the B $\rightarrow$ A emission data of Rytel (1970) and the B $\leftrightarrow$ X measurements of Eidelsberg et al. (1987) gives reason to believe that the energies relative to X $^1\Sigma^+$ (v=0, J=0) for most of the A state rovibronic levels displayed in Figure 7.1 have been established with an accuracy of about $\pm 0.10\ cm^{-1}$. Further evidence for the absence of gross measurements or calibration errors comes from the close agreement between the measured and calculated ^{13}C isotope shifts in three multiplets of C_I and C_{II}.

As part of a study of the $^{12}CO/^{13}CO$ abundance ratio in the atmosphere of ζ Ophiuchi, Wannier, Penzias and Jenkins (1982) have calculated the wavelengths of the progression of A $\leftarrow$ X R(0) lines that can be observed in absorption from the ground state of $^{13}C^{16}O$. The conversion of these wavelengths to wavenumbers for comparison with the experimentally established term values (e levels) for J′ = 1 in Table 7.2 reveals discrepancies of 18.7, 4.4, and 1.7 cm^{-1} for the 0-0, 1-0 and 6-0 transitions and smaller

errors for transitions to v′ =2 to 5. Since the set of molecular parameters used in the calculations has not been published, it is impossible to identify the origin of these differences, although it appears likely that they may result from the failure of the calculations to account for the many A state interactions with close-lying Σ and Λ levels. A more recent study of CO abundances in the direction of ζ Ophiuchi by Sheffer et al. (1992) helps to emphasize this point. These authors observe an interstellar feature at a rest wavenumber of 72960.2 cm^{-1}, unquestionably the R(0) line in the (6←0) band of $A \leftarrow X$ at 72959.85 cm^{-1} listed in Table 7.2, but they rejected this assignment because of the poor agreement of the rest wavenumber with the predicted position by 3.6 cm^{-1} to the red region of the interstellar line where a much weaker feature, just barely visible above noise, can be detected. As may be appreciated from an inspection of Fig. 7.1 and from the discussion of the preceding section, the discrepancy between prediction and observation comes from the neglect of a consideration of the interaction of A(v=6) with the lower-lying level $d\ ^3\Delta_1$ (v=12) which pushes the lowest J levels in $A\ ^1\Pi$ by as much as 3 cm^{-1} to higher energies. The correct modelling of the 6-0 interstellar lines must also take into account the upper-state mixing ratios in accordance with the data in Table 7.3. The results presented in this chapter have appeared in a publication (Haridass, C., and Huber, K. P., *Astrophys. J.* **420**, 433 (1994)). A reprint of this paper is included in the Appendix.

REFERENCES

Brown, J. M., Hougen, J. T., Huber, K. P., Johns, J. W. C., Kopp, I., Lefebvre-Brion, H., Merer, A. J., Ramsay, D. A., Rostas, J., and Zare, R.N., *J. Mol. Spectrosc.* **55**, 500 (1975).

Clark, C. W., *Astrophys. J.* **285**, 322 (1984).

Comer, K. R., and Foster, S. C., *Chem. Phys. Lett.* **202**, 216 (1993).

Crosswhite, H. M., *J. Res. Nat. Bur. Stand.* **79 A**, 17 (1975).

Domin, J., *Acta. Phys. Hung.* **60**, 43 (1986).

Eidelsberg, M., Benayoun, J. J., Viala, Y., and Rostas, F., *Astron. Astrophys.* **90**, 231 (1991).

Eidelsberg, M., Benayoun, J. J., Viala, Y., Rostas, F., Smith, P. L., Yoshino, K., Stark, G., and Shettle, C. A., *Astron. Astrophys.* **265**, 839 (1992).

Eidelsberg, M., Roncin, J. -Y., Le Floch, A. C., Launay, F., Letzelter, C., and Rostas, J., *J. Mol. Spectrosc.*, **121**, 309 (1987).

Eidelsberg, M., and Rostas, F., *Astron. Astrophys.* **235**, 472 (1990).

Farrenq, R., Guelachvili, G., Sauval, A. J., Grevesse, N., and Farmer, C. B., *J. Mol. Spectrosc.* **149**, 375 (1991).

Field, R. W., Ph. D. thesis, Harvard University, 1971.

Field, R. W., private communication. M. I. T, Cambridge, Masssachusetts, 1993.

Field, R. W., Wicke, B. G., Simmons, J. D., and Tilford, S. G., *J. Mol. Spectrosc.* **44**, 383 (1972).

Garetz, B. A., Kittrell, C., and Le Floch, A. C., *Chem. Phys.* **94**, 843 (1991).

Hanson, M. M., Snow, T. P., and Black, J. H., *Astrophys. J.* **392**, 571 (1992).

Huber, K. P., Holland, F., and Coxon, J. A., *J. Chem. Phys.* **96**, 1005 (1992).

Huber, K. P., Klug, C. A., and Alberti, F., *J. Mol. Spectrosc.* **124**, 407 (1987).

Huber, K. P., and Sears, T. J., *Chem. Phys. Lett.* **113**, 129 (1985).

Huber, K. P., and Vervloet, M., *J. Mol. Spectrosc.* **153**, 17 (1992).

Janjić, J., Danielak, J., Kepa, R., and Rytel, M., *Acta. Phys. Pol.* **A 41**, 757 (1972).

Kaufman, V., and Edlén, B., *J. Phys. Chem. Ref. Data* **3**, 825 (1974).

Kelly, R. L ., *J. Chem. Ref. Data* **16**, Suppl. 1 (1987).

Kepa, R., *Acta. Phys. Hung.* **45**, 133 (1978).

Kepa, R., Para, A., and Rytel, M., *Acta. Phys. hung.* **68**, 205 (1990).

Kepa, R., Rytel, M., and Rzeszut, Z., *Acta. Phys. Pol.* **A 54**, 355 (1978).

Le Floch, A. C., *J. Mol. Spectrosc.* **155**, 177 (1992).

Le Floch, A. C., Rostas, J., and Schamps, J., *Mol. Phys.* **63**, 677 (1988).

Le Floch, A. C., Ph. D. thesis, University Paris-Sud, Orsay, 1989.

Le Floch, A. C., Launay, F., Rostas, J., Field, R. W., Brown, C. M., and Yoshino, K., *J. Mol. Spectrosc.* **121**, 337 (1987).

Rytel, M., *Acta. Phys. Pol.* **A 37**, 559 (1970).

Sheffer, Y., Federman, S. R., Lambert, D. L., and Cardelli, J. A., *Astrophys. J.* **397**, 482 (1992).

Simmons, J. D., and Bass, A. M., and Tilford, S. G., *Astrophys. J.* **155**, 345 (1969).

Tilford, S. G., and Simmons, J. D., *J. Phys. Chem. Ref. Data* **1**, 147 (1972).

Veeken, K., and Reuss, J., *Appl. Phys.* **B 38**, 117 (1985).

Wannier, P. G., Penzias, A. A., and Jenkins, E. B., *Astrophys. J.* **254**, 100 (1982).

CHAPTER 8

COMET-TAIL ($A\ ^2\Pi_i - X\ ^2\Sigma^+$) SYSTEM OF $^{12}C^{16}O^+$: REINVESTIGATION

8.1 Introduction

The spectra of the molecular ion CO^+ are of considerable importance for the understanding of the chemical and physical processes that take place in the solar and stellar atmospheres, comet-tails and the interstellar space. For example, the comet-tail ($A\ ^2\Pi_i - X\ ^2\Sigma^+$) system of CO^+ was first observed in the tail of the comet Morehouse 1908c by Pluvinel and Baldet (1909, 1911); strong evidence of CO^+ in Orion molecular cloud 1 was provided by Erickson et al. (1981); CO^+ was the first terrestrial molecular ion observed in the microwave region by Dixon and Woods (1975). This molecular ion has also been used as a monitoring probe for chemical dynamics in the investigations of the environmental research and combustion processes. The comet-tail system of CO^+ which occurs in the region 3080 - 8500 Å has applications in the study of radiative heating of hypersonic spacecraft at escape velocity and in the atmospheric fringe of the planet Venus which contains considerable amounts of CO_2. Observation of the pure rotational emission line of the neutral CO molecule from the interstellar space by Wilson et al. (1970) proves that neutral CO has been by far the most abundant molecule in the interstellar medium. From radio-astronomical observations, the abundance rations $^{12}C/^{13}C$ and $^{16}O/^{18}O$ were obtained for the interstellar medium and are compared with the theoretical models (see Audouze, 1977). Precise laboratory data on the spectra of CO and CO^+ and their various isotopomers would be very useful in the study of their spectra resulting from the astrophysical phenomena mentioned above. With this objective in

prespective, a systematic study of several electronic band systems of $^{12}C^{16}O$, $^{12}C^{18}O$, $^{13}C^{18}O$, $^{12}C^{16}O^+$, $^{12}C^{18}O^+$, and $^{13}C^{18}O^+$ has been undertaken in our laboratory. For example, Prasad and Reddy (1988, 1989, and 1990) and Reddy and Prasad (1989a) performed detailed rotational anlayses of the Herzberg ($C\ ^1\Sigma^+ - A\ ^1\Pi$) and the Angström ($B\ ^1\Sigma^+ - A\ ^1\Pi$) systems of $^{13}C^{18}O$ and the comet-tail ($A\ ^2\Pi_i - X\ ^2\Sigma^+$), the first-negative ($B\ ^2\Sigma^+ - X\ ^2\Sigma^+$), and the Baldet -Johnson ($B\ ^2\Sigma^+ - A\ ^2\Pi_i$) systems of $^{13}C^{18}O^+$. Molecular constants for the $X\ ^2\Sigma^+$, $A\ ^2\Pi_i$, and $B\ ^2\Sigma^+$ states of $^{12}C^{16}O^+$ have been obtained by Haridass et al. (1992) by using a merge technique (Albritton et al., 1977 and Coxon, 1978). In this paper the authors have analyzed the rotational structure of the individual bands of the A-X system, and reanalyzed the data of the B-X (Rao, 1950 and Misra et al., 1987), and B-A (Jakubek et al., 1987) systems, and the infrared (Davies and Rothwell, 1985) and microwave data of the v=0, 1 and 2 levels (Sastry et al., 1981 and Bogey et al., 1983). The molecular constants and the band origins thus obtained from these analyses were combined and all multiple estimates were reduced to a single set of values using a grand merge procedure. It was believed that the non-smooth variations of molecular constants in the $A\ ^2\Pi_i$ state, especially the higher-order constants such as D_v, A_{Dv}, p_v, q_v, are attributed to the neglect of perturbations. Recently Bembenek et al. (1994) recorded new bands in the Baldet-Johnson ($B^2\Sigma^+ - A\ ^2\Pi_i$) system of $^{12}C^{16}O^+$ and performed rotational analysis. In their analysis they have excluded the perturbed lines of the bands with a common lower $v''=0$ level and claimed that the molecular constants of the $B\ ^2\Sigma^+$ and $A\ ^2\Pi_i$ states thus obtained show a smooth variation with the vibrational quantum number (v+1/2). These authors found that the Λ-doubling parameters p_v and q_v of the $A\ ^2\Pi_i$ state

obtained by Haridass et al. (1992) do not obey tradionally recognized polynomial dependence on the vibrational quantum number (v+1/2). Wang et al. (1996) from our laboratory recently analyzed the gamma ($A\ ^2\Sigma^+ - X\ ^2\Pi_r$) system of $^{15}N^{18}O$ together with the available infrared vibration-rotation absorption bands of the same isotopomer and found that the Λ-doubling parameters p_v and q_v of the ground $X\ ^2\Pi_i$ state show a smooth variation with (v+1/2). These authors have also discussed the nature of the signs of these parameters. The information about the $A\ ^2\Pi_i$ state of CO' can be obtained from the rotational anlaysis of the A-X and B-A systems and similarly the information about the $B\ ^2\Sigma^+$ state can be obtained from the rotational analysis of the B-A and B-X systems. The present author (Haridass, 1990) reanalyzed the data of B-A system reported by Jakubek et al. (1987) and those of the B-X system reported by Rao (1950) and Misra et al. (1987) and obtained the merged molecular constants for the B, A, and X states. The constants thus obtained agree well within the error limits with those reported by Jakubek et al. (1987) and Misra et al. (1987). This agreement implies that our method of determining the merged constants is basically correct. However, when Haridass et al. (1992) included their data of the A-X system with those of Jakubek et al. (1987), Rao (1950), Misra et al. (1987), infrared data of Davies and Rothwell (1985) and the microwave data of Sastry et al. (1981) and Bogey et al. (1983) the variation in the values of the molecular constants p_v and q_v as a function of (v+1/2) is found to be irregular. After publication of the paper (Haridass et al., 1992) we have noted that in the recorded spectra there are some systematic shifts of the rotational lines of several bands of the A-X system due to inherent difficulties in the experimental procedure. Because of this situation we now decided to

make corrections to these shifts and reanalyze the data of the A-X system.

Weak perturbations in the A $^2\Pi_i$, v=0 state at $2.5 \leq J \leq 6.5$ due to X $^2\Sigma^+$, v=10 state resulting in extra lines of the sub-band of A $^2\Pi_{1/2}$ - X $^2\Sigma^+$, which have been observed by Katayama and Welsh (1981) in the laser-induced spectra of CO^+. Deperturbation analysis for the A $^2\Pi_i$ state of CO^+ from the available spectroscopic data (Bulthuis and co-workers, 1932, 1935; Rao, 1950; Katayama and Welsh, 1981) of the perturbed levels A, v=0, 5, and 10 using a modern direct fitting approach was carried out by Coxon and Foster (1982). These authors have also calculated an accurate RKR potential curve for the X $^2\Sigma^+$ state and tabulated the term values and the RKR turning points for high-lying vibrational levels. Remeasurement and subsequent analysis of the 0-0 band of the A-X system of CO^+ using laser-induced fluorescence excitation was also carried out by Brown et al. (1984).

In the present chapter, the rotational structure of 10 bands (4-0, 3-0, 2-0, 1-0 (with common $v'' = 0$), 0-1, 0-2, 0-3, 0-4 (with common $v' = 0$), 2-1 and 1-1) photographed under high resolution is analyzed. In our recorded spectra extra lines were not observed and therefore we have analyzed the 0-1, 0-2, 0-3, and 0-4 bands for rotational levels $J \geq 6.5$ but did not include lines with $J < 6.5$) because of perturbations. We have combined the experimental data of the ten bands referred to above with those of the infrared data of Davies and Rothwell (1985) and the microwave data of Bogey et al. (1983) for v=0, 1, 2, 3 and 4, in a global fit, using an effective Hamiltonian for the $^2\Pi$ state given by Brown et al. (1979) and the matrix elements for the $^2\Pi$ and $^2\Sigma^+$ states given by Amiot et al. (1981) and Douay et al. (1988) and molecular constants were derived for the A $^2\Pi_i$

and $X\ ^2\Sigma^+$ states. From the values of the T_v for the A, $v' = 0$ to 4 and X, $v'' = 0$ to 4 levels, the equilibrium vibrational constants were obtained for both states with respect to the $X\ ^2\Sigma^+$, v=0.

8.2 Experimental Details

The molecular ion CO^+ was excited in the cathode column of the hollow - cathode discharge tube. The high resolution spectra of seven bands were photographed on the 3.4 m Jarrell-Ash spectrograph equipped with a 1200 grooves/mm grating blazed at 1.4 μm, five bands (4-0, 3-0, 2-0, 1-0, and 2-1) in the third order, and two bands (1-1 and 0-2) in the second order. Three bands were photographed on the 2.0 m Bausch and Lomb spectrograph, two bands (0-1 and 0-3) in the second order of a 1200 grooves/mm grating blazed at 1.0 μm, and one band (0-4) in the third order of a 600 grooves/mm grating blazed at 2.5 μm. The slit width was maintained at 30 μm for the former and 20 μm for the latter. The reciprocal dispersions of the spectra photographed varied from 0.60 Å/mm at 3820 Å in the third order to 1.05 Å/mm at 7200 Å in the second order. Overlapping orders of the spectra were eliminated by using Corning and Hoya glass filters. The exposure times on the photographic plates (103 a-o, 103-F, and 1-N) varied from 45 min to 12 hr. An Fe-Ne hollow-cathode lamp was used as source for the reference spectra whose wavelengths were taken from Crosswhite (1975). The spectral measurements made on the Gaertner Optical Company comparator (Model M 1205C) have an accuracy of ±0.03 Å for the high resolution spectra.

8.3 Analysis of the Spectra

The upper A $^2\Pi_i$ state of the comet-tail system belongs to intermediate Hund's case (a) $\rightarrow$ case (b) (case (a) for small rotation and case (b) for large rotation) as shown later in this section. Its lower state X $^2\Sigma^+$ belongs to Hund's case (b). The rotational structure of a band for a $^2\Pi_i$ - $^2\Sigma^+$ transition exhibits 12 branches designated as $^2\Pi_{1/2}$ - $^2\Sigma^+$: R_{21ee}, R_{22ff}, Q_{21fe}, Q_{22ef}, P_{21ee}, and P_{22ff} and $^2\Pi_{3/2}$ - $^2\Sigma^+$: R_{11ee}, R_{12ff}, Q_{11fe}, Q_{12ef}, P_{11ee}, and P_{22ff} as shown schematically in Fig. 8.1. The parity of the levels in the e/f notation is according to Brown et al. (1975). As the bands are degraded to longer wavelengths, the R_{21ee}, Q_{21fe}/R_{22ff}, R_{11ee}, and Q_{11fe}/R_{12ff} branches form four distinct heads of a band in the decreasing order of wavenumber. The effective Hamiltonian for the $^2\Pi$ state discussed in detail by Brown et al. (1979) was used in the present work to analyze the rotational structure of the comet-tail bands. The matrix elements of the Hamiltonian for the $^2\Pi$ and $^2\Sigma^+$ states used in the present work are taken from Amiot et al. (1981) and Douay et al. (1988). The matrix elements of these Hamiltonians which are relevant to the present work are

$$^2\Sigma^{e,f} \quad : T_v + B_v\, x\, (x \mp 1) - D_v\, x^2(x \mp 1)^2 \pm 0.5\, \gamma_v\, (x \mp 1)$$

$$^2\Pi_{1/2}^{e,f} \; : T_v - 0.5\, A_v - 0.5\, A_{Dv}\, |x^2 + 1| + B_v\, |x^2 + 1| - D_v\, x^2\, |x^2 + 3| \mp$$

$$0.5\, p_v\, x \mp q_v\, x$$

$$^2\Pi_{3/2}^{e,f} \; : T_v + 0.5\, A_v + 0.5\, A_{Dv}\, |x^2 - 1| + B_v\, |x^2 - 1| - D_v\, x^2\, |x^2 - 1|$$

$$\{^2\Pi_{1/2},^2\Pi_{3/2}\}^{e,f} : - B_v\, |x^2 - 1|^{1/2} + 2.0\, D_v\, x^2\, |x^2 - 1|^{1/2} \pm 0.5\, q_v\, x\, |x^2 - 1|^{1/2}, \qquad [8.1]$$

where B_v and D_v are the rotational constants, γ_v is the spin-rotation constant, A_v and A_{Dv} are the spin-orbit constants, p and q are the Λ-doubling constants, and $x = (J + 0.5)$. The

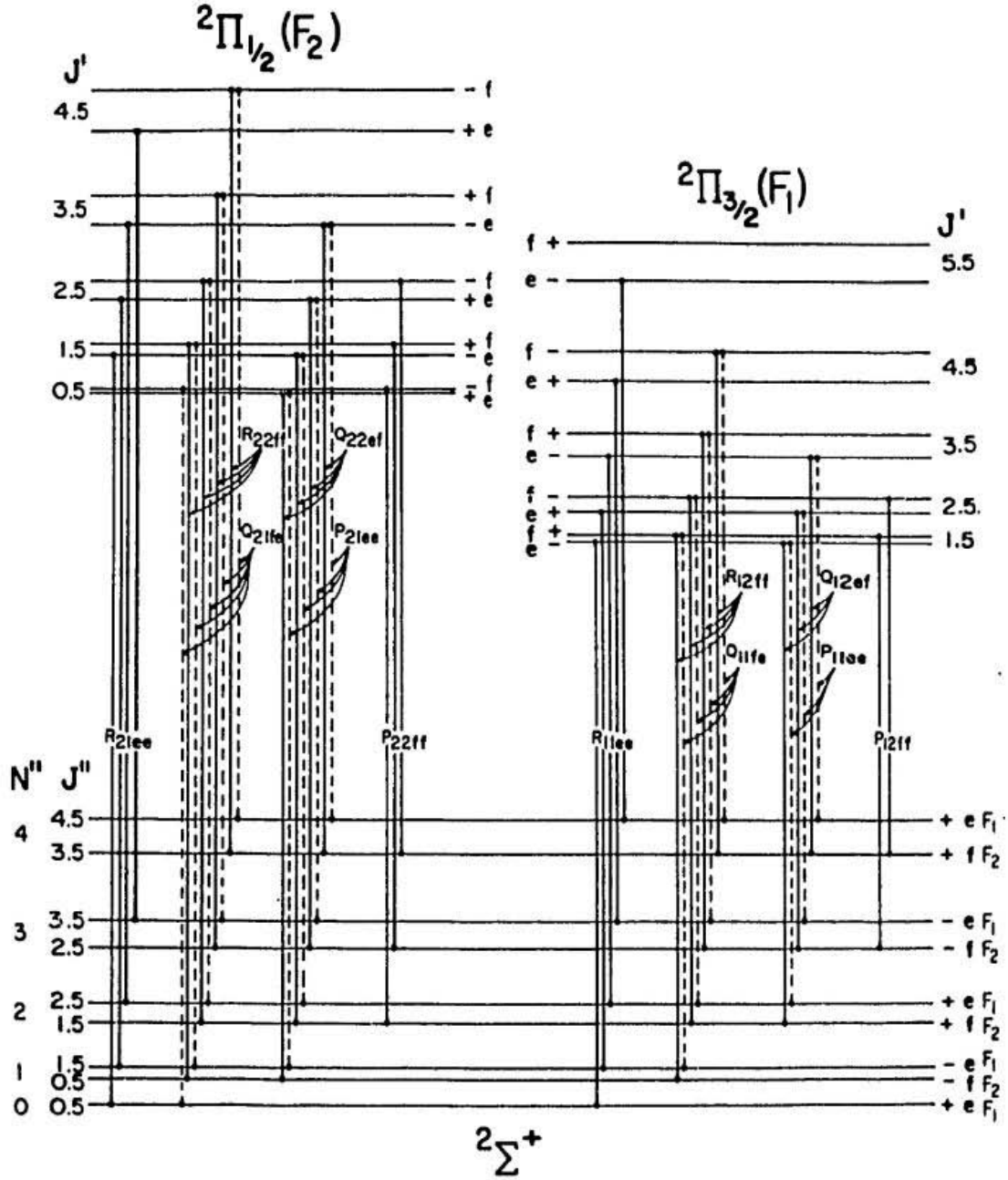

Figure 8.1 A schematic energy level diagram showing the first few rotational transitions for all 12 branches of a band of a $^2\Pi_i$ - $^2\Sigma^+$ system.

upper and lower state signs ± or ∓ in the above matrix elements refer to the e/f levels, respectively.

The rotational structure of a section of the 0-2 band of the comet-tail system photographed on the 3.4 m Jarrell-Ash spectrograph in the second order of the 1200 grooves/mm grating is shown in Fig. 8.2. In this figure the four heads and the ten branches (out of the expected twelve) of their rotational structure are clearly identified. It is to be noted that each of the branches, Q_{22ef}/P_{21ee} in the $^2\Pi_{1/2}$ - $^2\Sigma^+$ sub-band and R_{12f}/Q_{11fe} in the $^2\Pi_{3/2}$ - $^2\Sigma^+$ sub-band form two close pairs and appear as one branch. The intensities of the lines of the resolved pairs (R_{22ff}, Q_{21fe}) and (Q_{12ef}, P_{11ee}) are found to be approximately equal. These pairs of branches give directly the spin-splitting in the ground $^2\Sigma^+$ state. To verify the observed intensity pattern of a band in the $^2\Pi_i$ - $^2\Sigma^+$ transition of CO^+, intensities of the branches were calculated using the following expressions given by Earls (1935):

Branches	Line Strength S_J
R_{21ee} R_{11ee}	$((2J + 1)^2 \mp (2J + 1)\ U\ \lvert 4J^2 + 4J + 1 - 2\lambda \rvert)/32J$
R_{22ff} R_{12ff}	$((2J + 1)^2 \pm (2J + 1)\ U\ \lvert 4J^2 + 4J - 7 + 2\lambda \rvert)/32J$
Q_{21fe} Q_{11fe}	$((2J + 1)\ \lvert (4J^2 + 4J - 1) \mp U\ (8J^3 + 12J^2 - 2J - 7 + 2\lambda\}\rvert)/32J(J + 1)$
Q_{22ef} Q_{12ef}	$((2J + 1)\ \lvert (4J^2 + 4J - 1) \pm U\ (8J^3 + 12J^2 - 2J + 1 - 2\lambda\}\rvert)/32J(J + 1)$
P_{21ee} P_{11ee}	$((2J + 1)^2 \mp (2J + 1)\ U\ \lvert 4J^2 + 4J - 7 + 2\lambda \rvert)/32(J + 1)$
P_{22ff} P_{12ff}	$((2J + 1)^2 \pm (2J + 1)\ U\ \lvert 4J^2 + 4J + 1 - 2\lambda \rvert)/32(J + 1)$

Figure 8.2 Rotational structure of the 0-2 band of the comet-tail ($A\ ^2\Pi_i$ - $X\ ^2\Sigma^+$) system of $^{12}C^{16}O^+$, photographed on the 3.4 m Jarrell - Ash spectrograph in the second order of a 1200 grooves/mm grating. In this figure, the rotational lines at J = 3.5 of the P_{22ff} branch and J = 6.5 of the P_{12ff} branch are very weak to identify.

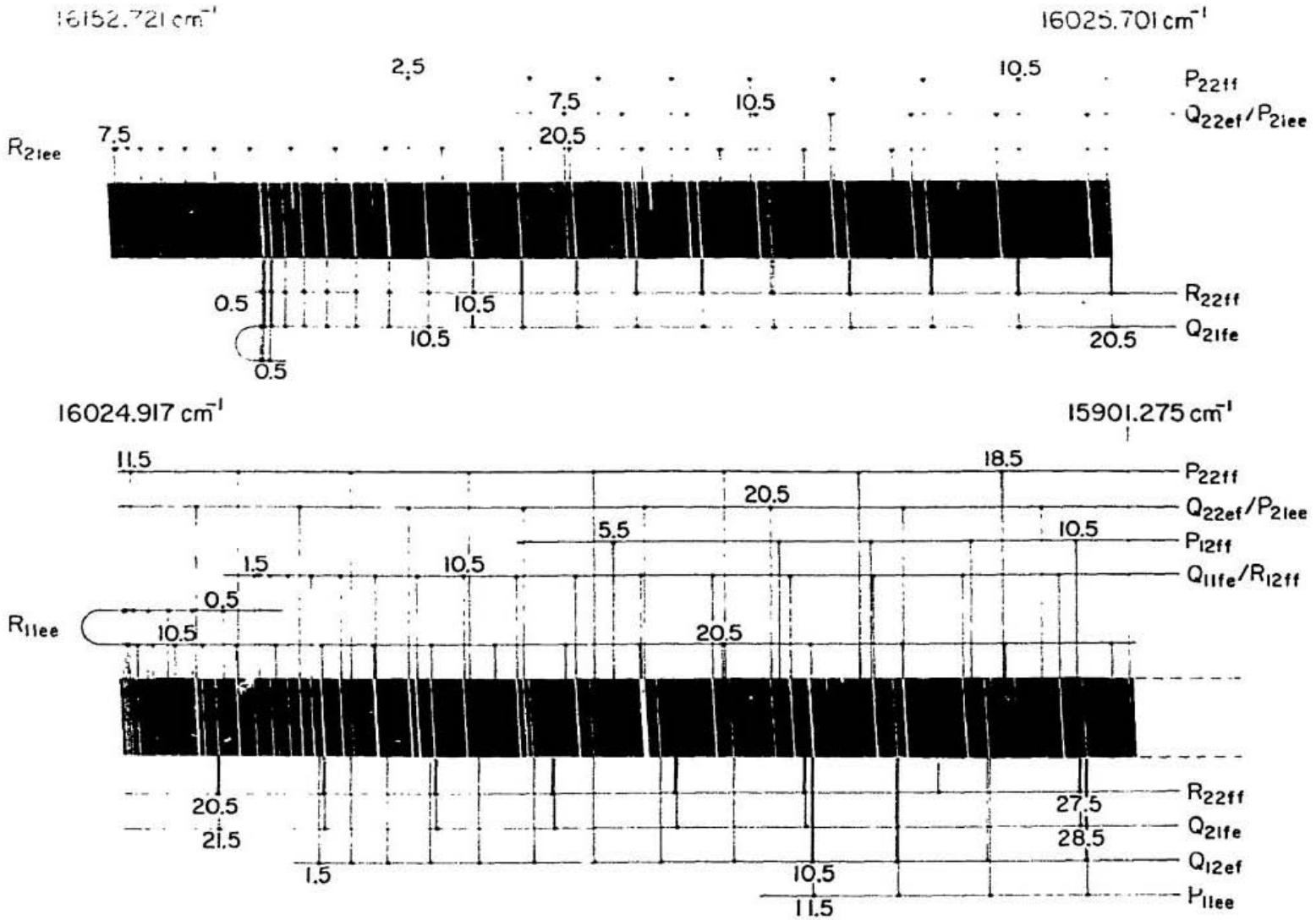
16152.721 cm⁻¹
16025.701 cm⁻¹
2.5
7.5
10.5
7.5
20.5
10.5
P22ff
Q22ef/P21ee
R21ee
0.5
10.5
10.5
20.5
R22ff
Q21fe
0.5
16024.917 cm⁻¹
15901.275 cm⁻¹
11.5
18.5
P22ff
20.5
Q22ef/P21ee
5.5
10.5
P12ff
1.5
10.5
Q11fe/R12ff
0.5
R11ee
10.5
20.5
20.5
27.5
R22ff
21.5
28.5
Q21fe
1.5
10.5
Q12ef
11.5
P11ee

Here $U = [\lambda^2 - 4\lambda + (2J + 1)^2]^{-1/2}$, $\lambda = A/B$, A is the spin-orbit constant, and B is the rotational constant. The upper and lower signs of notation $\pm$ and $\mp$ refer to the branches arising from the $^2\Pi_{1/2} - ^2\Sigma^+$ and $^2\Pi_{3/2} - ^2\Sigma^+$ transitions, respectively. The calculated intensities are displayed in Figs. 8.3 and 8.4. In these figures, it is clearly seen that the ratio of the intensities of the unresolved pairs (Q_{22ef}/P_{21ee} and Q_{11fe}/R_{12ff}) is approximately 3:1 and that of the resolved pairs (Q_{22ef} and P_{21ee}, and Q_{12ef} and P_{11ee}) is approximately 1:1. In the case of the 1-0 and 1-1 bands, i.e., bands with a common upper level, it was possible to observe 12 branches since the bands were strong and the rotational lines are resolved.

To rule out the possibility of systematic shifts in the observed spectra due to various experimental procedures, the spectra can in principle be calibrated with the atomic lines of carbon and oxygen if they appear in the CO^+ spectrum itself. However, these atomic lines were not observed in the present work. The emission spectrum has the advantage of displaying several bands involving the same upper vibrational levels and therefore provides a critical check of the assignments and systematic shifts. As the ground state rotational levels of CO^+ are known accurately, it is possible to calculate the shifts for the bands arising from the same v' and different v'', by combining the observed wavenumbers of the rotational levels with the corresponding term values of the ground state. The ground state term values for v=0, 1, 2, 3 and 4 for both e and f levels are calculated from the Dunham parameters and the spin-rotation constant γ_v given by Bogey et al. (1983) and the G(v) values calculated by Coxon and Foster (1981). For example, the rovibrational term values of A $^2\Pi_i$, v=0, e and f levels are obtained by combining the

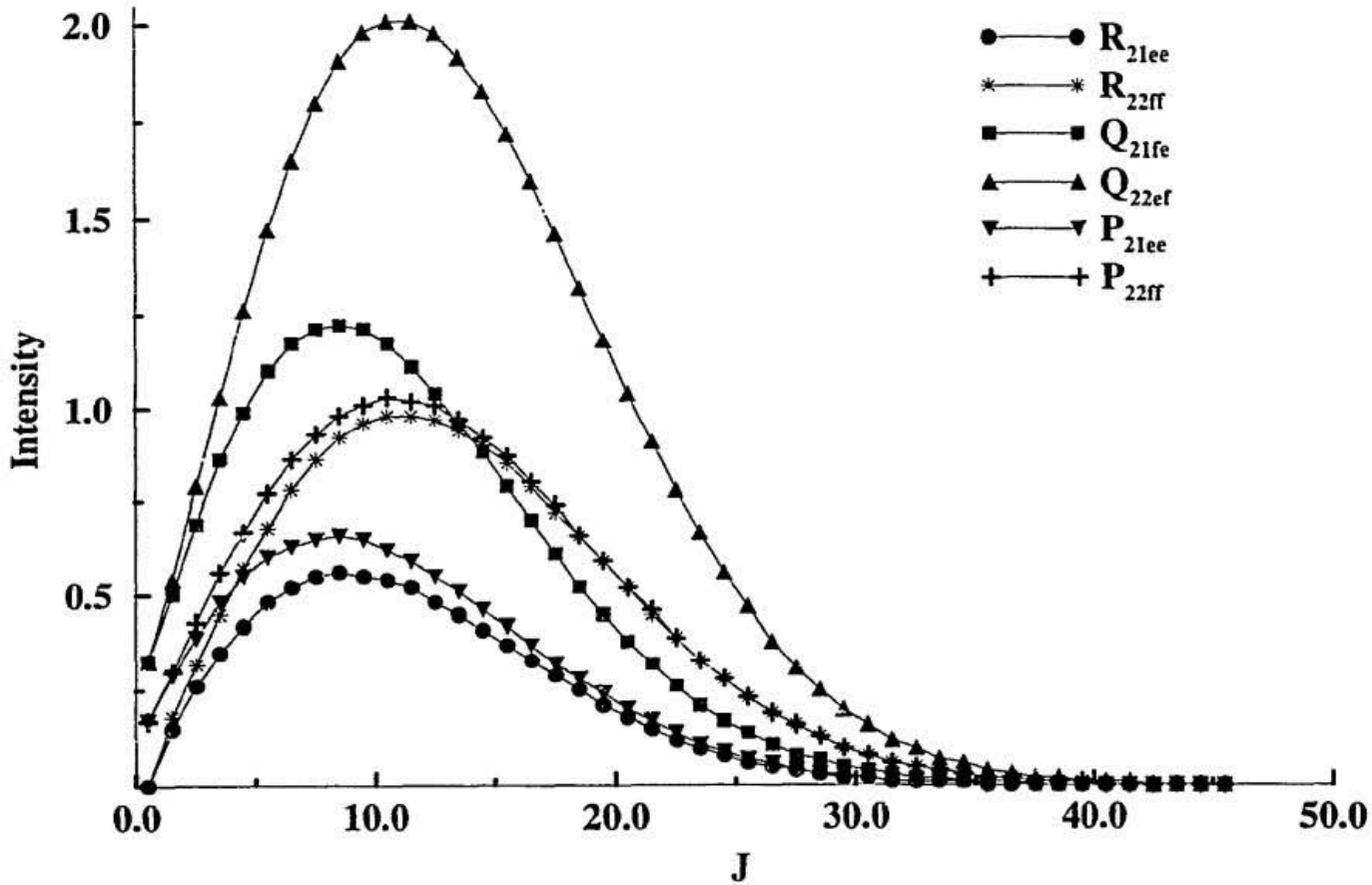

Figure 8.3 Intensity distribution of the six branches in the 0-2 band of the comet-tail sub-band ($^2\Pi_{1/2}$ - $^2\Sigma^+$) system of $^{12}C^{16}O^+$

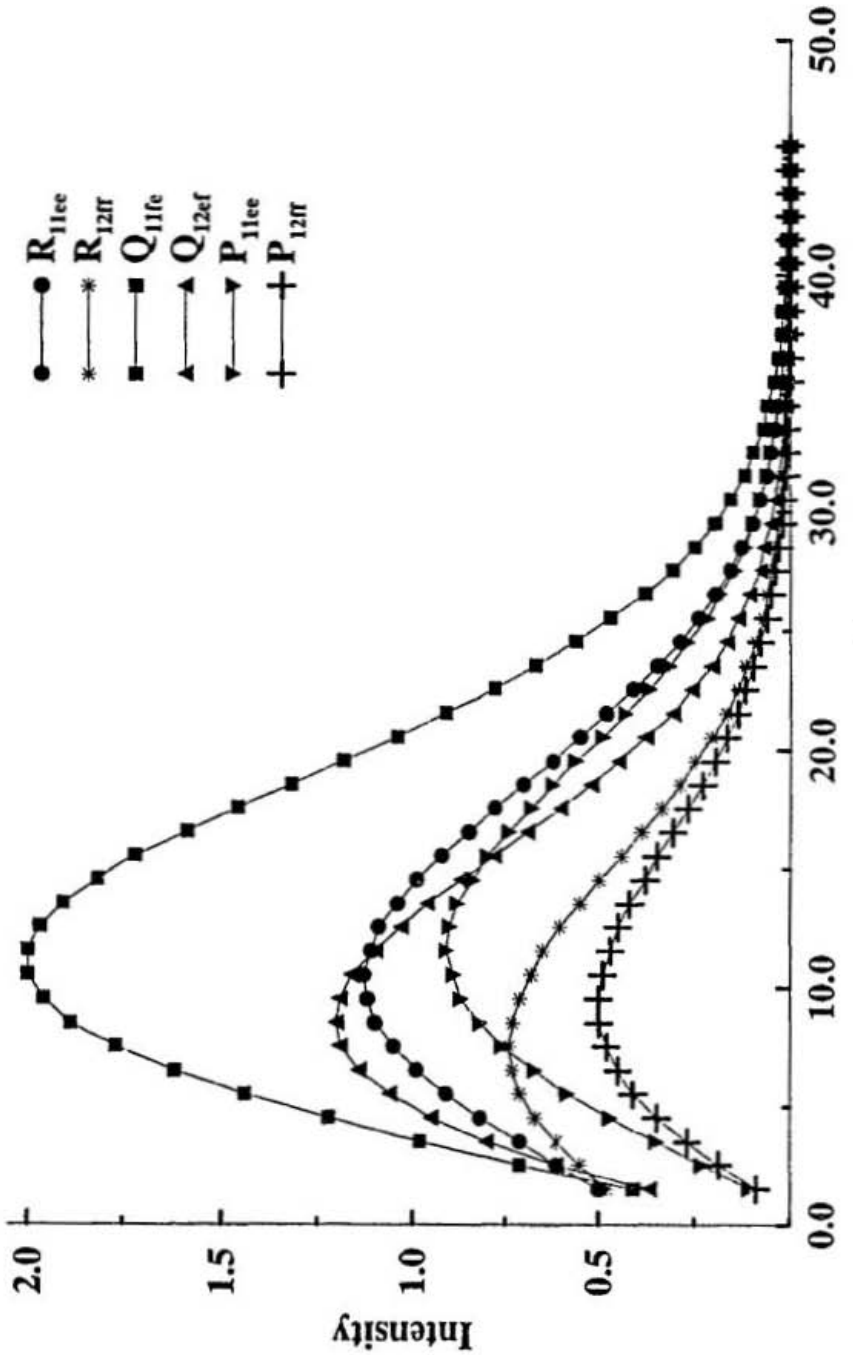

Figure 8.4 Intensity distribution of the six branches in the 0-2 band of the comet-tail sub-band ($^2\Pi_{3/2}$ - $^2\Sigma^+$) system of $^{12}C^{16}O^+$

observed wavenumbers of the 0-1, 0-2, 0-3 and 0-4 bands of the A-X system to the corresponding term values of the v=1, 2, 3 and 4 levels of the X $^2\Sigma^+$ state. The term values of the v′=0 level calculated from the 0-2 band are found to be consistently lower by 0.197 cm^{-1} than those calculated from the 0-1, 0-3 and 0-4 bands. Using a similar procedure, the rovibronic term values of the A $^2\Pi_i$, v=1 and 2 levels are calculated by combining the wavenumbers of the 1-0 and 1-1, 2-0 and 2-1 bands, respectively, of the A-X system to the corresponding term values of the X $^2\Sigma^+$, v″ =0 and 1 as mentioned above. The calculated term values of the v′=1 level from the 1-0 band are found to be consistently lower by 0.265 cm^{-1} than those calculated from the 1-1 band. A systematic shift was observed for the term values of the v′=2 level calculated from the 2-1 band with those calculated from the 2-0 band and is found to be -0.113 cm^{-1}. The corrections for the observed wavenumber of the 0-2 band with respect to 0-1, 0-3 and 0-4 bands was made by adding the constant value of 0.197 cm^{-1}. Following the same procedure the shifts of the other bands were corrected. After making these corrections for the systematic shifts the rotational quantum numbers and the vacuum wavenumbers of the spectral lines of all the ten bands (4-0, 3-0, 2-0, 1-0, 2-1, 1-1, 0-1, 0-2, 0-3, and 0-4) are listed in Table 8.1.

In the present work, the wavenumber data of the ten bands, the infrared data of the rovibronic spectra (Davies and Rothwell, 1985), and the microwave data of the v=0, 1, 2, 3, and 4 levels both for the X $^2\Sigma^+$ state (Sastry et al., 1981 and Bogey et al., 1983), a total of 2513 transitions were used simultaneously in a nonlinear least-squares fit. The weights were calculated from the expression $w = 1/\sigma^2$, where σ is the uncertainty for the

TABLE 8.1 Vacuum wavenumbers (in cm^{-1}) of the rotational lines of the bands of the $A\ ^2\Pi_i - X\ ^2\Sigma^+$ system of $^{12}C^{16}O^+$

4-0 Band ($A\ ^2\Pi_{3/2} - X\ ^2\Sigma^+$)					
J	$R_{21ee}(J)$	$R_{22f}(J)$	$Q_{21e}(J)$	$Q_{22f}(J)$	$P_{22f}(J)$
0.5	26453.235(21)	26449.311(5)	26448.690(23)	26444.741(8)	
1.5	456.850(-20)	449.034(-11)	449.277(-15)	441.423(0)	
2.5	459.639(9)	447.875(-13)	449.034(12)	437.220(1)	26429.612(-29)
3.5	461.506(11)	445.827(- 9)	447.875(19)	432.109(-11)	421.503(- 9)
4.5	462.477(15)	442.899(12)	445.785(-10)	426.106(-20)	412.477(-11)
5.5	462.515(-18)	439.038(- 4)	442.856(19)	419.229(- 8)	402.576(7)
6.5	461.702(- 3)	434.307(8)	438.975(- 8)	411.453(1)	391.749(- 7)
7.5	459.974(- 5)	428.663(5)	434.244(13)	402.781(10)	380.052(3)
8.5	457.347(- 7)	422.102(-17)	428.564(-17)	393.175(-19)	367.443(- 3)
9.5	453.822(- 6)	414.674(- 6)	422.014(-19)	382.699(-21)	353.967(19)
10.5	449.403(2)	406.360(19)	414.580(- 5)	371.335(-14)	339.566(12)
11.5	444.072(1)	397.112(11)	406.243(7)	359.081(2)	324.268(5)
12.5	437.850(11)	386.941(-18)	396.990(3)	345.929(18)	308.070(- 6)
13.5	430.698(- 4)	375.927(13)	386.823(-13)	331.845(1)	290.997(5)
14.5	422.670(10)	363.951(-14)	375.803(21)	316.899(23)	273.010(0)
15.5	413.703(- 9)	351.117(5)	363.801(-23)	301.015(8)	254.119(-10)
16.5	403.861(5)	337.351(- 1)	350.970(9)	284.236(- 1)	234.348(- 2)
17.5	393.086(- 5)	322.672(-14)	337.214(21)	266.544(-20)	213.677(7)
18.5	381.413(- 3)	307.123(11)	322.528(11)	247.993(5)	192.098(8)
19.5	368.825(- 6)	290.632(3)	306.954(20)	228.495(-12)	169.621(13)
20.5	355.380(48)	273.224(-11)	290.468(26)	208.114(- 7)	146.226(1)
21.5	340.948(27)	254.946(15)	273.046(6)	186.813(-17)	121.929(-10)
22.5	325.583(-12)	235.716(1)	254.728(2)	164.610(-21)	096.759(10)
23.5	309.347(- 6)	215.606(21)	235.497(- 4)	141.504(-20)	070.674(18)
24.5		194.568(27)	215.301(-61)	117.514(6)	043.665(8)
25.5		172.592(10)	194.305(- 4)	092.597(14)	015.774(22)
26.5		149.700(- 6)	172.330(-11)	066.717(-30)	25986.965(24)
27.5		125.908(- 5)	149.435(-21)	040.015(15)	957.217(- 5)
28.5		101.196(- 5)		012.321(-19)	926.591(- 5)
29.5				25983.775(8)	895.060(0)
30.5				954.289(10)	862.547(-68)
31.5				923.907(31)	829.250(- 9)
32.5				892.554(- 4)	795.004(11)
33.5				860.300(-22)	
34.5				827.167(- 2)	
35.5				793.121(23)	

TABLE 8.1 (Continued)

4-0 Band ($A\ ^2\Pi_{3/2}$ - $X\ ^2\Sigma^+$)					
J	$R_{11ee}(J)$	$Q_{11fe}(J)$	$Q_{12ef}(J)$	$P_{11ee}(J)$	$P_{12ff}(J)$
0.5	26328.246(8)				
1.5	331.729(11)	26324.294(- 5)	26316.452(4)		
2.5	334.240(10)	323.864(20)	312.055(-12)	26316.452(27)	
3.5	335.782(7)	322.413(- 9)	306.717(- 3)	312.055(20)	26296.329(- 5)
4.5	336.337(-15)	320.036(3)	300.406(0)	306.683(4)	287.067(14)
5.5	335.961(0)	316.691(14)	293.117(- 9)	300.331(-25)	276.806(- 2)
6.5	334.584(-19)	312.366(11)	284.884(4)	293.050(-17)	265.562(-35)
7.5	332.263(-16)	307.078(11)	275.652(-17)	284.831(19)	253.407(-14)
8.5	328.974(-13)	300.813(- 1)	265.490(- 4)	275.610(18)	240.277(- 5)
9.5	324.720(- 9)	293.611(16)	254.344(- 9)	265.397(-10)	226.182(2)
10.5	319.515(11)	285.407(- 4)	242.251(1)	254.258(0)	211.111(- 5)
11.5	313.305(- 8)	276.254(- 9)	229.173(-10)	242.148(3)	195.096(6)
12.5	306.168(11)	266.167(15)	215.171(18)	229.055(-14)	178.107(4)
13.5	298.036(0)	255.099(22)	200.165(3)	215.048(18)	160.139(-18)
14.5	288.944(- 6)	243.060(20)	184.225(15)	200.040(10)	141.255(4)
15.5	278.918(18)	230.042(1)	167.291(- 7)	184.079(10)	121.381(- 6)
16.5	267.886(0)	216.070(-10)	149.435(9)	167.160(13)	100.578(12)
17.5	255.891(-18)	201.156(- 3)	130.587(- 8)	149.234(-32)	078.791(2)
18.5	242.970(1)	185.272(- 6)	110.811(5)	130.429(3)	056.059(3)
19.5	229.084(18)	168.419(-18)	090.068(8)	110.622(- 6)	032.376(7)
20.5	214.225(23)	150.631(- 7)	068.360(3)	089.853(-20)	007.712(-16)
21.5	198.376(0)	131.865(-15)	045.677(-22)	068.155(- 6)	25982.118(-17)
22.5	181.605(16)	112.176(11)	022.111(26)	045.506(12)	955.603(13)
23.5	163.846(5)	091.482(-11)	25997.525(7)	021.858(-14)	928.061(-33)
24.5	145.154(21)	069.867(2)	971.992(- 5)	25997.303(8)	899.653(4)
25.5	125.466(0)	047.270(-11)	945.512(-11)	971.751(-14)	
26.5	104.834(- 5)	023.747(6)	918.081(-17)	945.269(-13)	
27.5	083.283(29)	25999.241(- 7)	889.733(12)	917.824(-23)	
28.5	060.726(17)	973.812(12)	860.412(19)	889.448(-13)	
29.5	037.179(-28)			860.101(-24)	
30.5	012.762(16)			829.818(-20)	
31.5				798.645(43)	

TABLE 8.1 (Continued)

3-0 Band ($A\ ^2\Pi_{1/2} - X\ ^2\Sigma^+$)					
J	$R_{21ee}(J)$	$R_{22f}(J)$	$Q_{21ff}(J)$	$Q_{22ef}(J)$	$P_{22f}(J)$
0.5		24994.994(- 4)	24994.307(8)	24990.369(6)	
1.5	25002.687(29)	994.834(- 3)	994.994(10)	987.117(5)	
2.5	005.577(20)	993.806(-14)	994.834(20)	982.994(-13)	24975.325(- 8)
3.5	007.611(12)	991.925(-22)	993.806(18)	978.039(- 7)	967.313(10)
4.5	008.814(29)	989.230(12)	991.925(19)	972.215(-16)	958.412(- 7)
5.5	009.128(15)	985.659(27)	989.147(-21)	965.548(-11)	948.687(6)
6.5	008.584(2)	981.213(25)	985.559(-13)	958.024(- 8)	938.089(2)
7.5	007.196(3)	975.884(- 1)	981.097(-22)	949.636(-12)	926.636(- 2)
8.5	004.956(13)	969.726(2)	975.794(-14)	940.381(-27)	914.341(7)
9.5	001.833(0)	962.703(0)	969.658(21)	930.283(-27)	901.179(4)
10.5	24997.853(- 8)	954.822(1)	962.593(-14)	919.335(-19)	887.155(- 3)
11.5	993.024(- 2)	946.081(4)	954.712(- 4)	907.515(-25)	872.290(4)
12.5	987.317(-10)	936.456(-15)	945.950(-13)	894.845(-21)	856.567(11)
13.5	980.760(- 3)	925.991(-10)	936.340(- 8)	881.359(27)	839.973(5)
14.5	973.325(- 8)	914.666(- 1)	925.862(- 7)	866.918(-19)	822.494(-28)
15.5	965.013(-23)	902.471(4)	914.551(25)	851.672(- 9)	804.234(18)
16.5	955.854(-16)	889.383(-18)	902.322(5)	835.546(-15)	785.063(12)
17.5		875.474(8)	889.243(2)	818.591(13)	765.039(14)
18.5	934.954(27)	860.666(3)	875.320(22)	800.737(6)	744.147(9)
19.5	923.155(7)	844.983(- 7)	860.506(21)	782.018(0)	722.379(-10)
20.5		828.440(- 5)	844.790(-13)	762.453(14)	699.771(- 5)
21.5		811.033(4)	828.250(0)	742.000(8)	676.299(- 1)
22.5			810.837(13)	720.688(11)	651.954(- 5)
23.5		773.554(-20)	792.529(4)	698.484(- 8)	626.764(11)
24.5		753.523(-10)	773.343(- 8)	675.446(9)	600.701(21)
25.5		732.605(-11)		651.507(- 4)	573.730(-11)
26.5		710.801(-19)	732.370(- 4)	626.718(6)	545.918(-15)
27.5		688.142(- 3)		601.038(- 2)	517.284(28)
28.5				574.503(9)	
29.5				547.077(5)	
30.5				518.787(13)	
31.5				489.558(-41)	
32.5				459.542(- 3)	
33.5				428.642(30)	

TABLE 8.1 (Continued)

3-0 Band ($A\ ^2\Pi_{3/2}$ - $X\ ^2\Sigma^+$)					
J	$R_{11ee}(J)$	$Q_{11fe}(J)$	$Q_{12ef}(J)$	$P_{11ee}(J)$	$P_{12ff}(J)$
0.5	24873.949(3)				
1.5	877.514(- 6)	24870.019(12)	24862.138(-17)		
2.5	880.163(- 1)	869.654(8)	857.867(- 2)		
3.5	881.887(8)	868.371(15)	852.639(-15)		24842.159(23)
4.5	882.581(-83)	866.147(10)	846.483(-27)		832.991(3)
5.5	882.533(14)	863.002(13)	839.462(24)		822.895(-17)
6.5	881.441(- 3)	858.931(19)	831.442(4)	24839.399(20)	811.897(-11)
7.5	879.421(-20)	853.929(22)	822.494(-16)	831.368(- 2)	799.963(-15)
8.5	876.504(- 4)	847.971(- 3)	812.676(20)	822.441(8)	787.135(13)
9.5	872.646(0)	841.126(12)	801.897(23)	812.566(- 3)	773.343(2)
10.5	867.836(-21)	833.350(23)	790.174(6)	801.785(6)	758.641(6)
11.5	862.138(- 1)	824.634(21)	777.545(10)	790.070(7)	743.000(- 5)
12.5	855.495(2)	814.943(-30)	763.994(15)	777.437(15)	726.452(- 1)
13.5	847.898(-23)	804.400(- 8)	749.521(23)	763.846(-10)	709.003(25)
14.5	839.399(-22)	792.928(10)	734.114(20)	749.369(3)	690.575(- 7)
15.5	829.981(-14)	780.518(14)	717.785(17)	733.881(-72)	671.251(-14)
16.5	819.649(6)	767.187(21)	700.524(3)	717.600(-18)	650.996(-33)
17.5	808.353(-13)	752.902(- 4)	682.331(-21)	700.367(6)	629.832(-43)
18.5	796.169(5)	737.720(- 3)	663.240(-23)	682.177(- 6)	607.810(8)
19.5	783.042(4)	721.626(8)	643.253(- 2)	663.078(- 8)	584.793(-21)
20.5	768.986(- 1)	704.589(- 3)	622.336(8)	643.072(4)	560.917(8)
21.5	754.018(5)	686.639(- 7)	600.523(39)	622.100(-33)	536.085(- 4)
22.5	738.131(15)	667.774(- 7)	577.756(33)	600.278(- 1)	510.348(- 8)
23.5	721.329(33)	647.983(-12)	554.074(29)	577.503(- 6)	483.741(31)
24.5	703.550(- 3)	627.291(- 1)	529.426(-25)	553.852(30)	
25.5	684.881(- 8)	605.662(- 8)	503.922(-21)	529.240(21)	
26.5	665.298(- 5)	583.141(10)		503.725(23)	
27.5	644.804(8)	559.678(4)		477.260(-10)	
28.5	623.337(-31)	535.301(- 1)		449.898(-27)	
29.5	601.038(18)	510.040(27)		421.719(52)	
30.5	577.756(5)	483.825(17)		392.456(-41)	
31.5		456.675(-14)			
32.5		428.642(-12)			
33.5		399.685(-21)			

TABLE 8.1 (Continued)

2-0 Band ($A\ ^2\Pi_{1/2}$ - $X\ ^2\Sigma^+$)					
J	$R_{21ee}(J)$	$R_{220}(J)$	$Q_{210}(J)$	$Q_{22ef}(J)$	$P_{220}(J)$
0.5				23509.324(3)	
1.5	23521.758(-15)		514.029(24)	506.125(- 4)	23501.428(-40)
2.5	524.811(1)		513.921(-14)	502.113(- 9)	494.369(15)
3.5	527.011(-19)		513.057(8)	497.323(24)	486.423(- 2)
4.5	528.431(- 1)		511.362(16)	491.667(6)	477.693(13)
5.5	529.012(- 5)	505.558(9)	508.845(18)	485.197(-10)	468.133(12)
6.5	528.769(-14)	501.428(24)	505.469(-21)	477.934(- 2)	457.743(- 3)
7.5	527.736(6)	496.462(23)	501.326(- 9)	469.839(-10)	446.558(2)
8.5	525.857(1)	490.670(15)	496.362(0)	460.929(-16)	434.552(2)
9.5	523.168(7)	484.057(6)	490.554(-15)	451.216(- 7)	421.729(1)
10.5	519.645(1)		483.955(0)	440.663(-19)	408.093(3)
11.5	515.302(- 1)	468.391(14)	476.566(46)	429.311(-12)	393.636(2)
12.5	510.140(2)	459.309(3)	468.270(7)	417.134(- 9)	378.376(16)
13.5	504.151(3)	449.415(4)	459.173(-10)	404.143(0)	362.260(- 8)
14.5	497.323(- 8)	438.699(8)	449.278(- 1)	390.333(11)	345.371(14)
15.5	489.665(-21)	427.156(12)	438.555(5)	375.689(11)	327.622(- 4)
16.5	481.215(3)	414.778(7)	426.976(-18)	360.213(2)	309.083(8)
17.5	471.902(- 5)	401.572(4)	414.603(- 8)	343.922(2)	289.711(8)
18.5	461.749(-22)	387.554(17)	401.425(25)	326.799(- 5)	269.514(6)
19.5	450.802(0)	372.686(12)	387.401(42)	308.871(9)	248.498(7)
20.5	438.982(-16)	356.988(8)	372.485(- 2)	290.108(15)	226.659(9)
21.5	426.353(- 6)	340.452(0)	356.788(4)	270.516(21)	204.002(17)
22.5	412.872(-12)	323.092(1)	340.240(- 8)	250.084(15)	180.504(10)
23.5		304.905(11)	322.868(- 9)	228.835(22)	156.202(25)
24.5		285.864(4)	304.709(38)	206.742(16)	131.020(-13)
25.5		265.990(1)		183.824(18)	105.017(-44)
26.5		245.307(28)		160.084(30)	078.246(-14)
27.5				135.489(21)	050.674(44)
28.5				110.063(16)	022.176(7)
29.5				083.829(40)	22992.884(7)
30.5				056.669(-26)	
31.5				028.779(16)	

TABLE 8.1 (Continued)

2-0 Band ($A\ ^2\Pi_{3/2}$ - $X\ ^2\Sigma^+$)					
J	$R_{11ee}(J)$	$Q_{11f}(J)$	$Q_{12ef}(J)$	$P_{11ee}(J)$	$P_{12f}(J)$
0.5	23392.855(6)				
1.5	396.516(- 2)	23388.910(0)	23381.048(-10)		
2.5	399.304(10)	388.662(18)	376.858(- 9)		
3.5	401.179(0)	387.488(2)	371.766(-18)		
4.5	402.167(- 5)	385.439(2)	365.786(-24)		23352.114(- 3)
5.5	402.283(10)	382.505(7)	358.932(-14)		342.233(21)
6.5	401.503(20)	378.684(17)	351.159(-33)		331.422(5)
7.5	399.799(- 2)	373.966(20)	342.529(-20)		319.736(3)
8.5	397.221(- 7)	368.365(29)	332.981(-35)		307.151(-10)
9.5	393.791(26)	361.870(34)	322.571(-24)		293.696(- 6)
10.5	389.423(12)	354.436(-11)	311.296(10)		279.343(-14)
11.5	384.174(7)	346.186(17)	299.071(-19)		264.125(0)
12.5	378.048(14)	337.019(15)	285.992(-15)		248.020(11)
13.5	371.016(5)	326.930(-22)	272.034(- 4)	23285.864(-20)	230.989(-20)
14.5	363.097(- 3)	316.017(4)	257.194(9)	271.907(1)	213.113(-13)
15.5	354.301(0)	304.189(1)	241.438(- 9)	257.057(13)	194.353(- 7)
16.5	344.620(6)	291.477(- 1)	224.821(- 5)	241.296(- 1)	174.723(10)
17.5	334.031(- 9)	277.872(-11)	207.324(2)	224.655(-12)	154.176(-10)
18.5	322.571(- 8)	263.415(11)	188.932(- 5)	207.158(4)	132.747(-33)
19.5	310.243(11)	248.043(1)	169.688(18)	188.769(10)	
20.5	297.009(9)	231.797(- 1)	149.512(-11)	169.498(15)	
21.5	282.888(6)	214.682(10)	128.516(19)	149.345(18)	
22.5	267.893(13)	196.667(3)	106.602(10)	128.300(8)	
23.5	251.991(- 3)	177.787(11)	083.829(20)	106.395(17)	
24.5	235.219(- 5)	158.013(5)		083.571(-15)	
25.5	217.581(10)	137.373(13)		059.918(0)	
26.5	199.055(21)	115.840(6)		035.402(29)	
27.5	179.639(23)	093.423(- 6)			
28.5		070.141(- 6)			
29.5		045.961(-26)			
30.5		020.965(14)			
31.5		22995.055(16)			

TABLE 8.1 (Continued)

1-0 Band ($A\ ^2\Pi_{1/2}$ - $X\ ^2\Sigma^+$)						
J	$R_{21ee}(J)$	$R_{22f}(J)$	$Q_{21ef}(J)$	$Q_{22ef}(J)$	$P_{21ee}(J)$	$P_{22f}(J)$
0.5	22010.319(2)	22006.434(18)	22005.617(20)	22001.652(- 7)		
1.5	014.284(15)	006.462(7)	006.399(- 4)	21998.547(21)	22001.652(7)	21993.813(7)
2.5	017.447(3)	005.731(15)	006.434(2)	994.628(10)	21998.518(14)	986.758(6)
3.5	019.852(10)	004.207(5)	005.706(21)	989.948(14)	994.598(12)	
4.5	021.478(16)	001.912(3)	004.178(17)	984.465(- 8)	989.903(10)	970.332(16)
5.5	022.307(3)	21998.855(16)	001.869(10)	978.247(10)	984.418(- 5)	960.952(17)
6.5	022.382(15)	994.988(- 3)	21998.782(2)	971.233(9)	978.175(- 3)	950.718(-61)
7.5	021.664(14)	990.383(20)	994.931(9)	963.433(0)	971.160(5)	939.868(22)
8.5	020.160(7)	984.961(5)	990.294(8)	954.875(10)	963.363(7)	928.151(13)
9.5	017.883(9)	978.788(20)	984.880(11)	945.536(16)	954.800(21)	915.664(12)
10.5	014.814(2)	971.814(16)	978.690(18)	935.396(1)	945.432(8)	902.403(13)
11.5	010.963(- 4)	964.054(8)	971.711(18)	924.500(9)	935.292(2)	888.357(6)
12.5	006.350(13)	955.519(8)	963.947(15)	912.808(1)	924.376(- 1)	873.546(13)
13.5	000.911(-11)	946.188(- 3)	955.408(20)	900.339(- 3)	912.699(15)	857.954(17)
14.5	21994.683(-36)	936.099(13)	946.076(17)	887.105(10)	900.238(28)	841.566(4)
15.5	987.736(7)	925.192(- 3)	935.951(6)	873.067(1)	887.005(51)	824.406(0)
16.5	979.959(10)	913.521(5)	925.046(1)	858.254(0)	872.936(20)	806.476(6)
17.5		901.054(5)	913.368(11)	842.650(- 8)		787.764(11)
18.5	962.025(7)	887.793(0)	900.894(13)	826.274(- 2)	842.493(4)	768.255(1)
19.5	951.853(-10)	873.768(22)	887.632(17)	809.120(11)	826.107(8)	747.960(-12)
20.5		858.910(3)	873.565(6)	791.157(3)		726.921(15)
21.5	929.151(-20)	843.268(- 8)	858.712(1)	772.412(0)		705.053(- 3)
22.5	916.620(-11)	826.805(-46)	843.031(-40)	752.865(-16)		682.409(-12)
23.5	903.281(-12)	809.616(-14)	826.628(- 9)	732.544(-16)		658.993(- 7)
24.5	889.178(22)	791.601(-13)	809.393(-14)	711.418(-31)		634.783(- 9)
25.5		772.781(-20)		689.525(-21)		609.803(6)
26.5		753.169(-21)		666.835(-16)		
27.5			752.931(- 9)	643.319(-44)		
28.5			732.515(- 5)	619.043(-37)		
29.5		689.525(-33)		593.961(-42)		

TABLE 8.1 (Continued)

1-0 Band ($A\ ^2\Pi_{1/2} - X\ ^2\Sigma^+$)						
J	$R_{11ee}(J)$	$R_{12ff}(J)$	$Q_{11fe}(J)$	$Q_{12ef}(J)$	$P_{11ee}(J)$	$P_{12ff}(J)$
0.5	21885.112(3)	21881.194(10)				
1.5	888.881(9)	881.044(23)	21881.194(24)	21873.323(5)		
2.5	891.784(3)	880.010(5)	881.015(17)	869.220(- 1)	21873.323(27)	
3.5	893.854(18)	878.138(2)	879.989(16)	864.265(- 6)	869.206(16)	21853.511(23)
4.5	895.037(0)	875.417(4)	878.110(15)	858.480(12)	864.233(3)	844.615(10)
5.5	895.389(5)	871.863(25)	875.358(- 5)	851.804(- 8)	858.438(20)	834.857(-12)
6.5	894.877(- 1)	867.410(0)	871.790(12)	844.321(17)	851.762(9)	824.297(15)
7.5	893.538(20)	862.125(- 5)	867.334(- 7)	835.960(16)	844.244(9)	812.844(0)
8.5	891.314(9)	856.000(1)	862.055(2)	826.760(27)	835.884(17)	800.577(20)
9.5	888.239(- 1)	849.039(22)	855.927(14)	816.693(21)	826.665(18)	787.440(21)
10.5	884.340(17)	841.181(- 4)	848.930(8)	805.779(18)	816.593(17)	773.448(14)
11.5	879.560(6)	832.498(- 6)	841.096(15)	794.012(11)	805.673(16)	758.617(16)
12.5	873.950(17)	822.975(1)	832.411(21)		793.889(1)	742.927(6)
13.5	867.459(- 4)	812.575(-20)	822.848(- 3)	767.951(13)		726.411(16)
14.5	860.154(12)	801.400(30)	812.467(4)	753.646(10)	767.814(8)	709.033(8)
15.5	851.977(6)	789.313(15)	801.237(8)	738.505(16)	753.495(0)	690.810(- 1)
16.5	842.966(14)		789.162(15)	722.512(15)	738.351(12)	671.765(11)
17.5	833.105(20)	762.625(9)	776.223(3)	705.684(23)	722.345(8)	651.880(24)
18.5	822.383(13)	748.008(- 1)	762.460(12)	687.998(16)	705.499(7)	631.110(- 7)
19.5	810.825(17)	732.568(10)	747.831(- 1)	669.477(16)	687.807(3)	609.534(- 5)
20.5	798.410(10)	716.283(18)	732.390(18)	650.109(10)	669.287(13)	
21.5	785.155(9)		716.066(- 3)	629.892(- 5)	649.909(6)	
22.5	771.042(- 5)		698.924(- 1)	608.845(-11)	629.671(-21)	
23.5	756.111(7)		680.940(1)		608.658(16)	
24.5	740.318(2)		662.122(8)			
25.5	723.689(4)		642.445(- 3)			
26.5	706.212(0)		621.928(-16)			
27.5	687.896(0)		600.597(- 5)			
28.5	668.730(- 8)					
29.5	648.687(-53)					
30.5	627.866(-34)					

TABLE 8.1 (Continued)

2-1 Band ($A\ ^2\Pi_{1/2}$ - $X\ ^2\Sigma^+$)					
J	$R_{21ee}(J)$	$R_{22ff}(J)$	$Q_{21fe}(J)$	$Q_{22ef}(J)$	$P_{22ff}(J)$
0.5	21333.999(- 1)	21330.140(4)	21329.342(4)		
1.5	337.892(1)	330.156(5)	330.113(- 9)	21322.330(7)	
2.5	341.005(2)	329.393(5)	330.129(1)	318.422(- 8)	
3.5	343.327(-10)	327.853(6)	329.342(-15)	313.757(- 2)	21302.890(6)
4.5	344.899(7)	325.528(1)	327.811(5)	308.320(9)	294.337(7)
5.5	345.664(- 3)	322.430(2)	325.472(- 5)	302.092(7)	284.993(- 6)
6.5	345.664(2)	318.560(12)	322.356(-13)	295.070(-11)	274.900(9)
7.5	344.868(- 7)	313.886(- 2)	318.482(2)	287.291(- 7)	264.001(- 4)
8.5	343.302(- 4)	308.453(6)	313.804(- 7)	278.745(8)	252.334(- 8)
9.5	340.962(9)	302.216(- 7)	308.361(0)	269.378(-17)	239.911(10)
10.5	337.813(- 4)	295.216(0)	302.114(-14)		226.681(0)
11.5	333.899(4)	287.417(- 8)	295.102(-10)	248.359(-12)	212.672(-10)
12.5	329.188(1)	278.860(11)	287.313(1)	236.690(4)	197.898(- 5)
13.5	323.690(- 2)	269.493(6)	278.720(- 7)	224.212(- 8)	182.352(8)
14.5	317.411(3)	259.333(- 5)	269.360(4)	210.975(6)	166.006(1)
15.5	310.33b\ 4)	248.400(- 2)	259.202(4)	196.952(17)	148.876(- 7)
16.5	302.470(0)	236.673(- 3)	248.265(13)	182.122(6)	130.986(6)
17.5	293.802(-11)	224.160(1)	236.511(- 6)	166.501(-10)	112.283(-11)
18.5	284.356(- 7)	210.844(- 8)	223.971(-21)	150.128(9)	092.811(-12)
19.5	274.122(4)	196.754(2)	210.681(6)	132.949(9)	072.559(-10)
20.5		181.855(- 3)	196.551(-15)	114.976(5)	051.522(- 7,
21.5	251.236(- 3)		181.649(-15)	096.215(2)	029.693(- 9)
22.5	238.609(6)	149.676(-10)	165.949(-18)	076.668(3)	007.087(- 2)
23.5	225.157(-10)	132.390(-15)	149.471(- 3)	056.303(-21)	20983.674(-14)
24.5	210.921(- 8)	114.308(-18)	132.178(- 5)	035.167(-24)	959.490(- 8)
25.5		095.436(-12)	114.067(-28)	013.241(-24)	
26.5		075.754(-15)	095.189(-19)	20990.524(-20)	
27.5		055.263(-26)		967.001(-26)	

TABLE 8.1 (Continued)

2-1 Band ($A\ ^2\Pi_{3/2}$ - $X\ ^2\Sigma^+$)					
J	$R_{11ee}(J)$	$Q_{11fe}(J)$	$Q_{12ef}(J)$	$P_{11ee}(J)$	$P_{12ff}(J)$
0.5	21208.921(- 7)				
1.5	212.627(- 8)	21205.031(4)	21197.268(16)		
2.5	215.491(3)	204.841(4)	193.183(9)		
3.5	217.487(0)	203.805(11)	188.239(- 5)	21193.150(8)	21177.600(7)
4.5	218.631(- 1)	201.896(- 1)	182.450(-10)	188.199(- 4)	168.758(- 9)
5.5	218.917(- 6)	199.143(- 5)	175.830(5)	182.415(4)	159.097(7)
6.5	218.371(10)	195.553(7)	168.332(- 5)	175.761(- 5)	148.558(- 4)
7.5	216.937(- 9)	191.082(- 9)	160.008(10)	168.276(7)	137.183(1)
8.5	214.686(8)	185.787(2)	150.803(- 5)	159.917(- 4)	124.935(-18)
9.5	211.564(7)	179.639(11)	140.772(5)	150.716(- 6)	111.877(2)
10.5	207.588(4)	172.621(1)	129.881(4)	140.669(- 3)	097.948(0)
11.5	202.766(7)	164.750(-11)	118.151(13)	129.776(3)	083.170(- 3)
12.5	197.079(- 3)	156.055(2)	105.545(- 5)	118.025(1)	067.542(-10)
13.5	190.553(- 2)	146.486(- 9)	092.120(5)	105.423(- 5)	051.077(- 8)
14.5	183.179(2)	136.096(6)	077.838(6)	091.983(0)	033.782(9)
15.5	174.952(3)	124.839(3)	062.713(9)	077.698(6)	015.613(- 4)
16.5	165.877(5)	112.727(- 9)	046.728(- 3)	062.562(7)	20996.607(-11)
17.5	155.946(0)	099.790(1)	029.919(6)	046.573(0)	976.774(- 3)
18.5	145.166(- 5)	086.008(12)	012.243(- 9)	029.736(-10)	956.099(4)
19.5	133.557(8)	071.357(- 2)	20993.763(15)	012.067(- 8)	
20.5	121.069(-10)	055.876(- 1)	974.395(- 7)	20993.537(-25)	
21.5	107.751(-11)	039.535(-17)		974.195(-12)	
22.5	093.601(2)	022.372(-11)			
23.5	078.594(3)	004.350(-23)			
24.5	062.730(- 7)	20985.507(-13)			
25.5	046.017(-21)	965.807(-20)			
26.5	028.487(- 7)				
27.5	010.094(-13)				
28.5	20990.846(-30)				

TABLE 8.1 (Continued)

1-1 Band ($A\ ^2\Pi_{1/2} - X\ ^2\Sigma^+$)

J	$R_{21ee}(J)$	$R_{22f}(J)$	$Q_{21ef}(J)$	$Q_{22ef}(J)$	$P_{21ee}(J)$	$P_{22f}(J)$
0.5		19822.520(-14)		19817.758(-18)		
1.5	19830.395(9)	822.615(-33)	19822.520(0)	814.712(- 8)	19817.758(- 5)	
2.5	833.621(-16)	822.014(-10)	822.615(-10)	810.922(- 3)	814.671(-26)	19803.054(- 5)
3.5	836.157(7)	820.625(-36)	821.966(-26)	806.385(- 8)	810.878(-16)	795.377(- 4)
4.5	837.914(- 8)	818.544(-15)	820.625(4)	801.128(5)	806.339(-14)	786.935(-31)
5.5	838.961(6)	815.726(8)	818.459(-50)	795.104(-11)	801.069(- 5)	777.837(24)
6.5	839.219(-27)	812.153(18)	815.631(-28)	788.356(-12)	795.046(-10)	767.934(11)
7.5	838.770(-25)	807.813(1)	812.060(- 8)	780.878(- 4)	788.263(-37)	757.302(7)
8.5	837.623(21)	802.735(-12)	807.757(22)	772.651(- 6)	780.775(-30)	745.922(- 7)
9.5	835.676(10)	796.929(-11)	802.641(-20)	763.672(-20)	772.554(-17)	733.825(0)
10.5	832.994(9)	790.369(-20)	796.844(- 1)	753.983(- 3)	763.577(-20)	720.995(14)
11.5	829.542(-17)	783.089(- 5)	790.268(-17)	743.523(-16)	753.879(- 3)	707.403(4)
12.5	825.402(16)	775.062(8)	782.954(-27)	732.343(- 7)	743.419(- 7)	693.067(- 9)
13.5	820.480(15)	766.256(-11)	774.923(- 9)	720.397(-21)	732.208(-20)	677.993(-20)
14.5	814.794(- 2)	756.745(11)	766.119(-17)	707.733(-10)	720.260(-27)	662.219(10)
15.5	808.361(-16)	746.426(-26)	756.599(5)	694.310(-14)	707.587(-16)	645.665(1)
16.5	801.214(7)	735.405(-16)	746.324(21)	680.153(- 6)	694.155(-19)	628.369(- 6)
17.5	793.277(- 8)	723.626(-14)	735.263(0)	665.273(24)	680.008(7)	610.327(-17)
18.5	784.620(10)	711.112(4)	723.466(- 7)	649.617(26)	665.050(-31)	591.549(-20)
19.5		697.813(-11)	710.929(- 3)	633.187(1)	649.419(4)	572.053(3)
20.5	764.990(- 4)	683.804(18)	697.623(-15)		633.034(33)	551.804(19)
21.5	754.032(-19)	669.004(10)	683.593(2)	598.160(30)	615.850(12)	530.784(10)
22.5	742.321(-29)	653.444(- 2)	668.769(-21)	579.473(- 3)	597.937(11)	509.019(2)
23.5	729.893(3)	637.127(-15)	653.244(11)	560.083(11)	579.282(18)	486.533(22)
24.5	716.651(-18)	620.081(1)		539.924(9)	559.818(-32)	463.298(39)
25.5		602.273(13)		519.047(42)		
26.5		583.702(22)	602.060(40)	497.342(1)	518.788(23)	414.513(10)
27.5		564.313(-26)	583.424(- 7)	474.907(-15)	497.132(40)	389.016(15)
28.5		544.268(31)	564.100(19)	451.741(- 7)	474.660(- 4)	362.742(- 5)
29.5		523.367(- 6)		427.789(-28)	451.519(38)	335.733(- 8)
30.5		501.734(-11)	523.097(0)		427.578(37)	
31.5					402.850(6)	
32.5			479.077(19)		377.408(19)	
33.5					351.208(33)	
34.5					324.214(12)	
35.5					296.481(13)	

TABLE 8.1 (Continued)

I-I Band ($A\ ^2\Pi_{3/2}$ - $X\ ^2\Sigma^+$)						
J	$R_{11ee}(J)$	$R_{12f}(J)$	$Q_{11fe}(J)$	$Q_{12ef}(J)$	$P_{11ee}(J)$	$P_{12ff}(J)$
0.5	19701.182(- 7)	19697.271(-30)				
1.5	704.966(-24)	697.222(7)	19697.271(-16)	19689.475(-37)		
2.5		696.311(- 2)	697.177(-15)	685.513(-16)	19689.475(-14)	
3.5	710.135(- 9)	694.575(-20)	696.259(-22)	680.719(-12)	685.461(-36)	19669.951(3)
4.5	711.499(2)	692.040(-23)	694.536(-19)	675.102(-16)	680.678(-12)	661.218(-37)
5.5	712.027(- 8)	688.728(12)	692.037(24)	668.670(-20)	675.058(-10)	651.757(10)
6.5	711.755(- 2)	684.530(-24)	688.671(14)	661.464(16)	668.632(1)	641.430(3)
7.5	710.625(-38)	679.584(5)	684.446(-41)	653.397(4)	661.353(-27)	630.283(-10)
8.5	708.765(10)	673.782(- 9)	679.479(-23)	644.525(0)	653.329(13)	618.337(-11)
9.5	706.038(6)	667.162(-28)	673.706(1)	634.856(12)	644.428(-11)	605.596(4)
10.5	702.480(-16)	659.788(11)	667.066(-29)	624.344(- 8)	634.740(- 9)	592.029(4)
11.5	698.131(-14)	651.545(- 7)	659.634(-38)	613.035(-14)	624.222(-26)	577.648(0)
12.5	692.961(-21)	642.523(6)	651.429(-10)	600.939(2)	612.913(-23)	562.474(10)
13.5	686.975(-31)	632.674(2)	642.378(-17)	587.995(-19)	600.812(- 2)	546.480(9)
14.5	680.200(-19)	622.009(- 8)	632.503(-37)	574.273(-11)	587.862(-21)	529.668(- 4)
15.5	672.632(12)	610.571(16)	621.869(- 8)	559.740(- 6)	574.161(17)	512.046(-22)
16.5	664.194(-16)	598.271(-13)	610.382(-23)	544.408(6)	559.561(-36)	493.632(-27)
17.5	654.986(- 5)	585.178(-29)	598.084(-42)	528.244(- 8)	544.220(-23)	
18.5	644.947(-15)	571.294(-30)	585.061(21)	511.306(9)	528.069(-15)	454.420(-12)
19.5	634.132(7)		571.123(-25)	493.561(22)	511.137(16)	433.633(16)
20.5	622.454(-25)		556.437(-14)	474.947(-31)	493.347(- 6)	411.987(-14)
21.5	610.015(-11)		540.933(-16)		474.805(22)	389.599(12)
22.5	596.754(-12)		524.660(16)		455.434(23)	366.327(-47)
23.5	582.694(- 6)		507.529(- 7)		435.267(28)	342.360(- 5)
24.5	567.837(8)		489.623(- 3)		414.276(10)	
25.5	552.150(- 2)		470.915(0)			291.947(-15)
26.5	535.664(- 8)		451.430(26)		369.929(4)	
27.5	518.391(4)		431.112(19)		346.582(24)	
28.5	500.317(18)				322.445(50)	

TABLE 8.1 (Continued)

0-1 Band ($A\ ^2\Pi_{1/2} - X\ ^2\Sigma^+$)					
J	$R_{21ee}(J)$	$R_{22f}(J)$	$Q_{21e}(J)$	$Q_{22f}(J)$	$P_{22f}(J)$
0.5			18286.503(14)		
1.5			287.353(-40)		
2.5			287.602(2)		18267.912(-21)
3.5			287.093(-16)		260.358(2)
4.5			285.922(3)		252.086(3)
5.5			284.001(-28)		243.103(- 9)
6.5	18305.314(5)		281.441(1)		233.435(- 8)
7.5	305.218(21)		278.154(4)	18246.920(-25)	223.075(- 2)
8.5	304.416(33)		274.145(-14)	239.056(- 3)	212.030(18)
9.5	302.892(27)		269.470(4)	230.489(17)	200.265(16)
10.5	300.637(- 4)		264.070(0)	221.183(- 2)	187.772(-14)
11.5	297.704(- 8)		257.939(-31)	211.202(7)	174.636(12)
12.5	294.083(7)		251.173(8)	200.456(-47)	160.778(17)
13.5	289.737(6)		243.652(- 2)	189.122(14)	146.232(34)
14.5	284.669(- 8)		235.430(- 7)	176.995(-14)	130.912(-20)
15.5	278.887(-24)		226.511(0)	164.236(32)	114.962(- 2)
16.5	272.409(-25)		216.861(-14)	150.707(14)	098.280(-13)
17.5	265.267(25)		206.559(29)	136.503(28)	080.941(24)
18.5	257.355(19)		195.462(-11)	121.556(7)	062.801(-35)
19.5	248.714(0)		183.668(-34)	105.915(2)	
20.5			171.226(8)	089.571(4)	
21.5	229.356(41)		158.058(39)	072.450(-60)	
22.5	218.537(1)			054.738(- 1)	
23.5			129.457(-12)	036.245(-12)	
24.5	194.854(44)		114.115(- 1)	017.044(-16)	
25.5	181.895(33)	081.473(-15)		17997.127(-19)	
26.5	168.208(21)	063.965(-15)		976.506(-10)	
27.5		045.744(- 5)		955.159(- 9)	
28.5		026.773(-19)		933.114(13)	
29.5		007.061(-47)		910.229(-86)	
30.5		17986.687(-11)		886.818(11)	
31.5		965.548(-11)			

TABLE 8.1 (Continued)

0-1 Band ($A\ ^2\Pi_{3/2}$ - $X\ ^2\Sigma^+$)					
J	$R_{11ee}(J)$	$Q_{11fe}(J)$	$Q_{12ef}(J)$	$P_{11ee}(J)$	$P_{12ff}(J)$
0.5	18165.947(- 2)				
1.5	169.829(-16)	18162.051(3)	18154.279(7)		
2.5	172.927(-37)	162.051(4)			
3.5	175.331(27)	161.241(-29)	145.713(- 6)		
4.5	176.897(31)	159.697(-18)	140.278(1)		
5.5	177.657(6)	157.397(15)	134.059(0)		
6.5	177.657(- 1)	154.279(5)	127.086(21)		18106.770(-26)
7.5	176.897(9)	150.432(43)	119.278(-17)		095.895(-15)
8.5	175.331(-10)	145.713(-15)	110.790(40)	18119.196(-22)	084.249(- 1)
9.5	173.032(15)	140.278(-14)	101.463(33)	110.645(-19)	071.809(- 8)
10.5	169.910(- 8)	134.059(-22)	091.366(29)	101.315(-20)	
11.5	166.022(-20)	127.086(-10)	080.495(23)	091.217(-16)	044.597(-38)
12.5	161.407(15)	119.346(8)	068.818(-15)	080.359(1)	029.858(-29)
13.5	155.994(28)	110.790(-17)	056.440(16)	068.743(32)	014.382(12)
14.5	149.779(12)	101.463(-40)		056.258(-35)	17998.023(-61)
15.5	142.828(35)	091.485(57)		043.137(33)	
16.5	135.030(-17)	080.615(32)		029.175(30)	963.159(-51)
17.5	126.491(-37)	069.005(37)		014.436(19)	944.573(-51)
18.5	117.269(32)	056.561(-22)		17998.953(32)	925.298(24)
19.5	107.204(29)	043.423(- 7)	17965.787(-27)	982.657(- 1)	
20.5	096.366(24)	029.519(10)	948.031(3)	965.612(-17)	
21.5	084.763(24)	014.856(35)	929.497(19)	947.807(-27)	
22.5	072.354(-12)	17999.386(20)	910.229(65)	929.287(13)	
23.5	059.236(13)	983.135(-11)	890.062(-25)	909.950(- 1)	
24.5	045.325(13)	966.130(-31)		889.828(-37)	
25.5	030.642(10)	948.397(-15)			
26.5	015.210(25)				
27.5	17998.953(-17)				

TABLE 8.1 (Continued)

0-2 Band ($A\ ^2\Pi_{1/2} - X\ ^2\Sigma^+$)					
J	$R_{21ee}(J)$	$R_{22ff}(J)$	$Q_{21ef}(J)$	$Q_{22fe}(J)$	$P_{22ee}(J)$
0.5		16133.920(11)	16132.937(-15)		
1.5		134.199(- 2)	133.885(-10)		
2.5		133.820(-13)	134.171(- 7)		16114.624(- 1)
3.5		132.790(-14)	133.800(- 2)		
4.5		131.104(-11)	132.790(26)		099.115(- 3)
5.5		128.779(15)	131.071(5)		090.382(6)
6.5		125.755(5)	128.707(2)		080.981(6)
7.5	16152.721(- 9)	122.073(- 1)	125.676(- 7)	094.733(-50)	070.924(10)
8.5	152.222(1)	117.737(4)	122.002(4)	087.252(12)	060.190(- 3)
9.5	151.037(-10)	112.726(- 2)	117.641(- 7)	079.018(-18)	048.799(-13)
10.5	149.194(-11)	107.045(-13)	112.681(47)	070.159(- 9)	036.769(- 1)
11.5	146.707(10)	100.723(3)	106.953(- 1)	060.636(- 1)	024.066(0)
12.5	143.539(20)	093.719(4)	100.608(0)	050.437(- 5)	010.691(- 9)
13.5	139.684(13)	086.037(- 4)	093.582(-12)	039.571(-11)	15996.666(- 5)
14.5	135.160(9)	077.682(-16)	085.897(-14)	028.066(10)	981.976(- 3)
15.5	129.958(- 1)	068.672(-11)	077.536(-23)	015.858(- 5)	966.626(3)
16.5	124.101(8)	059.006(9)	068.518(-17)	003.009(7)	950.597(- 4)
17.5	117.613(61)	048.615(-22)	058.819(-21)	15989.471(- 1)	933.914(0)
18.5	110.335(0)	037.593(-10)	048.446(-25)	975.260(-13)	916.549(-11)
19.5	102.458(18)	025.885(- 8)	037.399(-29)	960.395(- 7)	898.522(17)
20.5	093.871(6)	013.485(-21)	025.701(- 8)	944.876(16)	879.832(-17)
21.5	084.606(- 4)	000.433(- 9)	013.327(14)	928.644(- 2)	860.478(-12)
22.5	074.668(- 5)	15986.706(8)	000.246(6)	911.768(11)	840.467(7)
23.5	064.056(3)	972.263(-10)	15986.481(- 6)	894.207(14)	819.722(-38)
24.5	052.804(56)	957.151(-17)	972.046(- 8)	875.962(9)	798.348(-39)
25.5		941.354(-25)	956.926(-13)	857.033(- 4)	776.335(- 7)
26.5		924.904(- 2)	941.136(- 5)	837.443(1)	753.627(4)
27.5		907.754(6)		817.179(11)	
28.5		889.889(-15)	907.505(12)	796.233(19)	
29.5		871.355(-18)	889.629(-10)	774.600(21)	
30.5		852.159(6)		752.281(19)	
31.5		832.247(4)		729.293(31)	
32.5		811.622(-20)			
33.5		790.344(- 6)			

TABLE 8.1 (Continued)

0-2 Band ($A\ ^2\Pi_{3/2} - X\ ^2\Sigma^+$)					
J	$R_{11ee}(J)$	$Q_{11fe}(J)$	$Q_{12ef}(J)$	$P_{11ee}(J)$	$P_{12ff}(J)$
0.5	16012.434(22)				
1.5	016.344(- 3)	16008.573(24)	16000.843(- 7)		
2.5	019.549(7)	008.620(- 5)	15997.076(- 1)		
3.5	022.013(16)	007.967(5)	992.566(2)		
4.5	023.724(12)	006.548(-12)	987.315(2)		
5.5	024.703(16)	004.419(0)	981.324(0)		15964.171(- 1)
6.5	024.917(- 7)	16001.532(- 7)	974.590(- 7)		
7.5	024.431(10)	15997.921(0)	967.135(3)		943.765(17)
8.5	023.172(- 7)	993.567(1)	958.923(- 8)		932.449(17)
9.5	021.207(7)	988.476(2)	950.008(14)		920.394(13)
10.5	018.490(8)	982.651(6)	940.330(9)		907.585(-10)
11.5	015.040(13)	976.083(3)	929.922(9)	15940.239(21)	
12.5	010.839(5)	968.786(5)	918.768(- 4)	929.806(5)	879.832(6)
13.5	005.922(16)	960.755(9)	906.899(1)	918.646(- 5)	864.855(11)
14.5	000.246(5)	951.983(5)	894.310(19)	906.773(6)	849.121(-10)
15.5	15993.850(9)	942.468(- 9)	880.960(7)	894.142(-10)	832.681(- 8)
16.5	986.706(- 1)	932.240(- 3)	866.892(8)	880.798(- 7)	815.525(6)
17.5	978.831(- 7)	921.272(- 6)	852.073(-12)	866.729(2)	797.625(4)
18.5	970.253(17)	909.587(6)	836.553(- 5)	851.913(- 6)	778.953(-45)
19.5	960.904(3)	897.160(5)	820.292(-11)	836.382(- 1)	759.632(-17)
20.5	950.852(19)	884.003(3)	803.310(-11)	820.126(7)	
21.5	940.037(3)	870.118(3)	785.626(13)	803.130(1)	
22.5	928.492(-11)	855.504(1)	767.184(4)	785.419(7)	
23.5	916.229(-12)	840.181(17)	748.018(- 5)	766.977(8)	
24.5	903.278(28)	824.099(0)	728.132(-10)	747.804(1)	
25.5	889.534(6)	807.311(4)		727.905(- 8)	
26.5	875.074(- 3)	789.803(12)			
27.5		771.546(- 4)			
28.5		752.575(-10)			
29.5		732.901(5)			

TABLE 8.1 (Continued)

0-3 Band ($A\ ^2\Pi_{1/2} - X\ ^2\Sigma^+$)

J	$R_{21ee}(J)$	$R_{22f}(J)$	$Q_{21e}(J)$	$Q_{22f}(J)$	$P_{22f}(J)$
0.5		14010.669(5)			
1.5		011.046(13)	14010.646(- 5)		
2.5		010.787(7)	011.009(- 2)		13991.561(-11)
3.5		009.927(22)	010.759(10)		984.311(9)
4.5		008.424(16)	009.853(-12)		976.421(10)
5.5		006.296(10)	008.371(13)		967.904(5)
6.5	14030.098(1)	003.561(20)	006.221(- 7)		958.750(-16)
7.5	030.507(-14)	000.170(- 2)	003.479(5)	13972.846(-35)	949.005(- 7)
8.5	030.329(10)	13996.172(- 4)	000.117(22)	965.687(4)	938.631(- 5)
9.5	029.499(10)	991.561(7)	13996.083(- 8)	957.860(- 2)	927.646(8)
10.5	028.033(1)	986.299(- 6)	991.465(5)	949.412(- 4)	916.030(13)
11.5	025.947(3)	980.436(8)	986.209(7)	940.341(- 4)	903.785(12)
12.5	023.225(- 1)	973.932(11)	980.329(13)	930.654(6)	890.920(14)
13.5	019.858(-19)	966.796(12)	973.805(5)	920.334(10)	877.429(15)
14.5	015.876(-18)	959.026(11)	966.669(15)	909.374(1)	863.277(-19)
15.5	011.268(- 9)	950.621(7)	958.891(15)	897.799(6)	848.555(2)
		941.596(18)	950.486(20)	885.583(0)	833.200(17)
17.5	000.117(-17)	931.916(8)	941.430(9)	872.735(- 8)	817.196(11)
18.5	13993.616(10)	921.604(2)	931.742(0)	859.262(-10)	800.573(14)
19.5		910.663(5)	921.445(18)	845.172(5)	783.310(6)
20.5	978.636(6)	899.046(-29)	910.475(1)	830.424(- 6)	765.384(-34)
21.5	970.190(11)	886.874(21)	898.910(27)	815.047(-10)	746.917(16)
22.5	961.079(- 6)	873.995(5)		799.063(14)	727.752(0)
23.5		860.470(-14)		782.395(- 9)	
24.5	940.972(13)	846.343(8)		765.123(2)	
25.5	929.929(4)	831.565(24)		747.195(- 4)	
26.5		816.091(-11)		728.630(- 7)	
27.5		800.030(15)		709.430(- 5)	
28.5		783.293(13)		689.599(9)	
29.5				669.086(-16)	

TABLE 8.1 (Continued)

0-3 Band ($A\ ^2\Pi_{3/2}$ - $X\ ^2\Sigma^+$)					
J	$R_{11ee}(J)$	$Q_{11f}(J)$	$Q_{12ef}(J)$	$P_{11ee}(J)$	$P_{12f}(J)$
0.5	13889.135(5)				
1.5	893.093(-10)	13885.308(3)			
2.5	896.390(16)	885.443(-15)	13874.042(18)		
3.5	898.940(- 4)	884.927(17)	869.647(-18)	13873.995(2)	
4.5	900.816(3)	883.664(3)	864.588(-18)	869.604(-21)	
5.5	901.968(-12)	881.719(8)	858.853(6)	864.546(-11)	
6.5	902.454(8)	879.069(7)	852.400(12)	858.792(4)	13832.113(- 6)
7.5	902.209(- 3)	875.710(- 2)	845.226(- 4)	852.293(-28)	821.854(8)
8.5	901.265(-12)	871.671(7)	837.378(4)	845.137(-17)	810.882(8)
9.5	899.639(- 3)	866.928(11)	828.825(5)	837.270(-19)	
10.5	897.302(- 6)	861.467(- 4)	819.568(- 1)	828.708(-18)	786.831(-12)
11.5	894.278(4)	855.319(- 9)	809.595(-26)	819.453(-12)	773.762(-22)
12.5	890.526(-16)	848.498(10)	798.980(2)	809.524(15)	760.025(- 7)
13.5	886.101(-11)	840.937(-15)	787.633(- 7)	798.847(-10)	745.589(3)
14.5	880.981(- 3)	832.715(- 5)	775.618(10)	787.490(-20)	730.448(0)
15.5	875.149(-10)	823.809(15)	762.855(-28)	775.476(7)	714.618(- 1)
16.5	868.634(- 3)	814.166(- 7)	749.468(3)	762.729(- 6)	698.105(4)
17.5	861.402(-18)	803.854(- 5)	735.355(- 2)	749.318(10)	
18.5	853.509(2)	792.852(- 1)	720.567(10)	735.196(5)	
19.5	844.900(0)	781.165(11)	705.060(- 8)	720.381(- 1)	
20.5	835.608(10)	768.761(- 4)	688.875(-16)	704.877(- 7)	
21.5	825.600(- 3)	755.678(- 7)	671.994(-31)	688.698(0)	
22.5	814.917(3)	741.920(5)		671.796(-27)	
23.5	803.540(7)	727.471(15)		654.234(-28)	
24.5	791.449(-11)	712.303(- 6)			
25.5	778.691(- 5)	696.475(0)			
26.5	765.263(23)	679.945(- 8)			
27.5	751.090(- 4)	662.711(-34)			
28.5	736.280(23)				

TABLE 8.1 (Continued)

0-4 Band ($A\ ^2\Pi_{1/2}$ - $X\ ^2\Sigma^+$)					
J	$R_{21ee}(J)$	$R_{22ff}(J)$	$Q_{21ee}(J)$	$Q_{22ef}(J)$	$P_{22ff}(J)$
0.5			11916.732(0)		
1.5			917.749(- 3)		
2.5			918.218(29)		
3.5			918.037(- 5)		
4.5			917.310(- 2)		11884.056(7)
5.5		11914.178(23)	916.011(14)		875.773(6)
6.5	11937.949(-18)	911.697(19)	914.086(-12)		866.897(- 6)
7.5	938.661(1)	908.627(11)	911.621(8)	11881.301(-24)	857.465(9)
8.5	938.748(-17)	904.984(18)	908.528(-13)	874.442(-31)	847.422(- 4)
9.5	938.282(1)	900.719(- 9)	904.883(0)		
10.5	937.191(-17)	895.904(2)	900.652(16)	859.010(- 2)	825.623(9)
11.5	935.540(- 3)	890.493(8)	895.815(14)	850.387(-15)	813.829(- 2)
12.5	933.274(-12)	884.492(14)	890.357(-19)	841.203(- 2)	801.474(11)
13.5	930.423(-13)	877.902(23)	884.375(15)	831.421(1)	788.518(9)
14.5	926.985(- 7)	870.700(13)	877.752(0)	821.026(-19)	774.967(- 1)
15.5	922.937(-15)	862.908(7)	870.552(1)	810.081(1)	760.847(7)
16.5	918.262(-53)	854.537(17)	862.753(- 4)	798.517(- 8)	746.123(- 1)
17.5	913.050(-29)	845.544(2)	854.372(5)	786.356(-21)	730.829(10)
18.5	907.242(- 2)		845.395(15)	773.630(- 7)	714.921(- 4)
19.5		825.796(2)		760.293(-10)	698.429(-10)
20.5		815.030(10)	825.623(9)	746.372(- 2)	681.364(2)
21.5		803.636(- 9)	814.843(11)	731.832(-17)	663.693(0)
22.5		791.685(16)	803.468(20)	716.722(- 6)	645.429(- 2)
23.5		779.093(4)		701.001(- 7)	626.565(-10)
24.5		765.933(29)		684.682(- 8)	607.114(-10)
25.5		752.128(15)		667.768(- 3)	
26.5		737.739(23)		650.234(-18)	
27.5		722.736(25)		632.108(-23)	
28.5		707.127(30)		613.410(3)	
29.5				594.049(-30)	
30.5		674.041(4)		574.119(-27)	
31.5		656.618(29)			

TABLE 8.1 (Continued)

0-4 Band ($A\ ^2\Pi_{3/2}$ - $X\ ^2\Sigma^+$)					
J	$R_{11ee}(J)$	$Q_{11fe}(J)$	$Q_{12ef}(J)$	$P_{11ee}(J)$	$P_{12ff}(J)$
0.5	11796.210(17)				
1.5	800.214(10)				
2.5	803.542(-10)	11792.627(- 9)	11781.307(-10)		
3.5	806.238(1)	792.190(-13)	777.108(- 3)		
4.5	808.245(-15)	791.109(1)	772.235(- 9)		
5.5	809.628(9)	789.353(3)	766.717(2)		
6.5	810.321(5)	786.927(- 4)	760.526(1)		
7.5	810.341(- 9)	783.841(-10)	753.674(0)		11730.303(13)
8.5	809.721(- 2)	780.120(10)	746.167(3)		719.660(- 4)
9.5	808.438(4)	775.694(-14)	737.997(3)	11746.094(14)	708.380(0)
10.5	806.474(-10)	770.655(8)	729.179(14)	737.918(16)	696.437(- 2)
11.5	803.884(11)	764.928(1)	719.699(20)	729.061(- 3)	683.834(- 8)
12.5	800.615(13)	758.556(8)	709.549(14)	719.581(12)	670.595(6)
13.5	796.672(0)	751.518(6)	698.744(9)	709.407(-10)	656.687(6)
14.5	792.082(0)	743.812(- 7)	687.268(-12)	698.630(22)	
15.5	786.829(- 5)	735.469(0)	675.133(-37)	687.137(- 7)	
16.5	780.936(8)	726.452(-12)	662.402(- 5)	675.036(10)	
17.5	774.359(- 6)	716.794(-10)	648.989(- 2)	662.242(-12)	
18.5	767.139(- 6)	706.480(-11)	634.927(4)	648.831(2)	
19.5	759.258(-)	695.535(11)	620.227(23)	634.737(-15)	
20.5	750.749(11)	683.911(7)	604.841(6)	620.025(1)	
21.5	741.548(- 4)	671.634(0)	588.828(11)	604.645(- 2)	
22.5		658.707(- 5)	572.149(- 2)	588.631(11)	
23.5	721.218(1)	645.130(-10)		571.946(1)	
24.5	710.058(-12)	630.903(-16)			
25.5	698.296(26)	616.058(9)			
26.5	685.816(- 2)	600.531(0)			
27.5	672.708(- 6)	584.364(- 1)			
28.5	658.941(-18)	567.540(-13)			

[a] Numbers in parentheses correspond to (ν_{obs} - ν_{cal}) in the last digit.

spectral positions of the lines. The values of σ are in the range 0.01 to 0.1 cm^{-1} for the optical data, 0.01 to 0.001 cm^{-1} for the infrared data and 0.2 to 0.6 × 10^{-5} cm^{-1} for the microwave data. The residuals between the calculated and observed wavenumber dataof the optical spectra for all the ten bands are also given in Table 8.1. The dimensionless variance in the fit is 2.5 and the root mean square deviation is ~0.016 cm^{-1}. A set of 54 molecular parameters for the v = 0 to 4 levels for both states A $^2\Pi_i$ and X $^2\Sigma^+$ thus obtained are listed in Table 8.2. From this table, it is noted that the value of the Λ-doubling parameters p_v and q_v do not show irregularities in their v-dependence. It is appropriate to comment on the values of the molecular constants obtained in this work and the values reported in the literature. For example, the B_0 value of the A $^2\Pi_i$ state obtained in the present work is 1.5796211(84) cm^{-1}. The high precision of the B_0 value upto 6th decimal place is due to the inclusion of the microwave data. This value is in agreement in the 4th decimal place within the error limits to the values 1.579629(102) cm^{-1} and 1.579710(104) cm^{-1} reported by Jakubek et al. (1987) from analysis of the individual bands 0-0 and 1-0 of the B $^2\Sigma^+$ - A $^2\Pi_i$ system. We have reanlayzed the 1-0 band of Jakubek et al. (1987) using our program and the value for B_0 of the A state is found to be 1.579606(74) cm^{-1}. Using the value of 1.579496(26) cm^{-1} and the values of the other molecular parameters reported by Bembenek et al. (1994) the wavenumbers of the 0-1, 0-2, 0-3 and 0-4 bands of the A-X system can be reproduced up to J=22.5 with an accuracy of 0.01 cm^{-1}. Beyond this J value there is a deviation in the (ν_{obs}-ν_{cal}) values from -0.028 cm^{-1} to -0.195cm^{-1} for J=24.5 to J=33.5. Thus we conclude that the molecular constants given in Table 8.2 can be used to reproduce the wavenumbers up to

TABLE 8.2 Rotational constants [a] (in cm^{-1}) of the A $^2\Pi_i$, and X $^2\Sigma^+$ states of $^{12}C^{16}O^+$ from the global fit

Molecular Constant	v=0	v=1	v=2	v=3	v=4
			A $^2\Pi_i$		
T_v	20406.2166(18)	21941.4793(12)	23449.2278(14)	24930.3444(18)	26384.7229(17)
B_v	1.5796211(84)	1.5600719(74)	1.5407277(96)	1.521349(11)	1.5019686(98)
$D_v \times 10^6$	6.735(11)	6.4641(96)	6.661(12)	6.690(12)	6.600(10)
$- A_v$	122.0513(18)	121.9829(20)	121.8874(23)	121.8126(30)	121.8720(29)
$- A_{Dv} \times 10^4$	2.179(55)	1.357(63)	1.467(70)	1.546(80)	0.804(81)
$- q_v \times 10^4$	2.619(75)	2.439(93)	2.61(11)	2.21(10)	3.16(12)
$p_v \times 10^2$	1.549(14)	1.293(17)	1.259(18)	1.054(21)	0.943(23)
			X $^2\Sigma^+$		
T_v	0	2183.92064(36)	4337.4571(19)	6460.7397(27)	8553.6771(28)
B_v	1.967462265(60)	1.94843818(64)	1.92935252(90)	1.910180(16)	1.890985(16)
$D_v \times 10^6$	6.3170(18)	6.3674(47)	6.4278(81)	6.399(22)	6.475(20)
$\gamma_v \times 10^3$	9.10556(50)	9.0495(34)	8.9729(38)	8.972(65)	8.766(63)

[a]Number in parantheses is the uncertainty in the last digit and corresponds to one standard deviation.

the J levels reported in Table 8.1. Since least-squares technique is only an inter polation method, extrapolation of the data to higher rotational quantum numbers will not give accurate values. From Table 8.2 we claim that the values of the Λ-doubling parameters p_v and q_v obtained in the present work do not show irregularities in their v-dependnce.

The B_v values listed in Table 8.2 were fitted to the standard spectroscopic relation

$$B_v = B_e - \alpha_e (v + 1/2) + \gamma_e (v + 1/2)^2 + \delta_e (v+1/)^3 \qquad [8.2]$$

and the resulting equilibrium molecular constants B_e, α_e, γ_e and δ_e along with their standard deviations are presented in Table 8.3. The D_v values were fitted to the relation

$$D_v = D_e + \beta_e (v+1/2) + \varepsilon_e (v+1/2)^2 \qquad [8.3]$$

and the resulting values of D_e, and β_e for the A state and D_e, β_e, and ε_e for the X state are listed in Table 8.3. It should be noted that the value of $D_1 = 6.4641(96) \times 10^{-6}$ cm^{-1} of the A state is not included in determining the parameters D_e and β_e. The equilibrium molecular constants p_e, α_p, and β_p are determined by fitting the values of the Λ-doubling parameter p_v given in Table 8.2 to the expression

$$p_v = p_e - \alpha_p (v + 1/2) + \beta_p (v + 1/2)^2 \qquad [8.4]$$

and their values are also given in Table 8.3. The term values T_v for both A and X states given in Table 8.2 were fitted to the expression:

$$T_v = T_e + \omega_e (v + 1/2) - \omega_e x_e (v + 1/2)^2 + \omega_e y_e (v + 1/2)^3 \qquad [8.5]$$

and the vibrational constants ω_e, $\omega_e x_e$, and $\omega_e y_e$ and T_e thus obtained along with their standard deviations are also listed in Table 8.3. In fitting the Eqs. [8.2] to [8.5] a weighted least-squares fit was used in each case. The $^2\Pi_i$ state of the comet-tail system of CO^+ belongs neither to Hund's case (a) nor to Hund's case (b), but belongs to

TABLE 8.3 Equilibrium molecular constants[a,b] (cm^{-1}) for the A $^2\Pi_i$ and B $^2\Sigma^+$ states of $^{12}C^{16}O^+$

Molecular Constants	A $^2\Pi_i$	X $^2\Sigma^+$
T_e	19628.298(69)	
G(0)		1103.23(21)
ω_e	1562.79(18)	2214.15(15)
$\omega_e x_e$	13.926(89)	15.150(25)
$\omega_e y_e$	0.65(12)	
B_e	1.589482(20)	1.97695082(80)
$\alpha_e \times 10^2$	1.9806(36)	1.89615(19)
$\gamma_e \times 10^4$	1.66(18)	-3.018(70)
$\delta_e \times 10^4$	-1.92(24)	
$D_e \times 10^6$	6.752(12)	6.2856(44)
$\beta_e \times 10^8$	-3.01(36)	6.52(81)
$\varepsilon_e \times 10^9$		-5.5(2.2)
$p_e \times 10^2$	1.631(22)	
$\alpha_p \times 10^3$	1.99(23)	
$\beta_p \times 10^4$	1.08(49)	

[a]In obtaining the molecular constants presented in this Table, a wieghted least-squares fits were used.

[b]Number in parantheses is the uncertainty in the last digit and corresponds to one standard deviation.

intermediate case (case (a) for small rotation and case (b) for large rotation). To confirm this a Fortrat diagram for the 0-2 band of the comet-tail system of $^{12}C^{16}O^{+}$ is constructed and shown in Fig. 8.5. In this figure, the branches R_{22e} and R_{11ee}, Q_{22e} and Q_{11ee}, and P_{22e} and P_{11ee} draw closer together with increasing J, as expected for the intermediate case (see for example, Herzberg (1991). For the $^2\Pi_i$ state, the value of A/B is found to be -77.

8.4 Conclusions

The rotational structure of 10 bands photographed under high resolution was analyzed together with the available infrared and microwave transitions using the matrix elements of the effective Hamiltonian for the $^2\Pi$ state and the $^2\Sigma^+$ state . A set of rotational constants along with the T_v values were obtained for the $A\ ^2\Pi_i$ and $X\ ^2\Sigma^+$ states from this global fit. The equilibrium vibrational and rotational constants were also calculated for the A and X states. From this reanalysis, we claim that the irregularities in the higher order molecular constants have been corrected. It is also shown that the $A\ ^2\Pi_i$ state changes from Hund's case (a) at lower J to case (b) at higher J.

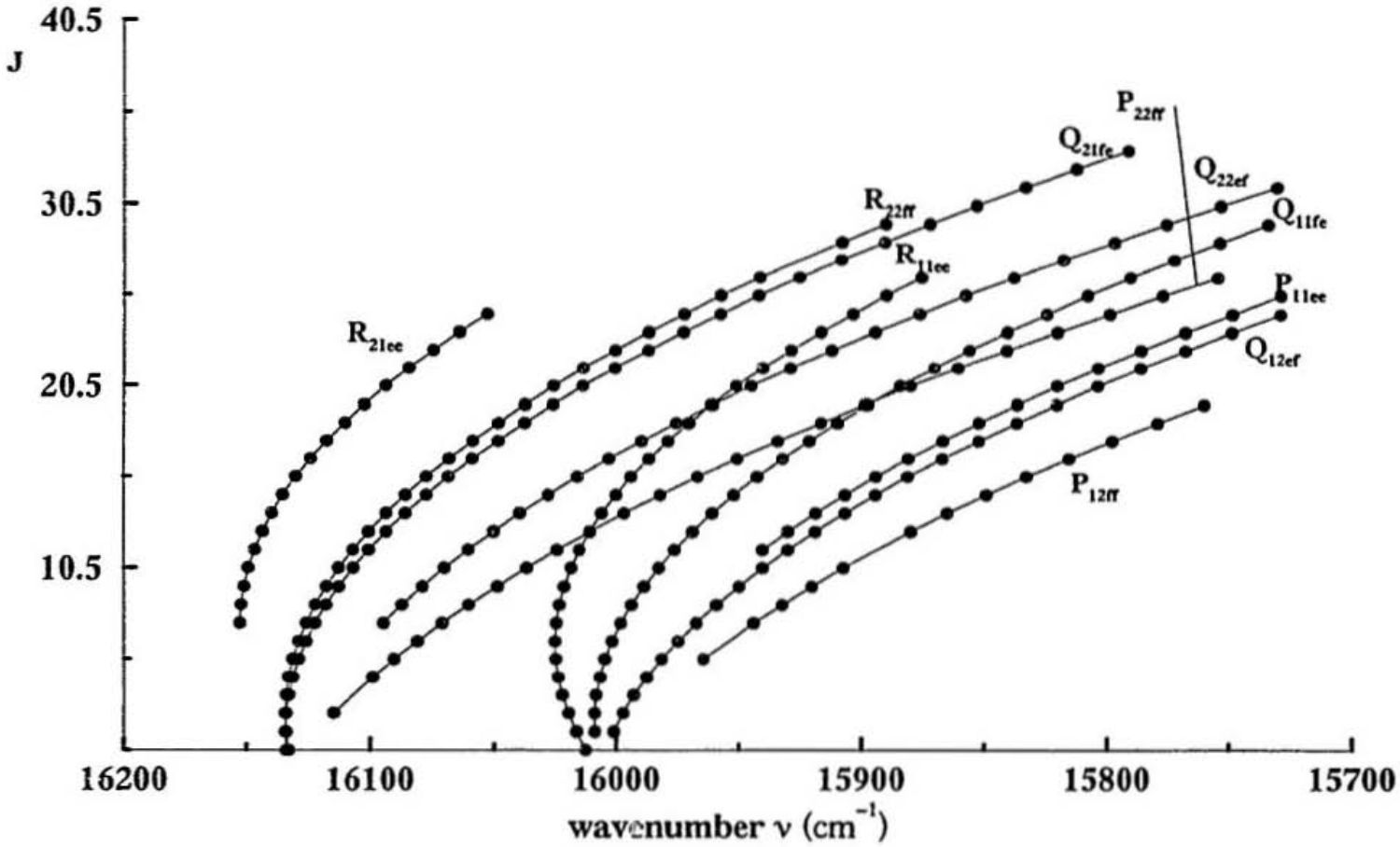

Figure 8.5 Fortrat diagram of the 0-2 band of the comet-tail (A $^2\Pi_i$ - X $^2\Sigma^+$) system of $^{12}C^{16}O^+$.

REFERENCES

Albritton, D. L., Schmeltekopf, A. L., and Zare, R. N., *J. Mol. Spectrosc.* **67**, 132 (1977).

Amiot, C., Maillard, J. P., and Chauville, J., *J. Mol. Spectrosc.*, **87** 196 (1981).

Audouze, J. in CNO Isotopes in Astrophysics (Dordrecht: Reidel) 5 (1977).

Bembenek, Z., Domin, U., Kepa, R., Porada, K., Rytel, M., Zachwieja, M., Jakubek, Z., and Janjić, J. D., *J. Mol. Spectrosc.* **165**, 205 (1994).

Bogey, M., Demuynck, C., and Destombes, J. L., *J. Chem. Phys.* **79**, 4704 (1983).

Brown, R. D., Dittman, R. G., and McGilvery, D. C., *J. Mol. Spectrosc.* **104**, 337 (1984).

Brown, J. M., Hougen, J. T., Huber, K. P., Johns, J. W. C., Kopp, I., Lefebvre-Brion, H., Merer, A. J., Ramsay, D. A., Rostas, J., and Zare, R. N., *J. Mol. Spectrosc.* **55**, 500 (1975).

Brown, J. M., Colbourn, E. A., Watson, J. K. G., and Wayne, F. D., *J. Mol. Spectrosc.* **74**, 294 (1979).

Bulthuis, H., *Proc. Acad. Sci.* Amsterdam. **38**, 604 (1935).

Coster, D., Brons, H. H., and Bulthuis, H., *Z. Physik.* **79**, 787 (1932).

Coxon, J. A., and Foster, S. C., *J. Mol. Spectrosc.* **93**, 117 (1982).

Coxon, J. A., *J. Mol. Spectrosc.* **72**, 252 (1978).

Crosswhite, H. M., *J. Res. Natl. Bur. Stds., A Phys. and Chem.* **79A**, 17 (1975).

Davies, P. B., and Rothwell, W. J., *J. Chem. Phys.* **83**, 5450 (1985).

Dixon, T. A., and Woods, R. C., *Phys. Rev. Lett.* **34**, 61 (1975).

Douay, M., Rogers, S. A., and Bernath, P. F., *Mol. Phys.* **64**, 425 (1988).

Earls, L. T., *Phys. Rev.* **48**, 423 (1935).

Erickson, N. R., Snell, R. L., Loren, R. B., Mundy, L., and Plambeck, R. L., *Astrophys. J.* **245**, L83 (1981).

Haridass, C., M.Sc. thesis, Memorial University of Newfoundland, Canada, 1990.

Haridass, C., Prasad, C. V. V., and Reddy, S. P., *Astrophys. J.*, **388**, 669 (1992).

Herzberg, G., "Molecular Spectra and Molecular Structure. I. Spectra of Diatomic Molecules," Kreiger, Malabar, FL, 1991.

Jakubek, Z., Kepa, R., Para, A., and Rytel, M., *Can. J. Phys.* **65**, 94 (1987).

Katayama, D. H., and Welsh, J. A., *J. Chem. Phys.* **75**, 4224 (1981).

Misra, P., Ferguson, D. W., Rao, K. N., Williams Jr. E., and Mathews, C. W., *J. Mol. Spectrosc.* **125**, 54 (1987).

Pluvinel, A. B., and Baldet, F., *Compt. Rend.* **148**, 759 (1909).

Pluvinel, A. B., and Baldet, F., *Astrophys. J.* **34**, 89 (1911).

Prasad, C. V. V., and Reddy, S. P., *J. Mol. Spectrosc.* **130**, 62 (1988).

Prasad, C. V. V., and Reddy, S. P., *J. Chem. Phys.* **90**, 3010 (1989).

Prasad, C. V. V., and Reddy, S. P., *J. Mol. Spectrosc.* **144**, 323 (1990).

Rao, K. N., *Astrophys. J.* **111**, 306 (1950a).

Rao, K. N., *Astrophys. J.* **111**, 50 (1950b).

Reddy, S. P., and Prasad, C. V. V., *J. Chem. Phys.* **91**, 1972 (1989a).

Reddy, S. P., and Prasad, C. V. V., *J. Phys. E. Sci. Instrum.* **22**, 306 (1989b).

Sastry, K. V. L. N., Helminger, P., Herbst, E., and DeLucia, F. C., *Astrophys. J.* **250**, L91 (1981).

Wang, D. X., Haridass, C., and Reddy, S. P., *J. Mol. Spectrosc.*, **175**, 73 (1996)

Wilson, R. W., Jefferts, K. B., and Penzias, A. A., *Astrophys. J.* **162**, L43 (1970)

SUMMARY

The conclusions arrived at from the study of the spectra of various isotopomers of CO and of $^{12}C^{16}O^{+}$ are discussed at length in the sections "Conclusions" in the respective chapters. To avoid repetition, a summary of the work presented in the thesis is not given.

LIST OF PUBLICATIONS

D. Wang, **C. Haridass** and S. P. Reddy
The Gamma ($A\ ^2\Sigma^+$-$X\ ^2\Pi_r$) System of the nitric oxide Isotopomers, J. Molec. Spectrosc. **175**, 73 (1996).*

C. Haridass, S. P. Reddy and A. C. Le Floch
Precise Rovibronic Term Values of Some Vibrational Levels of the $A\ ^1\Pi$, $B\ ^1\Sigma^+$, $C\ ^1\Sigma^+$, and $E\ ^1\Pi$ States of $^{12}C^{18}O$ and $^{13}C^{18}O$, J. Mol. Spectrosc. **168**, 429 (1994).*

C. Haridass, S. P. Reddy and A. C. Le Floch
The Fourth Positive ($A\ ^1\Pi$-$X\ ^1\Sigma^+$) System of $^{12}C^{18}O$ and $^{13}C^{18}O$: Perturbations in the $A\ ^1\Pi$ State, J. Mol. Spectrosc. **167**, 334 (1994).*

C. Haridass and K. P. Huber
A High-Resolution ^{13}C Isotope Study in the Vacuum Ultraviolet Spectra of CO (A-X), CI, and CII., Astrophysical Journal, 420, 433 (1994).*

C. G. Deacon, R. Goulding, **C. Haridass** and Brad de Young
Demonstration experiments with a Stirling Engine, Physics Education, **5**, 32 (1994).

C. Haridass, C. V. V. Prasad and S. P. Reddy
The Comet-Tail (A-X) System of $^{12}C^{16}O^+$: Precise Molecular Constants of its $X\ ^2\Sigma^+$, $A\ ^2\Pi_r$ and $B\ ^2\Sigma^+$ States. Astrophysical Journal 388, 669 (1992).*

C. Haridass, R. Sundararajan and N. Krishnamurthy
Lattice Dynamics of TlI, Can J. Phys. 66, 630 (1988).

T. Nageswari and **C. Haridass**
Intensity Distribution in Diffraction from Coarse Gratings, Physics Education 5, 32 (1988).

C. Haridass and P. Muthusubramanian
Infrared Spectra of Bis Glycine Cadmium Chloride, Proc. of the National Acadamey of Sciences, India, 56(A), 170 (1986).

C. Haridass, S. Natarajan and P. Muthusubramanian
Infrared Spectra of Barium Glycinate Dihydrate, Indian. J. Phys. 58B, 324 (1984).

C. Haridass and P. Muthusubramanian
Infrared Spectra of Trisarcosine Calcium Chloride, Indian. J. Phys. 58B, 315 (1984).

---

*A reprint of the publication is attached.

NOTE: FOR COPYRIGHT REASONS, THE ATTACHED REPRINTS ARE NOT INCLUDED FOR MICROFILMING.